Interaction Notes

Note 369

17 November 1978

Study of Corona in a Transmission Line Test Facility

P. S. Book
Kaman Sciences Corporation
Colorado Springs, Colorado

Abstract

The corona phenomenon may be an important factor in determining the current and voltage induced on long VLF antennas that are subjected to severe electromagnetic pulse environments. Because of the possible importance of these effects to several aircraft hardening programs and the incomplete characterization of corona under transient conditions, a basic study program was undertaken. The experimental configuration consisted of a single conductor suspended one meter over a ground plane with electric and magnetic field sensors attached to the ground plane at five locations along the test conductor. Measurements were made for five conductor types ranging from a 9.525 mm diameter copper tube to a 2.305 mm diameter beryllium copper wire. A charged coaxial line pulser was used to achieve an operating voltage from $\pm$ 40 kV to $\pm$ 90 kV. Selected data from the experimental phase of the program were numerically corrected for measurement errors and used to calculate basic transmission line quantities and the parameters of a simple empirical model of the corona phenomenon. These calculated results are presented in tabular and graphical form over the range of conductor and operating voltage.

PREFACE

This final report was prepared by Kaman Sciences Corporation, Colorado Springs, Colorado, under Contract F29601-77-C-0060 with the Air Force Weapons Laboratory, Kirtland Air Force Base, New Mexico. The Laboratory Project Officer was MSgt Harris A. Goodwin.

This report presents the results of an experimental program designed to study corona effects in a transmission line test facility. The work reported herein is a continuation and extension of an earlier corona study program carried out from May through October 1976. Much of the test facility and many of the experimental techniques developed under the previous program were modified as required and used to support this phase of the study program.

The author wishes to acknowledge important contributions by the following individuals: Dr. Carl E. Baum and Dr. Kenneth C. Chen of the Air Force Weapons Laboratory (AFWL) who provided technical guidance to both the experimental and analytical phases of the program; MSgt Harris A. Goodwin who arranged for the loan of needed government equipment and provided other administrative support; Dr. Wolfgang Bereuter of Kaman Sciences Corporation (KSC) who assisted with the analytical phase of the program and development of the data reduction methodology; and Roger Baer of KSC who assisted with all aspects of the experimental work.

TABLE OF CONTENTS

		Page
	PREFACE	2
I	INTRODUCTION	6
II	EXPERIMENTAL CONFIGURATION	8
	1. TEST FACILITY	8
	2. HIGH-VOLTAGE PULSER	12
	3. INSTRUMENTATION	14
III	CORONA MODEL	21
IV	TEST RESULTS	28
	1. DATA CORRECTION FACTORS	28
	2. DATA PRESENTATION	32
	3. CALCULATED PARAMETERS	36
V	DISCUSSION AND CONCLUSIONS	56
APPENDIX		
A	RAW TEST DATA	59
B	CORRECTED TEST DATA	111

LIST OF ILLUSTRATIONS

Figure		Page
1	Test Facility as Viewed From Line Termination.....	9
2	Diagram of Corona Test Facility.....	10
3	Diagram of High-Voltage Pulser.....	13
4	Response of Test Facility Cables and Oscilloscope to Step Input.....	16
5	Installation of Magnetic and Electric Field Sensors...	18
6	Simple Corona Model for Long Wire.....	22
7	Model Parameters for 4.115 mm Diameter Al Wire at 80 kV.....	44
8	Model Parameters for 4.115 mm Diameter Al Wire at 90 kV.....	45
9	Model Parameters for 4.115 mm Diameter Al Wire at -80 kV.....	46
10	Model Parameters for 4.115 mm Diameter Al Wire at -90 kV.....	47
11	Model Parameters for 2.305 mm Diameter BeCu Wire at 60 kV.....	48
12	Model Parameters for 2.305 mm Diameter BeCu Wire at 70 kV.....	49
13	Model Parameters for 2.305 mm Diameter BeCu Wire at 80 kV.....	50
14	Model Parameters for 2.305 mm Diameter BeCu Wire at 90 kV.....	51
15	Model Parameters for 2.305 mm Diameter BeCu Wire at -60 kV.....	52
16	Model Parameters for 2.305 mm Diameter BeCu Wire at -70 kV.....	53
17	Model Parameters for 2.305 mm Diameter BeCu Wire at -80 kV.....	54
18	Model Parameters for 2.305 mm Diameter BeCu Wire at -90 kV.....	55

LIST OF TABLES

Table		Page
1	Theoretical and Nominal Transmission Line Terminations.....	12
2	Summary of Corona Model and Transmission Line Relationships.....	27
3	Correction Factors for Test Facility Cables.....	31
4	Local Atmoshperic Conditions.....	33
5	Scope of Test Data.....	35
6	Parameters for 4.115 mm Diameter Al Wire.....	37
7	Parameters for 2.305 mm Diameter BeCu Wire.....	40
8	Test Conditions for Onset of Corona.....	57

SECTION I
INTRODUCTION

Certain types of military aircraft such as the E-4 and TACAMO employ long VLF trailing wire antennas. Moreover, these aircraft are required to survive exposure to a severe electromagnetic pulse (EMP) environment. It has been suggested that the corona phenomenon may be an important factor in determining the voltage and current induced on the antennas by the EMP environment. Because of the possible importance of corona effects and the incomplete characterization of corona under transient conditions, a basic study program was undertaken by KSC in May 1976. That program was directed by AFWL and culminated in a test report (ref. 1) describing the experimental procedure, test results and preliminary modelling effort.

The work reported herein is a continuation and extension of the earlier work. It was initiated in July 1977 and was designed to obtain better quality test data over a wider range of operating voltages and test conductor types. The basic experimental configuration consisted of a single conductor suspended 1m over a ground plane similar to the configuration used for the earlier work except that the conductor and ground plane lengths were increased by 30m. Electric and magnetic field sensors were attached to the ground plane at five locations along the test conductor. During the course of the experimental program, measurements were made for five conductors -- a 9.525 mm diameter (3/8 inch) copper tube, a sample of the TACAMO copper antenna wire (4.064 mm diameter), a sample of the TACAMO aluminum antenna wire (4.064 mm diameter), a 4.115 mm diameter (AWG No. 6) bare aluminum wire, and a 2.305 mm diameter (AWG No. 11) beryllium copper wire. Selected data for several of the test conductors were corrected for sensor and cable responses and used to calculate the parameters of a simple corona radius model.

---

1. Book, P. S. and Price, H. J., "A Transmission Line Corona Experiment," Electromagnetic Pulse Interaction Note No. 313, October 1976.

Section II of this report describes the transmission line test facility, the high-voltage pulser used to drive the test conductors, and the instrumentation used to acquire electric and magnetic field data. The simple corona radius model for the wire over ground plane test configuration is discussed in Section III. Raw and selected corrected data for some of the test conductors are presented in Section IV together with calculations and graphs of the model parameters based on these data; all of the recorded data were not corrected for instrumentation response because of the large quantity of raw data and also because only limited data are useful in support of the model concept. Discussion and conclusions relevant to the overall program are given in Section V.

SECTION II
EXPERIMENTAL CONFIGURATION

The three basic elements of the experimental configuration are the transmission line (single conductor over a ground plane) test facility, the high-voltage pulser used to drive a test conductor, and the field sensors and recording instrumentation. Each of these elements is discussed in considerable detail in the following paragraphs.

1. TEST FACILITY

The transmission line test facility is located on the northeast corner of KSC property in Colorado Springs, Colorado. The ground plane is comprised of eight rolls of plain weave copper wire cloth (No. 16 mesh size, AWG No. 25 wire size) spot-soldered at 10 to 15 cm intervals to form an overall surface area about 9.6m wide by 70m long. This ground plane was designed to accommodate a 60m test conductor with the pulser building and line termination resistor located 5m from opposite ends of the plane. Figure 1 is a photograph of the completed test facility as viewed from the line termination end and Figure 2 is a sketch illustrating some layout details that are not readily apparent from the photograph.

The test facility is configured for five measuring stations as indicated by the conduit outline shown in Figure 2. This conduit consists of 3.81 cm diameter copper water pipe with soldered joints in the main sections and clamped joints in the branch sections. The conduit in the region of the ground plane is buried about 10 cm into the test facility surface so as not to interfere with the ground plane itself. Cable pairs are routed from each of the measuring stations to the instrumentation trailer. An RG-8/U size cable with foam dielectric is used because of its compatibility with the small diameter conduit and its relatively low-loss characteristics (nominal attenuation of 5.41 db/100m at 100 MHz). The cable ends are fitted with locking type GR874 connectors at the sensors and with nonlocking type GR874 connectors at the instrumentation trailer.

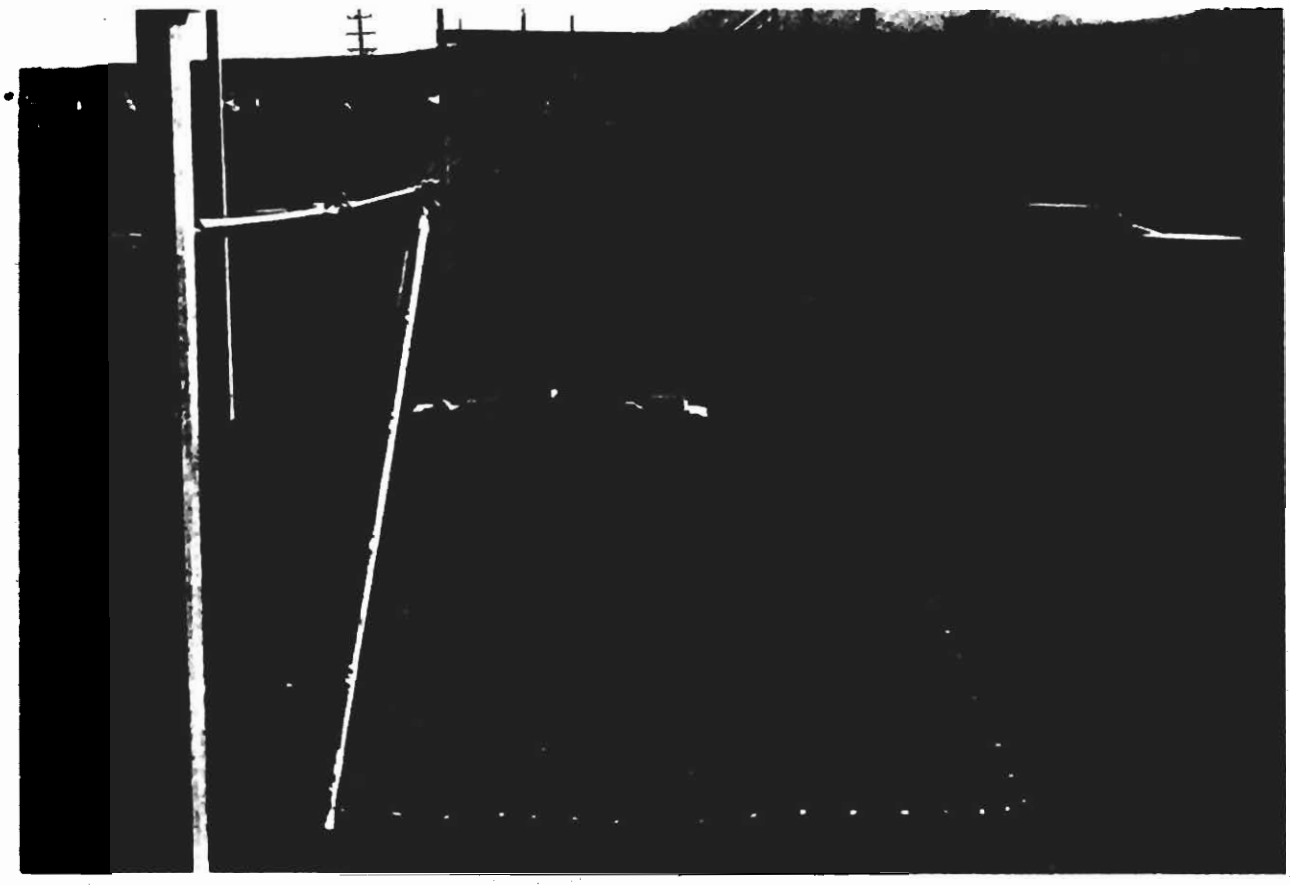

Figure 1
Test Facility As Viewed From Line Termination

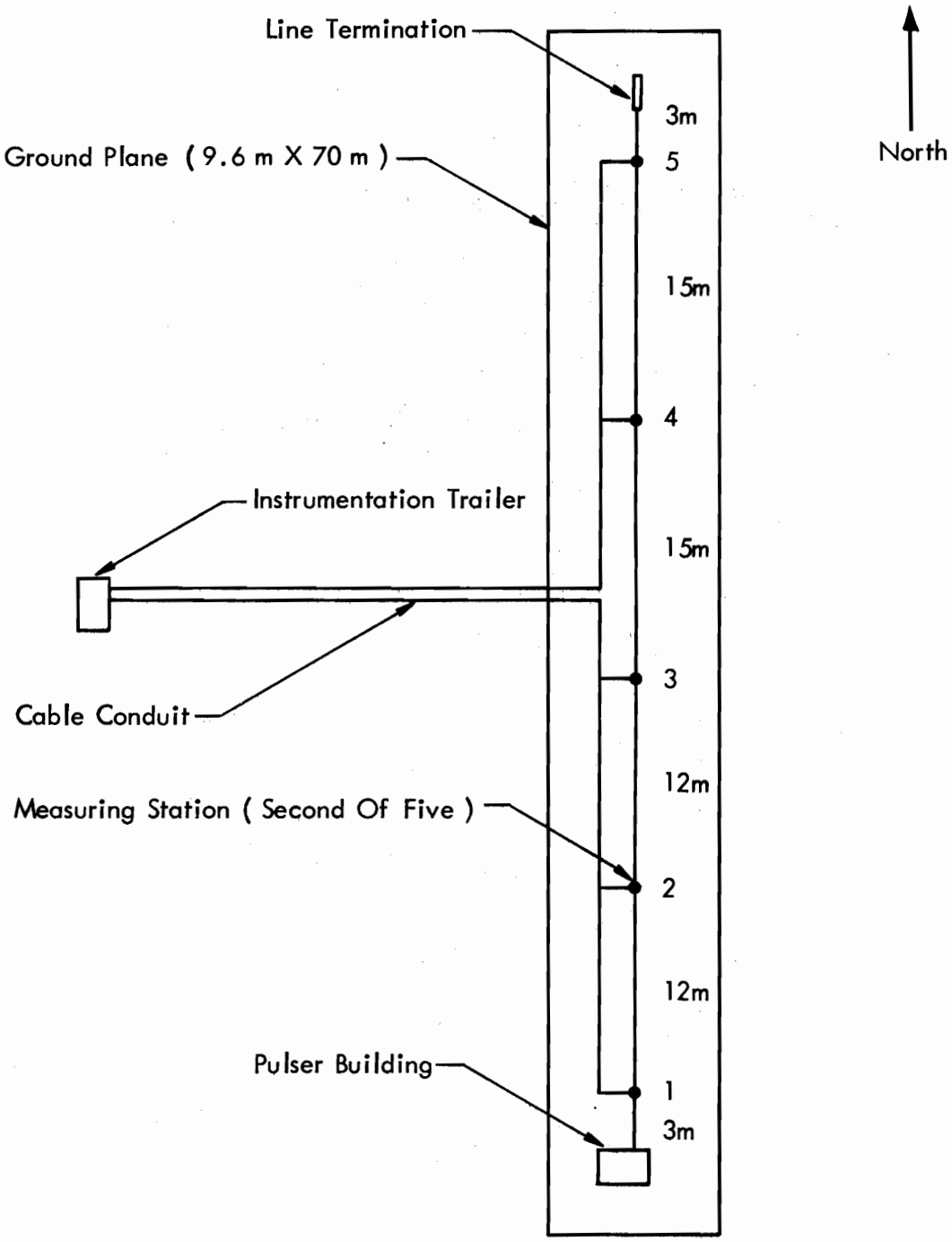

Figure 2
Diagram of Corona Test Facility

Power for the instrumentation trailer is via a commercial outlet in a KSC manufacturing building located about 30m west of the trailer site. A high-quality power line filter (Lindgren model C-30-2) is built into the trailer to prevent noise coupled onto the power cable from interfering with operation of the recording oscilloscopes. A 2.4m ground rod located near the trailer is used to provide a ground connection in addition to that provided by the main ground plain and buried conduit.

Each of the test conductors was suspended 1m above the ground plane with nylon cord fastened to the wood support structures shown in Figure 1. The cord was fastened to a test conductor at points near each of the support structures and at points midway between support structures. This fastening technique in combination with end supports designed to provide approximately 50 pounds of tension enabled the test conductors to be suspended with less than 2 cm deviation from a true parallel configuration.

In general, it is desirable to terminate a test conductor with its characteristic impedance in order to minimize the effects of a reflected pulse. High-power, low-inductance metal film resistors manufactured by Carborundum Company were used for this purpose throughout the experimental program. It is sometimes difficult to achieve a precise termination with this type of resistor because of the limited values that are available as standard items. The calculated characteristic impedance and measured value of termination resistor are compared in Table 1 for each of the test conductors.

Table 1

Theoretical and Nominal
Transmission Line Terminations

Test Conductor		Termination Resistance	
Type	Diameter	Calculated	Nominal
Copper tube	9.525 mm	362 ohms	393 ohms
Cu antenna wire	4.064	413	393
Al antenna wire	4.064	413	393
Bare Al wire	4.115	412	393
BeCu wire	2.305	447	447

2. HIGH-VOLTAGE PULSER

The high-voltage pulser used to drive the transmission line was designed and fabricated at KSC as part of the program carried out in 1976. It was also used for the current phase of the program with minor modifications to the control circuitry and gas enclosures. It consists of a 120 kV charging supply (Universal Voltronics model BPO-130-5-K3), a coaxial cable energy storage element (39.2m of RG-220/U), and a 100 kV spark gap output switch (Maxwell Laboratories model 40065). Figure 3 is a schematic of the pulser showing the basic components plus the charging resistor and spark gap grading resistors. Due to the nature of the design and limitations of various components, the maximum capability of this pulser is approximately $\pm$ 90 kV across a nominal 400-ohm load. Previous tests to characterize the pulser output waveform indicated a risetime of approximately 20 ns for a 500-ohm load over an operating range from $\pm$ 40 kV to $\pm$ 70 kV.

Three gas supplies were used to support operation of the pulser -- SF_6 at one atmosphere in the cylindrical enclosure around the charging resistor, Freon 12 at one atmosphere in the main rectangular enclosure around the spark gap and grading resistors, and dry air at

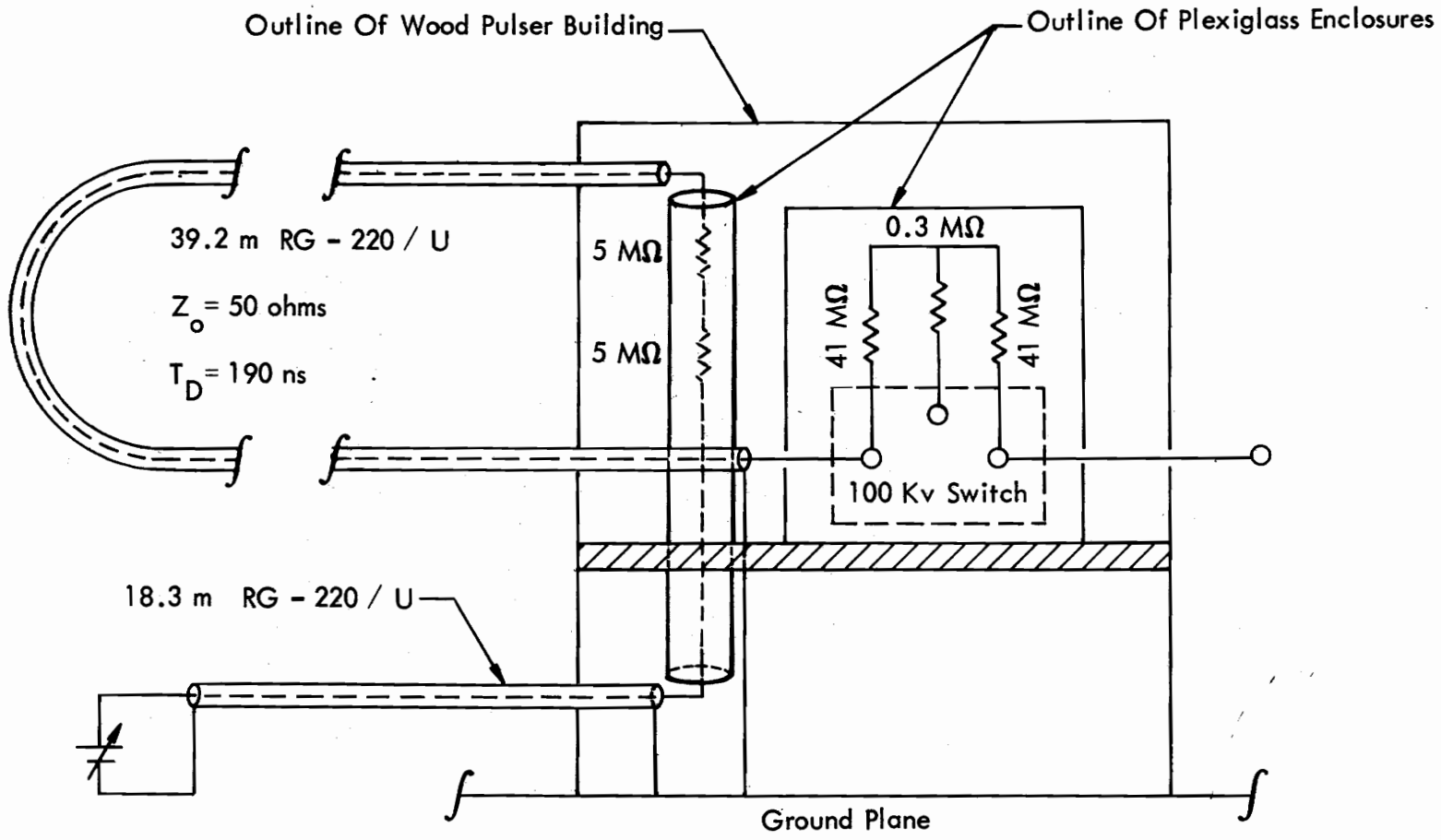

Figure 3
Diagram of High-voltage Pulser

up to 85 psi in the spark gap itself. SF_6 rather than Freon 12 could have been used in the main enclosure but the latter type gas is considerably less expensive and proved to be quite satisfactory for this application.

The spark gap was triggered by causing a momentary decrease in the air pressure from a value above the static breakdown level to a firing level. This was accomplished with a solenoid-actuated valve located near the spark gap vent port. This is a simple, reliable technique that is generally applicable if there is not a requirement for precise control of the firing time.

3. INSTRUMENTATION

The signal recording instrumentation consisted of Tektronix type R454 oscilloscopes equipped with type C-40 cameras. For deflection factor settings from 10 mV/div to 5 V/div, the bandwidth and risetime specifications for the type R454 are 150 MHz and 2.4 ns, respectively. The type C-40 camera is similar to the type C-32; both use an f/1.4 lens and provide a 1:1 object-to-image ratio. With 10,000 ASA film and P11 phosphor, the expected writing speed of the R454/C-40 combination is somewhat greater than 1.1 cm/ns.

Two oscilloscope/camera systems were assembled in a shielded enclosure located in the instrumentation trailer depicted in Figure 2. This enclosure is an integral part of the test facility shielding via a copper braid running from the end of the solid conduit to an entry port of the trailer screened enclosure. The use of two recording channels was based on the desire to record electric and magnetic field signals at a given measuring station for the same line excitation pulse. While it is apparent that the use of ten recording channels to enable simultaneous recording of data from all five measuring stations would have been preferred, such an approach was deemed to be outside the scope of this program. The oscillosopes were operated in the single sweep mode from the internal trigger source. Due to the delay line feature of the type R454 oscilloscopes,

the leading edges of waveforms could readily be recorded.

Pulse response measurements were made to characterize the bandwidth of the recording instrumentation in combination with the test facility cables. A Paravan model 1500 charged line pulser (risetime less than 0.5 ns) was used to drive each of the test facility cables at the cable/sensor connector interface. Figure 4* shows the responses as recorded in the instrumentation trailer.

Model MGL-S5A(A) $\dot{B}$ and model HSD-S3A(R) $\dot{D}$ sensors were used to measure the magnetic and electric fields at the ground plane. These types were chosen because of a comparatively small size compatible with a 1.0m transmission line height, sufficient sensitivity to generate a measurable signal at the lowest expected operating voltage, and a risetime specification (less than 1 ns for both types) considerably better than required.

Because of grounding and shielding requirements, installation of the sensors on the ground plane is relatively permanent. Figure 5 illustrates some details of a typical installation. Each sensor is bolted to a solid copper sheet which is soldered to the ground plane. Copper braid is used to shield the cable sections between the sensor output connectors and the cable conduit located just below the ground plane. Each braid is clamped to the connector shell on the sensor; it is spot-soldered around the entire periphery where it feeds through the ground plane. A 0.86m spacing between sensors was chosen to avoid mutual interference. Special care was taken in suspending a test conductor to assure that it was centered between the two sensors.

For an operating frequency range well below the cutoff frequency for the sensors (700 MHz for the $\dot{B}$ sensors and 350 MHz for the $\dot{D}$ sensors), the output voltages are given by

---

* In these figures and subsequent references, the station number designates the relative measuring station location where number one is closest to the pulser building.

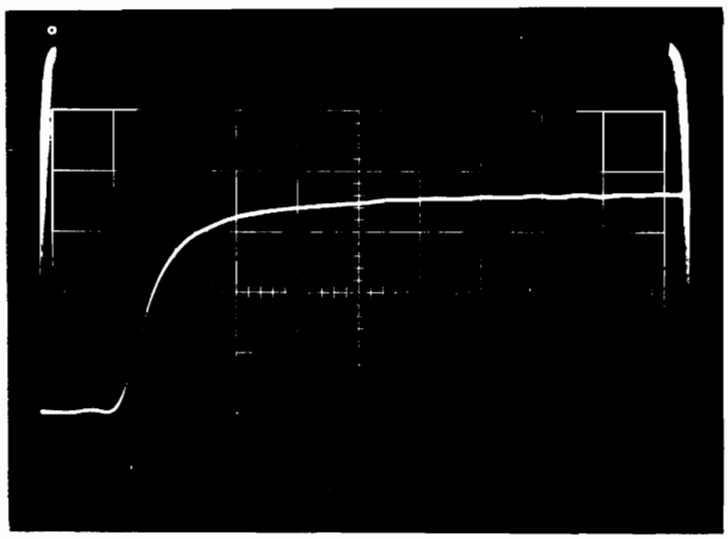

Station No. 1
S_V : 5 V/div
S_H : 5 ns/div

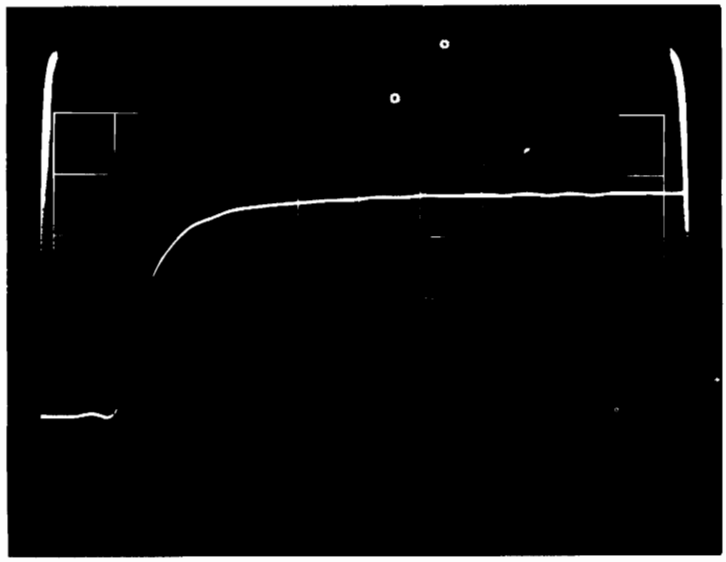

Station No. 2
S_V : 5 V/div
S_H : 5 ns/div

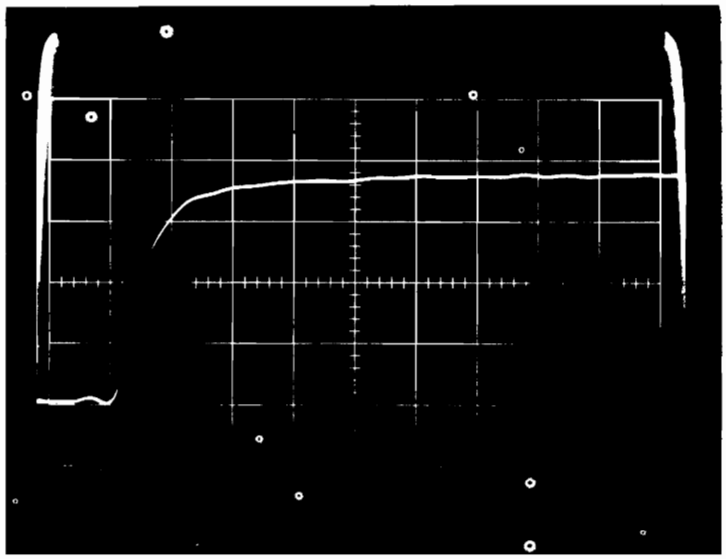

Station No. 3
S_V : 5 V/div
S_H : 5 ns/div

Figure 4

Response of Test Facility Cables and Oscilloscope to Step Input

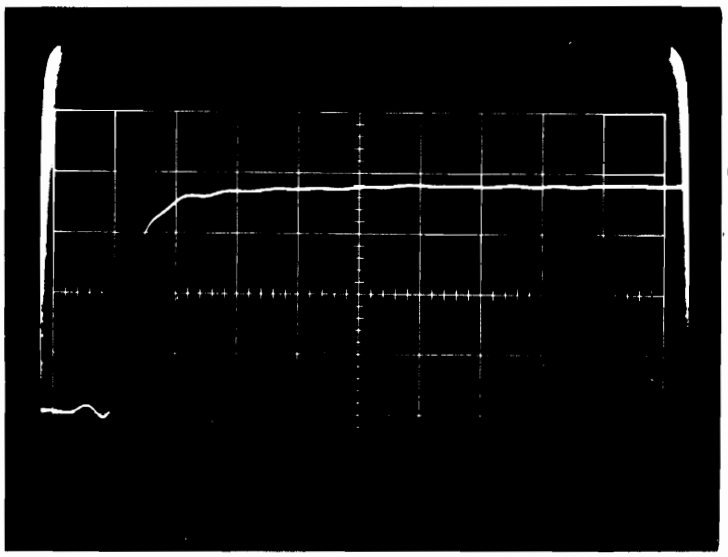

Station No. 4
S_V : 5 V/div
S_H : 5 ns/div

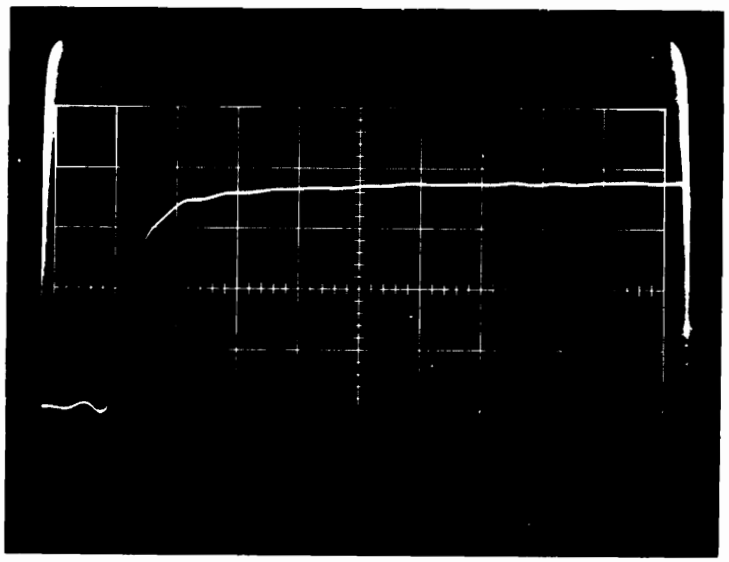

Station No. 5
S_V : 5 V/div
S_H : 5 ns/div

Figure 4 (Concluded)
Response of Test Facility Cables and Oscilloscope to Step Input

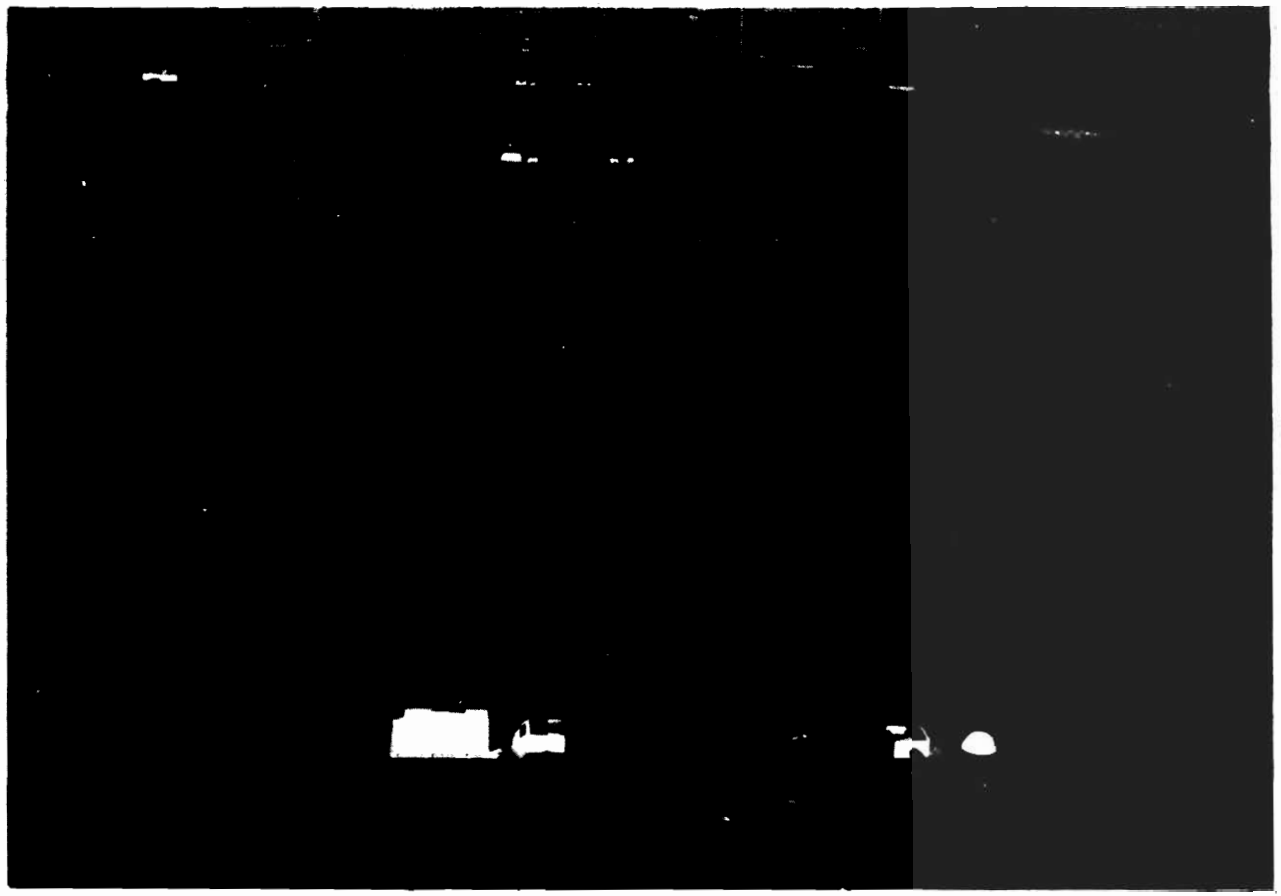

Figure 5
Installation of Magnetic and Electric Field Sensors

$$V_B^{\cdot} = A_{eq} \dot{B} \cos\theta \qquad (1)$$

where $A_{eq} = 10^{-3} m^2$ = sensor equivalent area

$\cos\theta = 1$

B = magnetic flux density in webers/m^2

and $$V_D^{\cdot} = A_{eq} R \dot{D} \qquad (2)$$

where $A_{eq} = 10^{-2} m^2$ = sensor equivalent area

R = 50 ohms = load resistance

D = electric flux density in C/m^2

The sensor output signals were electrically integrated with RCI-1C type integrators located at the oscilloscope inputs. For time intervals that are short compared to the 1 μs time constant* for this type of integrator, the integrated $\dot{B}$ signal is given by

$$V_B = \frac{1}{C_I}\int i dt = \frac{1}{C_I}\int \frac{V_B^{\cdot}}{R_I}\, dt$$

$$= \frac{1}{C_I R_I}\int 10^{-3}\, dB$$

$$= 10^3 B \qquad (3)$$

A similar manipulation for $V_D^{\cdot}$ yields

$$V_D = 5 \cdot 10^5 D \qquad (4)$$

---

* A latter section of this report deals with the case where this approximation is inappropriate.

The measured impedance at the surface of the ground plane, Z_m, is an important experimental parameter. It can be readily calculated from the basic definition of wave impedance and equations (3) and (4) as follows:

$$Z_m = \frac{E}{H} = \frac{D/\epsilon_o}{B/\mu_o}$$

$$= \frac{\mu_o}{\epsilon_o} \frac{V_D}{5 \times 10^5} \frac{10^3}{V_B}$$

$$= 283.9 \frac{V_D}{V_B} \qquad (5)$$

SECTION III
CORONA MODEL

Corona manifests itself as a highly ionized region in the vicinity of a conductor subjected to an applied voltage in excess of the corona threshold. For the transmission line test configuration, the ionized region is in the immediate vicinity of the test wire where the electric field is highest. From an elementary viewpoint, the radius of the ionized region would be expected to increase until the electric field at the boundary of the region becomes insufficient to support further ionization. Figure 6 is an equivalent circuit model of this phenomenological description.

Corona is a complex phenomenon and it is in general extremely difficult to relate model parameters to measured quantities. However, with the benefit of two simplifying assumptions, classical two wire transmission line theory is applicable and provides the necessary relationships: first, it must be assumed that the conductance of the corona region is very high compared to the shunt conductance of the transmission line; and second, it must be assumed that a new equilibrium state has been established (that is, transmission line theory is not directly applicable during transition from a normal to a corona condition). Two wire transmission line theory (equivalent to the single wire over ground plane test configuration when appropriate factors of two are included) is presented in various references. The following equations are taken from reference 2.

The electric field at the ground plane at a distance x from the wire centerline is given by

$$E = \left[1 + \left(\frac{x}{h}\right)^2\right]^{-1} \frac{2V}{h \ \ell n\left(\frac{2h}{r_c}\right)} \qquad (6)$$

---

2. Baum, C. E., "Impedances and Field Distributions for Symmetrical Two Wire and Four Wire Transmission Line Simulators", Electro-Magnetic Pulse Sensor and Simulation No. 27, June 1970.

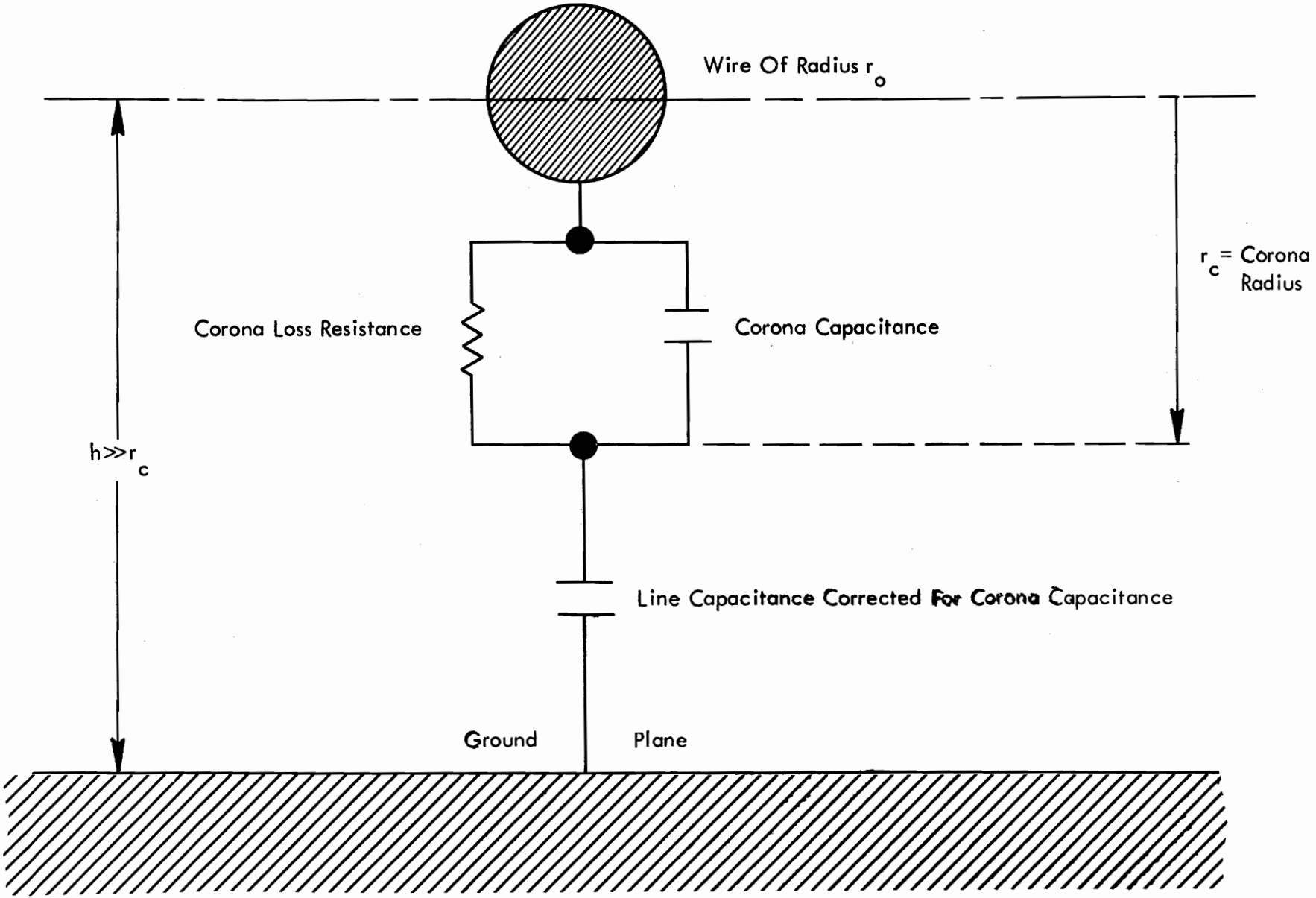

Figure 6

Simple Corona Model for Long Wire

or

$$E = \left[1 + \left(\frac{x}{h}\right)^2\right]^{-1} \frac{Q'}{\pi \epsilon_o h} \tag{7}$$

and the magnetic field at the same distance is given by

$$H = \left[1 + \left(\frac{x}{h}\right)^2\right]^{-1} \frac{I}{\pi h} \tag{8}$$

where

V is the wire voltage
h is the wire height
r_c is the corona radius parameter
Q' is the wire charge per unit length
I is the wire current

Thus, from equations (6) and (8), the impedance at the ground plane is simply

$$Z_{cm} = \frac{E}{H} = \frac{2\pi}{\ell n\left(\frac{2h}{r_c}\right)} \frac{V}{I} \tag{9}$$

where the terminology, Z_{cm}, is used to make a distinction between the expected impedance based on the corona radius model and the measured impedance, Z_m.

In equation (9), the quantity V/I is simply the characteristic impedance of a perfectly terminated transmission line for an operting voltage below corona threshold. For a single conductor over a ground plane, the characteristic impedance is given as

$$Z_{ot\ell} = \frac{1}{2\pi} \sqrt{\frac{\mu_o}{\epsilon_o}} \ell n\left(\frac{2h}{r_o}\right) \tag{10}$$

Substituting equation (10) into equation (9) gives

$$Z_{cm} = Z_{ofs} \frac{\ell n\left(\frac{2h}{r_o}\right)}{\ell n\left(\frac{2h}{r_c}\right)} \tag{11}$$

where Z_{ofs} is the characteristic impedance of free space

Therefore, for an operating voltage below the corona threshold where $r_o = r_c$, the expected value of Z_{cm} is simply 376.74 ohms.

Equation (9) cannot be solved in general for r_c as a function of measured parameters. However, for the measuring station near the wire termination where the ratio of V/I is determined by the termination resistor, equation (9) can be solved explicitly for r_c to yield

$$r_c = 2h\, e^{-\frac{2\pi R_t}{Z_{cm}}} \tag{12}$$

where R_t is the termination resistance

Experience has shown that equation (12) may not yield the expected results when the calculation is carried out with impedance values measured for operating conditions below corona threshold; this is due to the importance of small measurement errors in the exponential equation. One way to minimize the importance of systematic measurement errors is to normalize the calculation based on a measurement below corona threshold. That is, let the model impedance be a constant multiple of the measured impedance as expressed by

$$Z_{cm} = kZ_m \tag{13}$$

Substituting the above expression into eqution (12) gives

$$r_c = 2h\, e^{-\frac{2\pi R_t}{kZ_m}} \tag{14}$$

and since $r_c = r_o$ for an operating voltage below corona threshold

$$r_o = 2h\, e^{-\frac{2\pi R_t}{k Z_{mo}}} \qquad (15)$$

where Z_{mo} is the impedance measured at the end station for a test voltage below corona threshold

Solving equation (15) for k and substituting into equation (14) gives

$$r_c = 2h\, e^{\left(\ell n\, \frac{r_o}{2h}\right)\left(\frac{Z_{mo}}{Z_m}\right)}$$

$$= 2h \left(\frac{r_o}{2h}\right)^{\left(\frac{Z_{mo}}{Z_m}\right)} \qquad (16)$$

Other model parameters which can be computed from measured quantities include the line voltage near the termination, V_T, and the radial electric field at the boundary of the corona region, E_r. The first of these is given simply as the product of the wire current and the termination resistance where the wire current is related to the measured magnetic field by equation (8). These considerations result in the expression

$$V_T = I \times R_t$$

$$= \pi h \left[1 + \left(\frac{x}{h}\right)^2\right] H\, R_t \qquad (17)$$

or by incorporation of the magnetic field sensor constant as defined by equation (3)

$$V_T = \pi h \left[1 + \left(\frac{x}{h}\right)^2\right] \frac{10^{-3}}{\mu_o} V_B\, R_t \qquad (18)$$

The radial electric field at the boundary of a high conductivity corona region is given by

$$E_r = \frac{V_T}{r_c \, \ell n\left(\frac{2h}{r_c}\right)} \tag{19}$$

where r_c and V_T are as calculated from equations (16) and (18), respectively.

It is sometimes instructive to deal with basic transmission line parameters, Q' and I, rather than with corona model parameters. Equations (7) and (8) are the basic equations: with the appropriate sensor constants, these equations have the form

$$\begin{aligned} Q' &= \pi h \left[1 + \left(\frac{x}{h}\right)^2\right] D \\ &= \pi h \left[1 + \left(\frac{x}{h}\right)^2\right] 2 \cdot 10^{-6} \cdot V_D \end{aligned} \tag{20}$$

$$\begin{aligned} I &= \pi h \left[1 + \left(\frac{x}{h}\right)^2\right] H \\ &= h \left[1 + \left(\frac{x}{h}\right)^2\right] 2.5 \cdot 10^3 \cdot V_B \end{aligned} \tag{21}$$

These basic relationships are applicable all along the transmission wire independent of any particular corona model. They do, however, presume the existence of the normal TEM wave for a wire over ground plane transmission line.

Table 2 is a summary of the corona model and basic transmission line relationships developed in the foregoing paragraphs. Also included in Table 2 is a repetition of the definition of key terms used in the equations.

Table 2

Summary of Corona Model and Transmission Line Relationships

Corona Model Parameters:

$$r_c = 2h \left(\frac{r_o}{2h}\right)^{\left(\frac{Z_{mo}}{Z_m}\right)} \tag{16}$$

$$Z_m = 283.9 \frac{V_D}{V_B} \tag{5}$$

$$V_T = h\left[1 + \left(\frac{x}{h}\right)^2\right] 2.5 \cdot 10^3 \cdot V_B R_t \tag{18}$$

$$E_r = \frac{V_T}{r_c \, \ell n\left(\frac{2h}{r_c}\right)} \tag{19}$$

Transmission Line Parameters:

$$Q' = \pi h \left[1 + \left(\frac{x}{h}\right)^2\right] 2 \cdot 10^{-6} \cdot V_D \tag{20}$$

$$I = h \left[1 + \left(\frac{x}{h}\right)^2\right] 2.5 \cdot 10^3 \cdot V_B \tag{21}$$

Definition of Terms:

- r_c is the radius of the corona region
- h is the test wire height
- r_o is the test wire radius
- Z_{mo} is the impedance measured at the ground plane for a wire voltage below corona threshold
- Z_m is the impedance measured at the ground plane
- V_T is the wire voltage near the termination resistor
- x is the sensor distance from the wire centerline
- V_B is the integrated output of the B sensor
- R_t is the wire termination resistance
- E_r is the radial electric field at the boundary of the corona region
- Q' is the wire charge per unit length
- I is the wire current

SECTION IV
TEST RESULTS

This section consists of an evaluation and presentation of test results. The first part assesses the importance of and procedures for correcting the raw data for the nonideal response of an electrical integrator and for test facility cable attenuation. Raw data, corrected data for some test conditions, and calculations and graphs of corona model parameters are given in the second part.

1. DATA CORRECTION FACTORS

A cursory evaluation of the raw data shows that corona continues to affect the observed waveforms over the entire time interval corresponding to the pulse width of the charge line pulser - about 350 ns. It is clear that the nonideal response of a 1 μs time constant integrator must be accounted for in order to provide the best quality data over this time period. The correction algorithm is most easily developed in the frequency domain by noting that the actual output, $V_o(s)$, of an nonideal integrator is given by

$$V_o(s) = \frac{1}{\tau} \frac{V_i(s)}{s + \frac{1}{\tau}} \tag{22}$$

in comparison to the desired or corrected output, $V_{oc}(s)$, which is given as

$$V_{oc}(s) = \frac{V_i(s)}{\tau s} \tag{23}$$

where τ is the integrator time constant

$V_i(s)$ is the Laplace transform of the input to the integrator

Solving equation (22) for $V_i(s)$ and substituting into equation (23) yields

$$V_{oc}(s) = V_o(s) + \frac{1}{\tau s} V_o(s) \tag{24}$$

or in the time domain

$$V_{oc}(t) = V_o(t) + \frac{1}{\tau} \int_{-\infty}^{t} V_o(t')dt' \qquad (25)$$

which is the desired expression for corrected voltage as a function of recorded voltage.

An additional consideration can be inferred from a preliminary evaluation of the raw data. That is, the risetime characteristics of the recorded D and B waveforms imply a very short pulse width (about 10 ns full width at half-maximum amplitude) for the D and B signals transmitted over the test facility cables. The response measurements presented in Figure 4 indicate that a 10 ns pulse would suffer some degradation. The simplest correction algorithm is one based on signal attenuation as a function of frequency. For a skin-effect-limited cable, the transmission characteristic is defined by (ref. 3)

$$v(\ell) = v_i e^{-\frac{r'\ell}{2Z_o}} \qquad (26)$$

where ℓ is cable length

r' is the series resistance per unit length of cable

Z_o is the characteristic impedance of the cable

v_i is the voltage at the cable input

Through consideration of the skin effect phenomenon, the quantity r' can be expressed in terms of the frequency and physical characteristics of a given cable type. However, for the present purpose, it is sufficient to note that r' is proportional to the square-root of

3. Landee, Davis and Albrecht, Electronic Designers' Handbook, McGraw-Hill Book Company, Inc., 1957.

frequency such that equation (26) has the form

$$v(\ell) = v_i e^{-k_1 \sqrt{f}\ \ell} \tag{27}$$

where k_1 is a constant to be calculated from specified attenuation characteristics rather than from physical characteristics of the cable.

The cellular dielectric RG-8/U size cable is specified for a nominal attenuation of 0.0541 db/m at 100 MHz. Substituting these values into equation (27) and solving for k_1 results in the expression

$$v(\ell) = v_i e^{-6.23 \cdot 10^{-7} \sqrt{f}\ \ell} \tag{28}$$

where f and ℓ are given in Hz and m, respectively.

Equation (28) accounts only for the attenuation term that is frequency-dependent. There is an additional term due to the dc resistance of the cable center conductor plus shield relative to the 50-ohm termination impedance. When this term is included, equation (28) has the approximate form

$$v(\ell) = \frac{50}{50 + R_\ell} v_i e^{-6.23 \cdot 10^{-7} \sqrt{f}\ \ell} \tag{29}$$

or

$$v_i = v(\ell) \frac{50 + R_\ell}{50} e^{6.23 \cdot 10^{-7} \sqrt{f}\ \ell} \tag{30}$$

This equation defines the correction factor to be applied to an observed voltage, $v(\ell)$, to recover the true sensor output or cable input voltage, v_i. Table 3 is a summary of the correction factors for each of the five different cable lengths. The cable for measuring stations 4 and 5 was purchased and installed at a later time

than the other test facility cables. Since the cellular dielectric cable is not an RG type subject to specific performance specifications, the difference in dc characteristics for the two lots of cable is not too surprising.

Table 3

Correction Factors for Test Facility Cables

Measuring Station	Cable Length	Measured Resistance	Correction Factor
1	64m	1.37 ohms	$1.027\ e^{3.99 \cdot 10^{-5} \sqrt{f}}$
2	52m	1.11 ohms	$1.022\ e^{3.24 \cdot 10^{-5} \sqrt{f}}$
3	40m	0.88 ohms	$1.018\ e^{2.49 \cdot 10^{-5} \sqrt{f}}$
4	44m	0.51 ohms	$1.010\ e^{2.74 \cdot 10^{-5} \sqrt{f}}$
5	59m	0.67 ohms	$1.013\ e^{3.68 \cdot 10^{-5} \sqrt{f}}$

A straightforward procedure was followed to apply the correction algorithms developed in the preceding paragraphs. The photographically recorded waveform of primary interest were first digitized with an in-house model GP-3 Graf/Pen digitizer manufactured by Science Accessories Corporation. Thirty to fifty data points were digitized such that the original waveform could be reconstructed with good fidelity by connecting the digitized points with a series of straight lines. Following digitization, a numerical integration routine based on Simpson's rule was used to correct for integrator response in accordance with equation (25). Filon's method for numerical evaluation of Fourier transforms was then applied to obtain the transform of the corrected data. This was multiplied by the appropriate frequency-dependent cable correction factor given in Table 3, inverse transformed back into the time domain, and presented in graphical form for comparison with raw data and calculation of corona model and/or transmission line parameters.

2. DATA PRESENTATION

Theoretical considerations indicate that atmospheric conditions may be an important factor in the final interpretation of the data (ref. 4). Table 4 is a summary of such data at specific time periods associated with experimental activity. Thus, the approximate atmospheric conditions for any test shot can be obtained by reference to the date and time identification of each raw data photograph. The primary atmospheric data given in Table 4 were obtained from NOAA records for the Peterson Field measuring station in Colorado Springs, Colorado. The air density data were calculated from the ideal gas law using a correction factor to account for the moisture content of air (ref. 5).

Appendix A is a compilation of raw test data acquired during the experimental program for the test conductor types and operating voltages summarized in Table 5. Some raw data were not included in the compilation either because the operating voltages were below corona threshold or the data were judged to be redundant with respect to data for some other test conductor. It is to be noted that the compilation includes data at all five measuring stations for each test condition. This format was chosen in the interest of completeness even though only data from station five were used for the modelling effort included in this report.

Appendix B is corrected station five data for the bare Al and BeCu test conductors over the full range of test voltages. The focus on station five data is consistent with the corona model discussed in Section III in that it is only for this station that

---

4. Baum, C. E.. "The Calculation of Conduction Electron Parameters in Ionized Air," Electromagnetic Pulse Theoretical Note No. 6, March 1965.

5. Weast, R. C., Handbook of Chemistry and Physics, The Chemical Rubber Company, Cleveland, Ohio, 1968.

Table 4

Local Atmospheric Conditions

Date	Time	Temp (°C)	Relative Humidity (Percent)	Dew Point (°C)	Absolute Barometric Pressure* (mm of Hg)	Density (g/ℓ)
Jan	10:00	7.2	24	-12.2	604.01	1.000
6	11:00	8.9	22	-11.7	603.50	0.993
1978	12:00	10.0	20	-11.7	603.76	0.990
	13:00	11.7	18	-11.7	601.98	0.981
	14:00	12.2	18	-11.1	601.35	0.978
Mar	10:00	12.8	20	- 9.4	610.62	0.991
27	11:00	14.4	17	-10.0	610.11	0.985
1978	12:00	15.6	16	-10.0	609.60	0.980
	13:00	16.7	15	-10.0	609.09	0.976
	14:00	17.2	15	-10.0	608.46	0.973
July	10:00	25.6	28	5.6	612.52	0.949
24	11:00	26.1	32	8.3	612.27	0.946
1978	12:00	27.8	28	7.8	612.14	0.940
	13:00	29.4	22	5.6	611.89	0.936
	14:00	30.0	18	3.3	611.63	0.934
July	09:00	27.8	22	4.4	611.63	0.941
25	10:00	30.6	15	1.1	611.51	0.933
1978	11:00	32.2	10	- 2.8	611.38	0.928
	12:00	32.8	9	- 3.9	611.25	0.926
	13:00	33.3	10	- 2.8	611.00	0.924
	14:00	34.4	10	- 1.7	610.87	0.921
Sept	09:00	22.2	24	0.6	601.47	0.943
11	10:00	22.8	20	- 1.1	601.73	0.942
1978	11:00	23.9	16	- 3.3	601.98	0.940
	12:00	24.4	15	- 3.9	601.73	0.938
	13:00	24.4	13	- 5.6	601.60	0.938
	14:00	25.6	12	- 5.0	601.22	0.933
Sept	09:00	12.2	36	- 2.2	607.44	0.987
13	10:00	15.0	32	- 1.7	607.70	0.978
1978	11:00	15.6	33	- 0.6	607.31	0.975
	12:00	17.2	32	0.6	607.06	0.969
	13:00	18.9	29	0.6	606.43	0.962
	14:00	20.6	25	0	605.79	0.956

* The reference altitude for these data is 1857m.

Table 4 (Concluded)

Local Atmospheric Conditions

Date	Time	Temp (°C)	Relative Humidity (Percent)	Dew Point (°C)	Absolute Barometric Pressure* (mm of Hg)	Density (g/ℓ)
Sept	10:00	7.2	31	- 8.9	612.52	1.014
19	11:00	8.9	27	- 8.9	612.52	1.008
1978	12:00	10.0	25	- 8.9	612.14	1.003
	13:00	12.2	24	- 7.8	611.38	0.994
	14:00	12.2	24	- 7.8	610.87	0.993
	15:00	13.3	23	- 7.2	610.49	0.989
	16:00	13.3	24	- 6.7	610.11	0.988
Sept	10:00	7.8	43	- 3.9	615.32	1.016
21	11:00	10.0	37	- 3.9	615.19	1.008
1978	12:00	11.7	38	- 2.2	614.81	1.001
	13:00	13.9	30	- 3.3	614.68	0.993
	14:00	13.9	28	- 4.4	614.17	0.992
	15:00	15.0	30	- 2.2	614.05	0.988
Sept	10:00	21.7	21	- 1.7	612.39	0.963
26	11:00	23.3	18	- 2.2	612.39	0.958
1978	12:00	24.4	16	- 2.8	611.89	0.953
	13:00	25.6	15	- 2.8	611.63	0.949
	14:00	26.1	15	- 2.8	611.38	0.947
	15:00	26.1	14	- 3.9	611.25	0.947
	16:00	26.7	14	- 3.3	611.12	0.945
Sept	09:00	16.7	34	0.6	614.93	0.983
27	10:00	21.1	26	1.1	615.32	0.969
1978	11:00	22.2	26	1.7	615.06	0.965
	12:00	22.8	25	1.7	615.06	0.963
	13:00	23.3	24	1.7	614.68	0.960
	14:00	24.4	23	1.7	614.05	0.956

Table 5

Scope of Test Data

Type	Test Conductor Diameter	Test Voltages for Raw Data	Data Included in Appendix
Copper tube	9.525 mm	-30, -80 kV 30, 40, 50, 60 70, 80 90	40, 90 kV
Cu antenna wire	4.064	-60,-70,-80,-90 60, 70, 80, 90	60, 80
Al antenna wire	4.064	-60, -80 60, 80	60, 80
Bare Al wire	4.115	-60,-70,-80,-90 60, 70, 80, 90	-70, -90 60, 70, 80, 90
BeCu wire	2.305	-40,-50,-60,-70 -80,-90 40, 50, 60, 70 80, 90	-60, -90 40, 50, 60, 70 80, 90

model parameters are explicityly related to test data. Emphasis on data for the bare Al and BeCu test conductors reflects the fact that these data are more manageable than but still representative of the entire body of raw data.

3. CALCULATED PARAMETERS

The corrected data presented in Appendix B and the equations summarized in Table 2 are the base for calculation and evaluation of corona model and transmission line parameters. Tables 6 and 7 are summaries of calculated parameters for the two primary test conductors for all of the positive and negative test voltages. Included in each of these data summary tables are values of Z_{mo} for a test voltage below corona threshold. The average of these values was computed and used in the calculation of corona radius. Nominal or measured values of R_t as given in Table 1 were used to compute the model parameter, V_T.

There is an extremely large number of potentially useful ways to graph the parametric data given in Tables 6 and 7. However, a particular viewpoint or data requirement is best served by a specific data presentation format. Rather than attempting to generate a wide range of formats to serve all possible interests, only a few basic graphs of general interest will be presented herein. Namely, Figures 7 through 18 which are graphs of the corona radius and radial electric field parameters as a function of retarded time at station five.

Table 6

Parameters for 4.115 mm Diameter Al Wire

Test Voltage	Parameter	Time in ns 50	100	150	200	250	300	350	Avg.
60 kV	Z_{mo} ohms	387*	377	378	381	382	386	387	382
	Q' nC/m	492	501	502	508	507	510	511	
	I A	144	149	150	151	150	149	149	
	V_T kV	56.6	58.6	59.0	59.3	59.0	58.6	58.6	
70 kV	Z_{mo} ohms	374	370	370	366	372	375	379	
	Q' nC/m	562	564	542	554	574	595	609	
	I A	170	172	166	171	174	179	181	
	V_T kV	66.8	67.7	65.2	67.0	68.4	70.3	71.3	
80 kV	Z_m ohms	364	422	459	488	494	515	528	
	Q' nC/m	568	660	750	837	884	927	962	
	I A	177	177	185	194	202	203	206	
	r_c mm	1.46	3.95	6.52	9.17	9.79	12.2	13.8	
	V_T kV	69.4	69.5	72.6	76.2	79.4	79.9	80.9	
	E_r MV/m	6.59	2.83	1.95	1.54	1.52	1.29	1.18	

* The values of r_c and E_r at this early time are of questionable validity because of pulse reflection from the parastic capacitance associated with the line termination.

Table 6 (Continued)

Parameters for 4.115 mm Diameter Al Wire

Test Voltage	Parameter		Time in ns 50	100	150	200	250	300	350
90 kV	Z_m	ohms	352	428	448	494	531	544	565
	Q'	nC/m	464	686	821	974	1082	1147	1216
	I	A	149	181	207	222	230	238	243
	r_c	mm	1.14	4.31	5.67	9.79	14.2	16.0	19.1
	V_T	kV	58.4	71.2	81.5	87.4	90.4	93.5	95.5
	E_r	MV/m	6.85	2.69	2.45	1.68	1.29	1.21	1.07
-60 kV	Z_{mo}	ohms	383	374	369	372	382	377	375
	Q'	nC/m	497	506	508	518	521	515	518
	I	A	148	153	156	157	154	154	156
	V_T	kV	58.1	60.1	61.2	61.8	60.5	60.7	61.2
-70 kV	Z_m	ohms	388	387	385	384	401	405	406
	Q'	nC/m	564	560	585	600	623	638	643
	I	A	164	164	172	177	176	177	179
	r_c	mm	2.29	2.25	2.17	2.13	2.85	3.04	3.09
	V_T	kV	64.4	64.4	67.6	69.6	69.2	69.6	70.3
	E_r	MV/m	4.16	4.22	4.56	4.77	3.70	3.52	3.52

Table 6 (Concluded)

Parameters for 4.115 mm Diameter Al Wire

Test Voltage	Parameter		Time in ns 50	100	150	200	250	300	350
-80 kV	Z_m	ohms	357	374	397	402	413	420	413
	Q'	nC/m	557	620	710	757	769	782	786
	I	A	176	187	202	212	210	210	215
	r_c	mm	1.27	1.77	2.67	2.89	3.45	3.83	3.45
	V_T	kV	69.2	73.5	79.4	83.3	82.5	82.5	84.5
	E_r	MV/m	7.39	5.89	4.49	4.40	3.76	3.44	3.85
-90 kV	Z_m	ohms	383	413	429	448	455	454	464
	Q'	nC/m	608	787	886	957	976	976	997
	I	A	179	215	234	242	242	243	242
	r_c	mm	2.09	3.45	4.37	5.67	6.20	6.13	6.94
	V_T	kV	70.3	84.5	91.9	95.1	95.1	95.5	95.1
	E_r	MV/m	4.89	3.85	3.43	2.86	2.65	2.69	2.42

Table 7

Parameters for 2.305 mm Diameter BeCu Wire

Test Voltage	Parameter		Time in ns 50*	100	150	200	250	300	350
40 kV	Z_{mo}	ohms	401	392	396	398	401	406	408
	Q'	nC/m	289	297	300	303	302	304	304
	I	A	81.4	85.7	85.5	86.0	85.2	84.7	84.1
	V_T	kV	36.4	38.3	38.2	38.4	38.1	37.9	37.6
50 kV	Z_m	ohms	399	394	418	448	466	486	499
	Q'	nC/m	387	382	407	437	455	478	497
	I	A	110	110	110	110	110	111	112
	V_T	kV	49.2	49.2	49.2	49.2	49.2	49.6	50.1
60 kV	Z_m	ohms	384	391	426	465	495	530	564
	Q'	nC/m	355	400	460	536	593	652	705
	I	A	104	115	122	130	135	139	141
	r_c	mm	1.11	1.27	2.32	4.09	5.96	8.75	12.1
	V_T	kV	46.5	51.4	54.5	58.1	60.3	62.1	63.0
	E_r	MV/m	5.59	5.51	3.48	2.29	1.74	1.31	1.02

* The values of r_c and E_r at this early time are of questionable validity because of pulse reflection from the parasitic capacitance associated with the line termination.

Table 7 (Continued)

Parameters for 2.305 mm Diameter BeCu Wire

Test Voltage	Parameter		Time in ns 50	100	150	200	250	300	350
70 kV	Z_m	ohms	401	421	474	554	590	614	637
	Q'	nC/m	385	460	575	711	804	874	925
	I	A	108	123	137	145	154	161	164
	r_c	mm	1.52	2.14	4.60	11.1	15.2	18.4	21.8
	V_T	kV	48.3	55.0	61.2	64.8	68.8	72.0	73.3
	E_r	MV/m	4.41	3.75	2.19	1.13	0.93	0.83	0.74
80 kV	Z_m	ohms	386	442	524	582	633	667	681
	Q'	nC/m	422	541	696	864	998	1083	1155
	I	A	123	138	150	168	178	183	191
	r_c	mm	1.15	2.97	8.22	14.2	21.2	26.7	29.2
	V_T	kV	55.0	61.7	67.0	75.1	79.6	81.8	85.4
	E_r	MV/m	6.40	3.19	1.48	1.07	0.83	0.71	0.69
90 kV	Z_m	ohms	388	478	549	593	630	656	679
	Q'	nC/m	396	635	913	1101	1230	1309	1370
	I	A	115	150	188	210	220	225	228
	r_c	mm	1.20	4.84	10.6	15.6	20.7	24.8	28.8
	V_T	kV	51.4	67.1	84.0	93.9	98.3	100	102
	E_r	MV/m	5.78	2.30	1.52	1.24	1.04	0.92	0.83

Table 7 (Continued)

Parameters for 2.305 mm Diameter BeCu Wire

Test Voltage	Parameter		Time in ns 50	100	150	200	250	300	350	Avg.
-40 kV	Z_{mo}	ohms	384	388	383	391	380	389	389	386
	Q'	nC/m	294	305	304	310	307	311	311	
	I	A	86.6	88.7	89.5	89.6	91.4	90.3	90.8	
	V_T	kV	38.7	39.7	40.0	40.0	40.9	40.3	40.6	
-50 kV	Z_{mo}	ohms	400	386	391	385	398	390	393	
	Q'	nC/m	370	367	374	371	384	379	381	
	I	A	104	108	108	109	109	110	109	
	V_T	kV	46.5	48.3	48.3	48.7	48.7	49.2	48.7	
-60 kV	Z_m	ohms	398	397	398	412	454	495	511	
	Q'	nC/m	399	417	437	473	532	582	613	
	I	A	113	119	124	130	132	133	135	
	r_c	mm	1.44	1.42	1.44	1.85	3.52	5.96	7.15	
	V_T	kV	50.5	53.2	55.4	58.1	59.0	59.4	60.3	
	E_r	MV/m	4.84	5.18	5.31	4.51	2.64	1.72	1.50	

Table 7 (Concluded)

Parameters for 2.305 mm Diameter BeCu Wire

Test Voltage	Parameter		Time in ns 50	100	150	200	250	300	350
-70 kV	Z_m	ohms	391	394	438	491	507	516	520
	Q'	nC/m	410	491	580	694	739	759	767
	I	A	118	141	150	160	165	166	167
	r_c	mm	1.27	1.34	2.79	5.68	6.84	7.55	7.88
	V_T	kV	52.7	63.0	67.1	71.5	73.7	74.2	74.6
	E_r	MV/m	5.65	6.43	3.65	2.15	1.90	1.76	1.71
-80 kV	Z_m	ohms	410	455	474	478	487	505	500
	Q'	nC/m	475	645	771	825	853	874	894
	I	A	130	160	184	195	198	196	202
	r_c	mm	1.78	3.57	4.60	4.84	5.41	6.68	6.31
	V_T	kV	58.1	71.5	82.2	87.1	88.5	87.6	90.3
	E_r	MV/m	4.64	3.16	2.94	2.99	2.76	2.30	2.48
-90 kV	Z_m	ohms	424	452	485	489	498	500	509
	Q'	nC/m	493	803	930	965	989	992	1018
	I	A	132	201	216	223	225	224	226
	r_c	mm	2.25	3.42	5.28	5.54	6.17	6.31	6.99
	V_T	kV	59.0	89.8	96.6	99.7	100	100	101
	E_r	MV/m	3.86	4.12	3.08	3.05	2.82	2.75	2.55

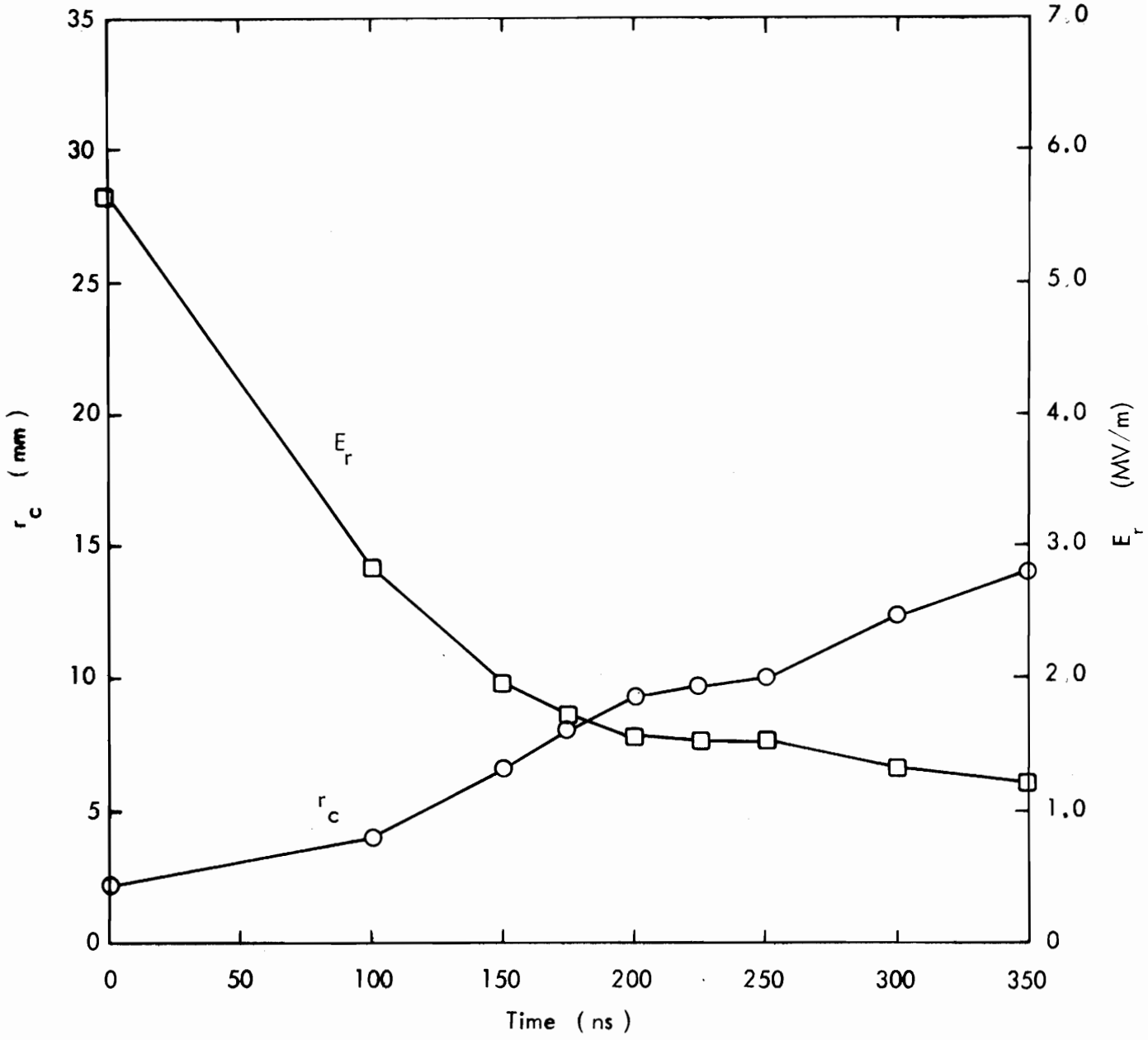

Figure 7

Model Parameters for 4.115 mm
Diameter Al wire at 80 kV

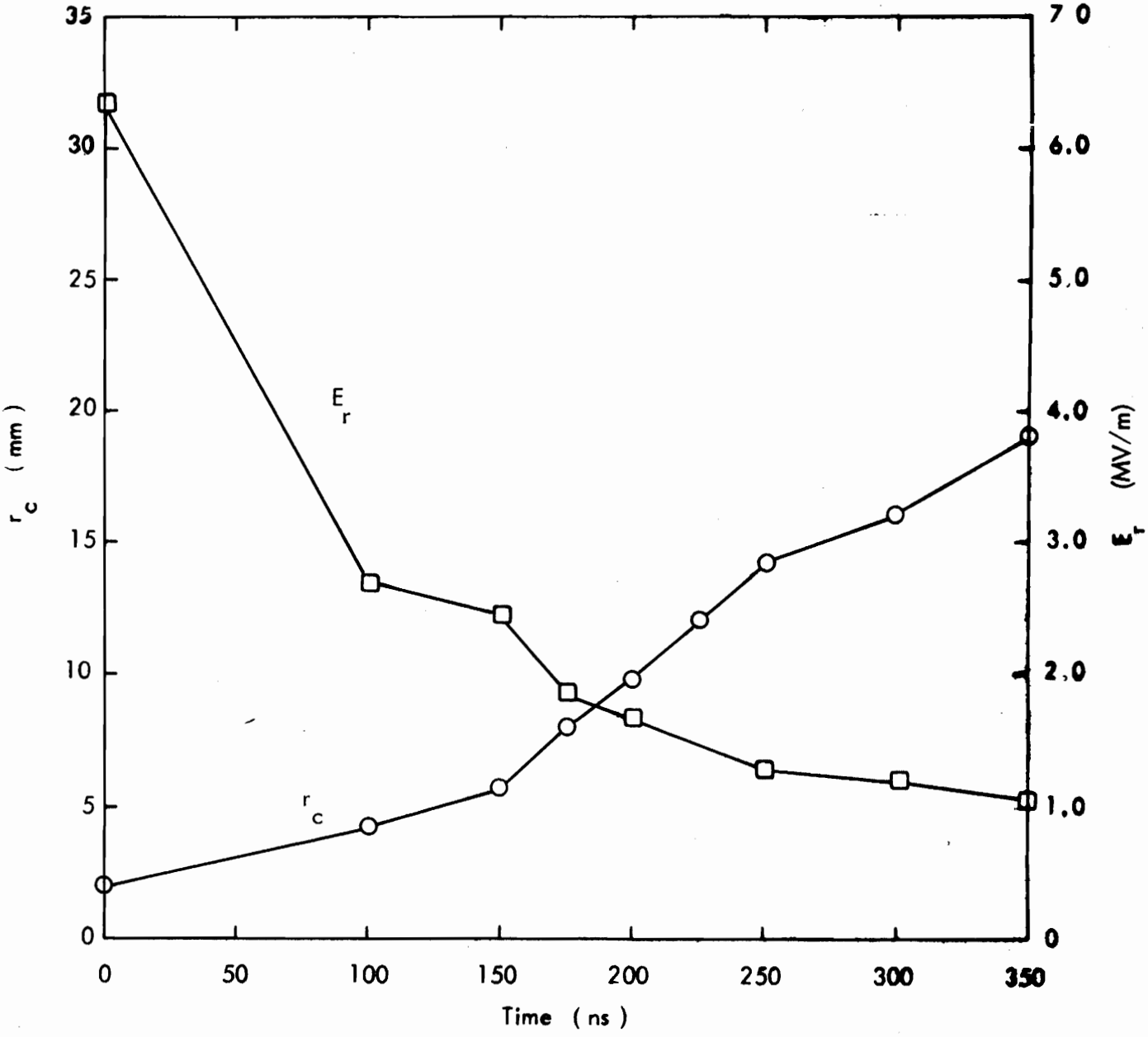

Figure 8

Model Parameters for 4.115 mm
Diameter Al wire at 90 kV

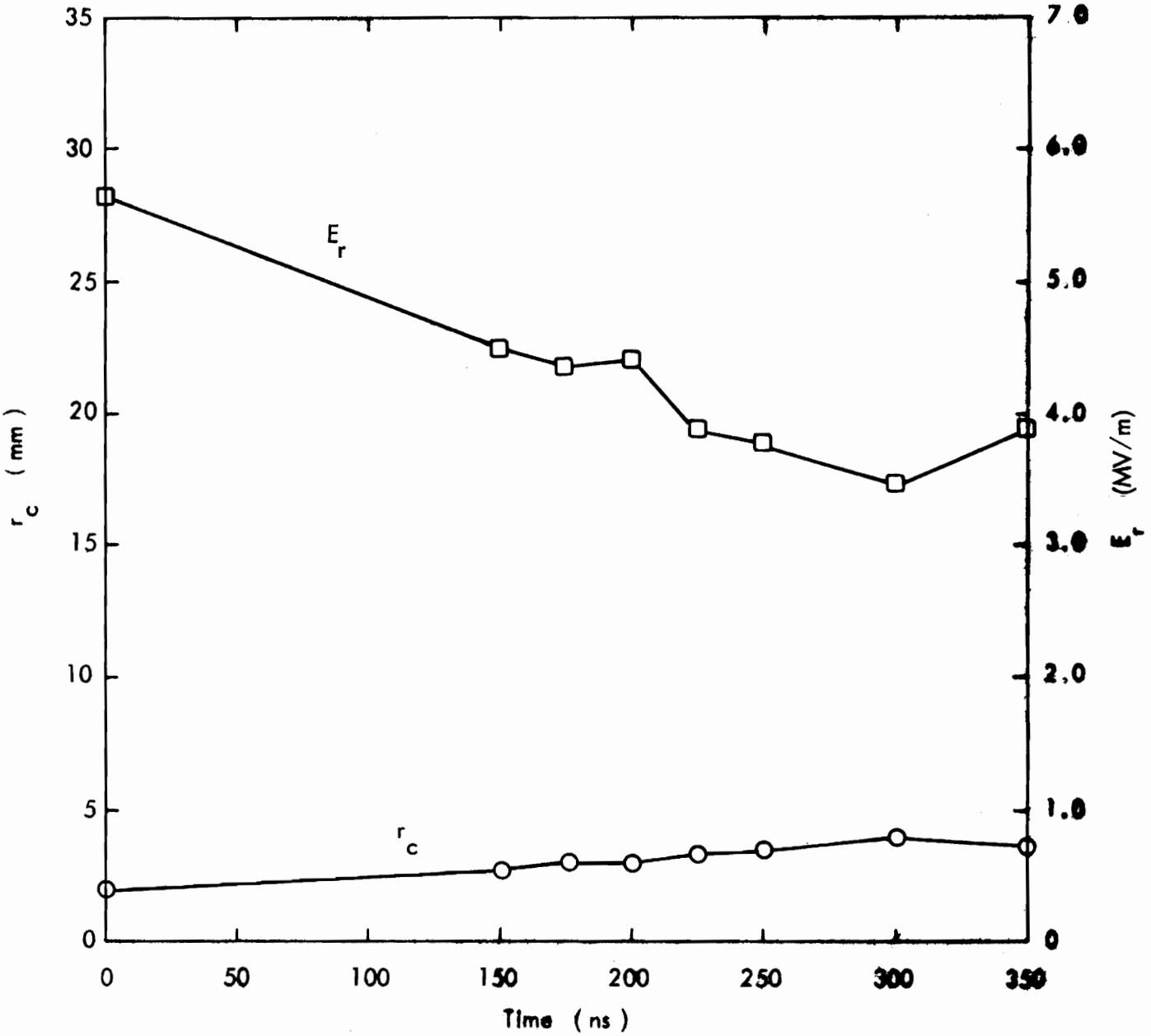

Figure 9

Model Parameters for 4.115 mm
Diameter Al wire at -80 kV

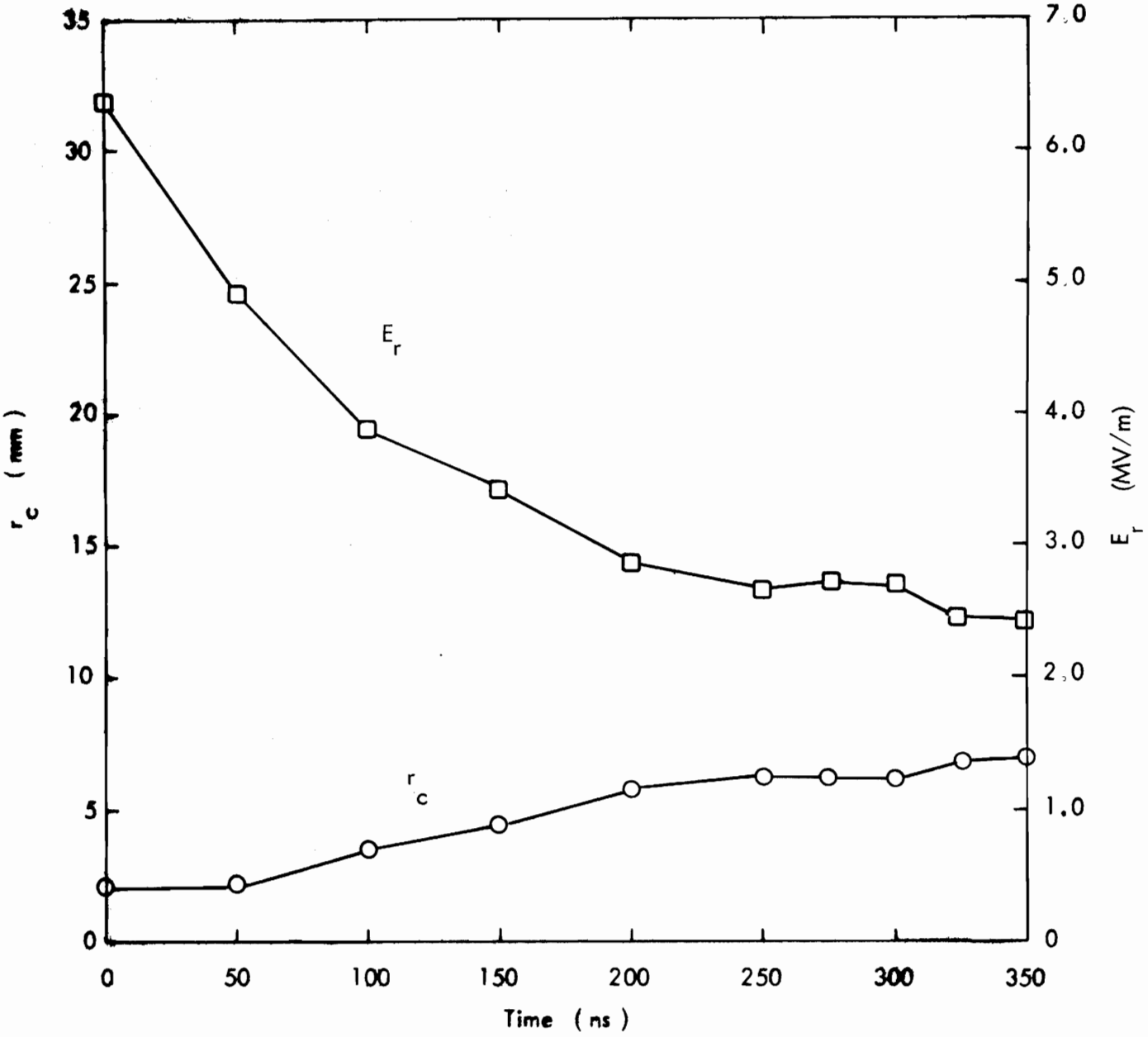

Figure 10

Model Parameters for 4.115 mm
Diameter Al wire at -90 kV

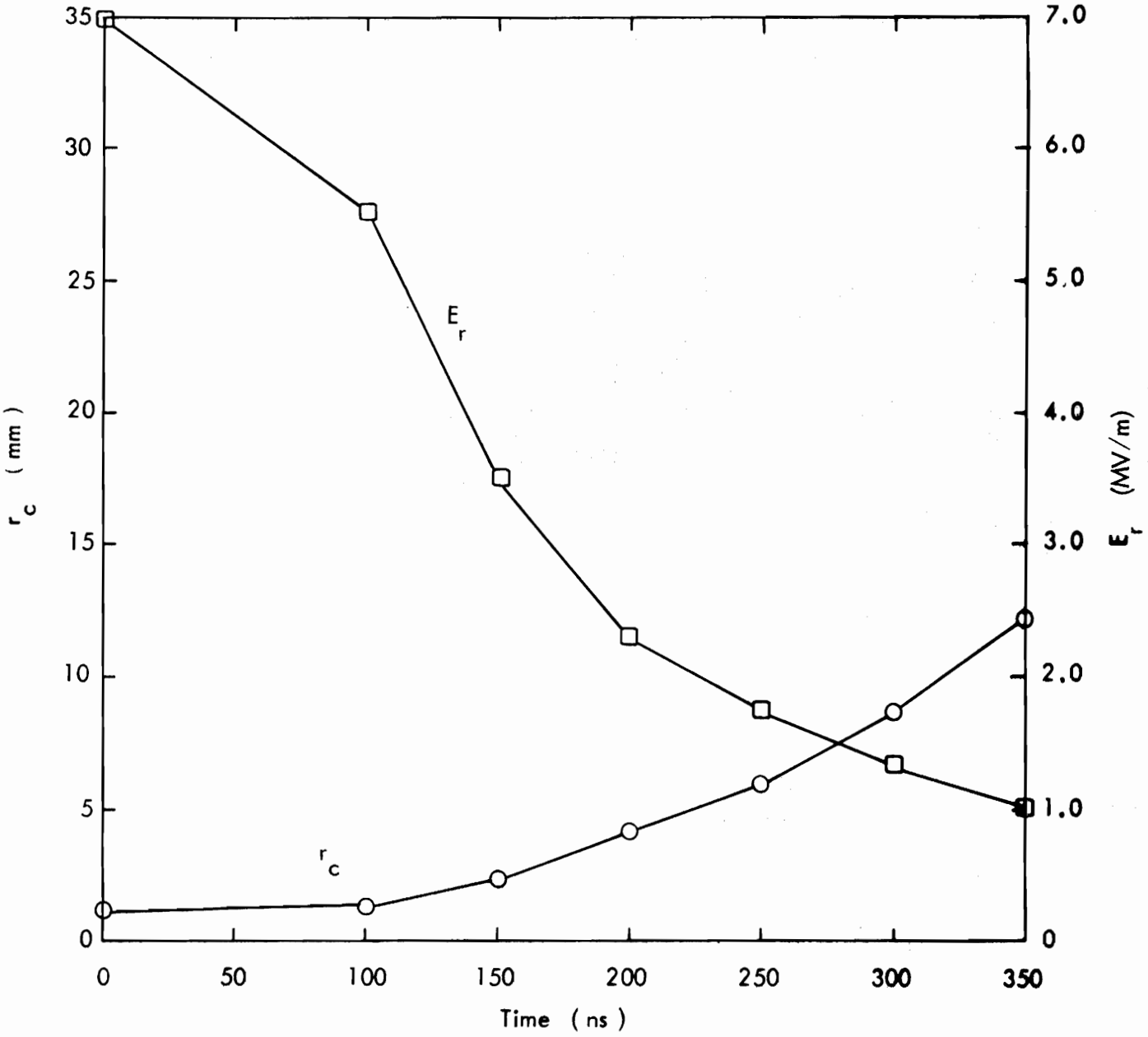

Figure 11

Model Parameters for 2.305 mm
Diameter BeCu wire at 60 kV

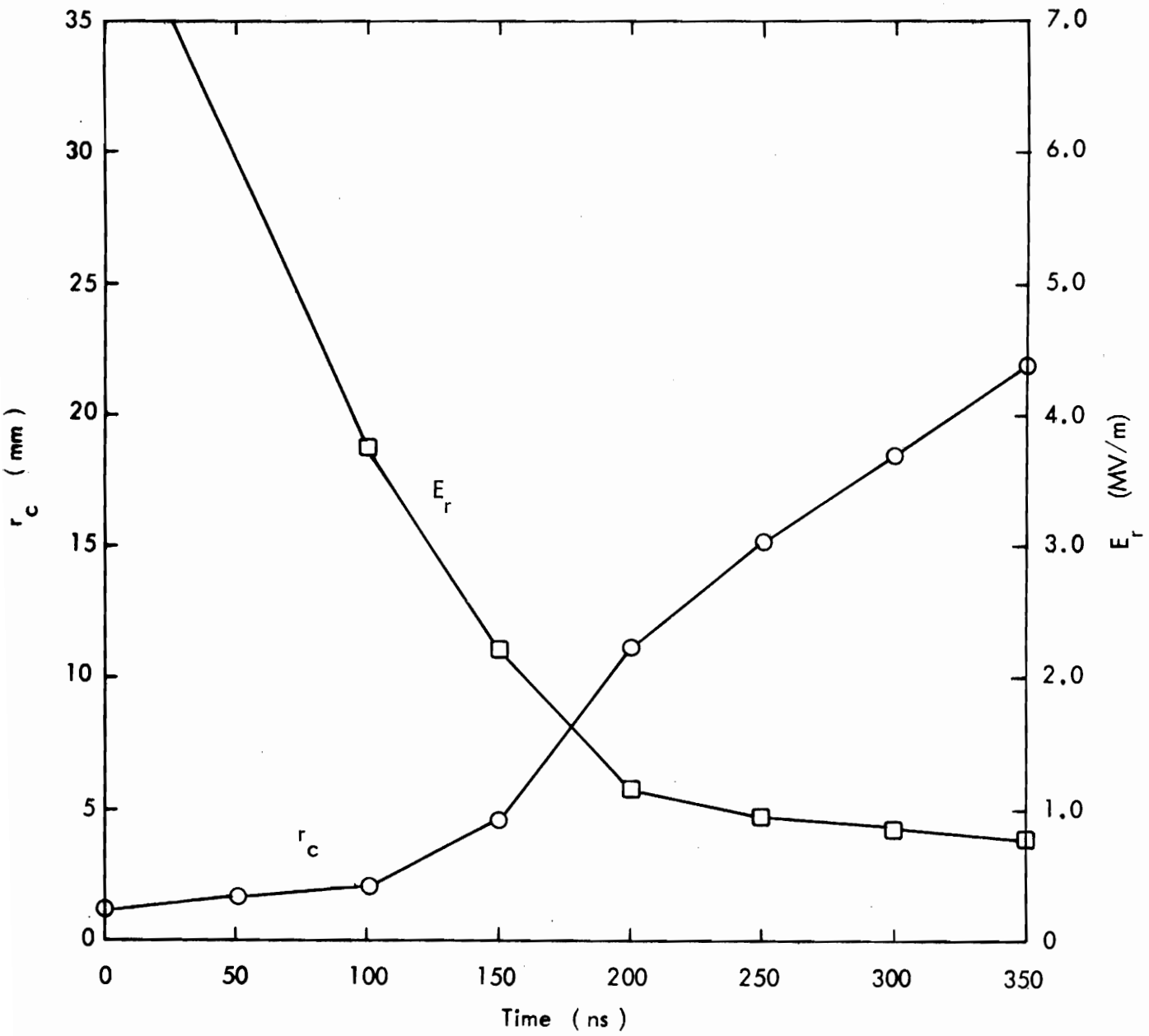

Figure 12

Model Parameters for 2.305 mm
Diameter BeCu wire at 70 kV

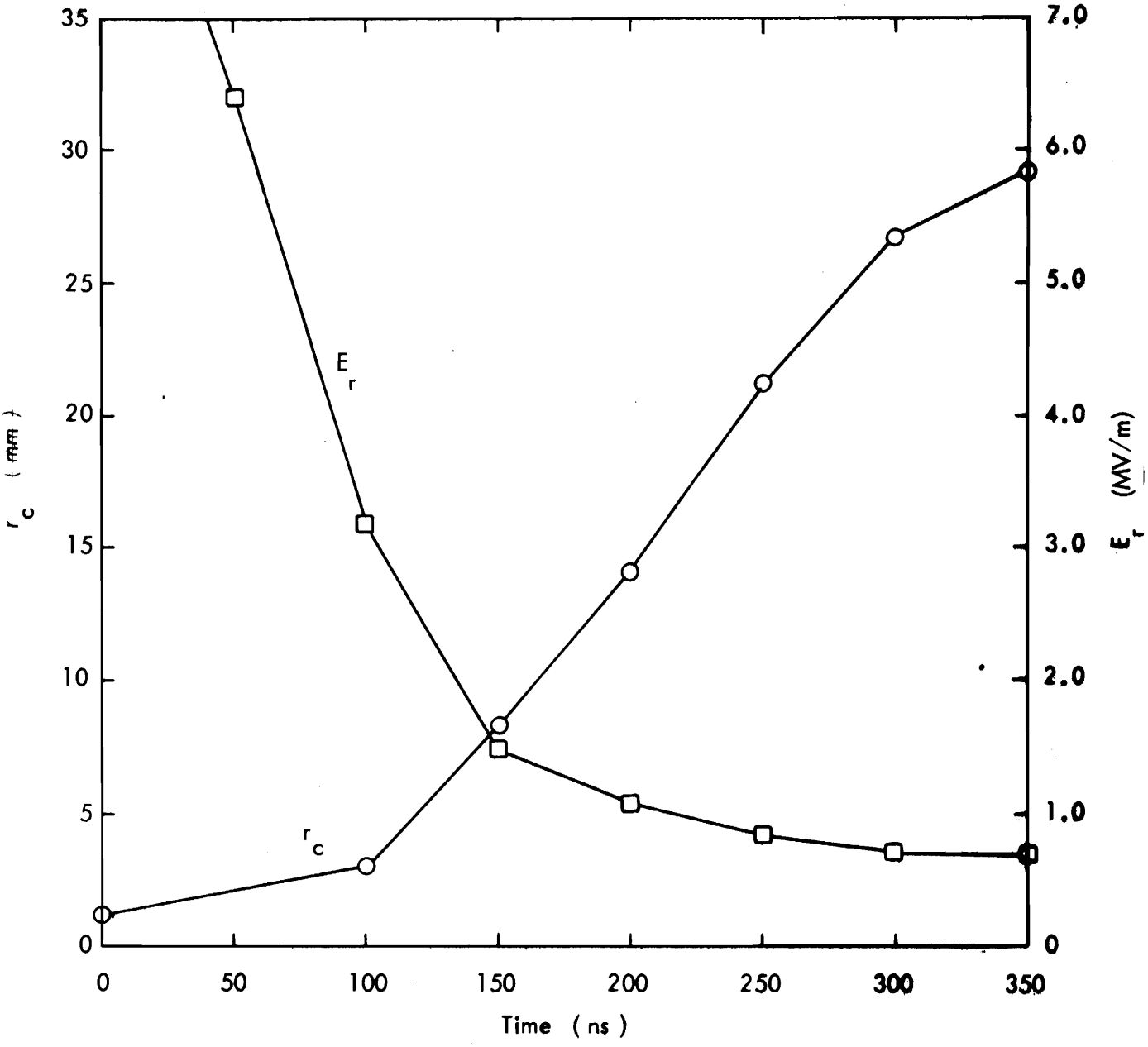

Figure 13

Model Parameters for 2.305 mm
Diameter BeCu wire at 80 kV

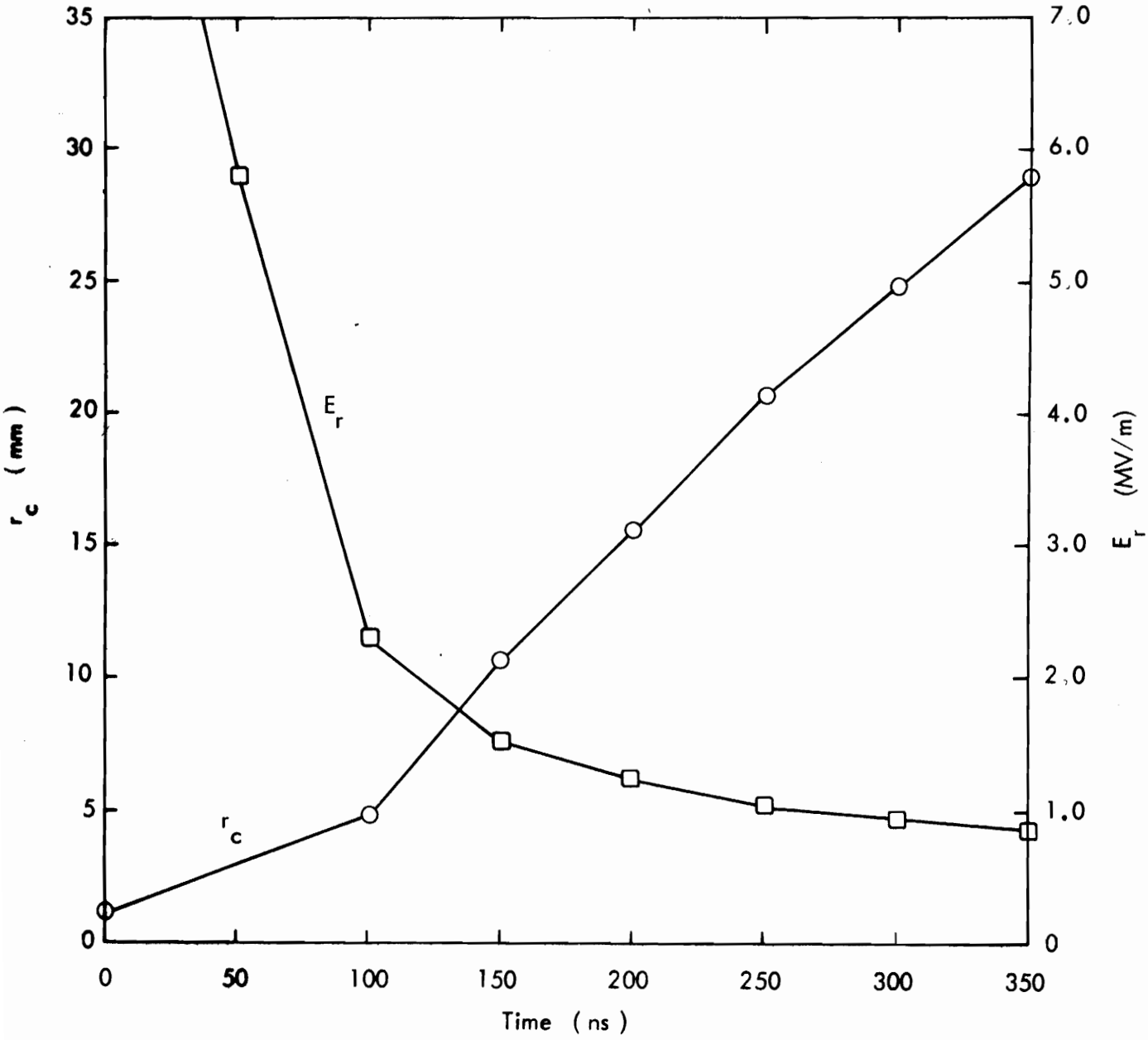

Figure 14

Model Parameters for 2.305 mm
Diameter BeCu wire at 90 kV

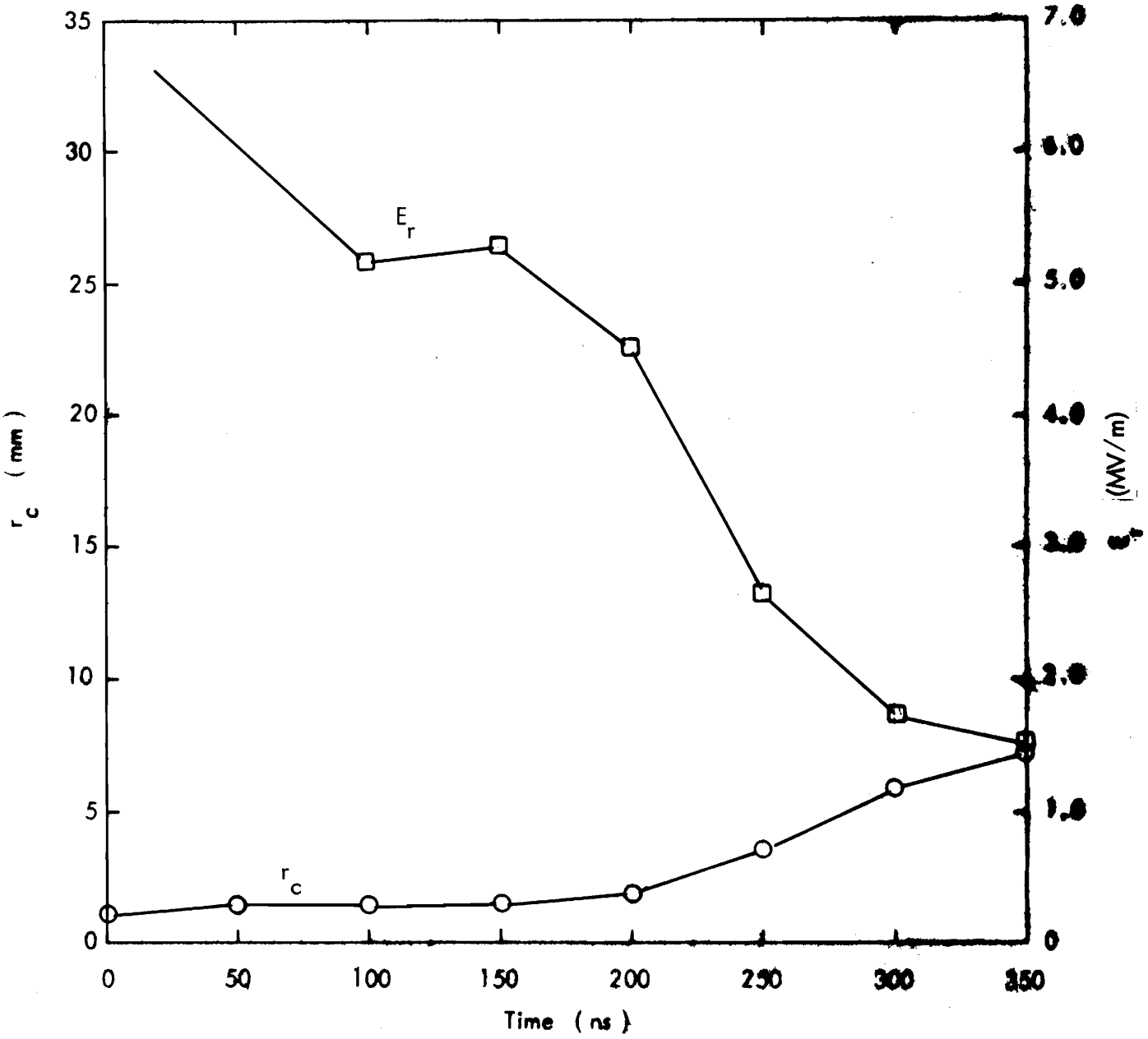

Figure 15

Model Parameters for 2.305 mm
Diameter BeCu wire at -60 kV

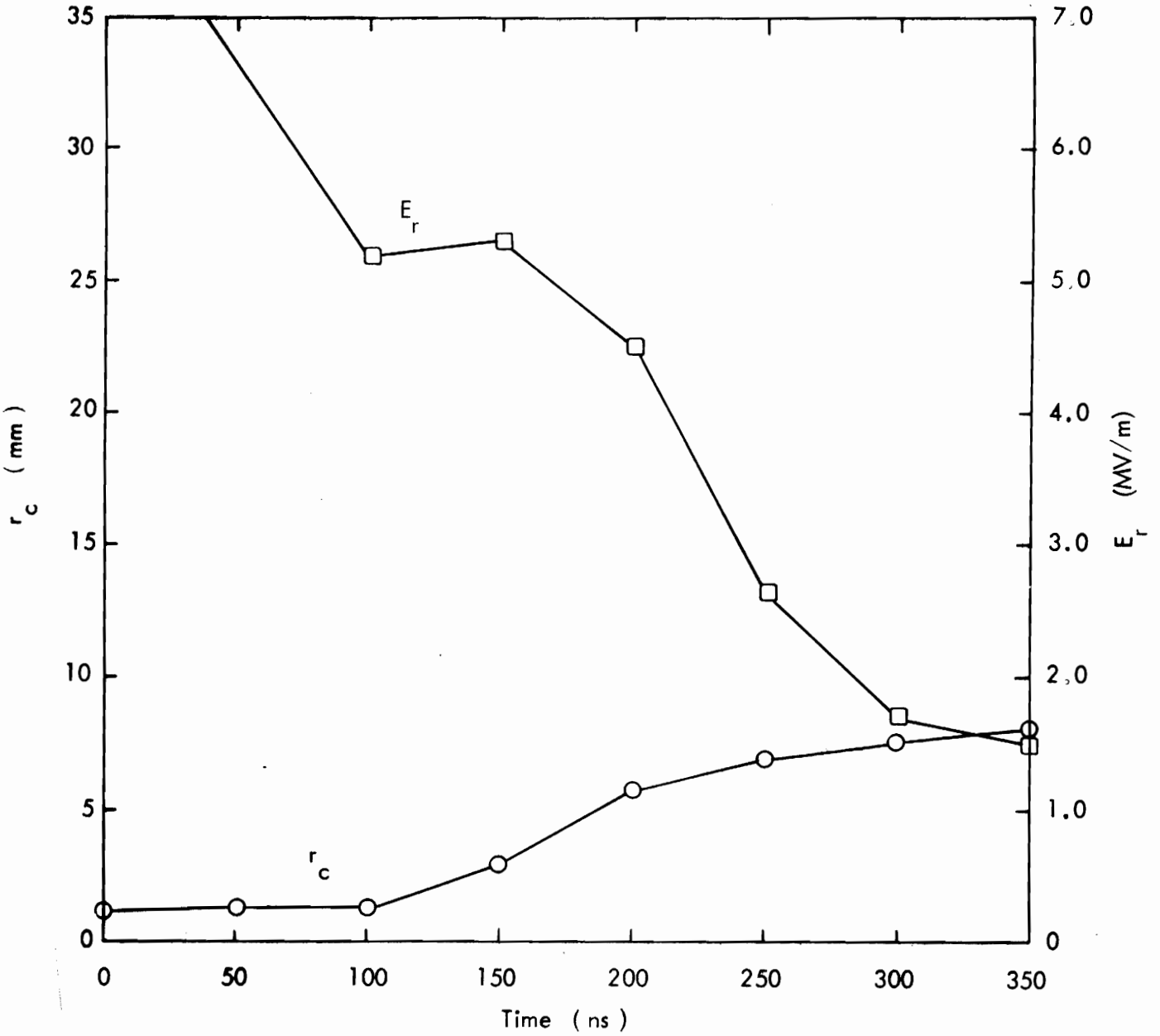

Figure 16

Model Parameters for 2.305 mm Diameter BeCu wire at -70 kV

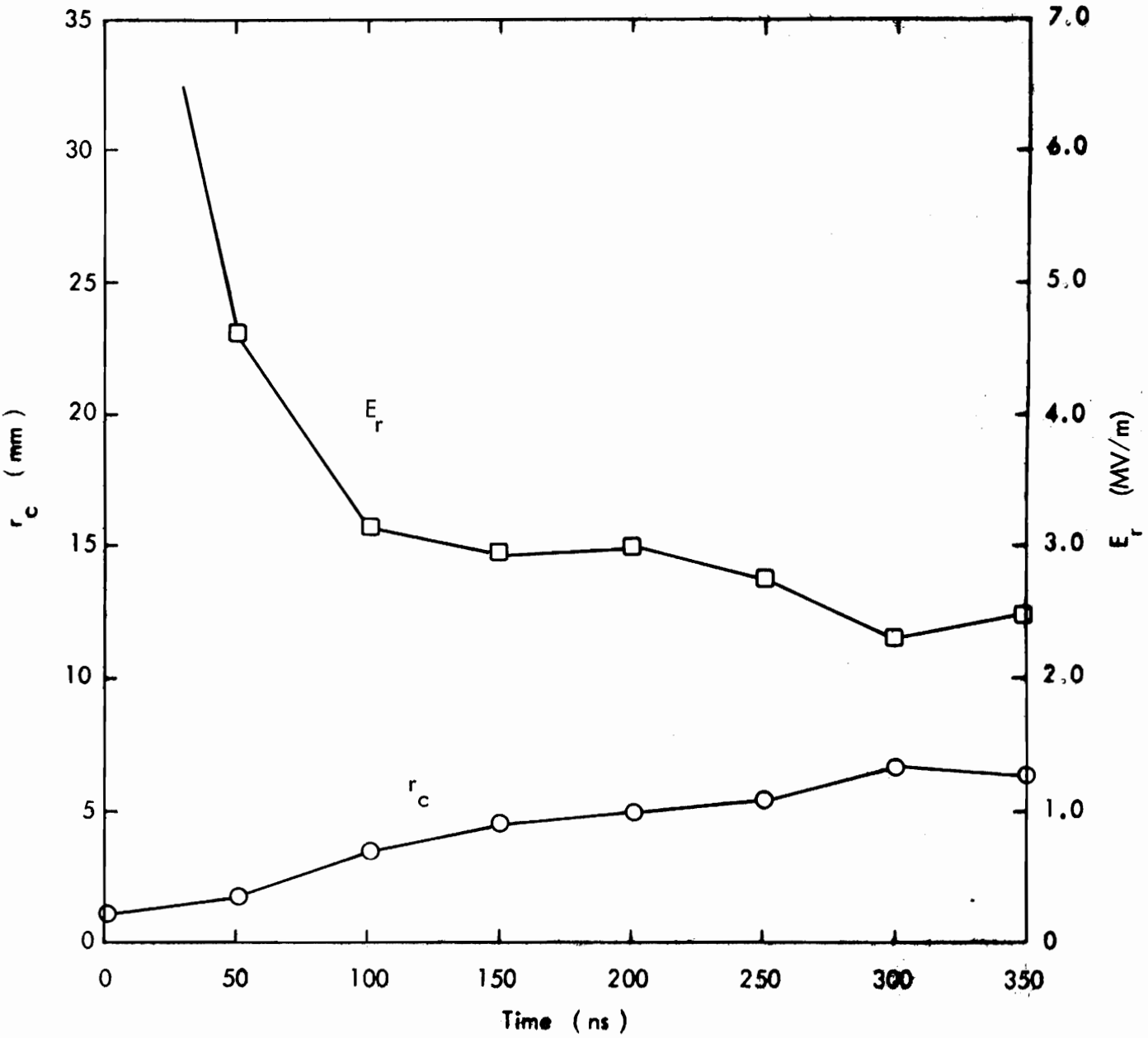

Figure 17

Model Parameters for 2.305 mm
Diameter BeCu wire at -80 kV

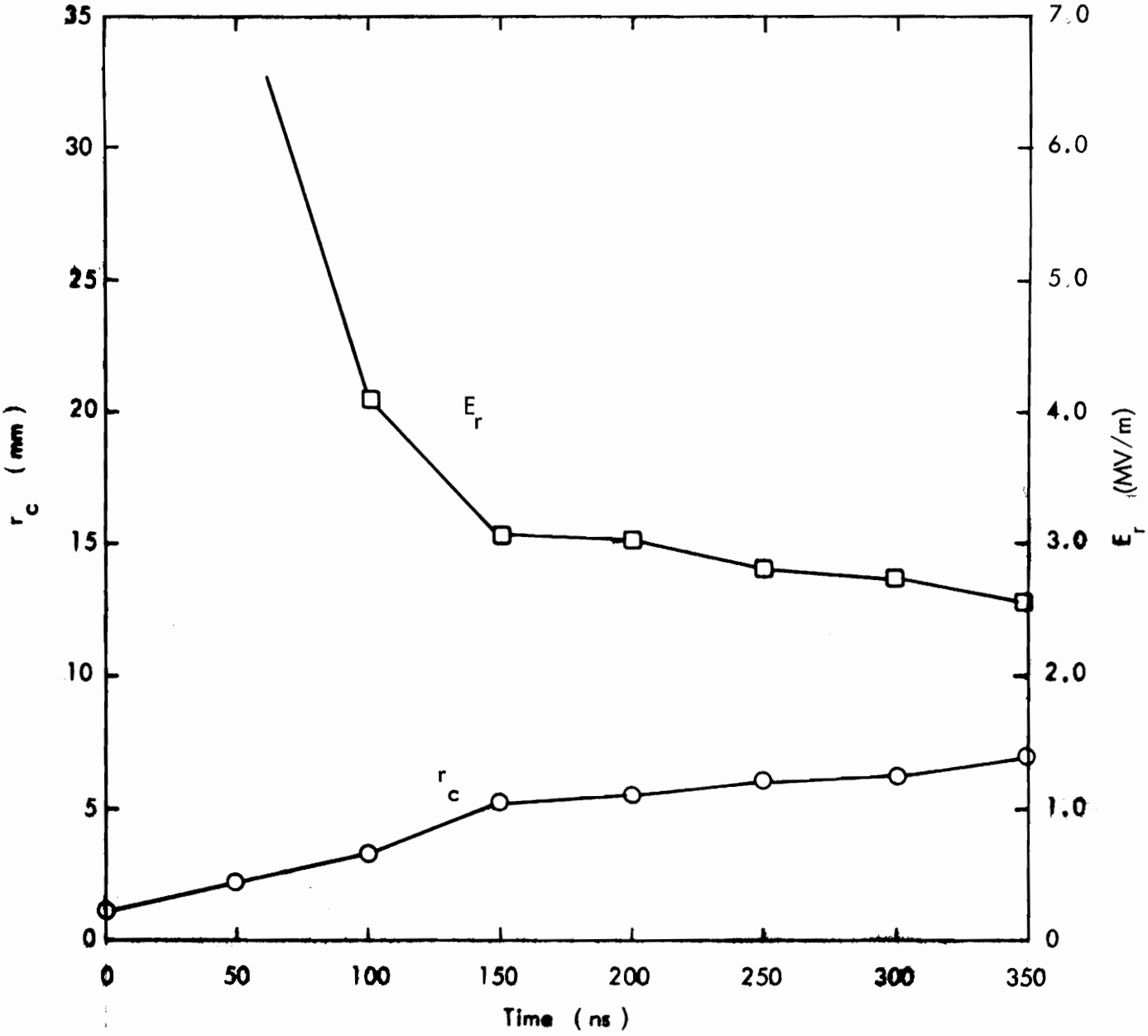

Figure 18

Model Parameters for 2.305 mm
Diameter BeCu wire at -90 kV

SECTION V
DISCUSSION AND CONCLUSIONS

A cursory review of the raw data and overall experience acquired throughout the test program indicates that the recorded signals were affected by a number of factors. Test conductor type, measuring station location, nominal voltage level and voltage polarity were the parameters of interest and could be well controlled. However, other variables such as atmospheric conditions near the test conductor and ambient temperature in the pulser building and instrumentation trailer could not be well controlled (ambient temperature variation is noted because of possible effects on pulser output voltage and sensitivity of signal measuring instrumentation). An important issue is whether changes in the uncontrolled variables corrupt or mask effects due to systematic variation of the test parameters of interest. Resolution of this issue really depends on the degree of corona effect under evaluation. For example, there are subtle differences in raw data for the copper and aluminum antenna wires. These differences are more likely due to changes in atmospheric conditions and ambient temperature than they are due to the different types of conducting material.

Subject to the caveat noted above, some conclusions can be drawn from the total assembly of raw data, corrected data, and calculated corona model and transmission line parameters:

(1) The dynamic corona threshold is very high compared to the expected static breakdown field which is about 2.63 MV/m for the 1857m altitude at which the testing was performed. Table 8 is a summary of test conditions which bracket the onset of corona and provide an indication of dynamic corona threshold for a 350 ns excitation pulse.

(2) Raw data for the copper antenna wire, aluminum antenna wire and bare aluminum wire are fairly similar. This implies that conductor diameter rather than conductivity or surface smoothness is the important factor.

Table 8

Test Conditions for Onset of Corona

Conductor Type	Maximum Test Voltage for No Corona Effects (kV)	Minimum Test Voltage for Apparent Corona* (kV)	Threshold Radial Electric Field (MV/m)
Cu tube	± 90	-	$3.13 < E_{rt}$
Cu antenna wire	± 60	± 70	$4.28 < E_{rt} < 5.00$
Al antenna wire	± 60	± 70	$4.28 < E_{rt} < 5.00$
Bare Al wire	± 60	± 70	$4.24 < E_{rt} < 4.94$
BeCu wire	± 40	± 50	$4.65 < E_{rt} < 5.82$

* The indication of corona onset is when the impedance measured at the ground plane deviates from the expected free-space value by more than the experimental uncertainty. Normally, corona is first apparent at the measuring station nearest to the pulser.

(3) The primary corona radius parameter, r_c, and the closely related radial electric field parameter begin to change radically at about $\pm$ 80 kV and $\pm$ 60 kV for the Al wire and BeCu wire, respectively. Corona effects are generally less severe for a negative pulse than for the same amplitude positive pulse.

(4) All of the model parameters continue to vary as a function of time for the entire 350 ns observation interval. Moreover, there is in general no clear indication that the parameters are approaching asymptotic values.

(5) In many cases, the radial electric field calculated from the corona model decreases to less than the static breakdown field. This indicates that the simple model tends to overestimate the radius of corona effects.

(6) The data correction procedure tends to smooth out some of the irregularities apparent in the raw data. Nevertheless, there are still some abrupt changes in the plotted data because the model parameters are so sensitive to experimental data.

Throughout this report, the emphasis has been on presentation rather than interpretation of test data. The corona radius model is recognized as a first order approximation that is subject to refinement and improvement. It is hoped that interested parties can use the data presented herein to develop and evaluate the corona radius or alternate models of the corona phenomenon.

APPENDIX A
RAW TEST DATA

This appendix is a compilation of raw test data for several conductor types and operating voltages. There are two features of these data that are to be noted in order to prevent possible confusion. First of all, the sharp decrease in the magnitude of recorded voltages at about 350 ns is simply a characteristic of the high-voltage pulser. This pulser uses a charged coaxial line which has a 50-ohm characteristic impedance and a 350 ns electrical length. Second, even though each of the test conductors was properly terminated, there was a small capacitive load due primarily to the method employed to attach the test conductor to the end support. The time interval from the leading edge of a recorded signal to the observed irregularity is simply the reflection arrival time for that particular measuring station. The terminology used in the data sheets is as defined in Table A1.

Table A1

Definition of Data Sheet Terminology

Term	Definition
NR	Not recorded
Test Voltage	Voltage that would be applied to the test wire if no corona existed
CT	Copper tube
CAW	Copper antenna wire
AAW	Aluminum antenna wire
BAW	Bare aluminum wire
BCW	Beryllium copper wire
V_{BX}	Integrated output of $\dot{B}$ sensor
V_{DX}	Integrated output of $\dot{D}$ sensor
X	Denotes the relative measuring station location where X = 1 is closest to the pulser and X = 5 is nearest to the line termination
S_V	Vertical sensitivity of data record
S_H	Horizontal sensitivity or sweep speed of data record

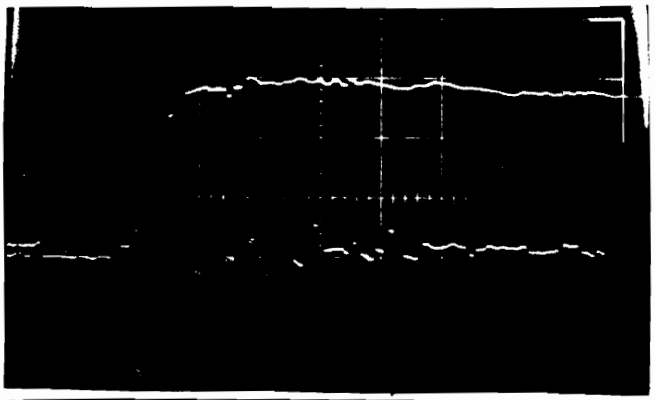

Trace: V_{B1}

S_V: 10 mV/div

S_H: 20 ns/div

Date: 1-6-78
Time: NR
Conductor Type: CT
Test Voltage: 40 kV

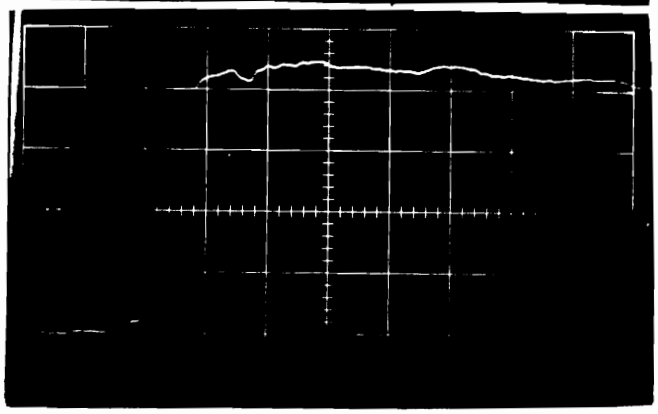

Trace: V_{D1}

S_V: 10 mV/div

S_H: 20 ns/div

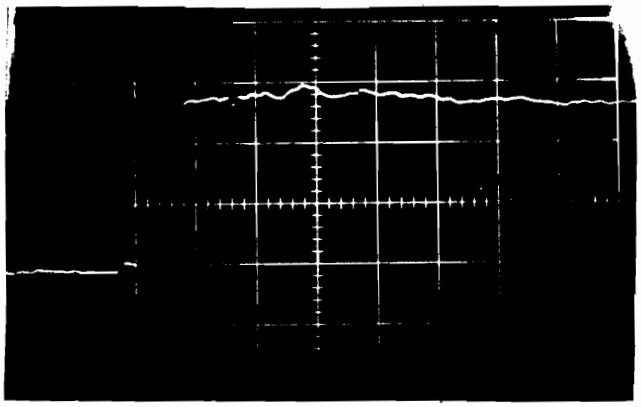

Trace: V_{B2}

S_V: 10 mV/div

S_H: 20 ns/div

Date: 1-6-78
Time: NR
Conductor Type: CT
Test Voltage: 40 kV

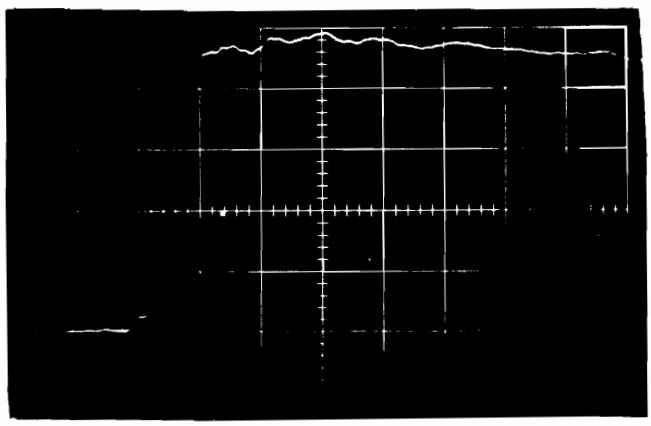

Trace: V_{D2}

S_V: 10 mV/div

S_H: 20 ns/div

Figure A1
Raw Test Data

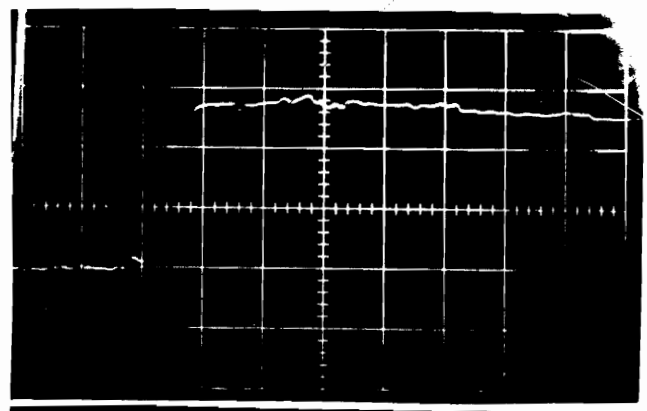

Trace: V_{B3}

S_V: 10 mV/div

S_H: 20 ns/div

Date: 1-6-78
Time: NR
Conductor Type: CT
Test Voltage: 40 kV

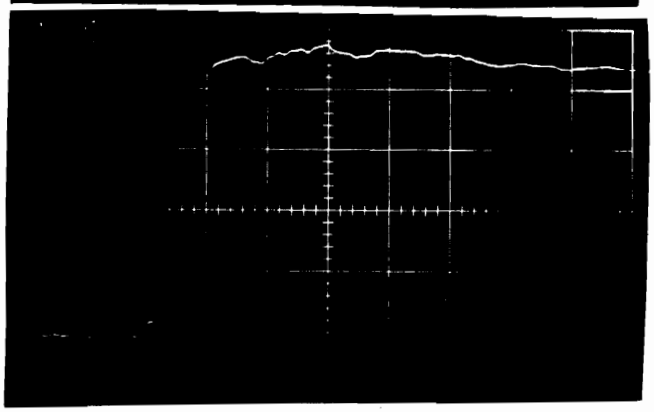

Trace: V_{D3}

S_V: 10 mV/div

S_H: 20 ns/div

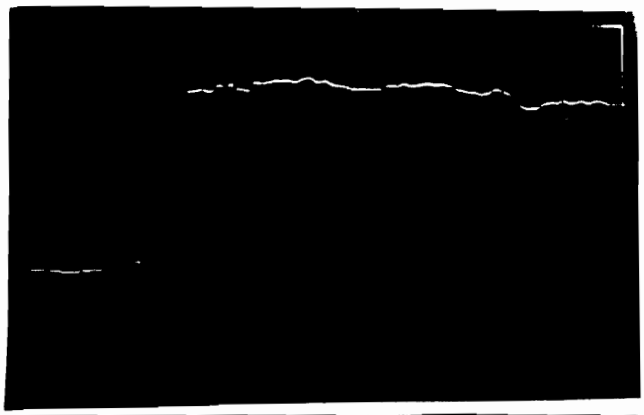

Trace: V_{B4}

S_V: 10 mV/div

S_H: 20 ns/div

Date: 1-6-78
Time: NR
Conductor Type: CT
Test Voltage: 40 kV

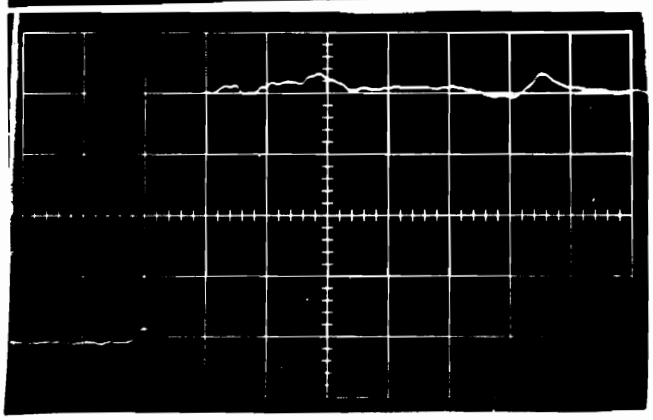

Trace: V_{D4}

S_V: 10 mV/div

S_H: 20 ns/div

Figure A2
Raw Test Data

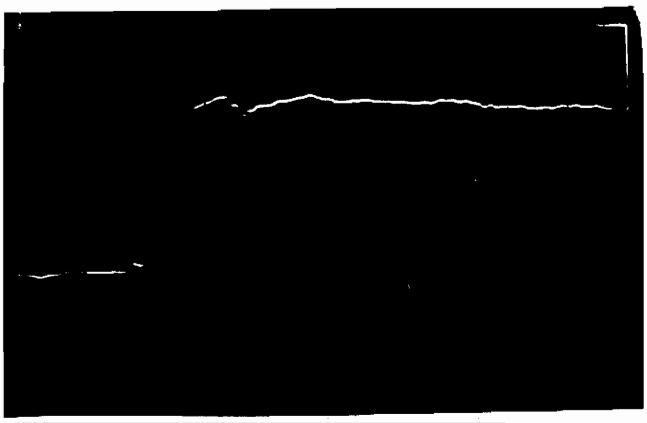

Trace: V_{B5}

S_V: 10 mV/div

S_H: 20 ns/div

Date: 1-6-78
Time: NR
Conductor Type: CT
Test Voltage: 40 kV

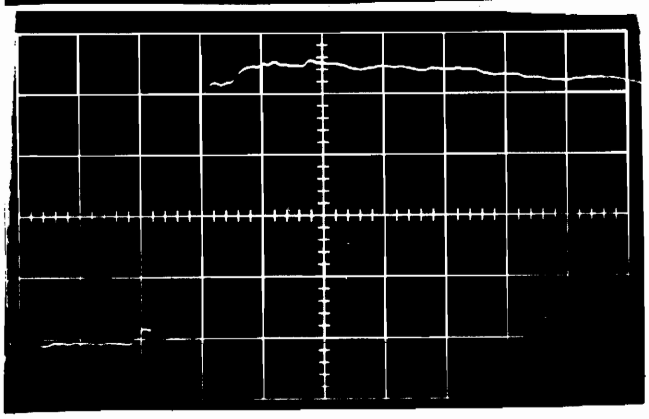

Trace: V_{D5}

S_V: 10 mV/div

S_H: 20 ns/div

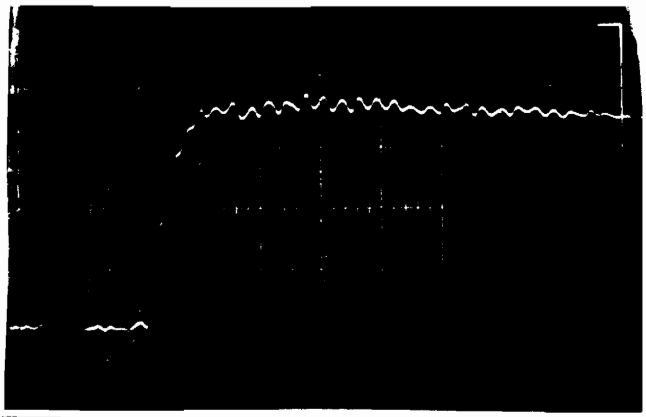

Trace: V_{B1}

S_V: 20 mV/div

S_H: 20 ns/div

Date: 3-27-78
Time: NR
Conductor Type: CT
Test Voltage: 90 kV

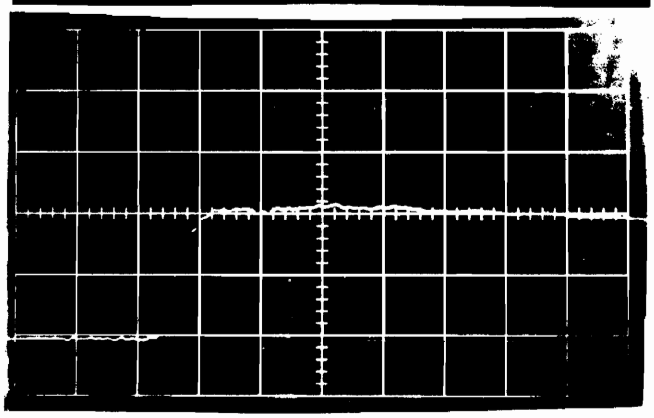

Trace: V_{D1}

S_V: 50 mV/div

S_H: 20 ns/div

Figure A3
Raw Test Data

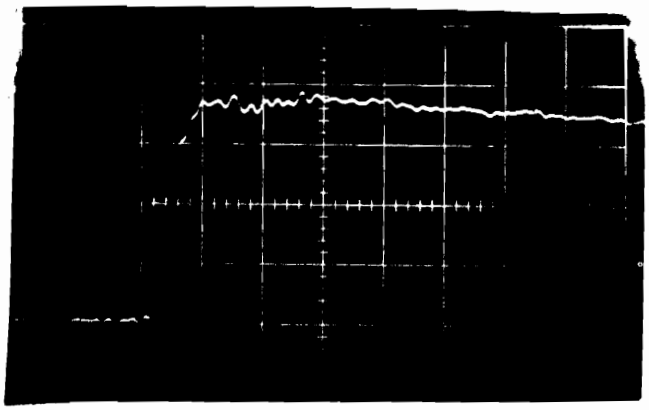

Trace: V_{B2}

S_V: 20 mV/div

S_H: 20 ns/div

Date: 3-27-78
Time: NR
Conductor Type: CT
Test Voltage: 90 kV

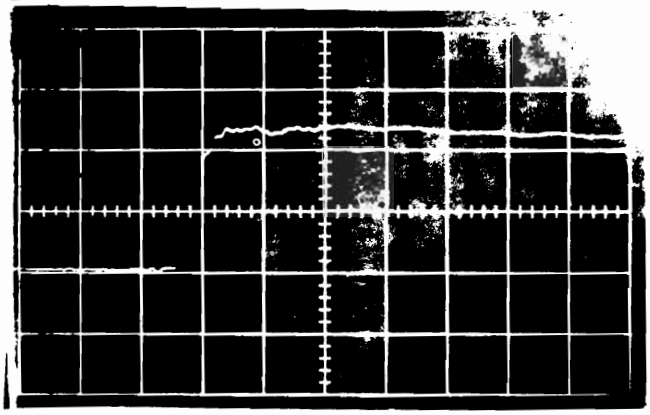

Trace: V_{D2}

S_V: 50 mV/div

S_H: 20 ns/div

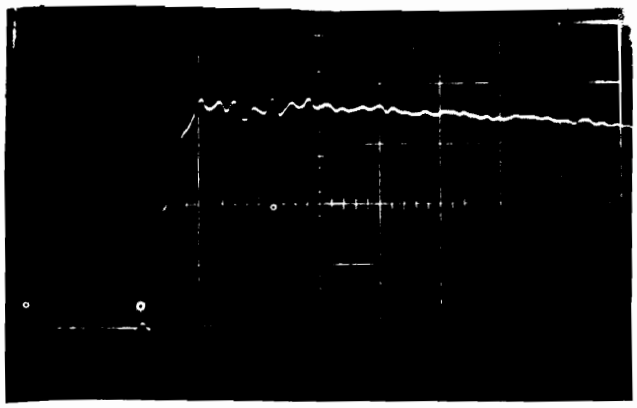

Trace: V_{B3}

S_V: 20 mV/div

S_H: 20 ns/div

Date: 3-27-78
Time: NR
Conductor Type: CT
Test Voltage: 90 kV

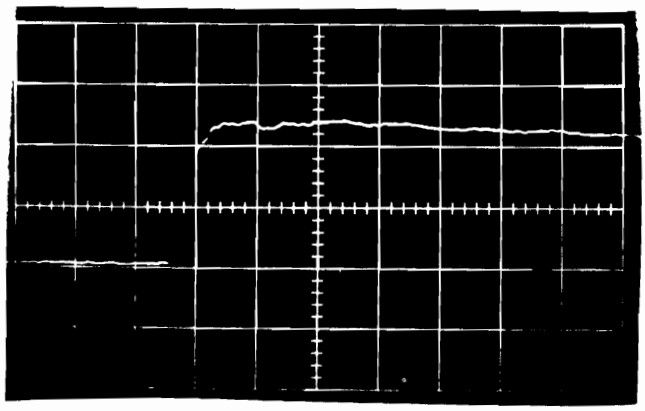

Trace: V_{D3}

S_V: 50 mV/div

S_H: 20 ns/div

Figure A4
Raw Test Data

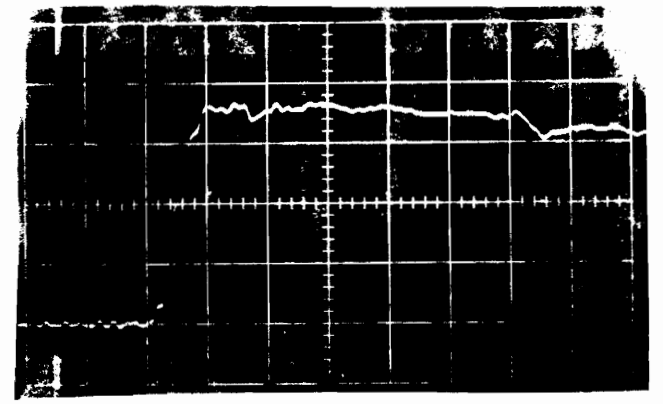

Trace: V_{B4}

S_V: 20 mV/div

S_H: 20 ns/div

Date: 3-27-78
Time: NR
Conductor Type: CT
Test Voltage: 90 kV

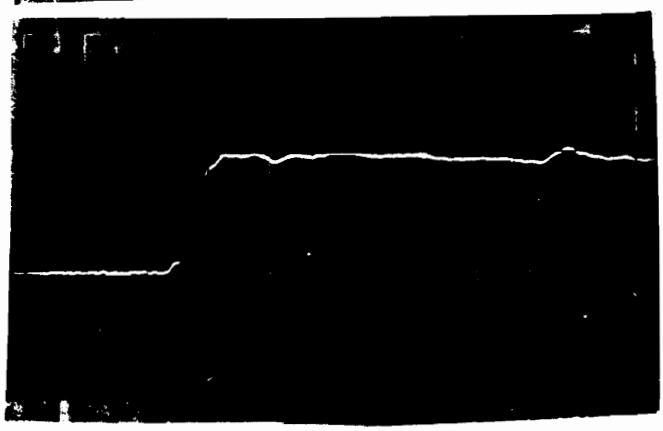

Trace: V_{D4}

S_V: 50 mV/div

S_H: 20 ns/div

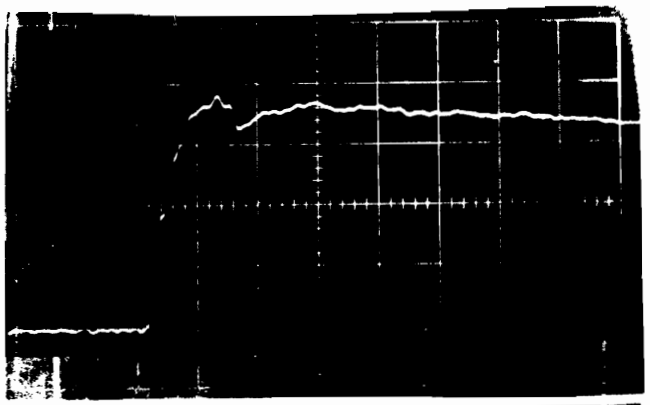

Trace: V_{B5}

S_V: 20 mV/div

S_H: 20 ns/div

Date: 3-27-78
Time: NR
Conductor Type: CT
Test Voltage: 90 kV

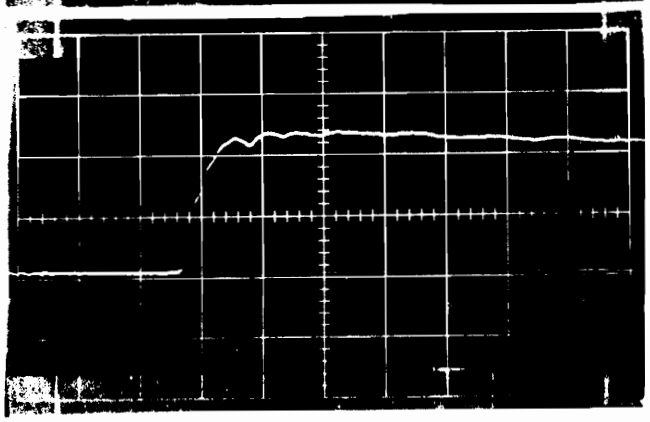

Trace: V_{D5}

S_V: 50 mV/div

S_H: 20 ns/div

Figure A5

Raw Test Data

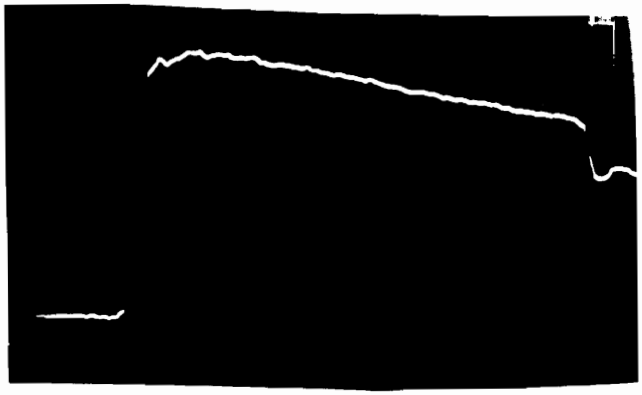

Trace: V_{B1}

S_V: 10 mV/div

S_H: 50 ns/div

Date: 7-24-78
Time: 10:45
Conductor Type: CAW
Test Voltage: 60 kV

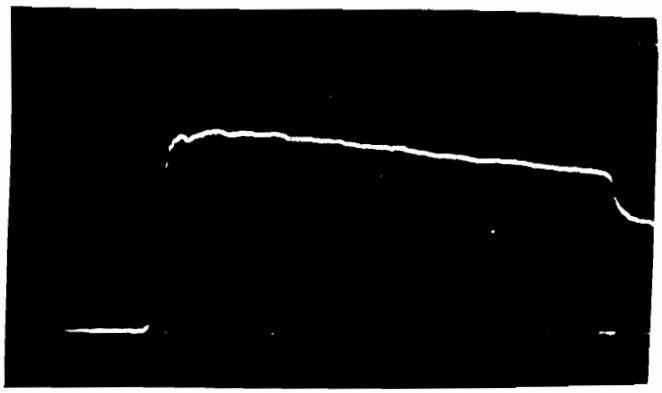

Trace: V_{D1}

S_V: 20 mV/div

S_H: 50 ns/div

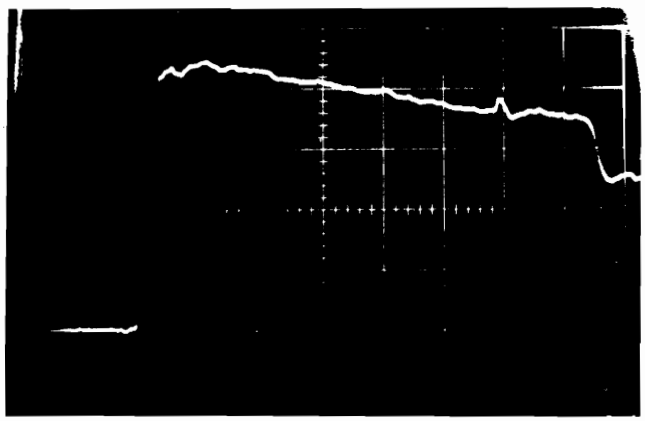

Trace: V_{B2}

S_V: 10 mV/div

S_H: 50 ns/div

Date: 7-24-78
Time: 10:40
Conductor Type: CAW
Test Voltage: 60 kV

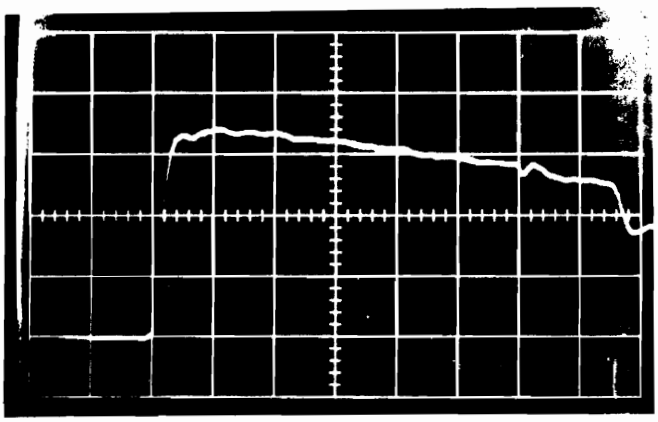

Trace: V_{D2}

S_V: 20 mV/div

S_H: 50 ns/div

Figure A6
Raw Test Data

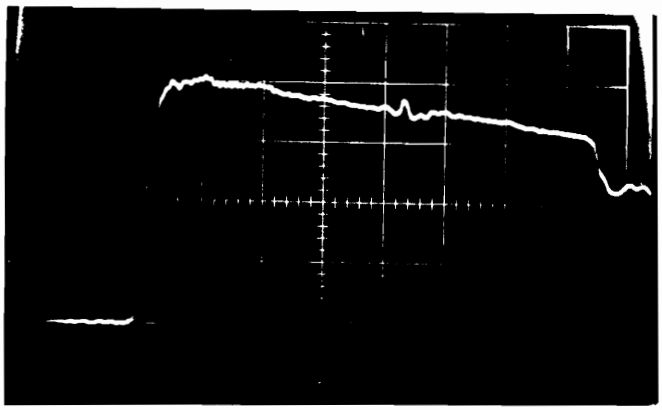

Trace: V_{B3}

S_V: 10 mV/div

S_H: 50 ns/div

Date: 7-24-78
Time: 10:35
Conductor Type: CAW
Test Voltage: 60 kV

Trace: V_{D3}

S_V: 20 mV/div

S_H: 50 ns/div

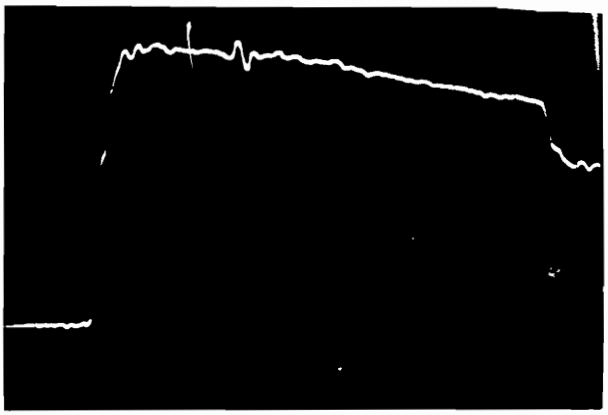

Trace: V_{B4}

S_V: 10 mV/div

S_H: 50 ns/div

Date: 7-24-78
Time: 10:30
Conductor Type: CAW
Test Voltage: 60 kV

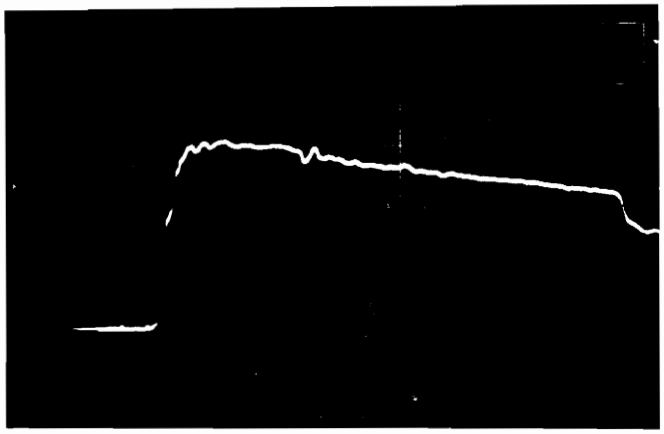

Trace: V_{D4}

S_V: 20 mV/div

S_H: 50 ns/div

Figure A7
Raw Test Data

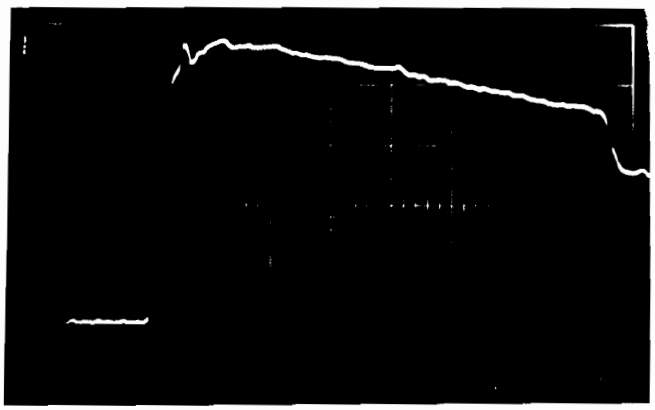

Trace: V_{B5}

S_V: 10 mV/div

S_H: 50 ns/div

Date: 7-24-78
Time: 10:20
Conductor Type: CAW
Test Voltage: 60 kV

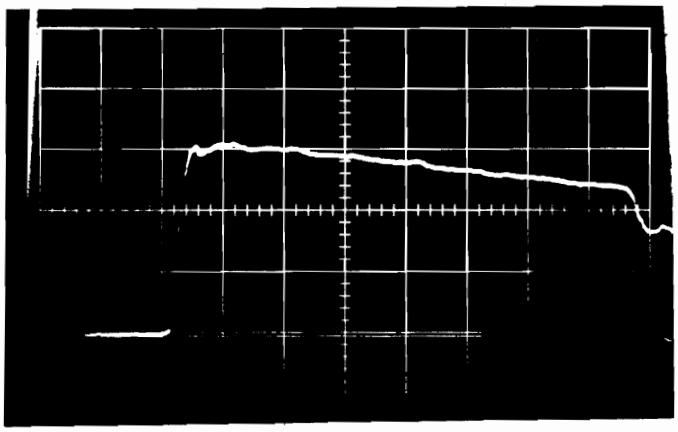

Trace: V_{D5}

S_V: 20 mV/div

S_H: 50 ns/div

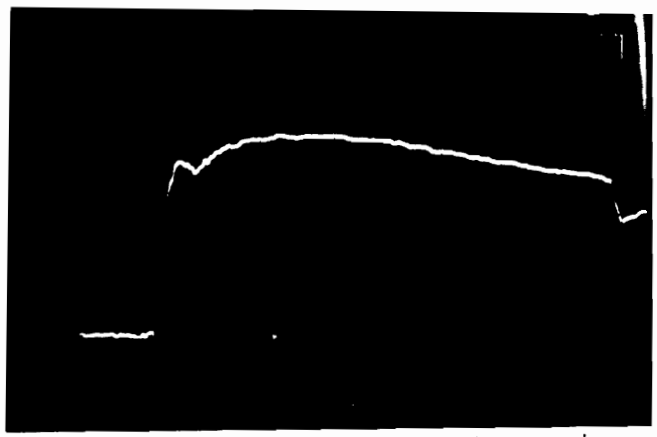

Trace: V_{B1}

S_V: 20 mV/div

S_H: 50 ns/div

Date: 7-25-78
Time: 08:40
Conductor Type: CAW
Test Voltage: 80 kV

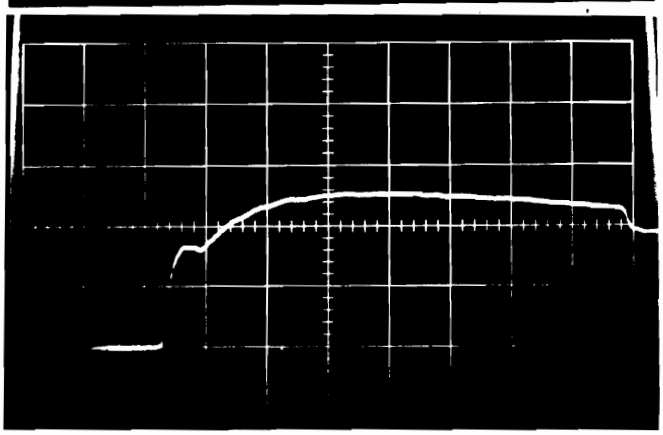

Trace: V_{D1}

S_V: 50 mV/div

S_H: 50 ns/div

Figure A8
Raw Test Data

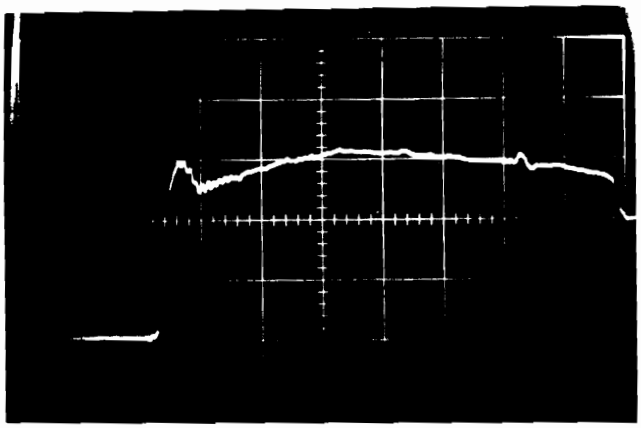

Trace: V_{B2}

S_V: 20 mV/div

S_H: 50 ns/div

Date: 7-25-78
Time: 08:50
Conductor Type: CAW
Test Voltage: 80 kV

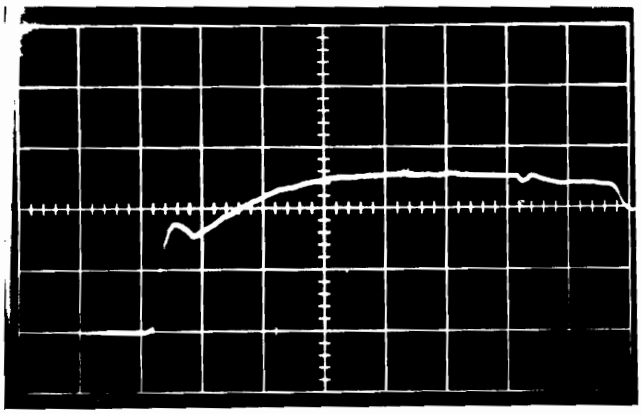

Trace: V_{D2}

S_V: 50 mV/div

S_H: 50 ns/div

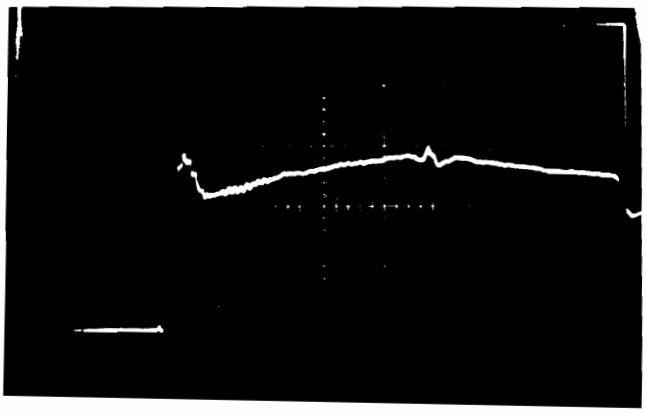

Trace: V_{B3}

S_V: 20 mV/div

S_H: 50 ns/div

Date: 7-25-78
Time: 08:48
Conductor Type: CAW
Test Voltage: 80 kV

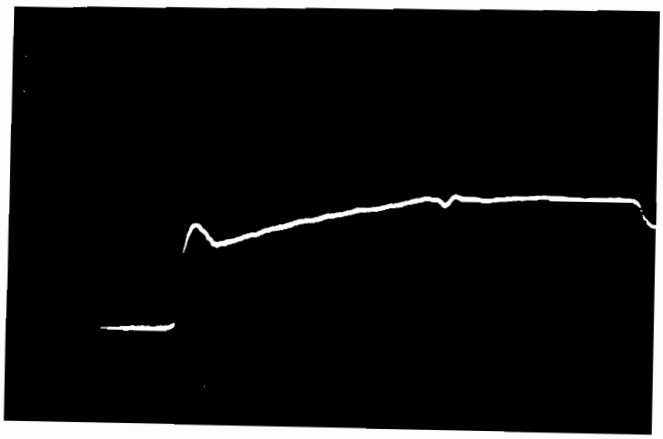

Trace: V_{D3}

S_V: 50 mV/div

S_H: 50 ns/div

Figure A9
Raw Test Data

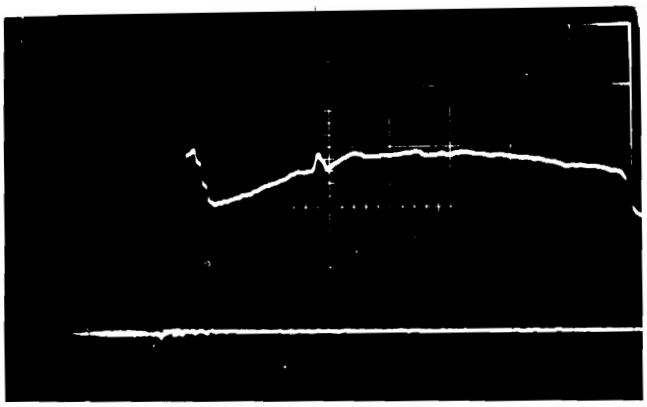

Trace: V_{B4}

S_V: 20 mV/div

S_H: 50 ns/div

Date: 7-25-78
Time: 09:02
Conductor Type: CAW
Test Voltage: 80 kV

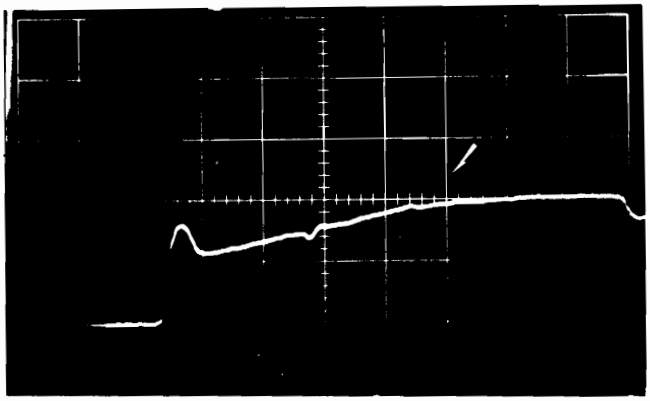

Trace: V_{D4}

S_V: 50 mV/div

S_H: 50 ns/div

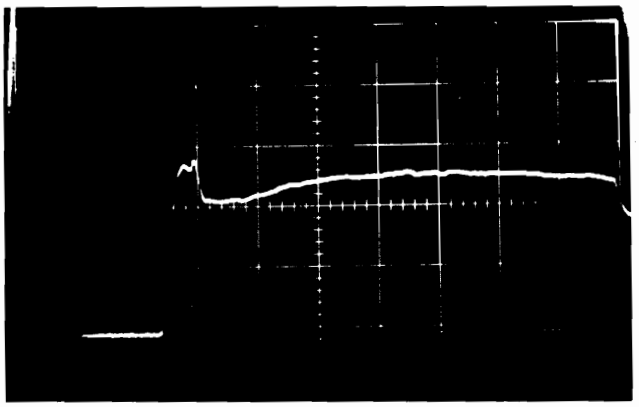

Trace: V_{B5}

S_V: 20 mV/div

S_H: 50 ns/div

Date: 7-25-78
Time: 09:08
Conductor Type: CAW
Test Voltage: 80 kV

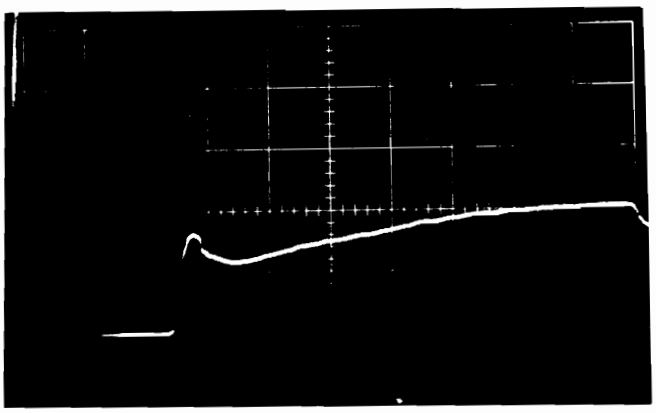

Trace: V_{D5}

S_V: 50 mV/div

S_H: 50 ns/div

Figure A10
Raw Test Data

Trace: V_{B1}

S_V: 10 mV/div

S_H: 50 ns/div

Date: 9-11-78
Time: 09:54
Conductor Type: AAW
Test Voltage: 60 kV

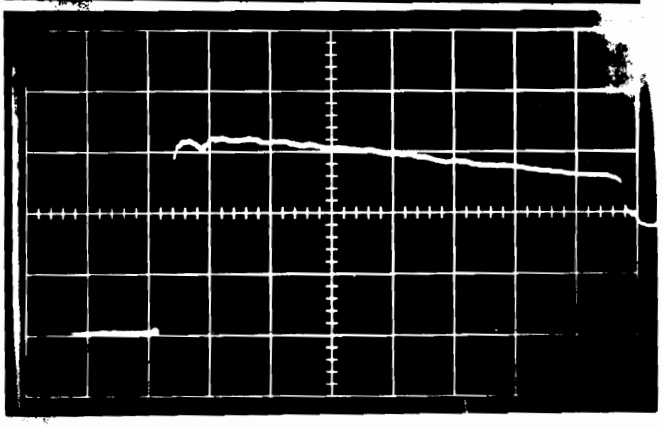

Trace: V_{D1}

S_V: 20 mV/div

S_H: 50 ns/div

Trace: V_{B2}

S_V: 10 mV/div

S_H: 50 ns/div

Date: 9-11-78
Time: 10:15
Conductor Type: AAW
Test Voltage: 60 kV

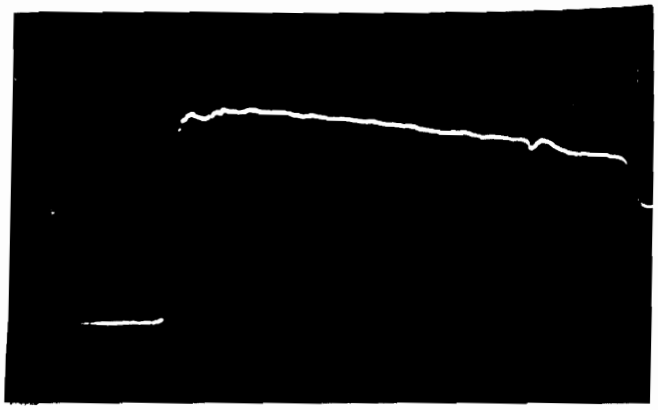

Trace: V_{D2}

S_V: 20 mV/div

S_H: 50 ns/div

Figure A11
Raw Test Data

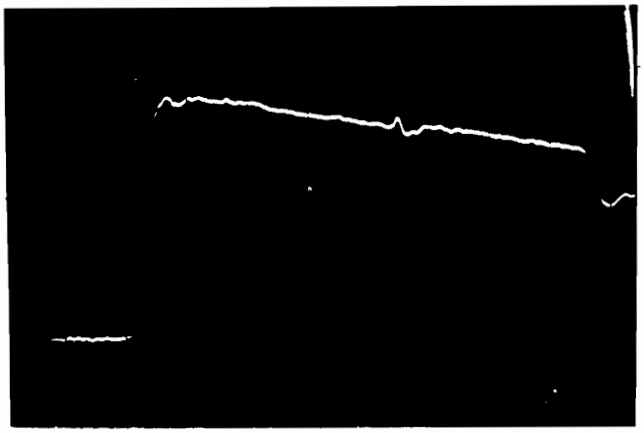

Trace: V_{B3}

S_V: 10 mV/div

S_H: 50 ns/div

Date: 9-11-78
Time: 10:02
Conductor Type: AAW
Test Voltage: 60 kV

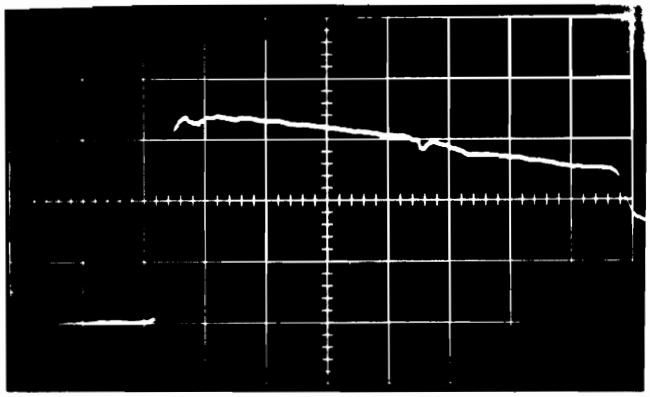

Trace: V_{D3}

S_V: 20 mV/div

S_H: 50 ns/div

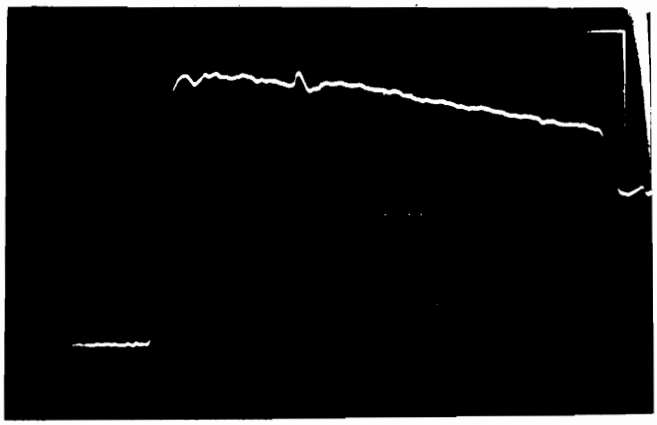

Trace: V_{B4}

S_V: 10 mV/div

S_H: 50 ns/div

Date: 9-11-78
Time: 10:06
Conductor Type: AAW
Test Voltage: 60 kV

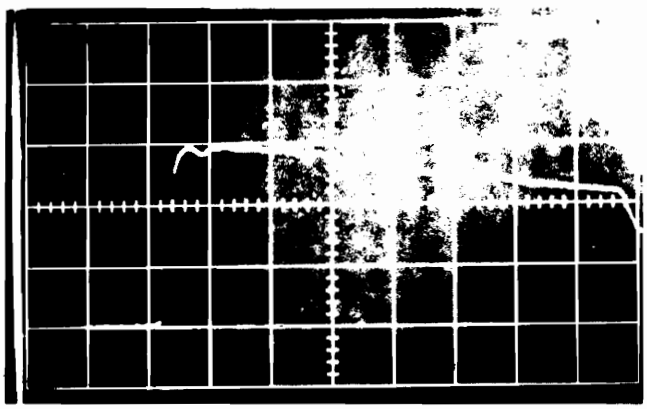

Trace: V_{D4}

S_V: 20 mV/div

S_H: 50 ns/div

Figure A12
Raw Test Data

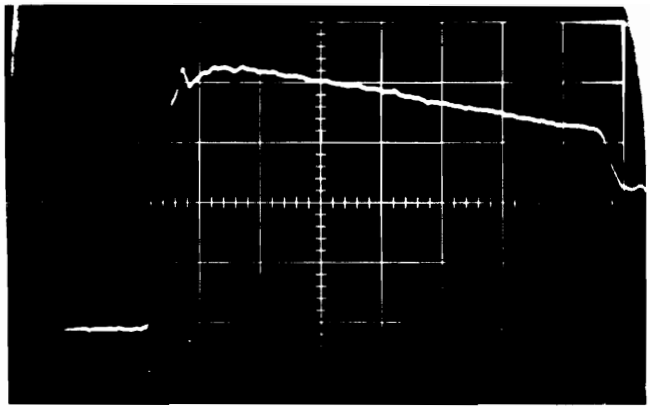

Trace: V_{B5}

S_V: 10 mV/div

S_H: 50 ns/div

Date: 9-11-78
Time: 10:11
Conductor Type: AAW
Test Voltage: 60 kV

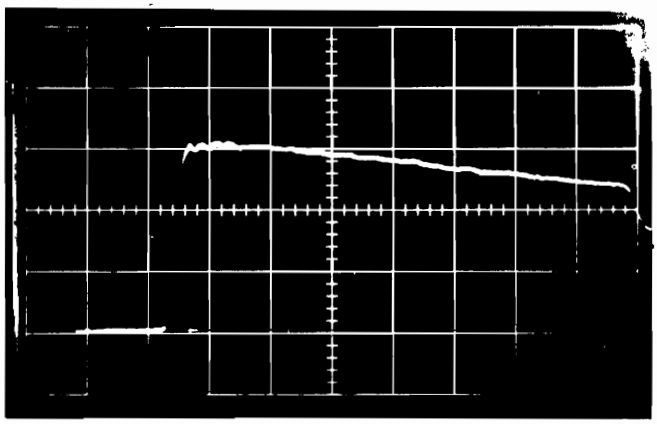

Trace: V_{D5}

S_V: 20 mV/div

S_H: 50 ns/div

Trace: V_{B1}

S_V: 20 mV/div

S_H: 50 ns/div

Date: 9-13-78
Time: 10:43
Conductor Type: AAW
Test Voltage: 80 kV

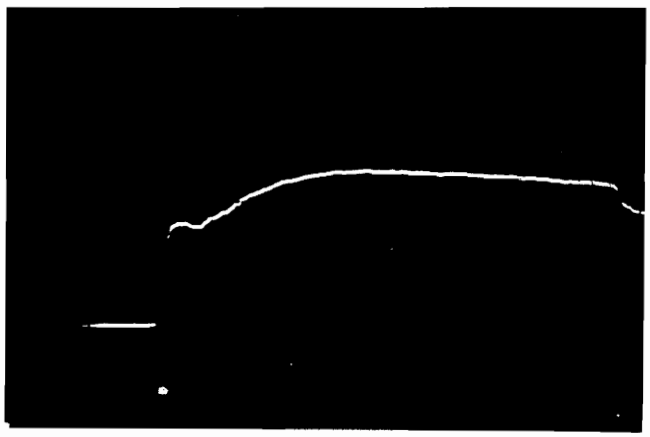

Trace: V_{D1}

S_V: 50 mV/div

S_H: 50 ns/div

Figure A13
Raw Test Data

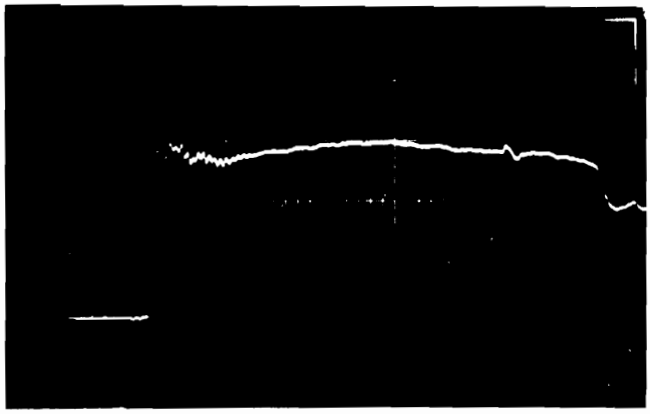

Trace: V_{B2}

S_V: 20 mV/div

S_H: 50 ns/div

Date: 9-13-78
Time: 10:06
Conductor Type: AAW
Test Voltage: 80 kV

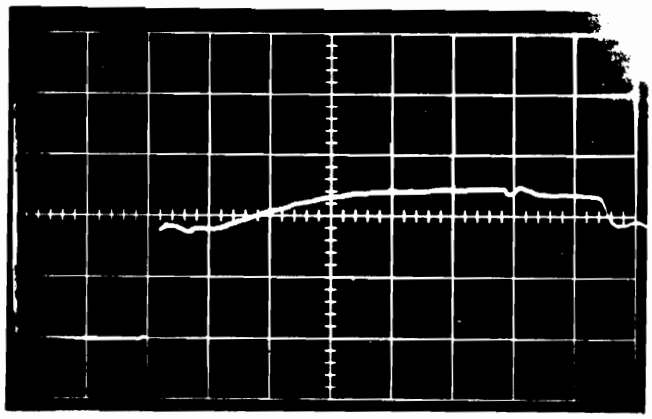

Trace: V_{D2}

S_V: 50 mV/div

S_H: 50 ns/div

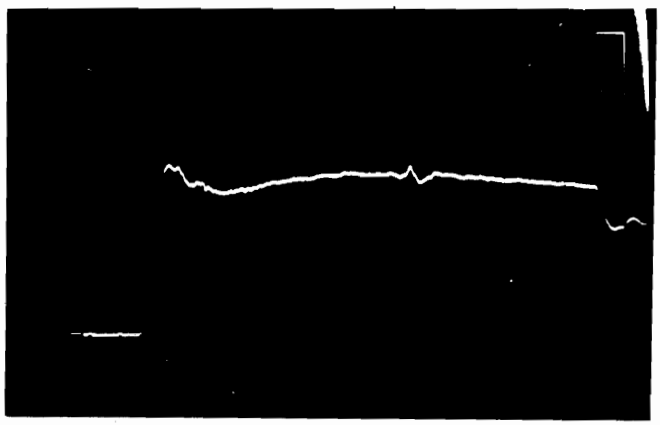

Trace: V_{B3}

S_V: 20 mV/div

S_H: 50 ns/div

Date: 9-13-78
Time: 10:35
Conductor Type: AAW
Test Voltage: 80 kV

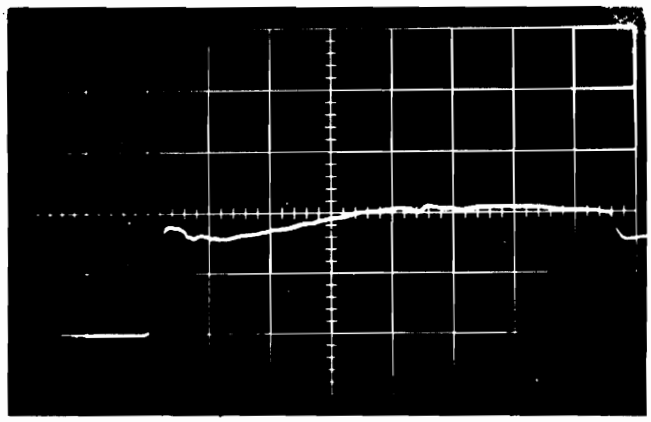

Trace: V_{D3}

S_V: 50 mV/div

S_H: 50 ns/div

Figure A14

Raw Test Data

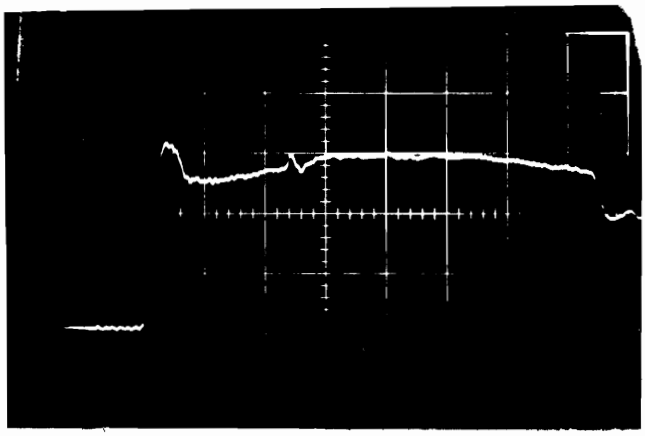

Trace: V_{B4}

S_V: 20 mV/div

S_H: 50 ns/div

Date: 9-13-78
Time: 10:16
Conductor Type: AAW
Test Voltage: 80 kV

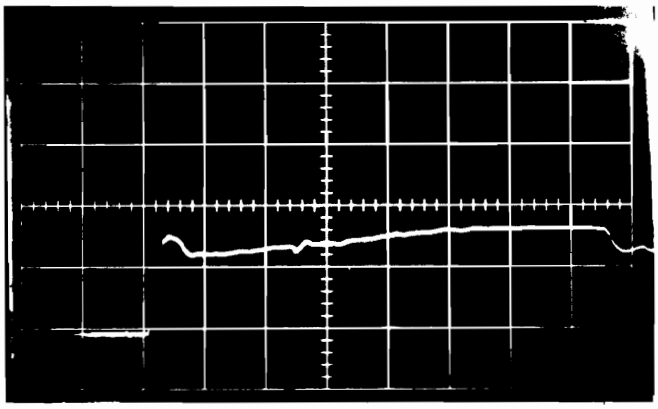

Trace: V_{D4}

S_V: 50 mV/div

S_H: 50 ns/div

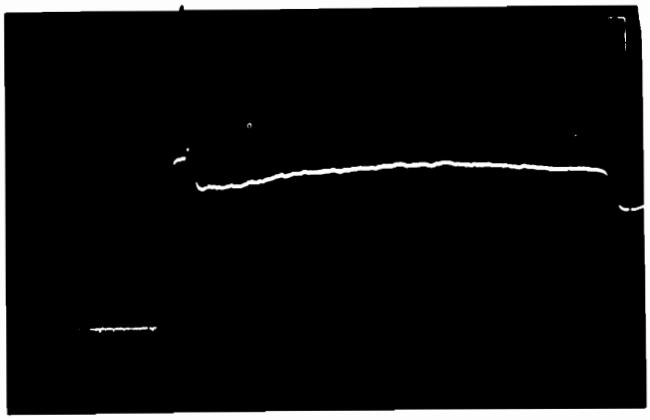

Trace: V_{B5}

S_V: 20 mV/div

S_H: 50 ns/div

Date: 9-13-78
Time: 10:51
Conductor Type: AAW
Test Voltage: 80 kV

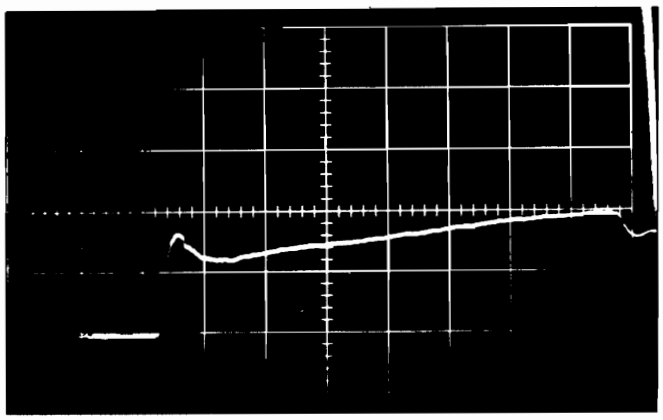

Trace: V_{D5}

S_V: 50 mV/div

S_H: 50 ns/div

Figure A15
Raw Test Data

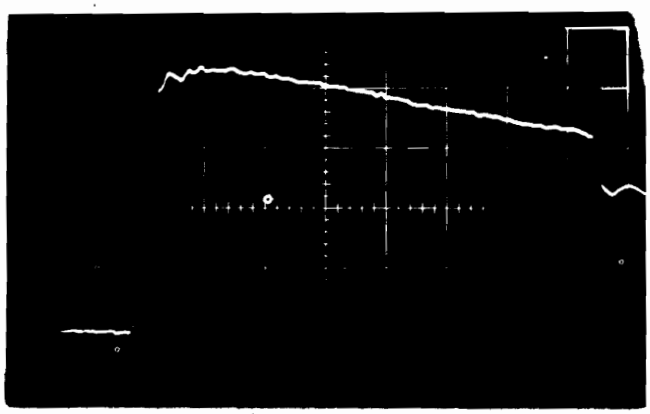

Trace: V_{B1}

S_V: 10 mV/div

S_H: 50 ns/div

Date: 9-19-78
Time: 13:43
Conductor Type: BAW
Test Voltage: 60 kV

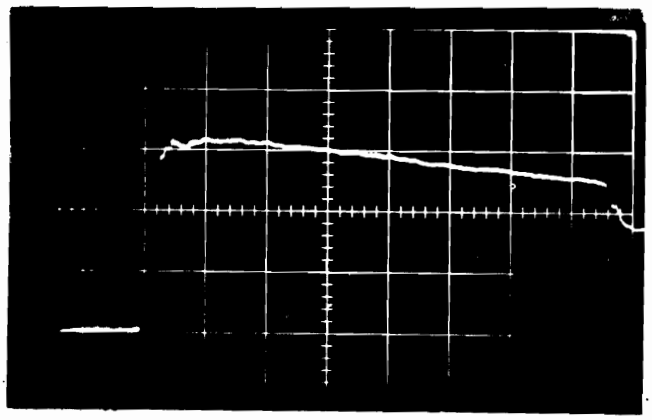

Trace: V_{D1}

S_V: 20 mV/div

S_H: 50 ns/div

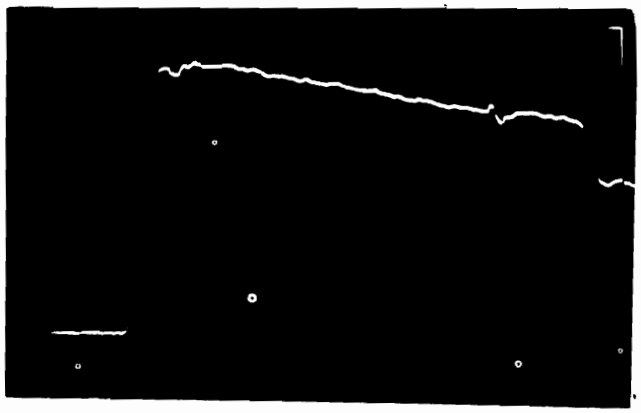

Trace: V_{B2}

S_V: 10 mV/div

S_H: 50 ns/div

Date: 9-19-78
Time: 13:47
Conductor Type: BAW
Test Voltage: 60 kV

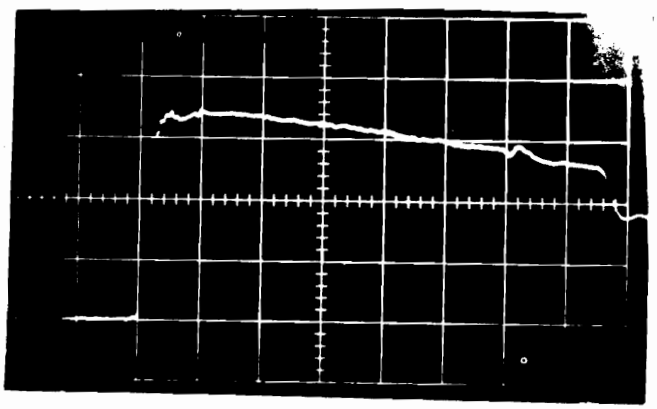

Trace: V_{D2}

S_V: 20 mV/div

S_H: 50 ns/div

Figure A16
Raw Test Data

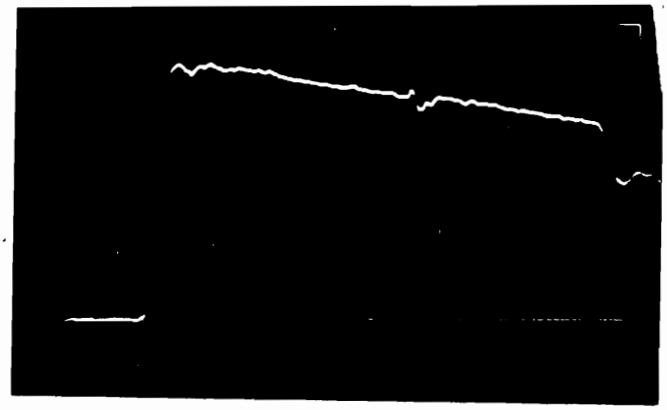

Trace: V_{B3}

S_V: 10 mV/div

S_H: 50 ns/div

Date: 9-19-78
Time: 13:51
Conductor Type: BAW
Test Voltage: 60 kV

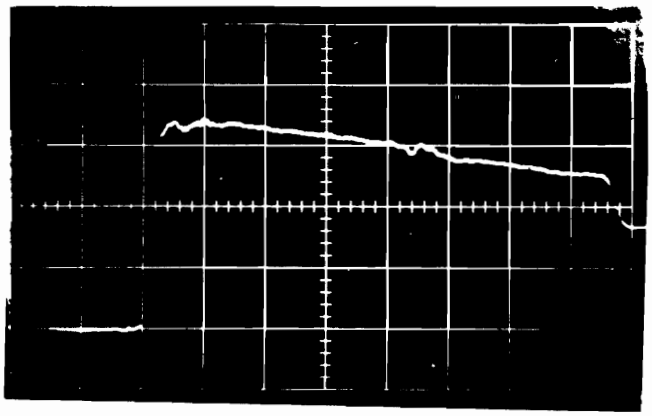

Trace: V_{D3}

S_V: 20 mV/div

S_H: 50 ns/div

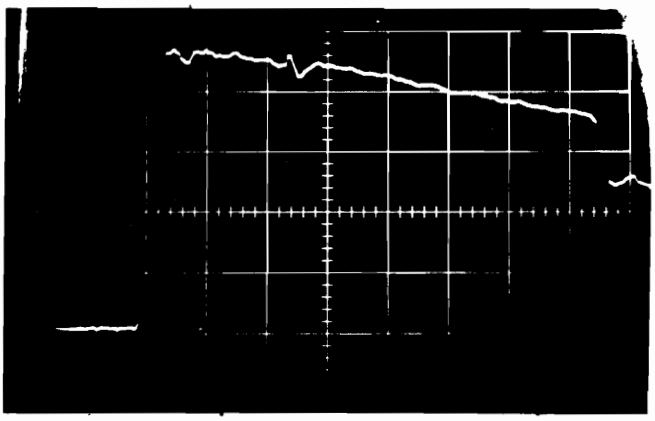

Trace: V_{B4}

S_V: 10 mV/div

S_H: 50 ns/div

Date: 9-19-78
Time: 13:55
Conductor Type: BAW
Test Voltage: 60 kV

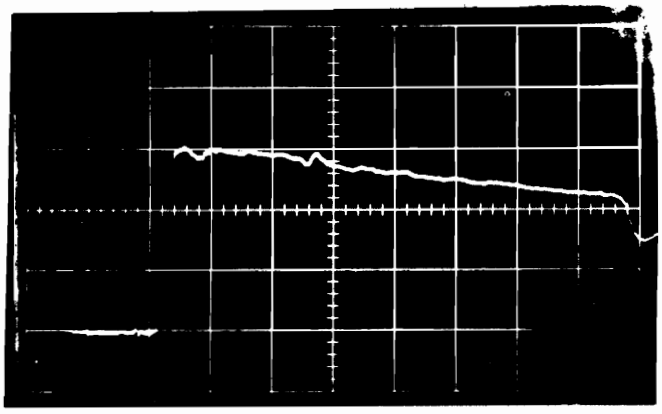

Trace: V_{D4}

S_V: 20 mV/div

S_H: 50 ns/div

Figure A17
Raw Test Data

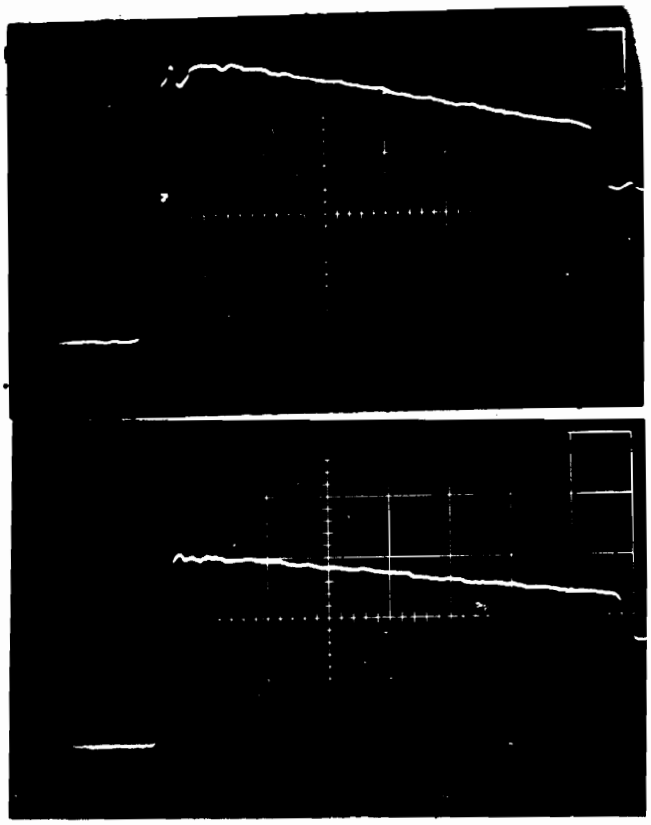

Trace: V_{B5}

S_V: 10 mV/div

S_H: 50 ns/div

Date: 9-19-78
Time: 14:00
Conductor Type: BAW
Test Voltage: 60 kV

Trace: V_{D5}

S_V: 20 mV/div

S_H: 50 ns/div

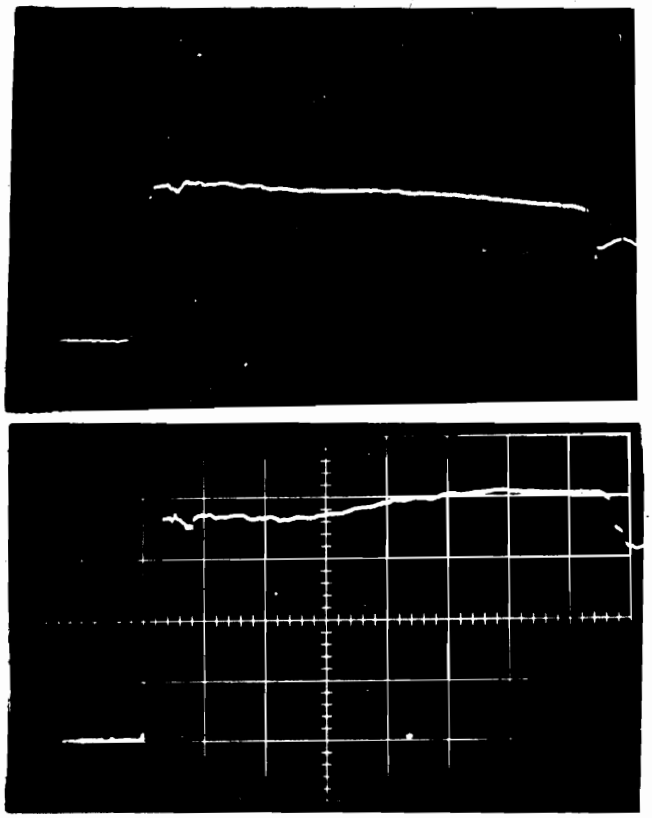

Trace: V_{B1}

S_V: 20 mV/div

S_H: 50 ns/div

Date: 9-19-78
Time: 14:28
Conductor Type: BAW
Test Voltage: 70 kV

Trace: V_{D1}

S_V: 20 mV/div

S_H: 50 ns/div

Figure A18
Raw Test Data

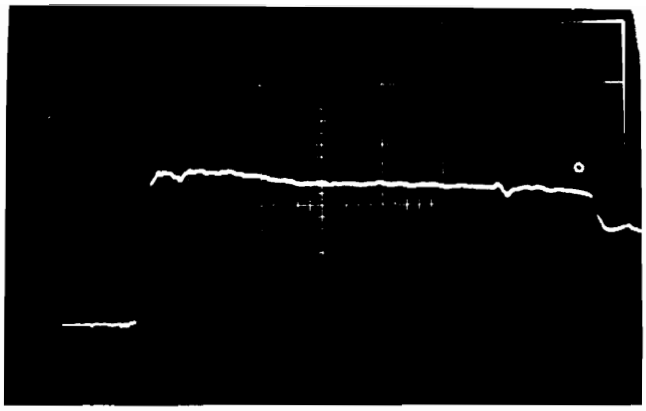

Trace: V_{B2}

S_V: 20 mV/div

S_H: 50 ns/div

Date: 9-19-78
Time: 14:25
Conductor Type: BAW
Test Voltage: 70 kV

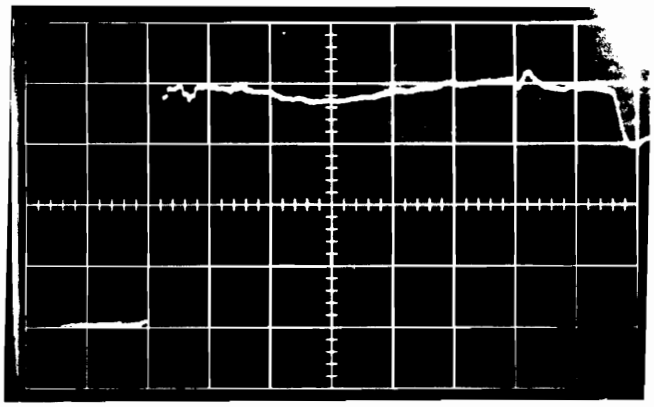

Trace: V_{D2}

S_V: 20 mV/div

S_H: 50 ns/div

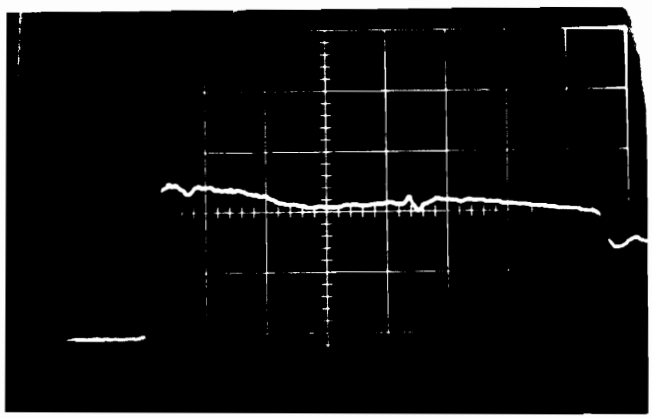

Trace: V_{B3}

S_V: 20 mV/div

S_H: 50 ns/div

Date: 9-19-78
Time: 14:20
Conductor Type: BAW
Test Voltage: 70 kV

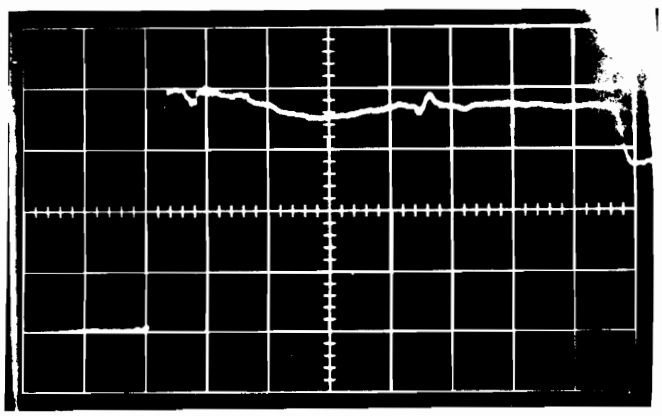

Trace: V_{D3}

S_V: 20 mV/div

S_H: 50 ns/div

Figure A19
Raw Test Data

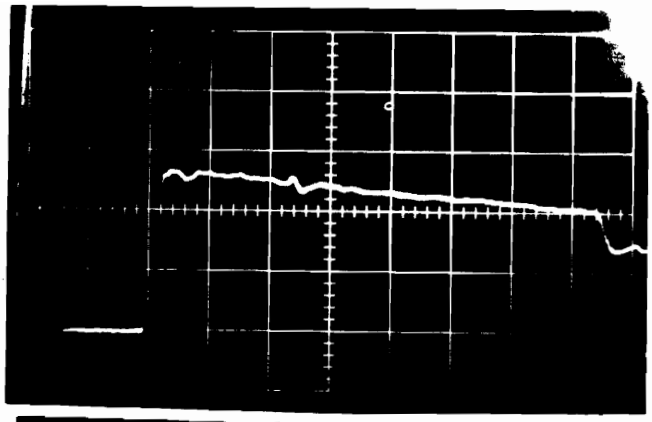

Trace: V_{B4}

S_V: 20 mV/div

S_H: 50 ns/div

Date: 9-19-78
Time: 14:32
Conductor Type: BAW
Test Voltage: 70 kV

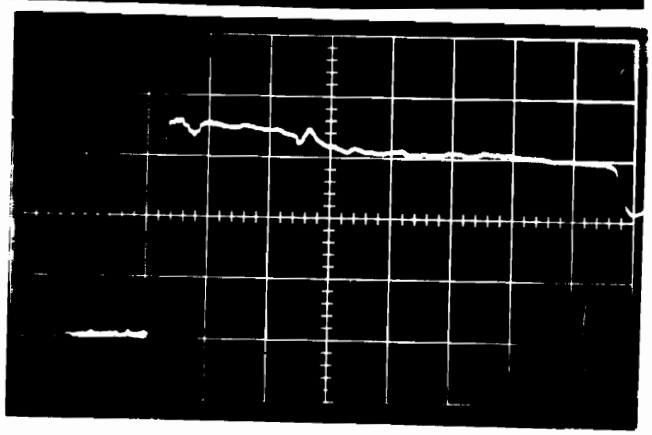

Trace: V_{D4}

S_V: 20 mV/div

S_H: 50 ns/div

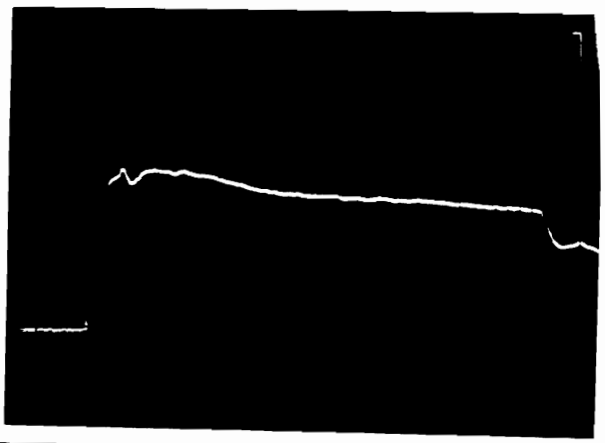

Trace: V_{B5}

S_V: 20 mV/div

S_H: 50 ns/div

Date: 9-19-78
Time: 14:13
Conductor Type: BAW
Test Voltage: 70 kV

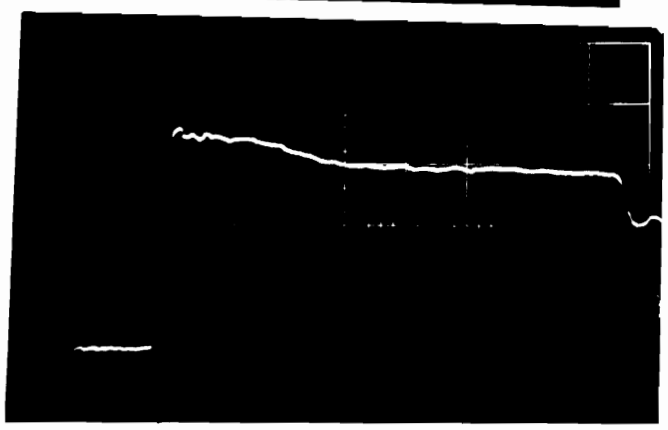

Trace: V_{D5}

S_V: 20 mV/div

S_H: 50 ns/div

Figure A20
Raw Test Data

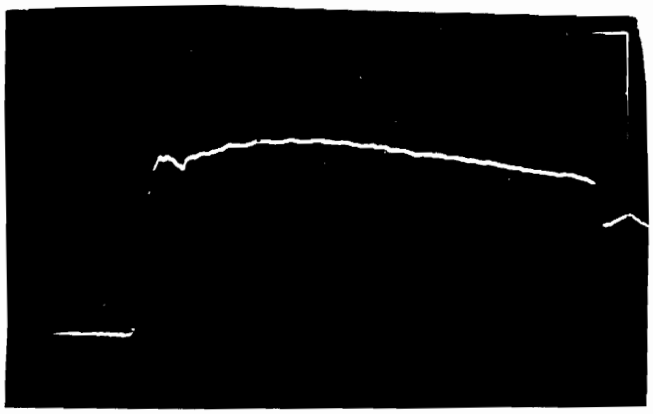

Trace: V_{B1}

S_V: 20 mV/div

S_H: 50 ns/div

Date: 9-19-78
Time: 14:52
Conductor Type: BAW
Test Voltage: 80 kV

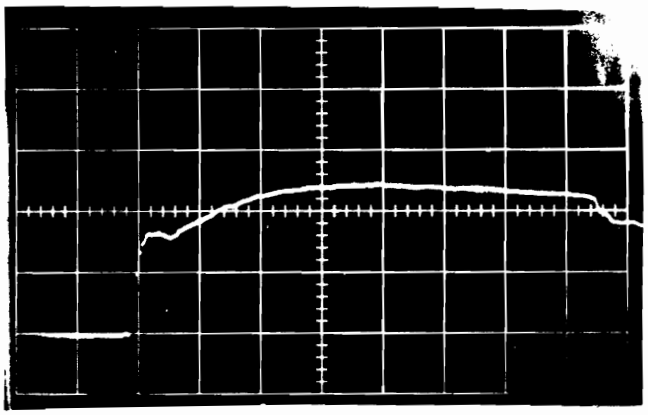

Trace: V_{D1}

S_V: 50 mV/div

S_H: 50 ns/div

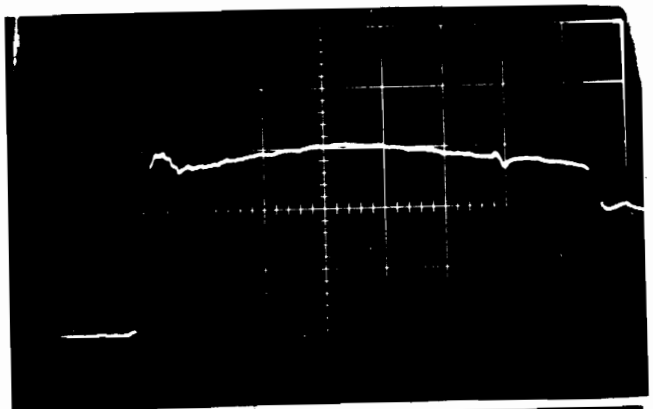

Trace: V_{B2}

S_V: 20 mV/div

S_H: 50 ns/div

Date: 9-19-78
Time: 15:09
Conductor Type: BAW
Test Voltage: 80 kV

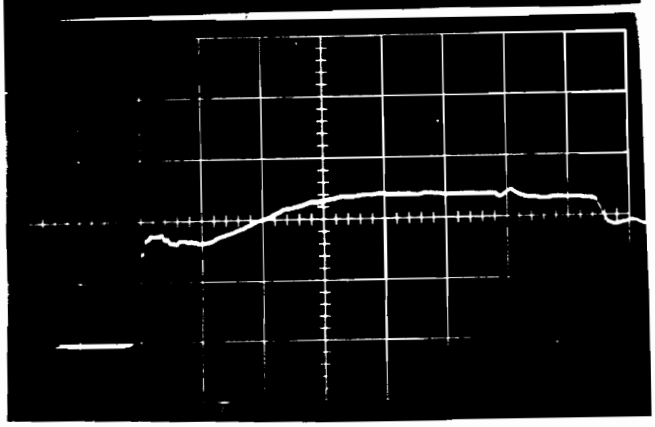

Trace: V_{D2}

S_V: 50 mV/div

S_H: 50 ns/div

Figure A21

Raw Test Data

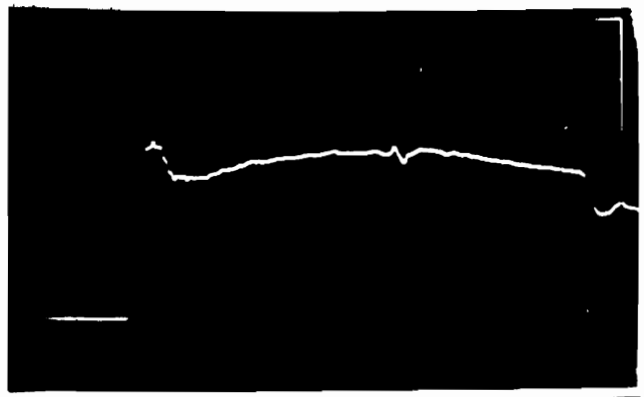

Trace: V_{B3}

S_V: 20 mV/div

S_H: 50 ns/div

Date: 9-19-78
Time: 15:13
Conductor Type: BAW
Test Voltage: 80 kV

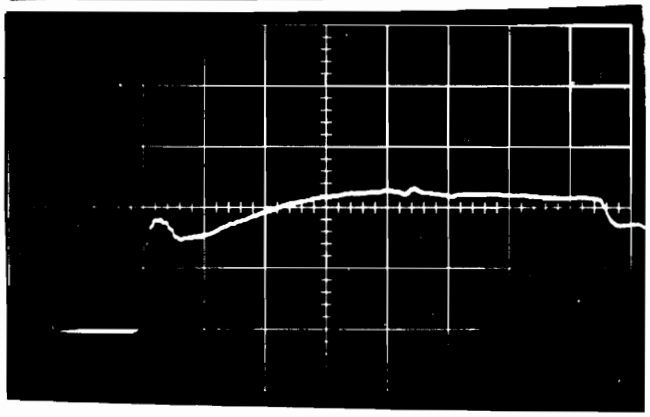

Trace: V_{D3}

S_V: 50 mV/div

S_H: 50 ns/div

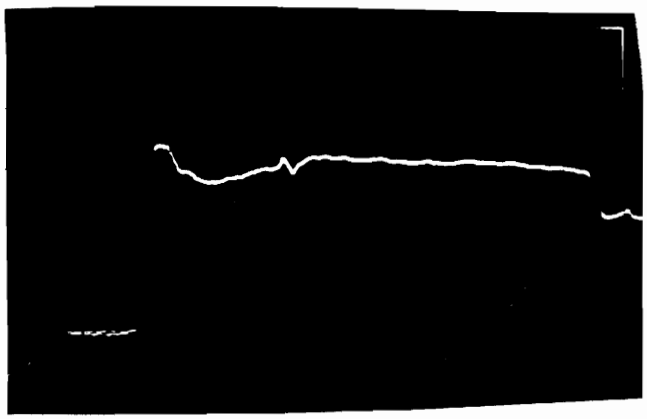

Trace: V_{B4}

S_V: 20 mV/div

S_H: 50 ns/div

Date: 9-19-78
Time: 15:17
Conductor Type: BAW
Test Voltage: 80 kV

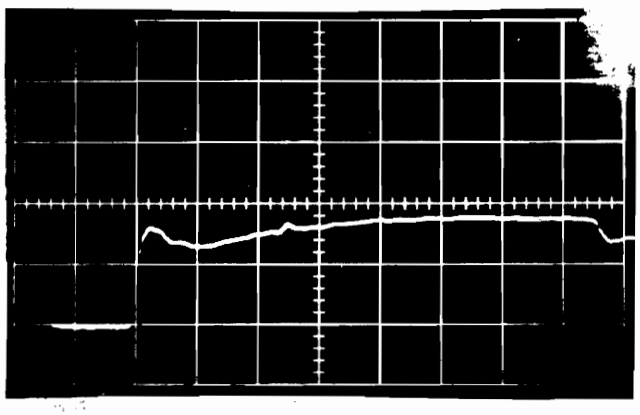

Trace: V_{D4}

S_V: 50 mV/div

S_H: 50 ns/div

Figure A22
Raw Test Data

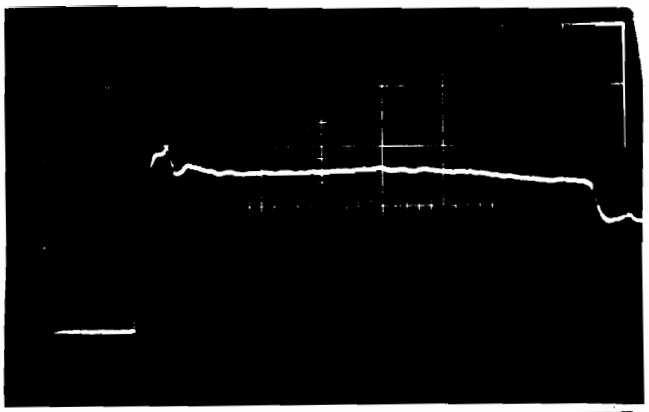

Trace: V_{B5}

S_V: 20 mV/div

S_H: 50 ns/div

Date: 9-19-78
Time: 15:27
Conductor Type: BAW
Test Voltage: 80 kV

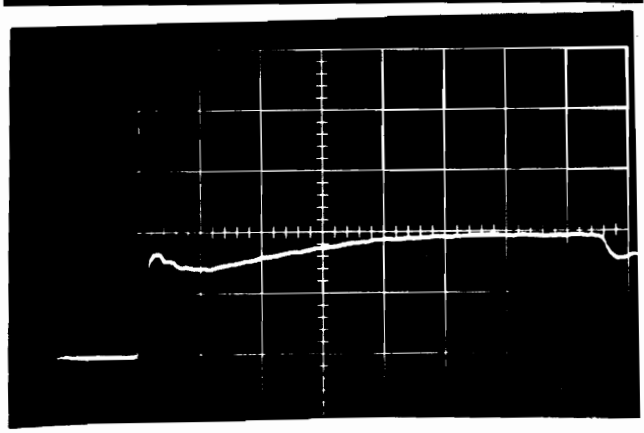

Trace: V_{D5}

S_V: 50 mV/div

S_H: 50 ns/div

Trace: V_{B1}

S_V: 20 mV/div

S_H: 50 ns/div

Date: 9-19-78
Time: 15:29
Conductor Type: BAW
Test Voltage: 90 kV

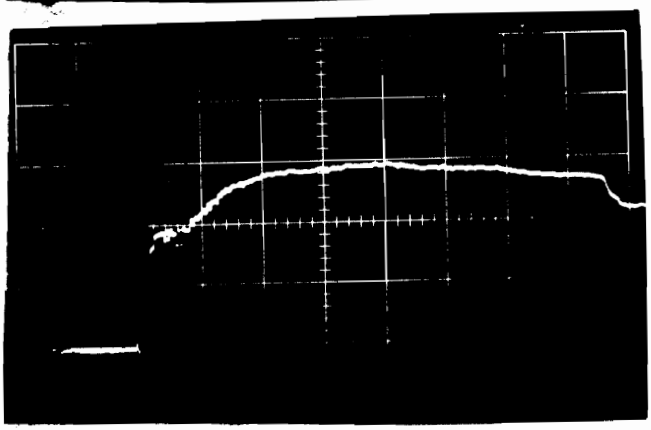

Trace: V_{D1}

S_V: 50 mV/div

S_H: 50 ns/div

Figure A23
Raw Test Data

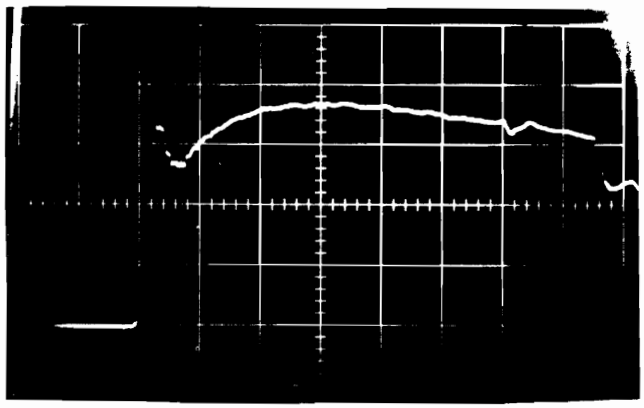

Trace: V_{B2}

S_V: 20 mV/div

S_H: 50 ns/div

Date: 9-19-78
Time: 15:31
Conductor Type: BAW
Test Voltage: 90 kV

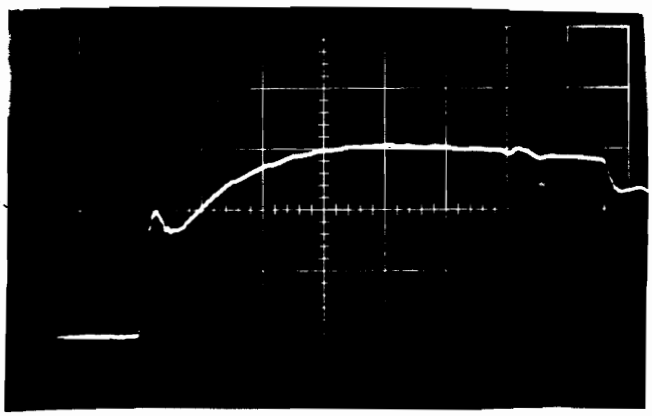

Trace: V_{D2}

S_V: 50 mV/div

S_H: 50 ns/div

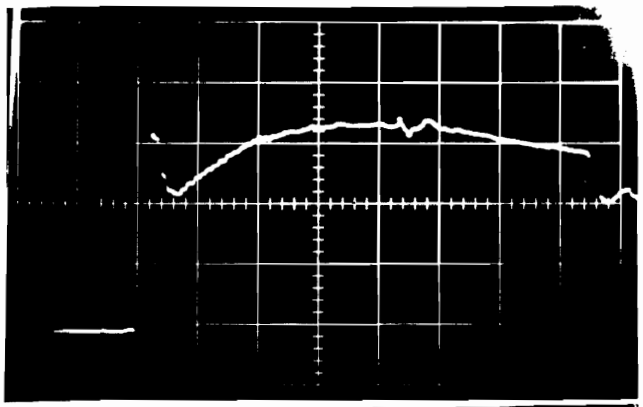

Trace: V_{B3}

S_V: 20 mV/div

S_H: 50 ns/div

Date: 9-19-78
Time: 15:35
Conductor Type: BAW
Test Voltage: 90 kV

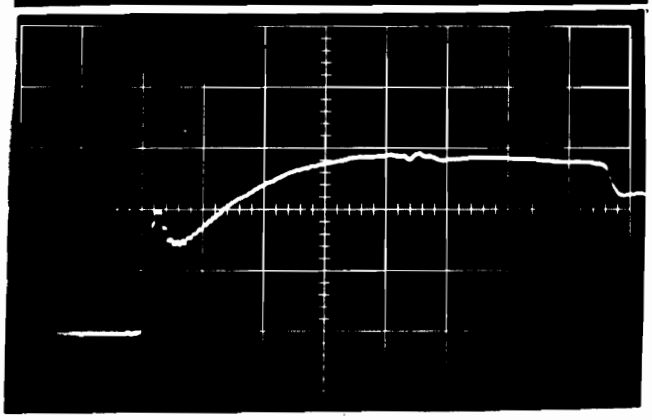

Trace: V_{D3}

S_V: 50 mV/div

S_H: 50 ns/div

Figure A24
Raw Test Data

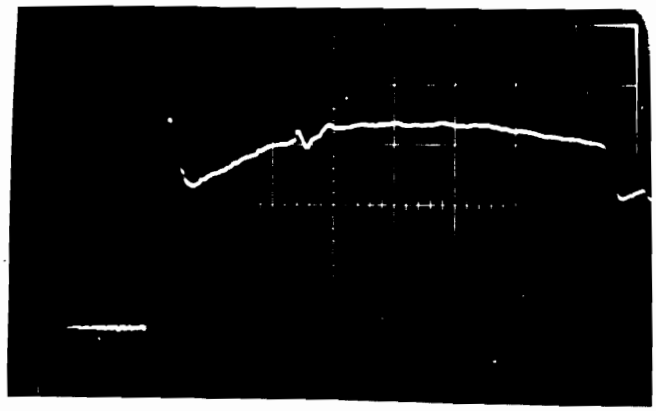

Trace: V_{B4}

S_V: 20 mV/div

S_H: 50 ns/div

Date: 9-19-78
Time: 15:38
Conductor Type: BAW
Test Voltage: 90 kV

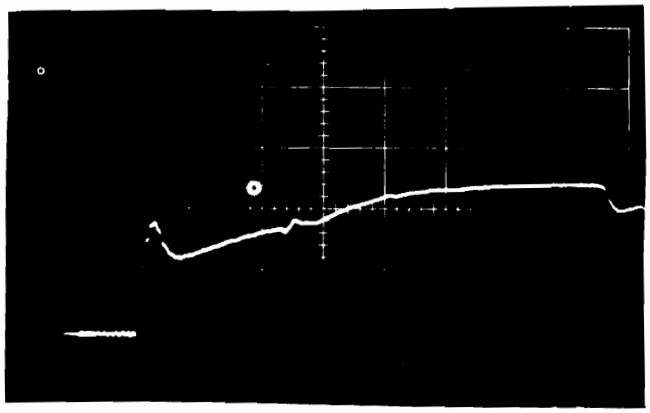

Trace: V_{D4}

S_V: 50 mV/div

S_H: 50 ns/div

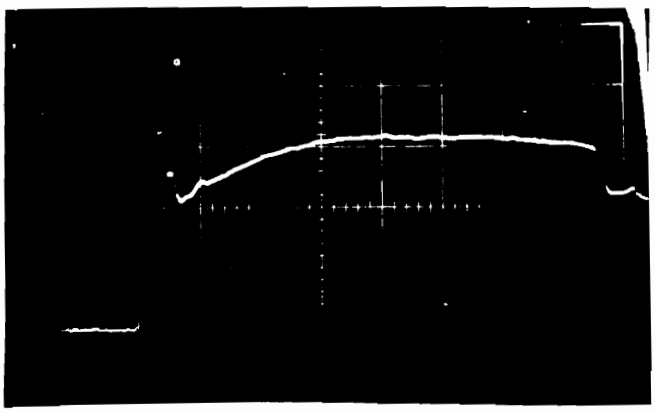

Trace: V_{B5}

S_V: 20 mV/div

S_H: 50 ns/div

Date: 9-19-78
Time: 15:42
Conductor Type: BAW
Test Voltage: 90 kV

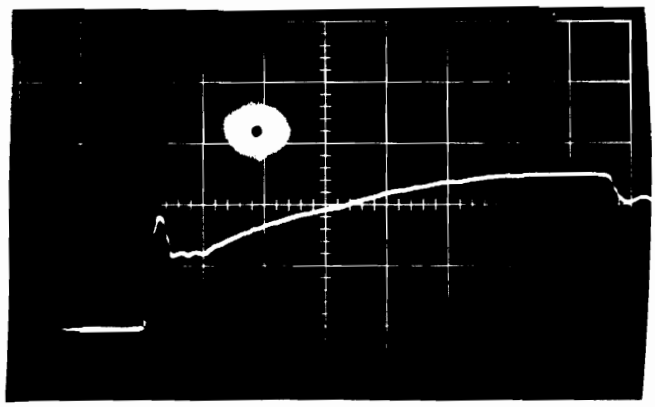

Trace: V_{D5}

S_V: 50 mV/div

S_H: 50 ns/div

Figure A25
Raw Test Data

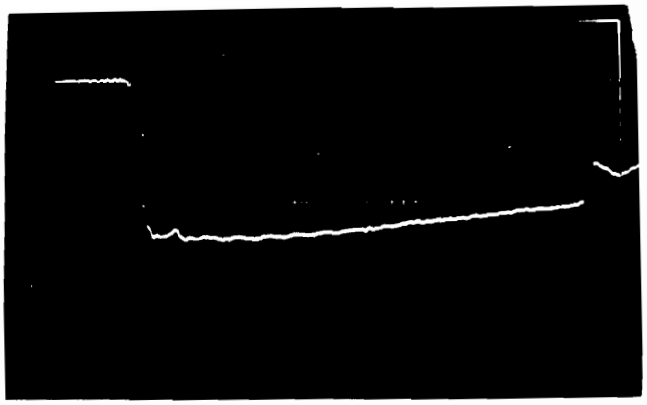

Trace: V_{B1}

S_V: 20 mV/div

S_H: 50 ns/div

Date: 9-21-78
Time: 10:58
Conductor Type: BAW
Test Voltage: -70 kV

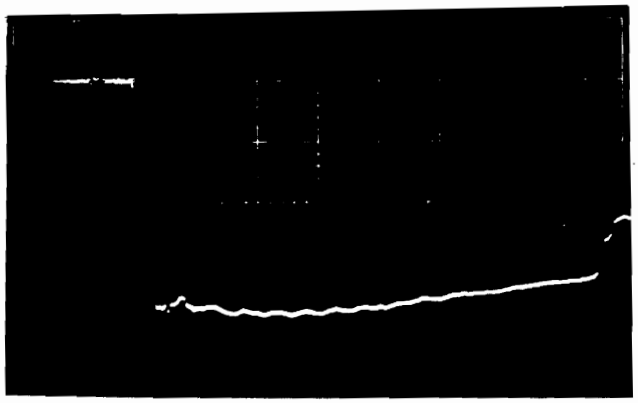

Trace: V_{D1}

S_V: 20 mV/div

S_H: 50 ns/div

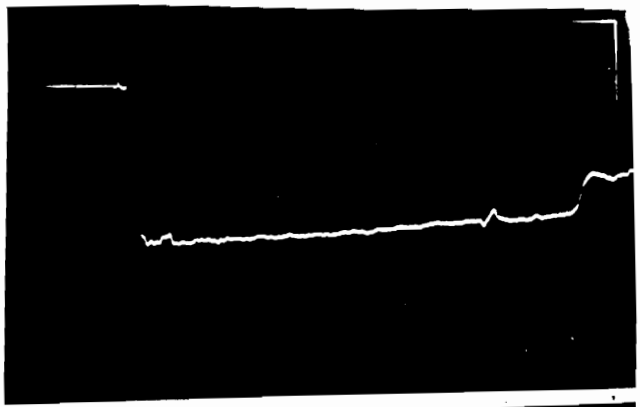

Trace: V_{B2}

S_V: 20 mV/div

S_H: 50 ns/div

Date: 9-21-78
Time: 11:02
Conductor Type: BAW
Test Voltage: -70 kV

Trace: V_{D2}

S_V: 20 mV/div

S_H: 50 ns/div

Figure A26

Raw Test Data

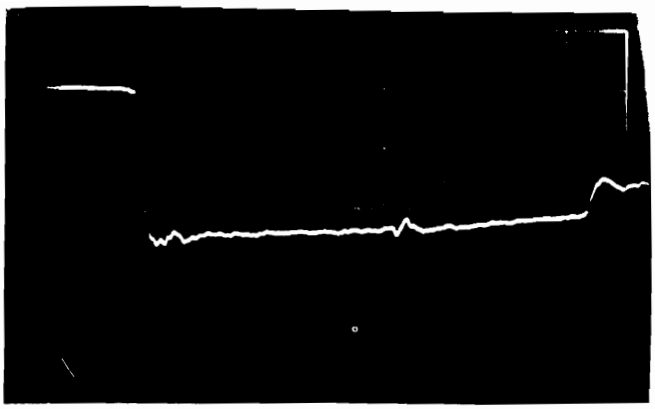

Trace: V_{B3}

S_V: 20 mV/div

S_H: 50 ns/div

Date: 9-21-78
Time: 11:06
Conductor Type: BAW
Test Voltage: -70 kV

Trace: V_{D3}

S_V: 20 mV/div

S_H: 50 ns/div

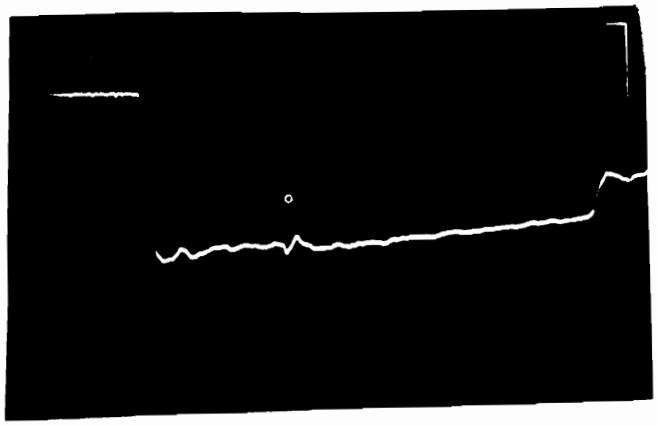

Trace: V_{B4}

S_V: 20 mV/div

S_H: 50 ns/div

Date: 9-21-78
Time: 11:11
Conductor Type: BAW
Test Voltage: -70 kV

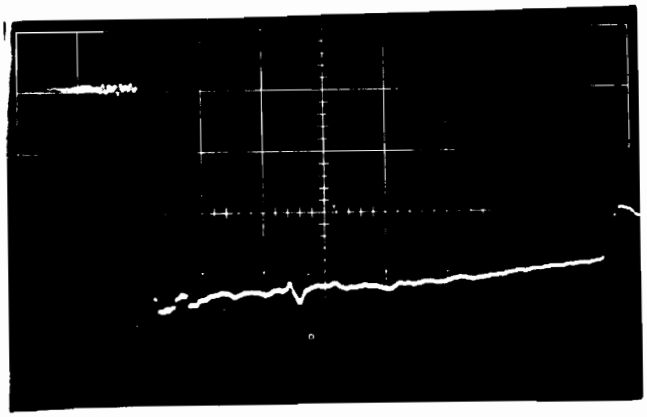

Trace: V_{D4}

S_V: 20 mV/div

S_H: 50 ns/div

Figure A27
Raw Test Data

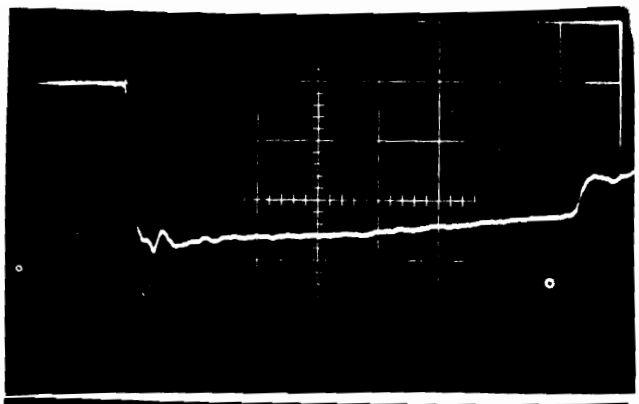

Trace: V_{B5}

S_V: 20 mV/div

S_H: 50 ns/div

Date: 9-21-78
Time: 11:15
Conductor Type: BAW
Test Voltage: -70 kV

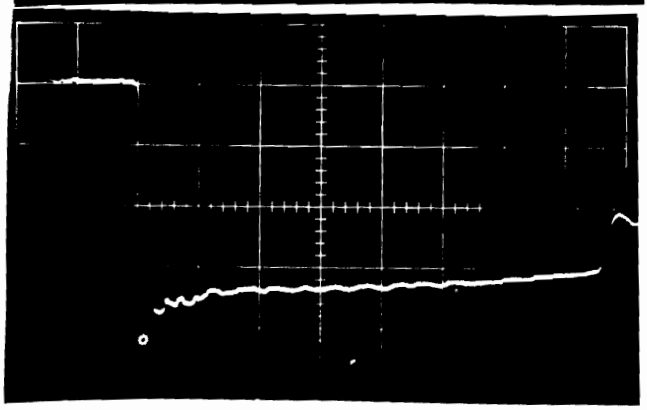

Trace: V_{D5}

S_V: 20 mV/div

S_H: 50 ns/div

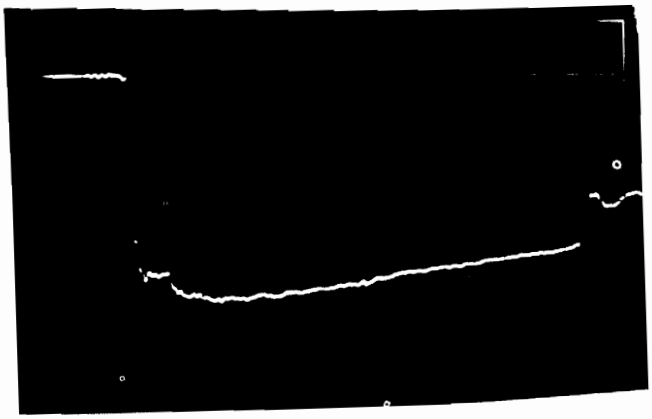

Trace: V_{B1}

S_V: 20 mV/div

S_H: 50 ns/div

Date: 9-21-78
Time: 14:48
Conductor Type: BAW
Test Voltage: -90 kV

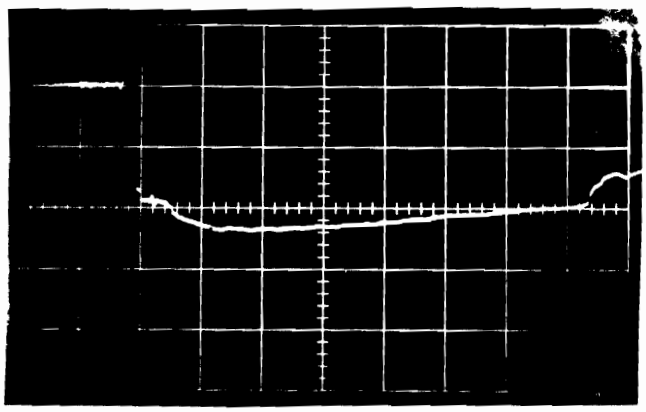

Trace: V_{D1}

S_V: 50 mV/div

S_H: 50 ns/div

Figure A28

Raw Test Data

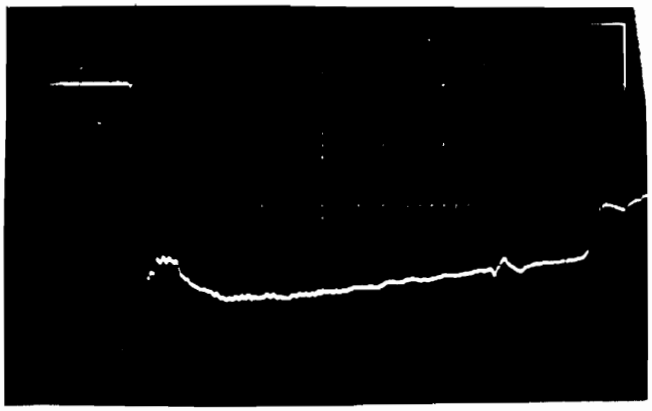

Trace: V_{B2}

S_V: 20 mV/div

S_H: 50 ns/div

Date: 9-21-78
Time: 14:03
Conductor Type: BAW
Test Voltage: -90 kV

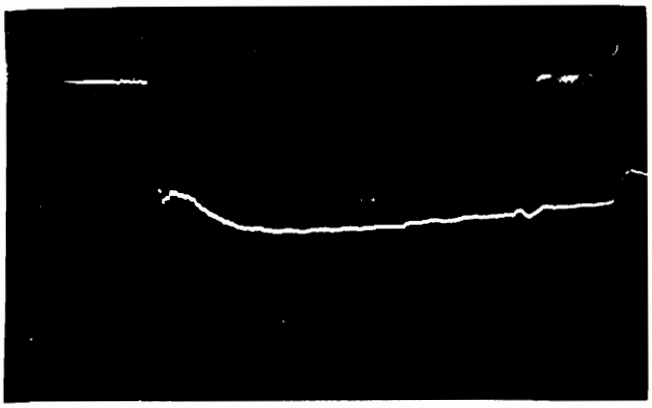

Trace: V_{D2}

S_V: 50 mV/div

S_H: 50 ns/div

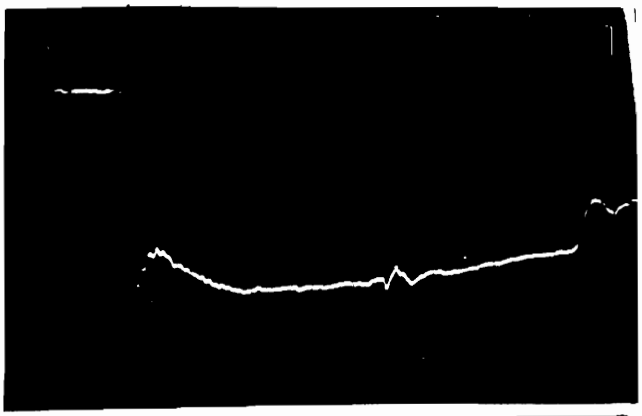

Trace: V_{B3}

S_V: 20 mV/div

S_H: 50 ns/div

Date: 9-21-78
Time: 14:09
Conductor Type: BAW
Test Voltage: -90 kV

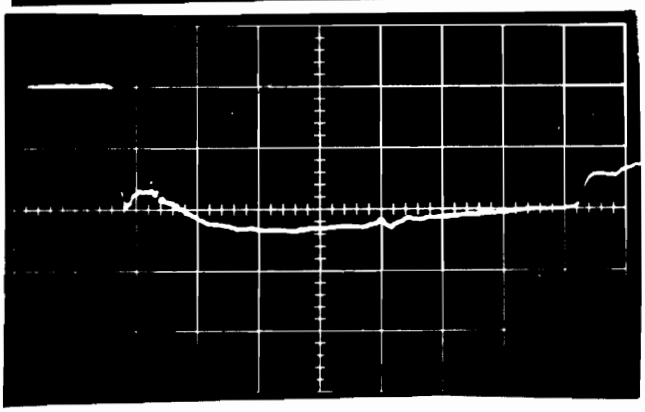

Trace: V_{D3}

S_V: 50 mV/div

S_H: 50 ns/div

Figure A29
Raw Test Data

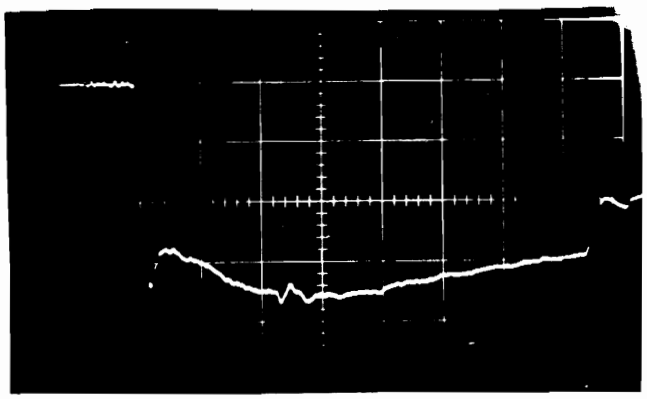

Trace: V_{B4}

S_V: 20 mV/div

S_H: 50 ns/div

Date: 9-21-78
Time: 14:17
Conductor Type: BAW
Test Voltage: -90 kV

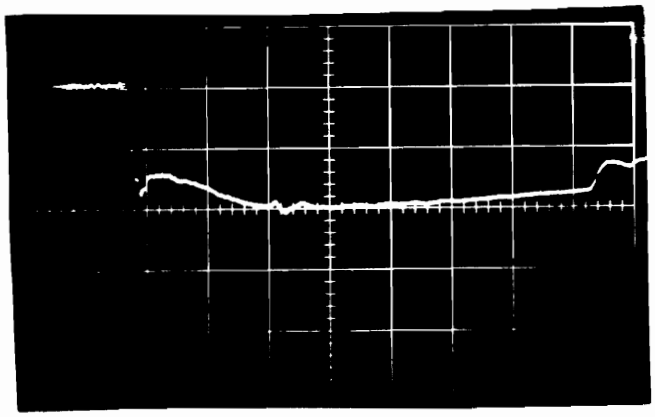

Trace: V_{D4}

S_V: 50 mV/div

S_H: 50 ns/div

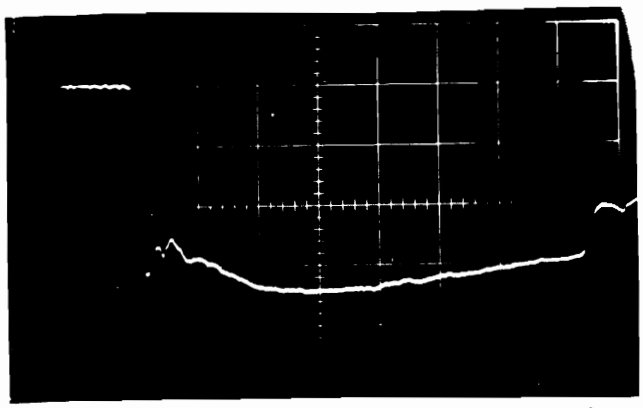

Trace: V_{B5}

S_V: 20 mV/div

S_H: 50 ns/div

Date: 9-21-78
Time: 14:20
Conductor Type: BAW
Test Voltage: -90 kV

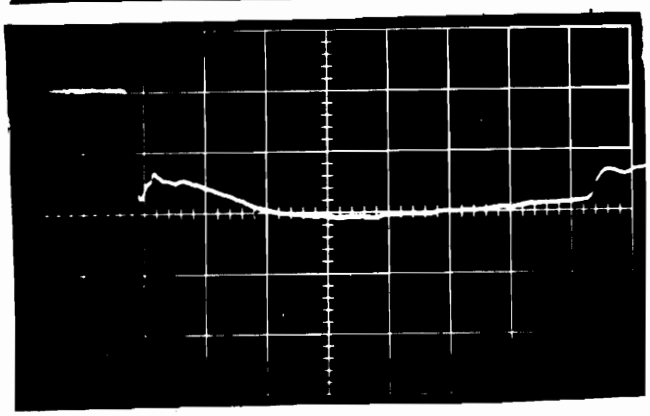

Trace: V_{D5}

S_V: 50 mV/div

S_H: 50 ns/div

Figure A30
Raw Test Data

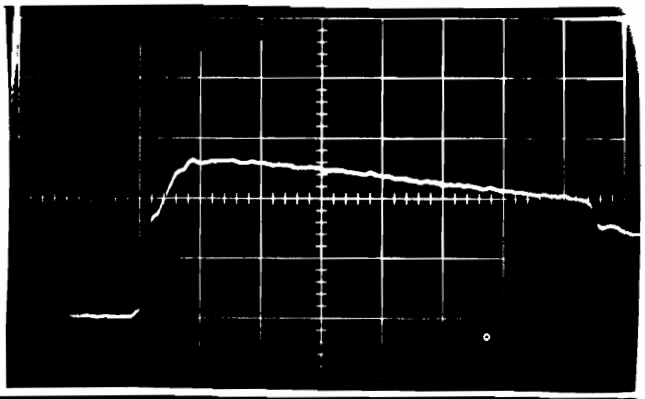

Trace: V_{B1}

S_V: 10 mV/div

S_H: 50 ns/div

Date: 9-27-78
Time: 09:40
Conductor Type: BCW
Test Voltage: 40 kV

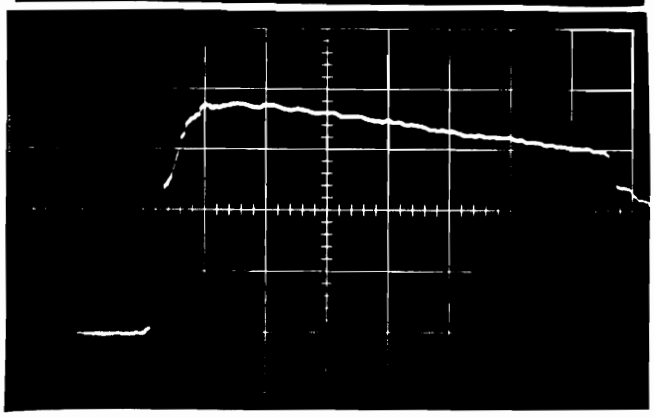

Trace: V_{D1}

S_V: 10 mV/div

S_H: 50 ns/div

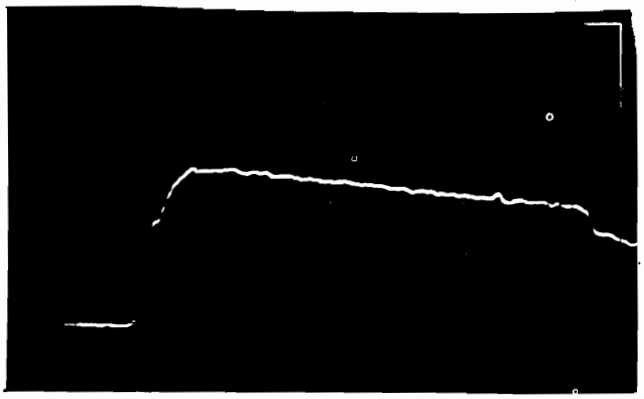

Trace: V_{B2}

S_V: 10 mV/div

S_H: 50 ns/div

Date: 9-27-78
Time: 09:45
Conductor Type: BCW
Test Voltage: 40 kV

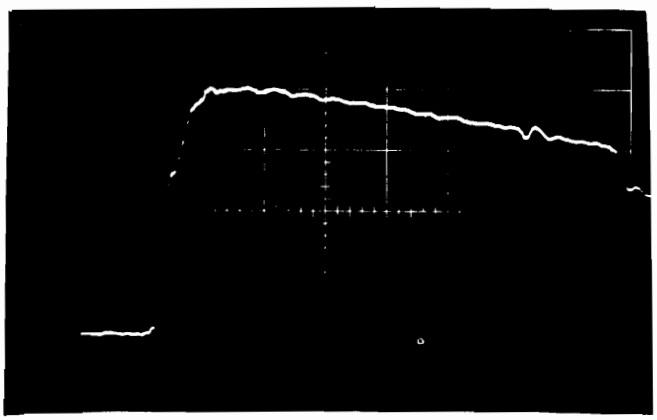

Trace: V_{D2}

S_V: 10 mV/div

S_H: 50 ns/div

Figure A31
Raw Test Data

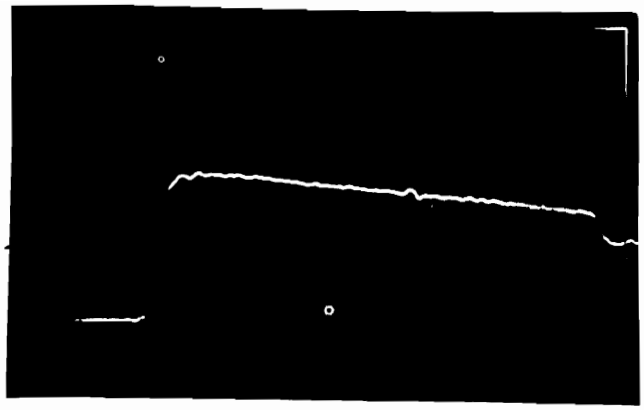

Trace: V_{B3}

S_V: 10 mV/div

S_H: 50 ns/div

Date: 9-27-78
Time: 09:50
Conductor Type: BCW
Test Voltage: 40 kV

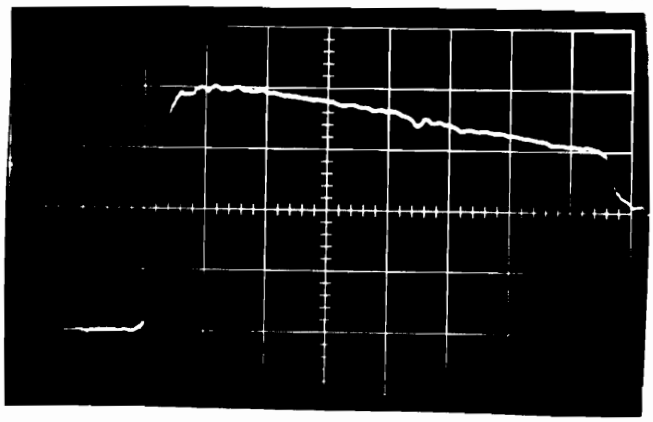

Trace: V_{D3}

S_V: 10 mV/div

S_H: 50 ns/div

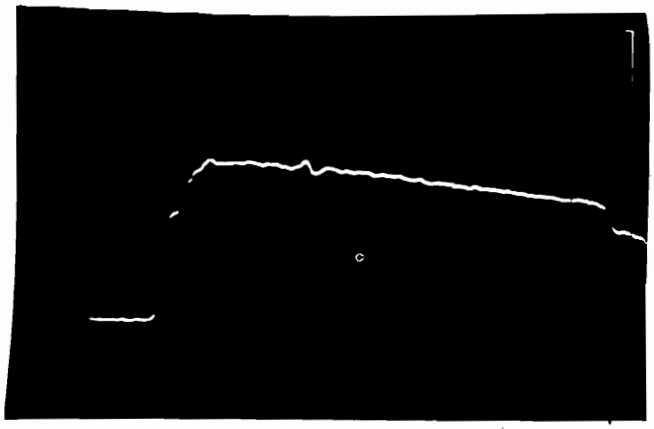

Trace: V_{B4}

S_V: 10 mV/div

S_H: 50 ns/div

Date: 9-27-78
Time: 09:53
Conductor Type: BCW
Test Voltage: 40 kV

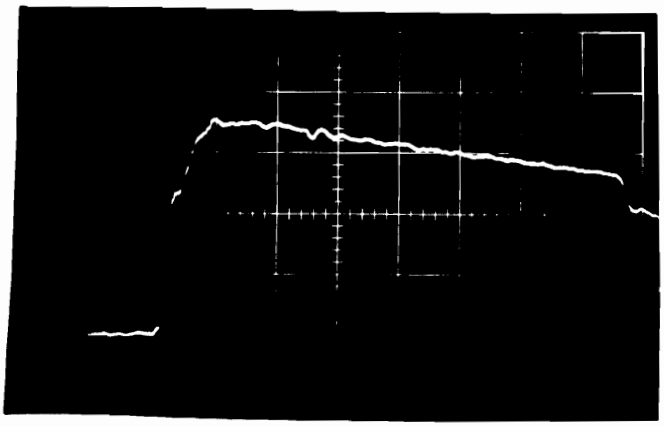

Trace: V_{D4}

S_V: 10 mV/div

S_H: 50 ns/div

Figure A32
Raw Test Data

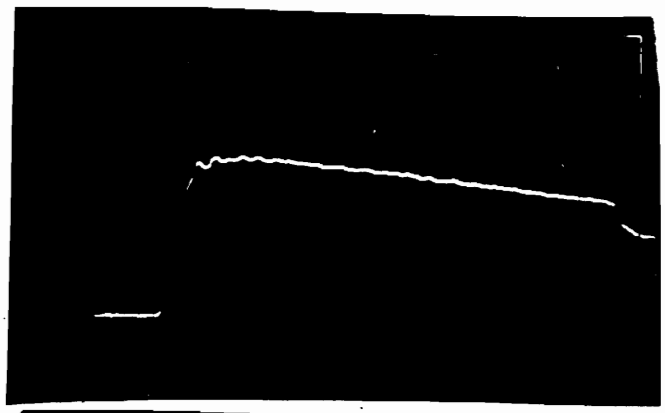

Trace: V_{B5}

S_V: 10 mV/div

S_H: 50 ns/div

Date: 9-27-78
Time: 09:57
Conductor Type: BCW
Test Voltage: 40 kV

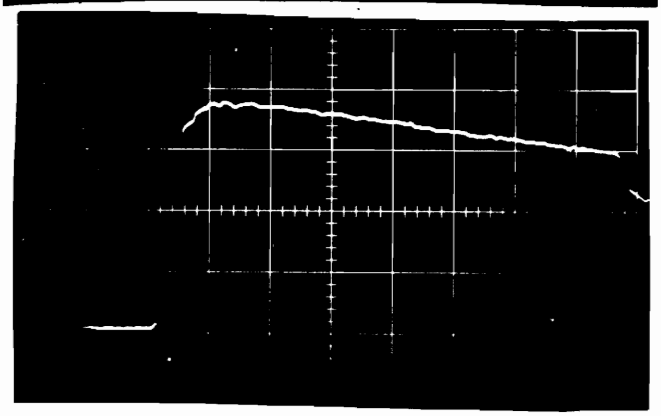

Trace: V_{D5}

S_V: 10 mV/div

S_H: 50 ns/div

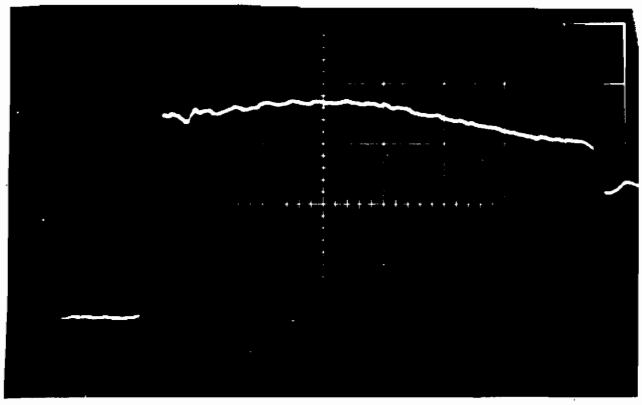

Trace: V_{B1}

S_V: 10 mV/div

S_H: 50 ns/div

Date: 9-27-78
Time: 10:18
Conductor Type: BCW
Test Voltage: 50 kV

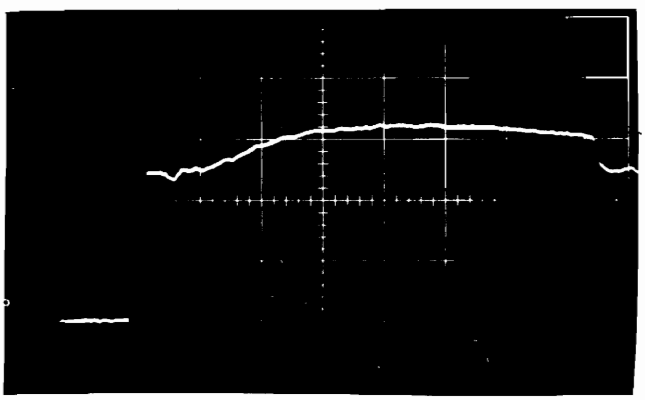

Trace: V_{D1}

S_V: 20 mV/div

S_H: 50 ns/div

Figure A33
Raw Test Data

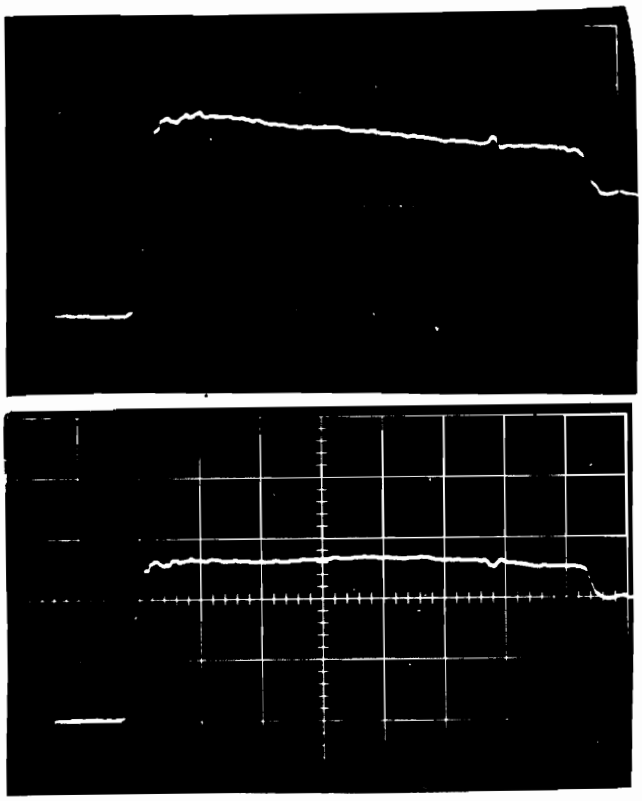

Trace: V_{B2}

S_V: 10 mV/div

S_H: 50 ns/div

Date: 9-27-78
Time: 10:14
Conductor Type: BCW
Test Voltage: 50 kV

Trace: V_{D2}

S_V: 20 mV/div

S_H: 50 ns/div

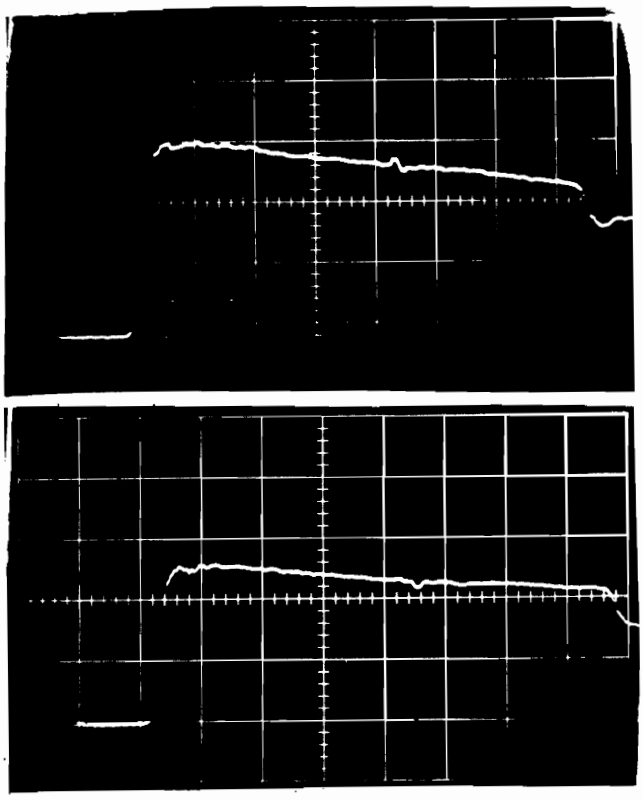

Trace: V_{B3}

S_V: 10 mV/div

S_H: 50 ns/div

Date: 9-27-78
Time: 10:10
Conductor Type: BCW
Test Voltage: 50 kV

Trace: V_{D3}

S_V: 20 mV/div

S_H: 50 ns/div

Figure A34
Raw Test Data

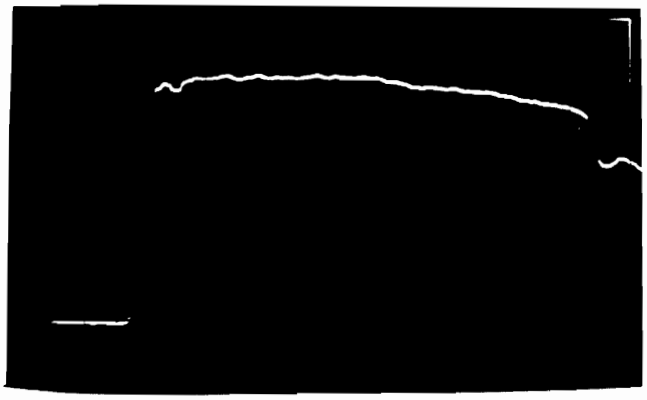

Trace: V_{B1}

S_V: 10 mV/div

S_H: 50 ns/div

Date: 9-27-78
Time: 10:23
Conductor Type: BCW
Test Voltage: 60 kV

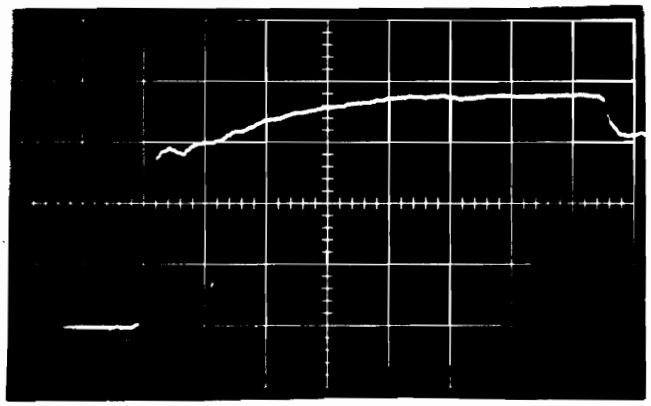

Trace: V_{D1}

S_V: 20 mV/div

S_H: 50 ns/div

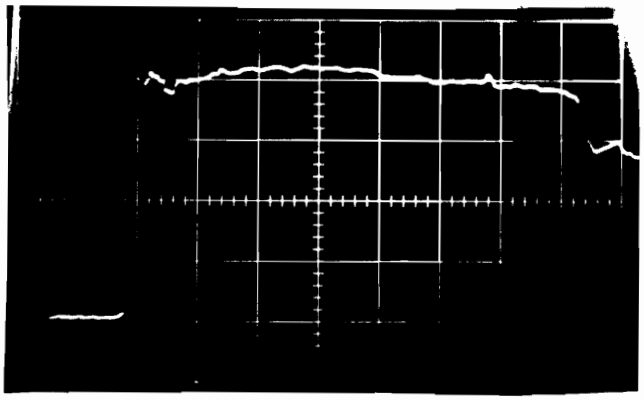

Trace: V_{B2}

S_V: 10 mV/div

S_H: 50 ns/div

Date: 9-27-78
Time: 10:27
Conductor Type: BCW
Test Voltage: 60 kV

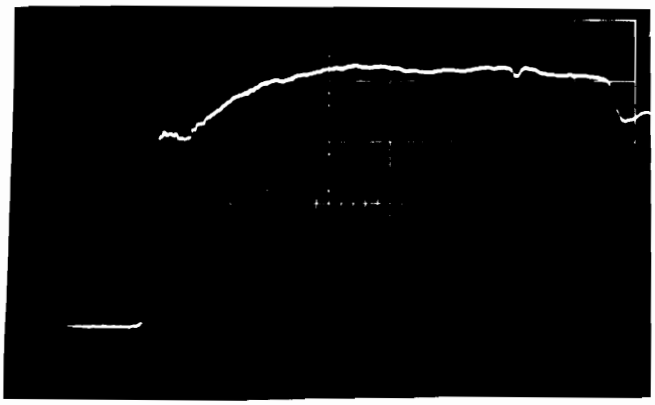

Trace: V_{D2}

S_V: 20 mV/div

S_H: 50 ns/div

Figure A36
Raw Test Data

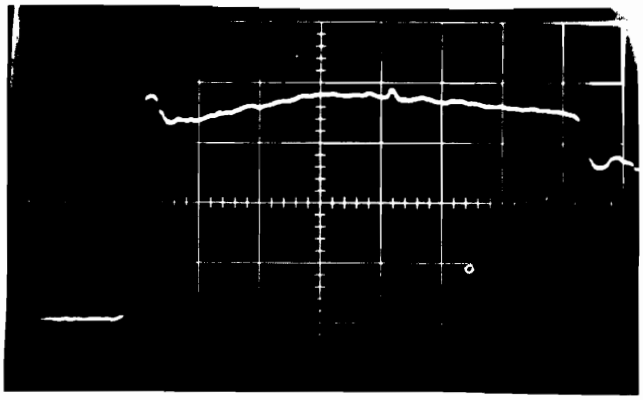

Trace: V_{B3}

S_V: 10 mV/div

S_H: 50 ns/div

Date: 9-27-78
Time: 10:30
Conductor Type: BCW
Test Voltage: 60 kV

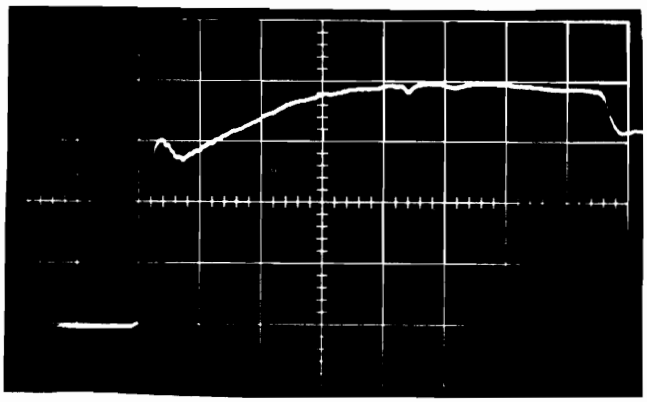

Trace: V_{D3}

S_V: 20 mV/div

S_H: 50 ns/div

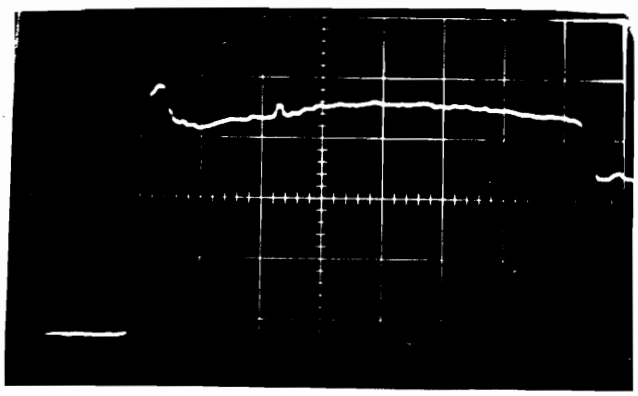

Trace: V_{B4}

S_V: 10 mV/div

S_H: 50 ns/div

Date: 9-27-78
Time: 10:35
Conductor Type: BCW
Test Voltage: 60 kV

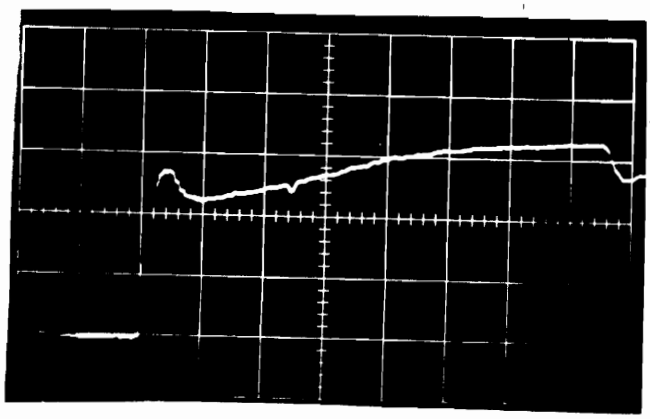

Trace: V_{D4}

S_V: 20 mV/div

S_H: 50 ns/div

Figure A37
Raw Test Data

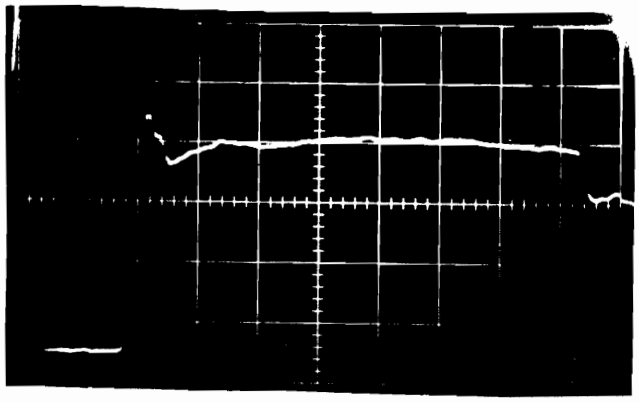

Trace: V_{B5}

S_V: 10 mV/div

S_H: 50 ns/div

Date: 9-27-78
Time: 10:40
Conductor Type: BCW
Test Voltage: 60 kV

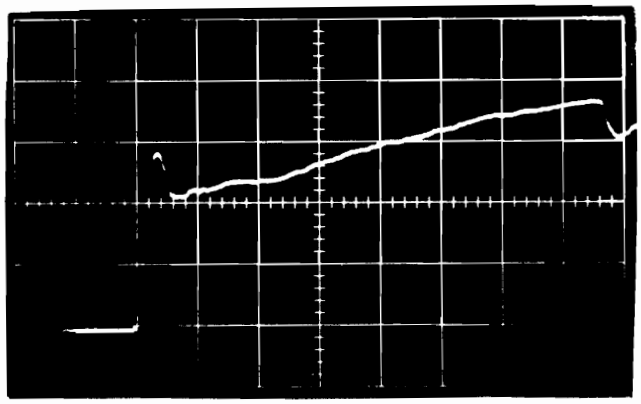

Trace: V_{D5}

S_V: 20 mV/div

S_H: 50 ns/div

Trace: V_{B1}

S_V: 20 mV/div

S_H: 50 ns/div

Date: 9-27-78
Time: 10:53
Conductor Type: BCW
Test Voltage: 70 kV

Trace: V_{D1}

S_V: 20 mV/div

S_H: 50 ns/div

Figure A38
Raw Test Data

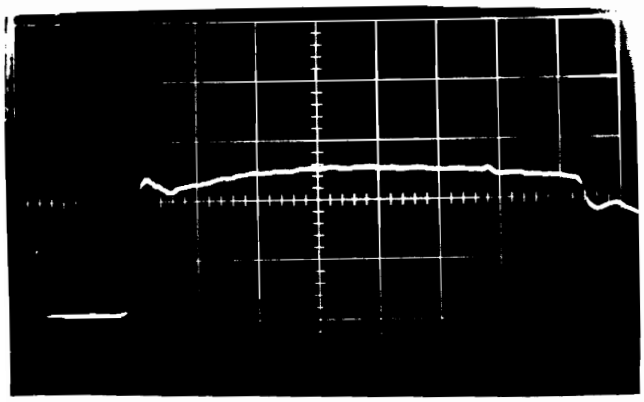

Trace: V_{B2}

S_V: 20 mV/div

S_H: 50 ns/div

Date: 9-27-78
Time: 10:58
Conductor Type: BCW
Test Voltage: 70 kV

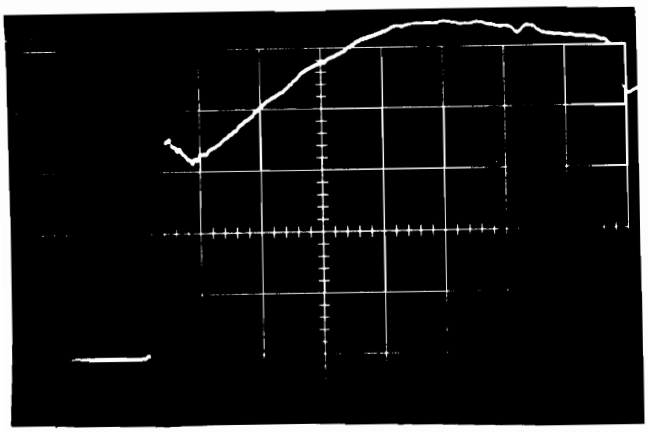

Trace: V_{D2}

S_V: 20 mV/div

S_H: 50 ns/div

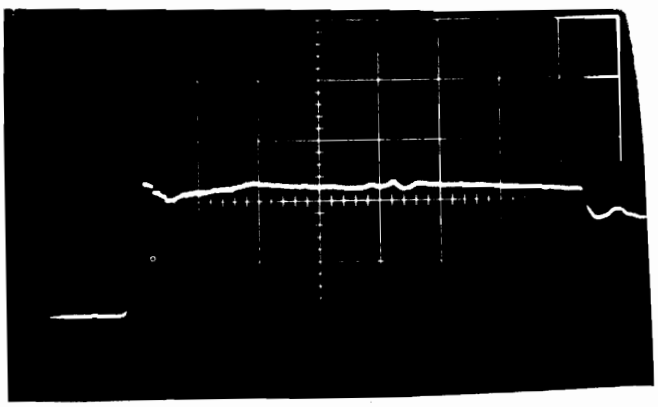

Trace: V_{B3}

S_V: 20 mV/div

S_H: 50 ns/div

Date: 9-27-78
Time: 11:03
Conductor Type: BCW
Test Voltage: 70 kV

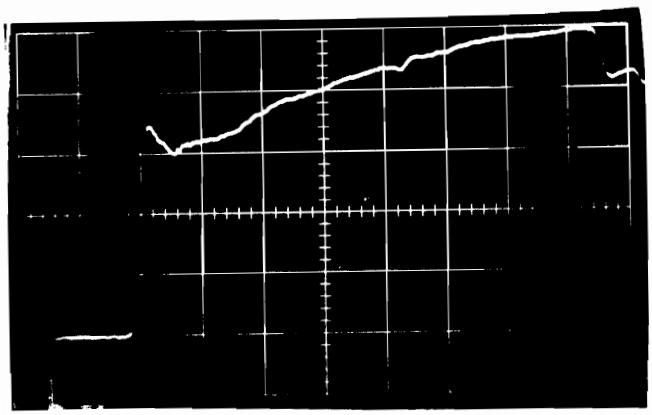

Trace: V_{D3}

S_V: 20 mV/div

S_H: 50 ns/div

Figure A39
Raw Test Data

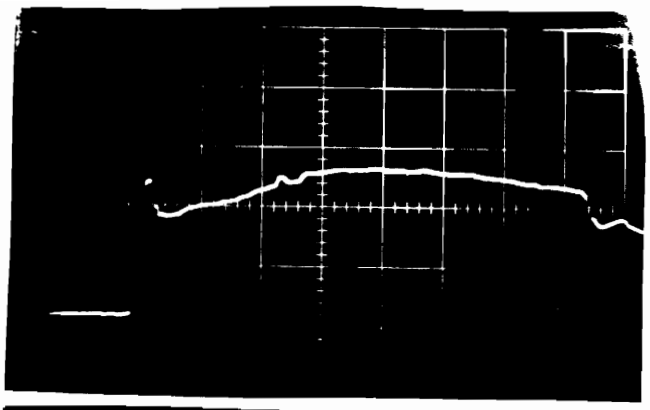

Trace: V_{B4}

S_V: 20 mV/div

S_H: 50 ns/div

Date: 9-27-78
Time: 11:06
Conductor Type: BCW
Test Voltage: 70 kV

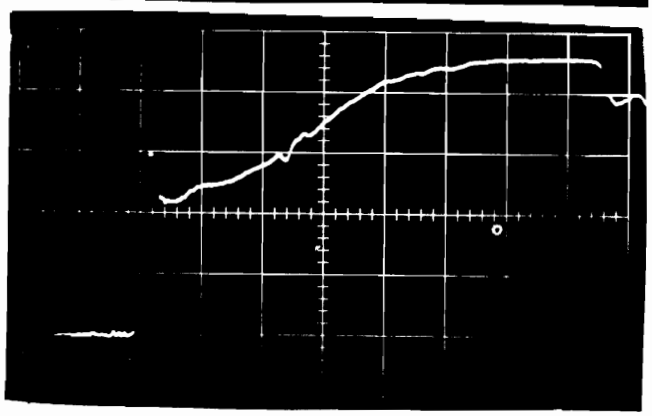

Trace: V_{D4}

S_V: 20 mV/div

S_H: 50 ns/div

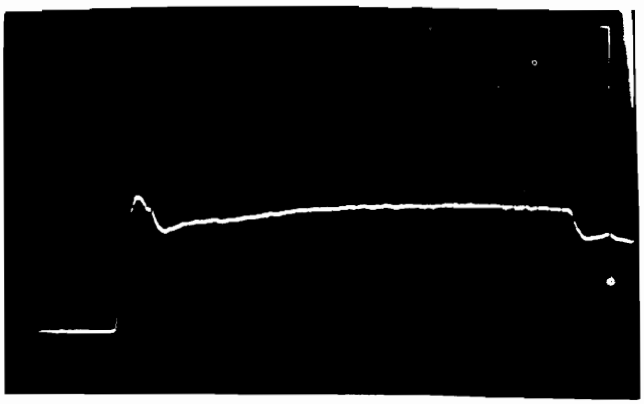

Trace: V_{B5}

S_V: 20 mV/div

S_H: 50 ns/div

Date: 9-27-78
Time: 11:10
Conductor Type: BCW
Test Voltage: 70 kV

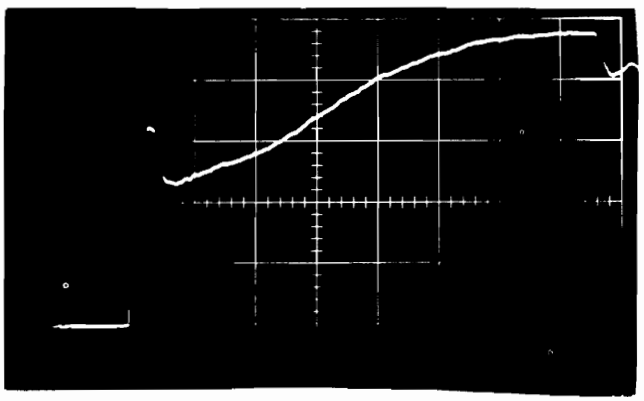

Trace: V_{D5}

S_V: 20 mV/div

S_H: 50 ns/div

Figure A40
Raw Test Data

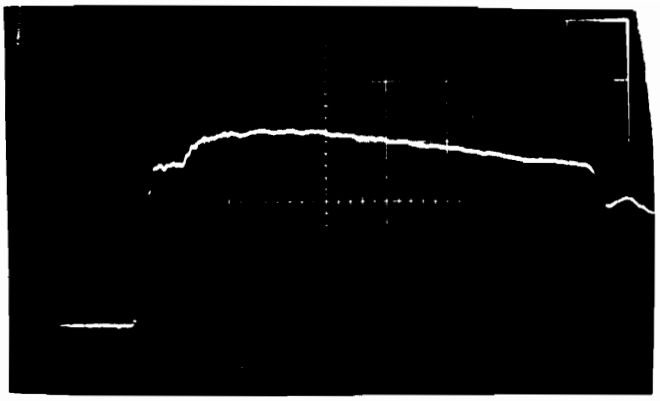

Trace: V_{B1}

S_V: 20 mV/div

S_H: 50 ns/div

Date: 9-27-78
Time: 11:15
Conductor Type: BCW
Test Voltage: 80 kV

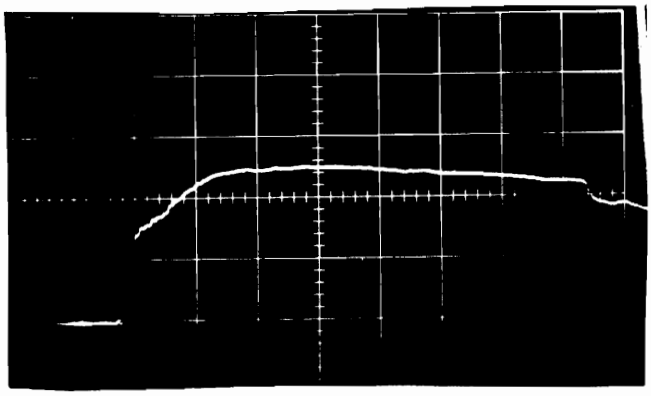

Trace: V_{D1}

S_V: 50 mV/div

S_H: 50 ns/div

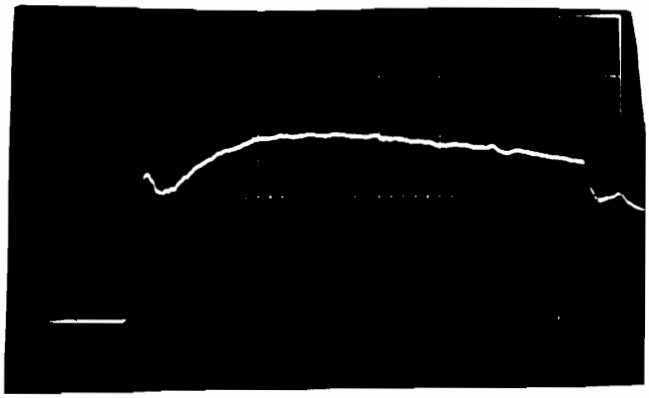

Trace: V_{B2}

S_V: 20 mV/div

S_H: 50 ns/div

Date: 9-27-78
Time: 11:19
Conductor Type: BCW
Test Voltage: 80 kV

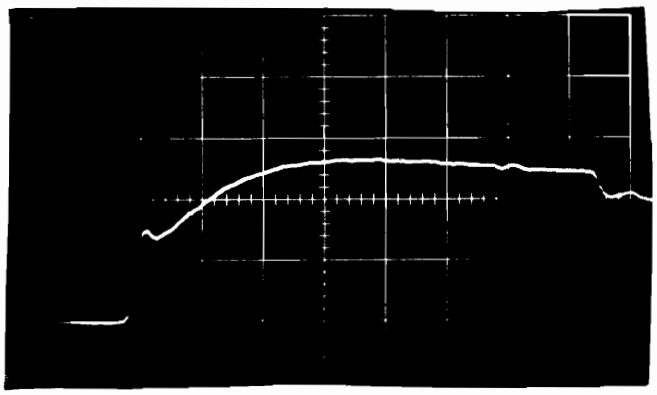

Trace: V_{D2}

S_V: 50 mV/div

S_H: 50 ns/div

Figure A41
Raw Test Data

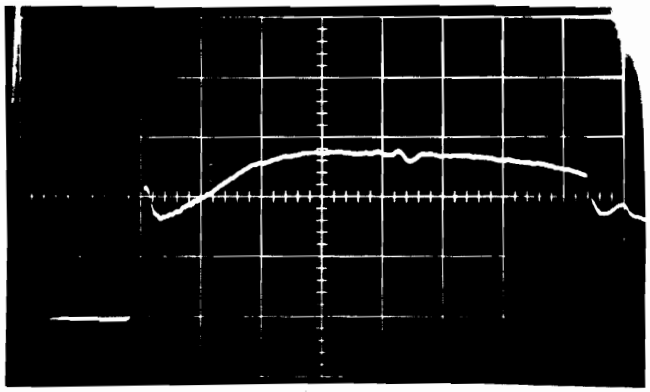

Trace: V_{B3}

S_V: 20 mV/div

S_H: 50 ns/div

Date: 9-27-78
Time: 11:23
Conductor Type: BCW
Test Voltage: 80 kV

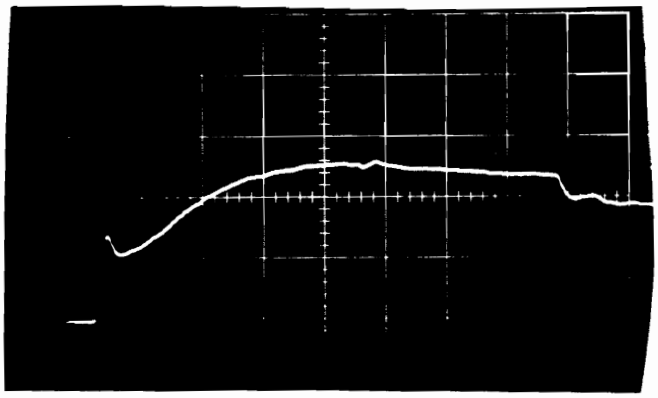

Trace: V_{D3}

S_V: 50 mV/div

S_H: 50 ns/div

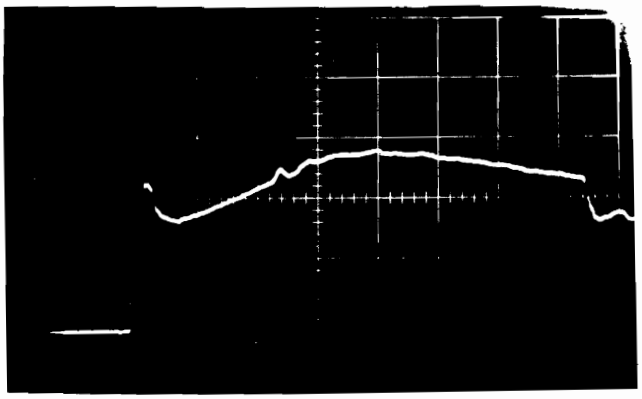

Trace: V_{B4}

S_V: 20 mV/div

S_H: 50 ns/div

Date: 9-27-78
Time: 11:28
Conductor Type: BCW
Test Voltage: 80 kV

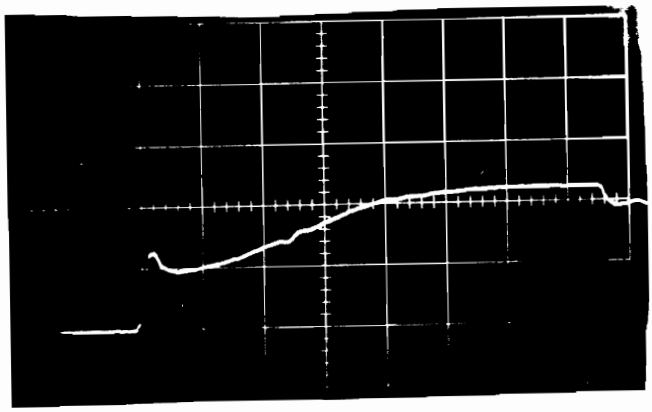

Trace: V_{D4}

S_V: 50 mV/div

S_H: 50 ns/div

Figure A42

Raw Test Data

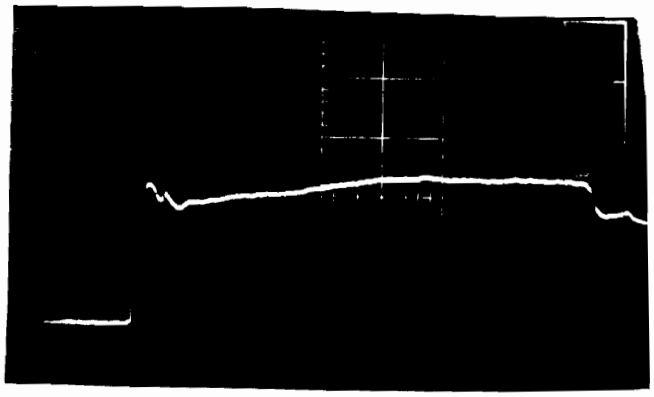

Trace: V_{B5}

S_V: 20 mV/div

S_H: 50 ns/div

Date: 9-27-78
Time: 11:35
Conductor Type: BCW
Test Voltage 80 kV

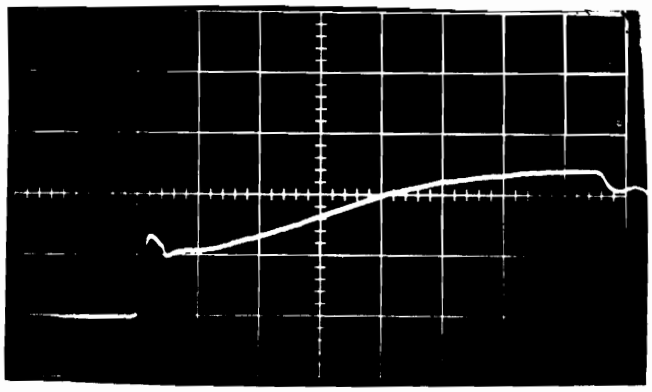

Trace: V_{D5}

S_V: 50 mV/div

S_H: 50 ns/div

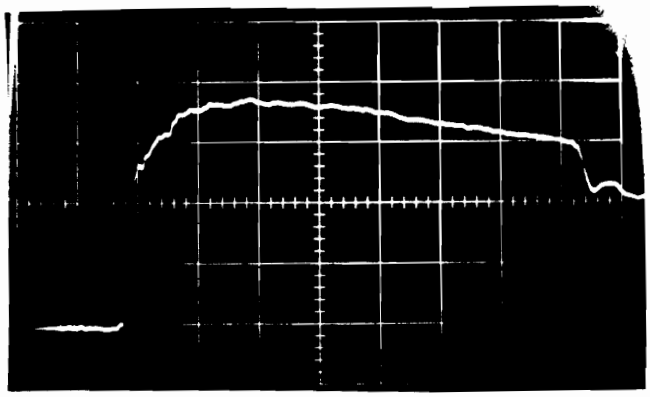

Trace: V_{B1}

S_V: 20 mV/div

S_H: 50 ns/div

Date: 9-27-78
Time: 13:20
Conductor Type: BCW
Test Voltage: 90 kV

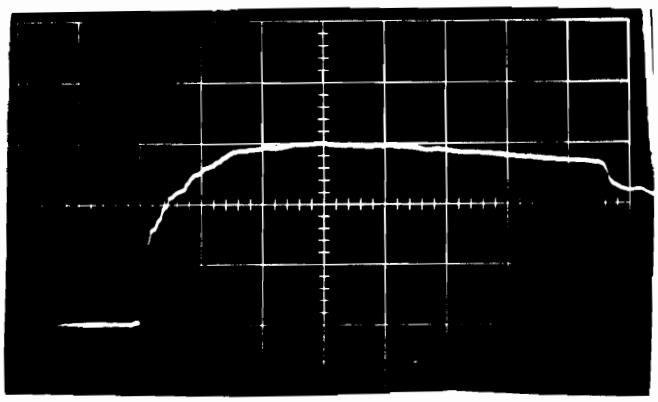

Trace: V_{D1}

S_V: 50 mV/div

S_H: 50 ns/div

Figure A43
Raw Test Data

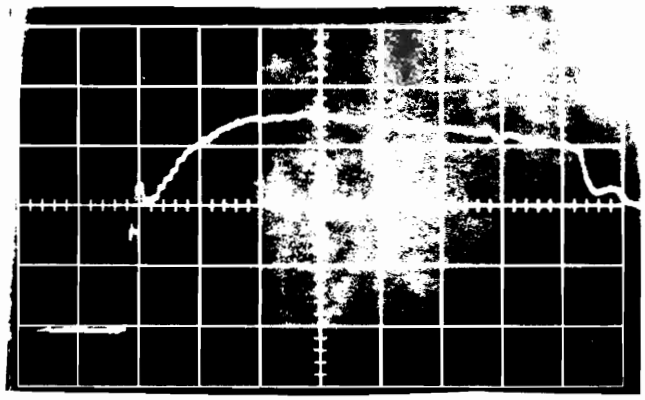

Trace: V_{B2}

S_V: 20 mV/div

S_H: 50 ns/div

Date: 9-27-78
Time: 13:25
Conductor Type: BCW
Test Voltage: 90 kV

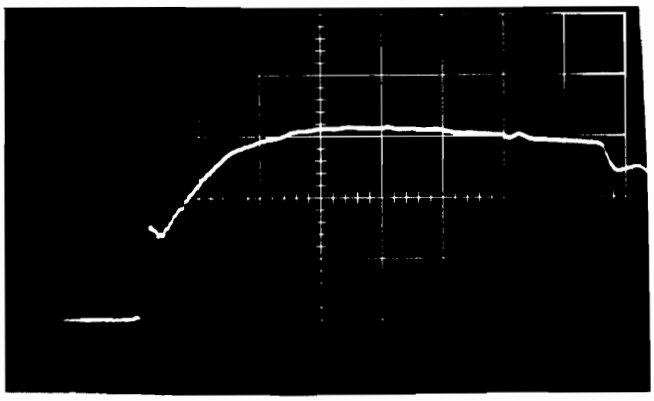

Trace: V_{D2}

S_V: 50 mV/div

S_H: 50 ns/div

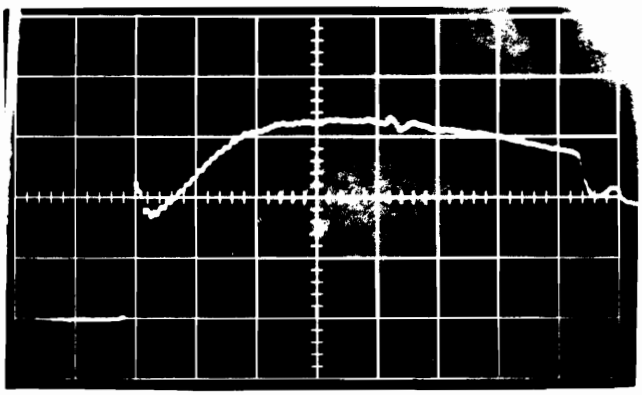

Trace: V_{B3}

S_V: 20 mV/div

S_H: 50 ns/div

Date: 9-27-78
Time: 13:30
Conductor Type: BCW
Test Voltage: 90 kV

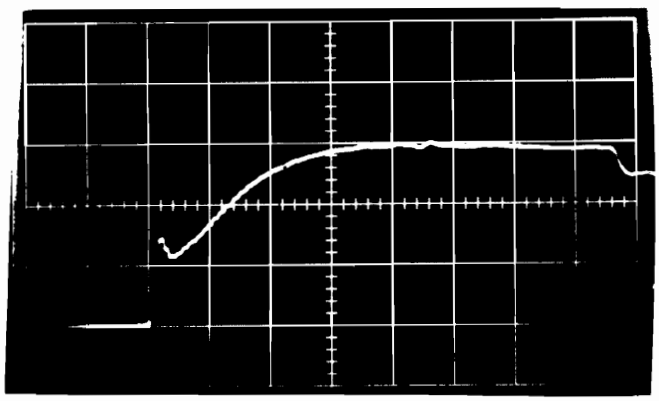

Trace: V_{D3}

S_V: 50 mV/div

S_H: 50 ns/div

Figure A44
Raw Test Data

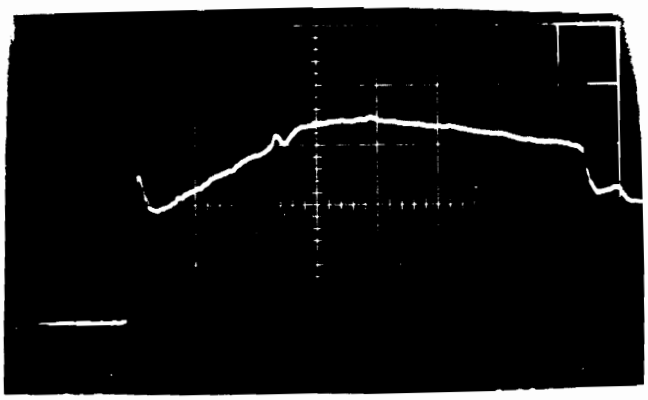

Trace: V_{B4}

S_V: 20 mV/div

S_H: 50 ns/div

Date: 9-27-78
Time: 13:34
Conductor Type: BCW
Test Voltage: 90 kV

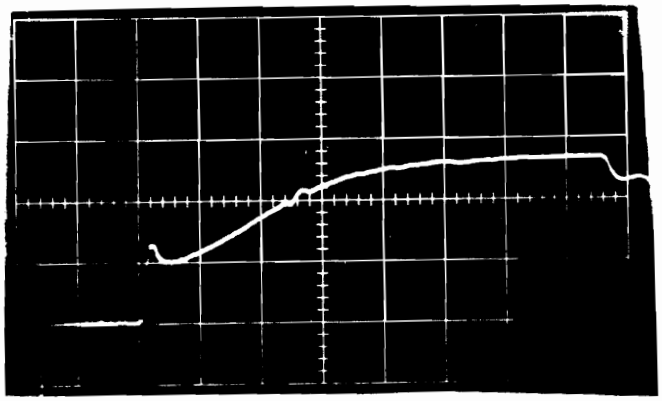

Trace: V_{D4}

S_V: 50 mV/div

S_H: 50 ns/div

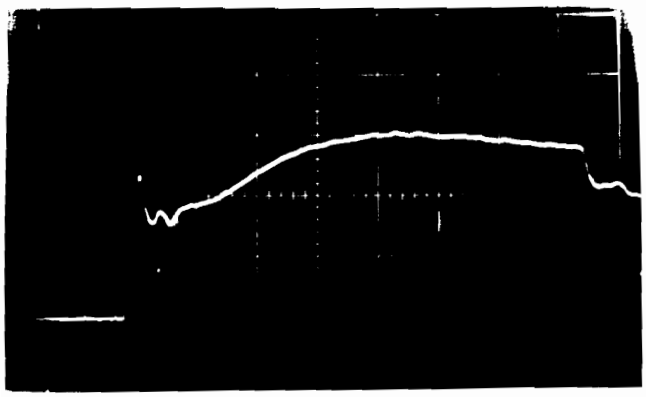

Trace: V_{B5}

S_V: 20 mV/div

S_H: 50 ns/div

Date: 9-27-78
Time: 13:38
Conductor Type: BCW
Test Voltage: 90 kV

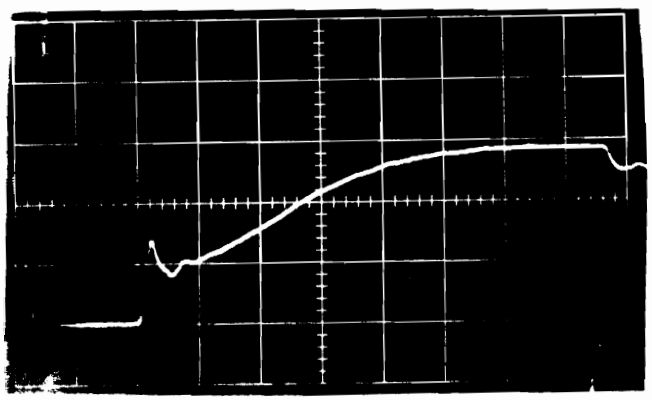

Trace: V_{D5}

S_V: 50 mV/div

S_H: 50 ns/div

Figure A45
Raw Test Data

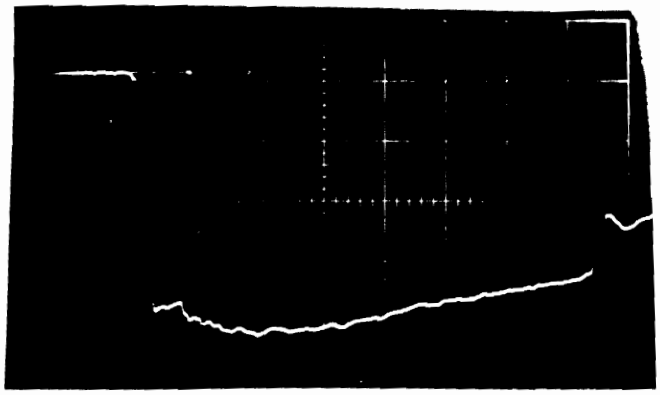

Trace: V_{B1}

S_V: 10 mV/div

S_H: 50 ns/div

Date: 9-26-78
Time: 11:15
Conductor Type: BCW
Test Voltage: -60 kV

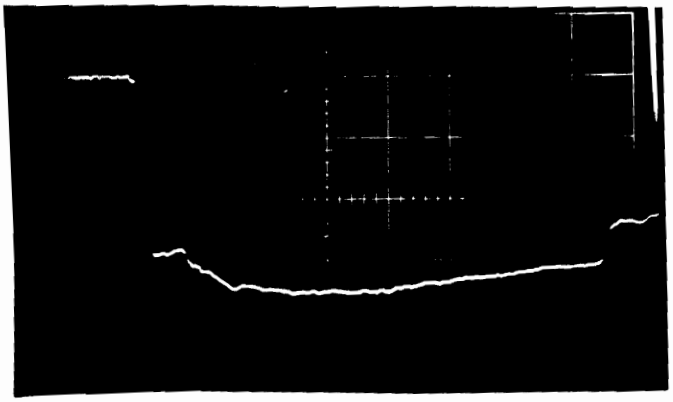

Trace: V_{D1}

S_V: 20 mV/div

S_H: 50 ns/div

Trace: V_{B2}

S_V: 10 mV/div

S_H: 50 ns/div

Date: 9-26-78
Time: 11:11
Conductor Type: BCW
Test Voltage: -60 kV

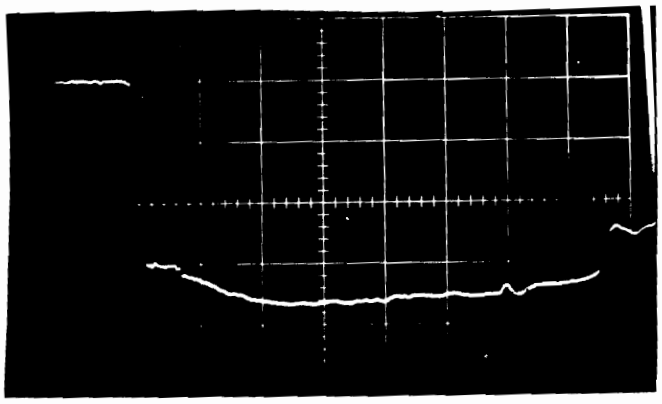

Trace: V_{D2}

S_V: 20 mV/div

S_H: 50 ns/div

Figure A46
Raw Test Data

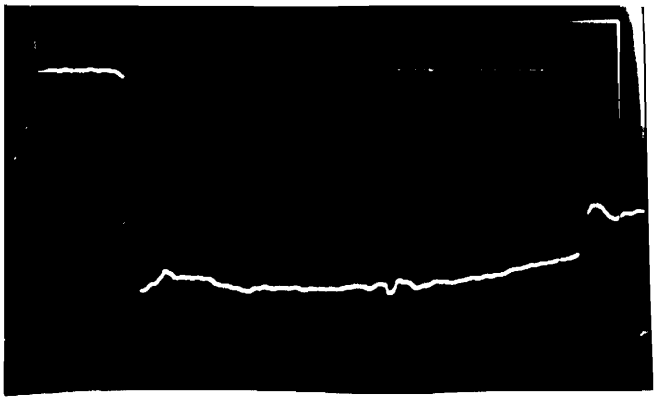

Trace: V_{B3}

S_V: 10 mV/div

S_H: 50 ns/div

Date: 9-26-78
Time: 11:05
Conductor Type: BCW
Test Voltage: -60 kV

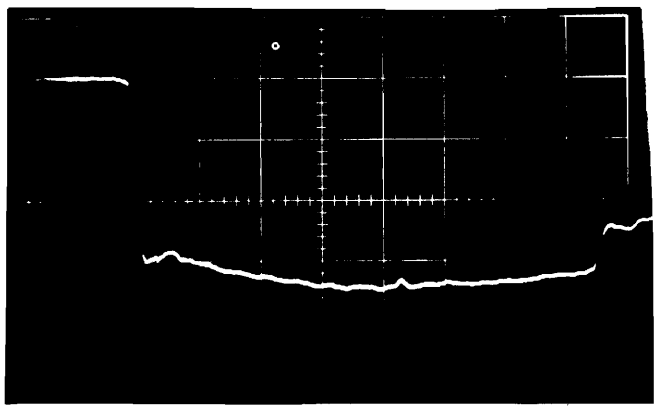

Trace: V_{D3}

S_V: 20 mV/div

S_H: 50 ns/div

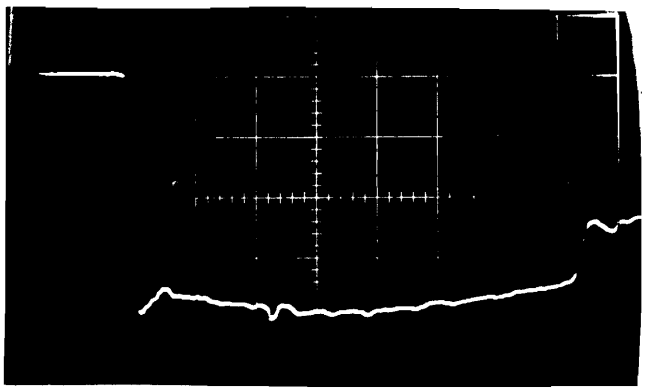

Trace: V_{B4}

S_V: 10 mV/div

S_H: 50 ns/div

Date: 9-26-78
Time: 10:57
Conductor Type: BCW
Test Voltage: -60 kV

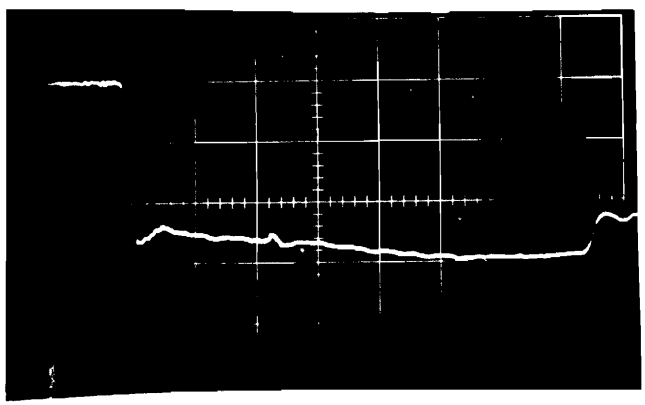

Trace: V_{D4}

S_V: 20 mV/div

S_H: 50 ns/div

Figure A47
Raw Test Data

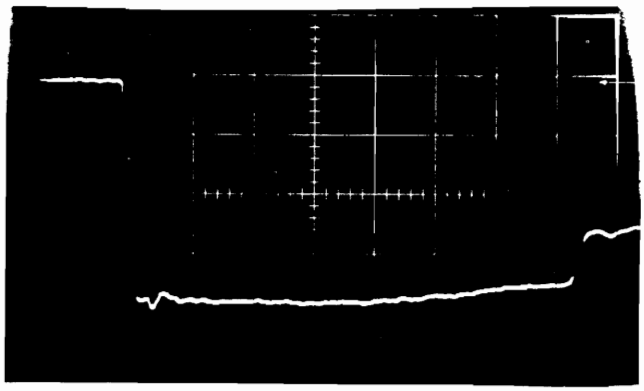

Trace: V_{B5}

S_V: 10 mV/div

S_H: 50 ns/div

Date: 9-26-78
Time: 10:53
Conductor Type: BCW
Test Voltage: -60 kV

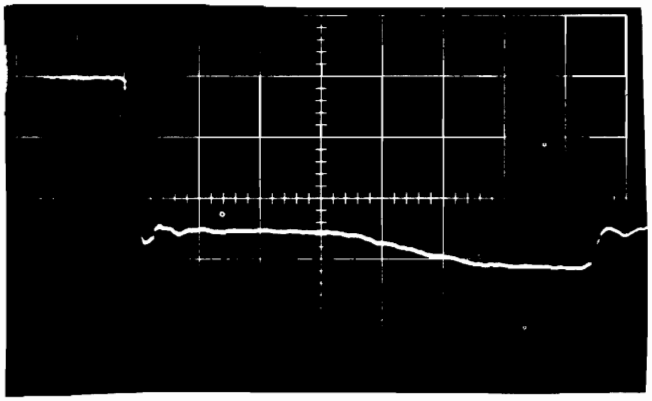

Trace: V_{D5}

S_V: 20 mV/div

S_H: 50 ns/div

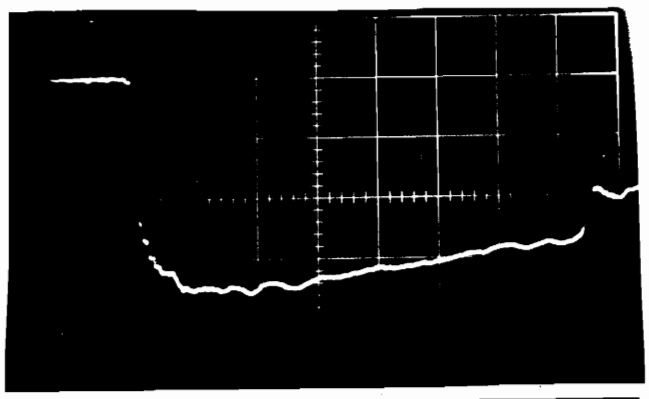

Trace: V_{B1}

S_V: 20 mV/div

S_H: 50 ns/div

Date: 9-26-78
Time: 15:27
Conductor Type: BCW
Test Voltage: -90 kV

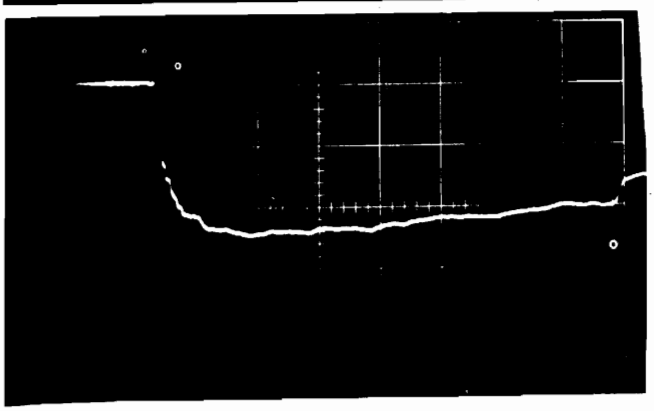

Trace: V_{D1}

S_V: 50 mV/div

S_H: 50 ns/div

Figure A48
Raw Test Data

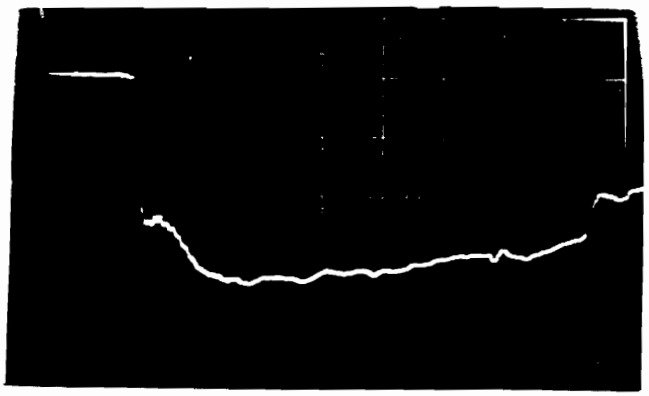

Trace: V_{B2}

S_V: 20 mV/div

S_H: 50 ns/div

Date: 9-26-78
Time: 15:32
Conductor Type: BCW
Test Voltage: -90 kV

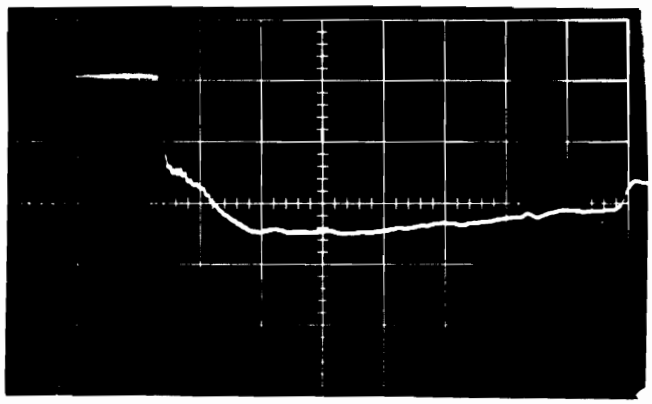

Trace: V_{D2}

S_V: 50 mV/div

S_H: 50 ns/div

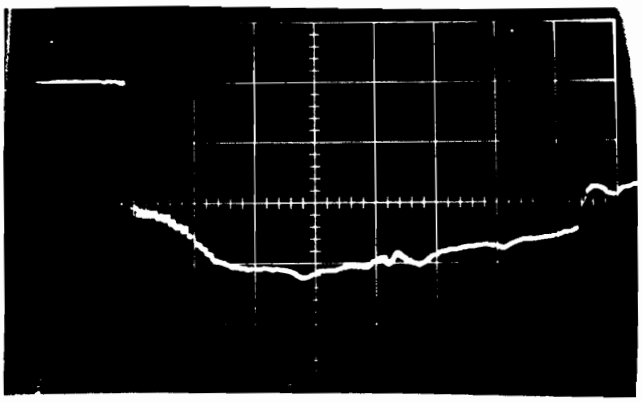

Trace: V_{B3}

S_V: 20 mV/div

S_H: 50 ns/div

Date: 9-26-78
Time: 15:36
Conductor Type: BCW
Test Voltage: -90 kV

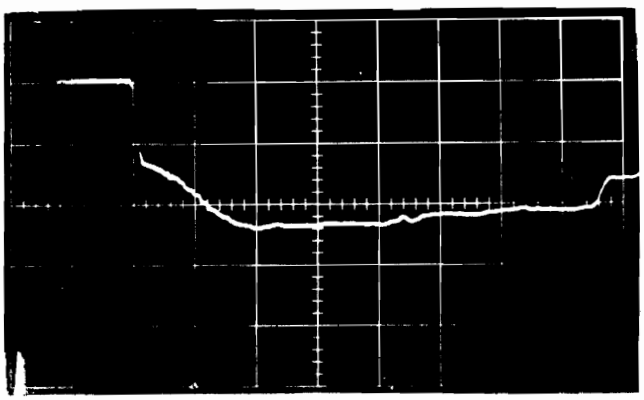

Trace: V_{D3}

S_V: 50 mV/div

S_H: 50 ns/div

Figure A49
Raw Test Data

Trace: V_{B4}

S_V: 20 mV/div

S_H: 50 ns/div

Date: 9-26-78
Time: 15:39
Conductor Type: BCW
Test Voltage: -90 kV

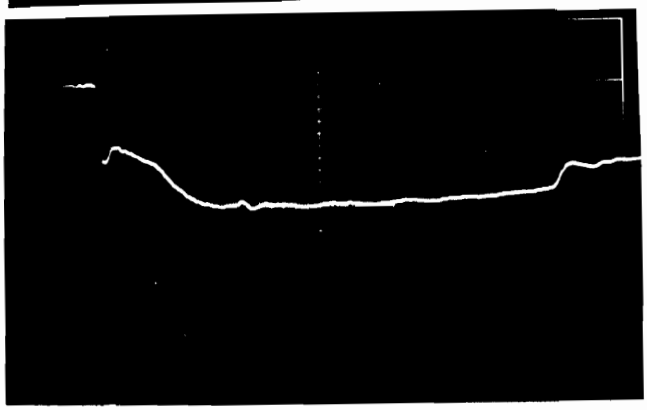

Trace: V_{D4}

S_V: 50 mV/div

S_H: 50 ns/div

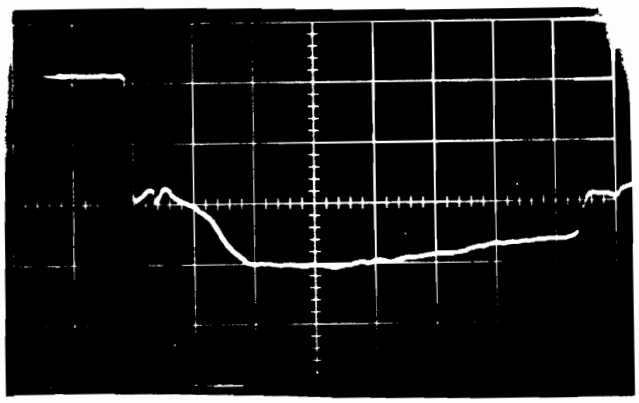

Trace: V_{B5}

S_V: 20 mV/div

S_H: 50 ns/div

Date: 9-26-78
Time: 15:44
Conductor Type: BCW
Test Voltage: -90 kV

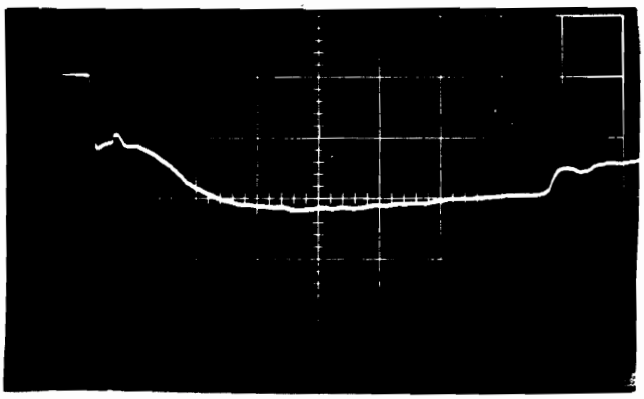

Trace: V_{D5}

S_V: 50 mV/div

S_H: 50 ns/div

Figure A50
Raw Test Data

APPENDIX B

CORRECTED TEST DATA

This appendix consists of corrected station [redacted] data for the bare Al and BeCu test conductors over the full range of test voltages. Figures B19, B20, B23, B24, B27 and B28 include representative raw data points in order to show the increasing importance of the correction procedure as corona effects become more pronounced. In accordance with the discussion presented in Section IV, the correction algorithms are equation (25) which corrects for the nonideal response of electrical integrators, and equation (30) which corrects for test facility cable attenuation. The terminology used in this appendix is as defined by Table A1 except that the form BX is substituted for V_{BX}.

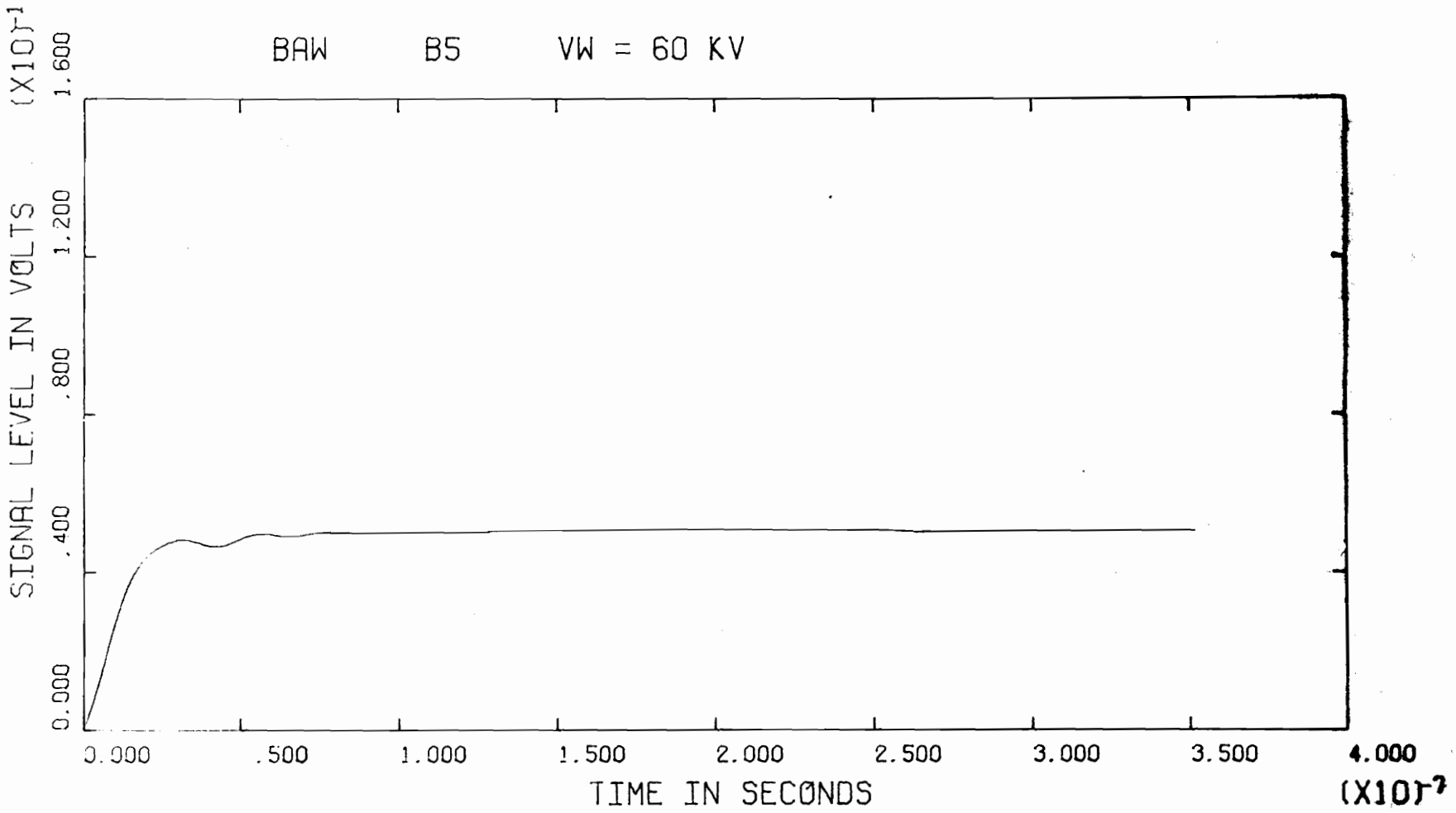

Figure B1

Corrected Test Data

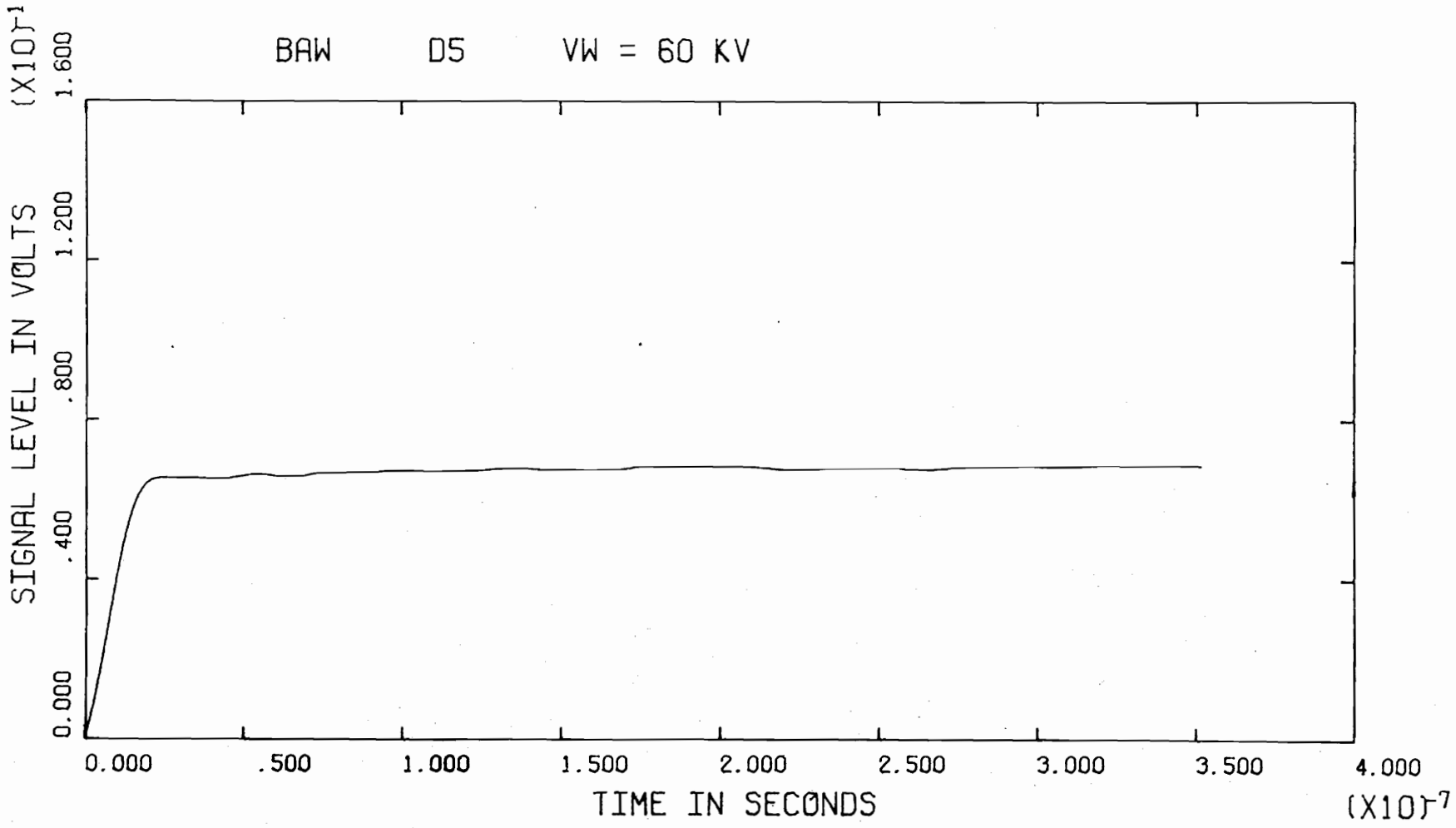

Figure B2

Corrected Test Data

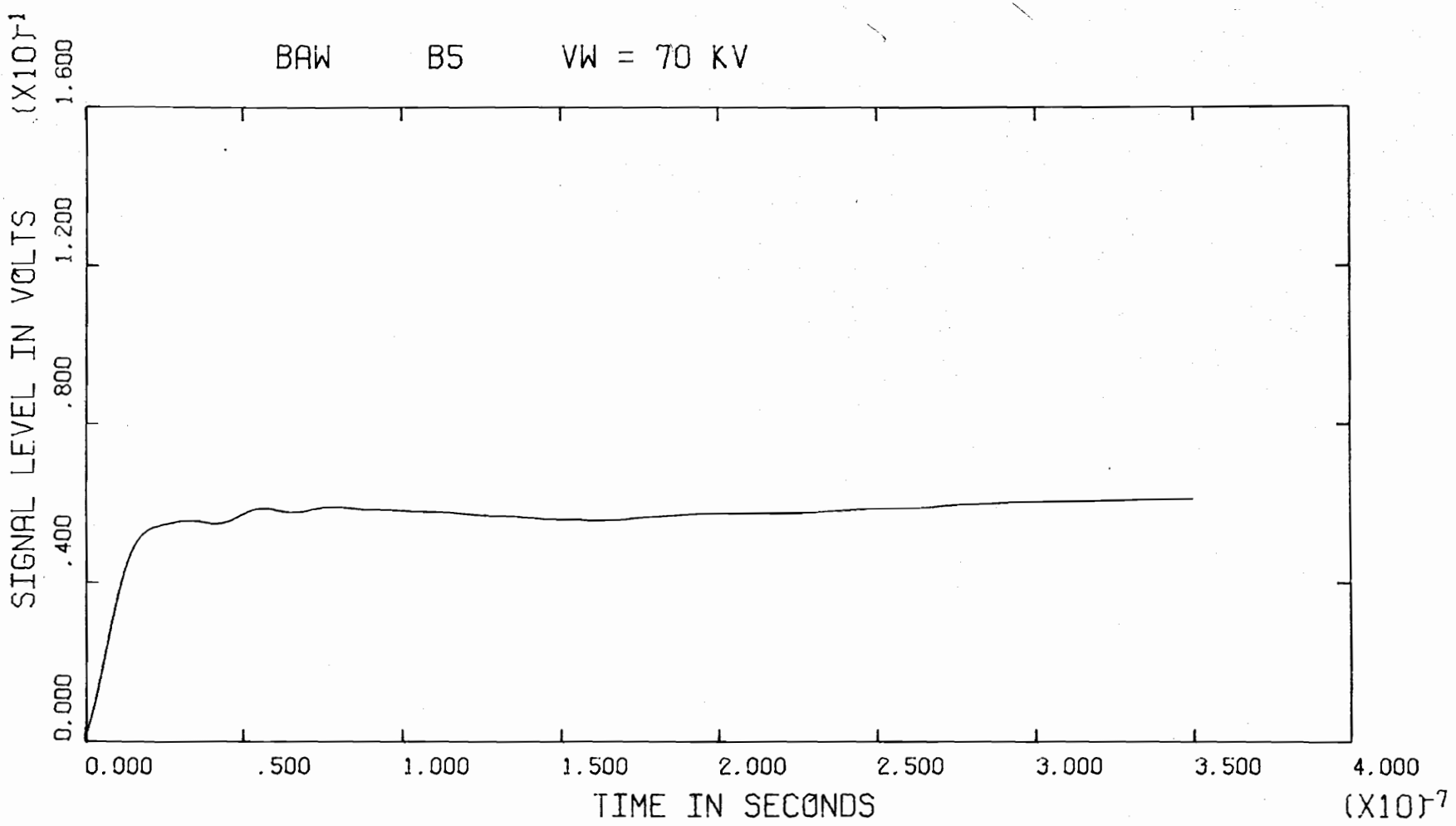

Figure B3

Corrected Test Data

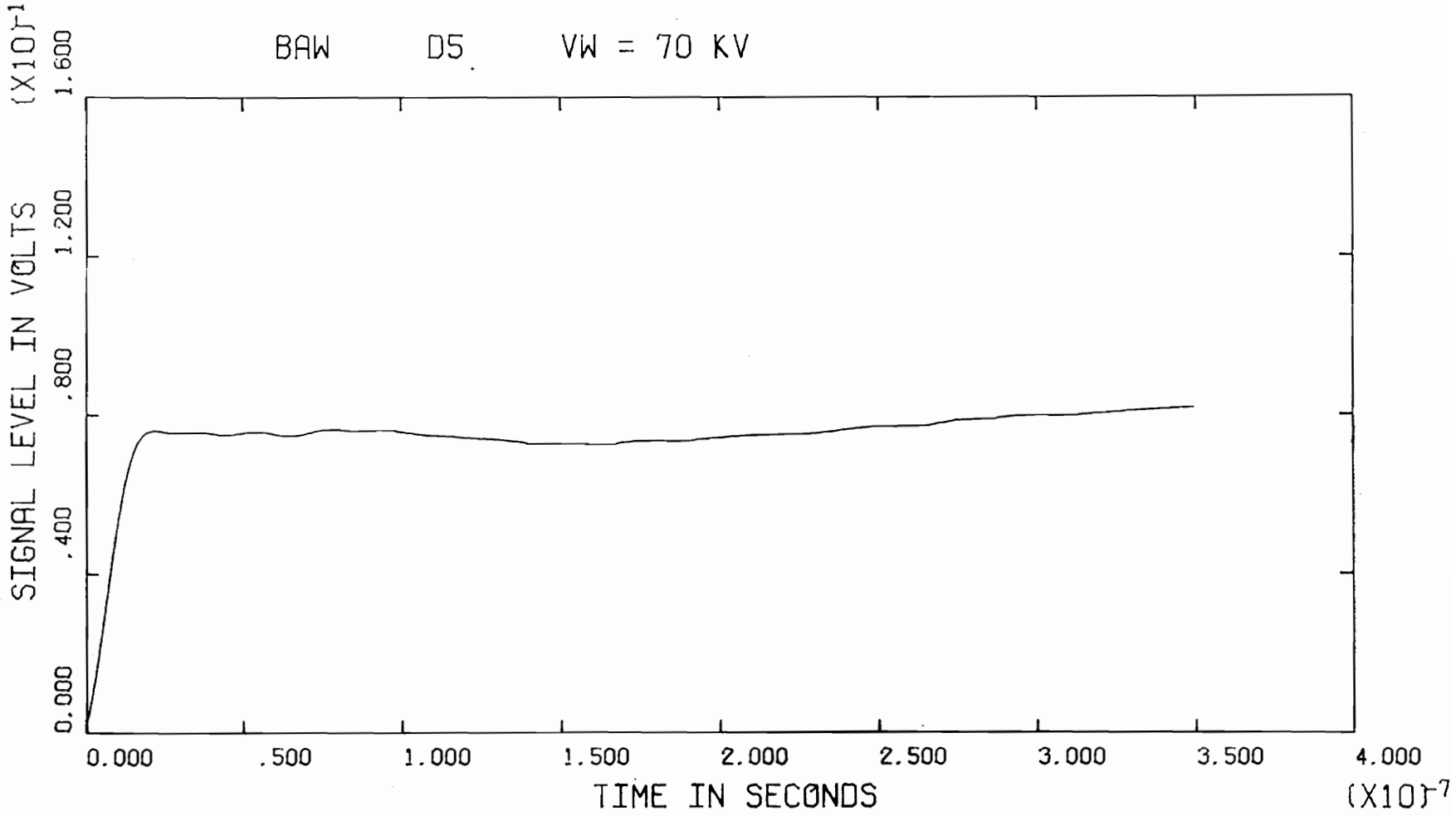

Figure B4

Corrected Test Data

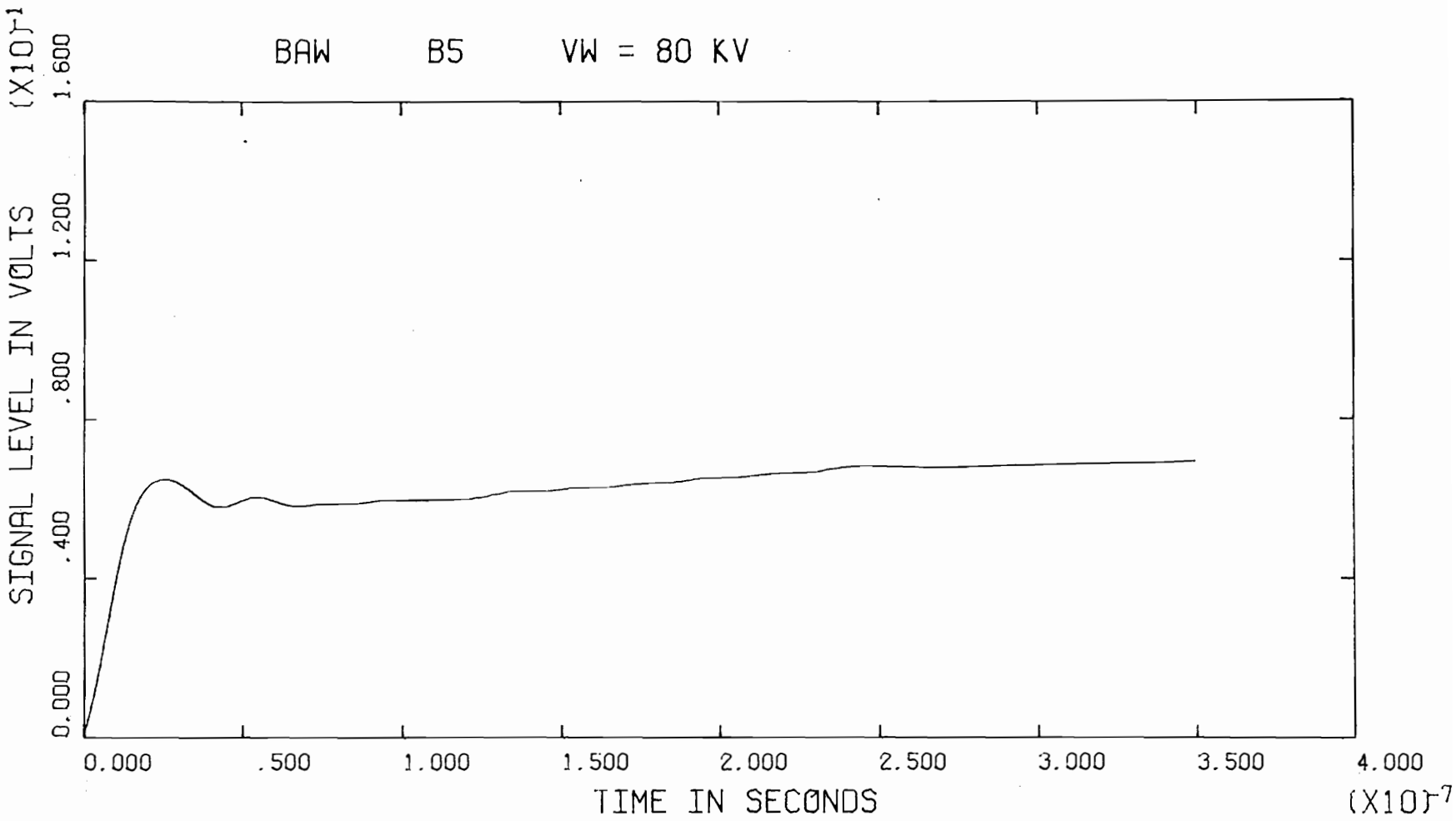

Figure B5

Corrected Test Data

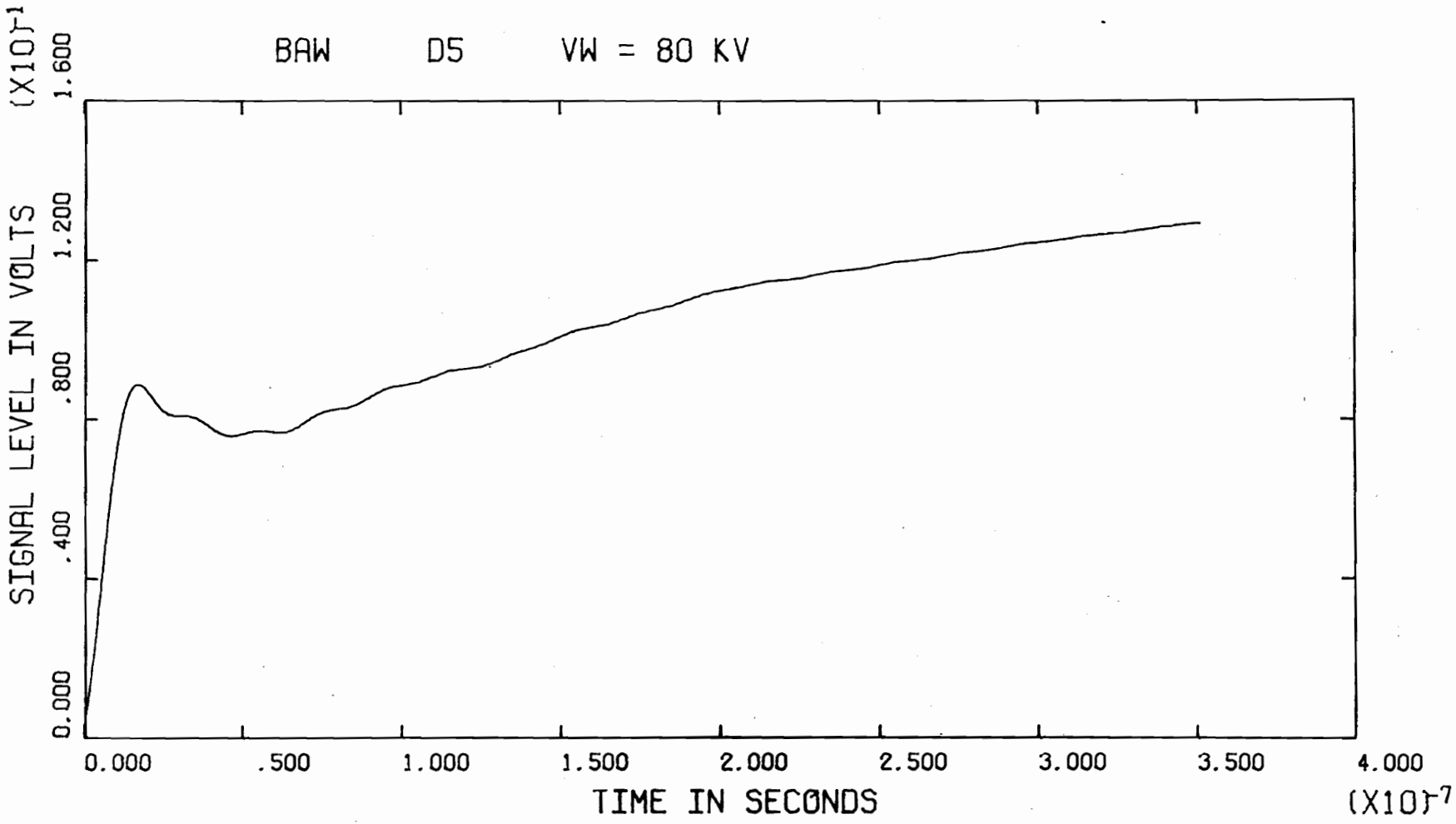

Figure B6

Corrected Test Data

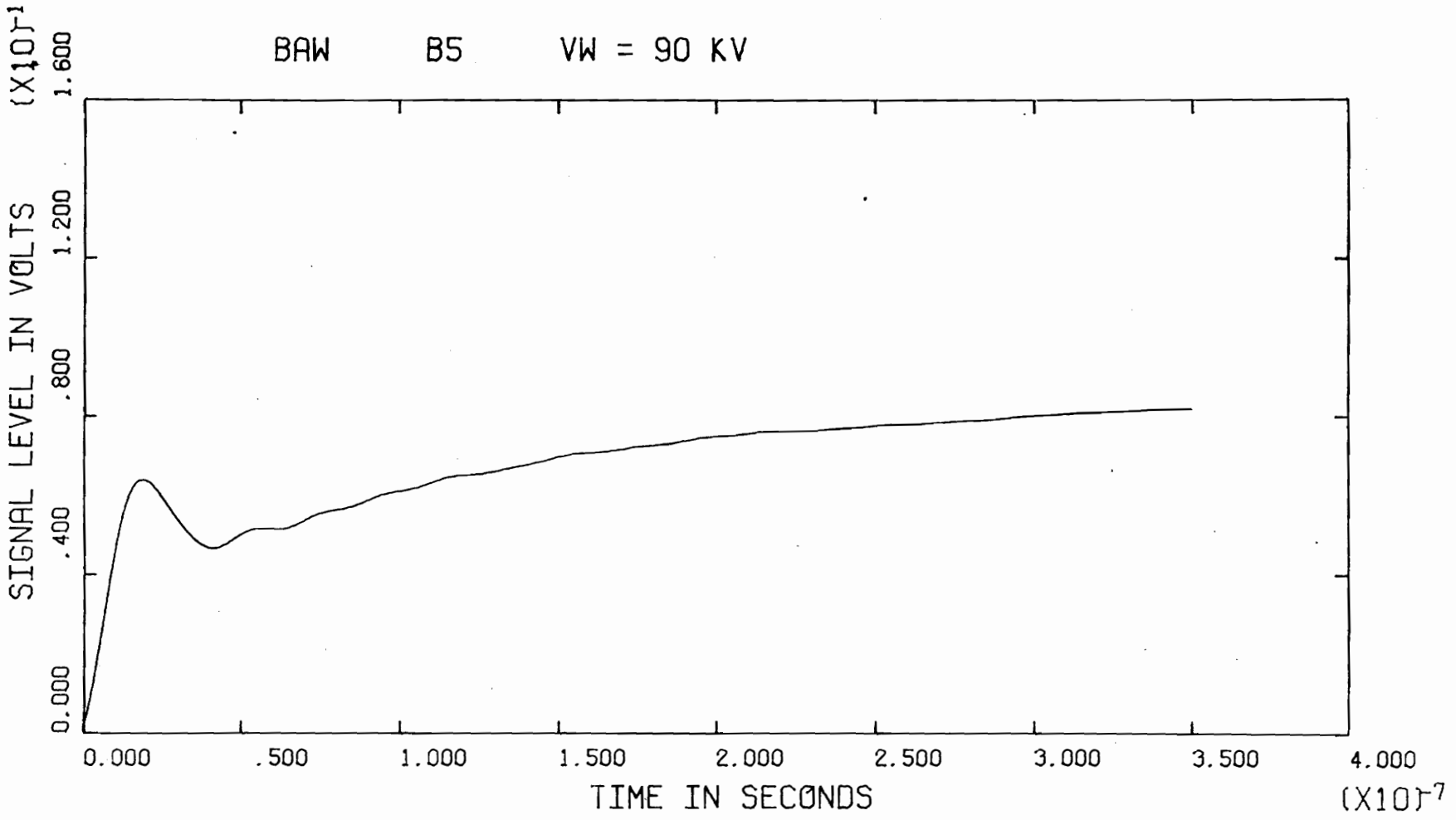

Figure B7

Corrected Test Data

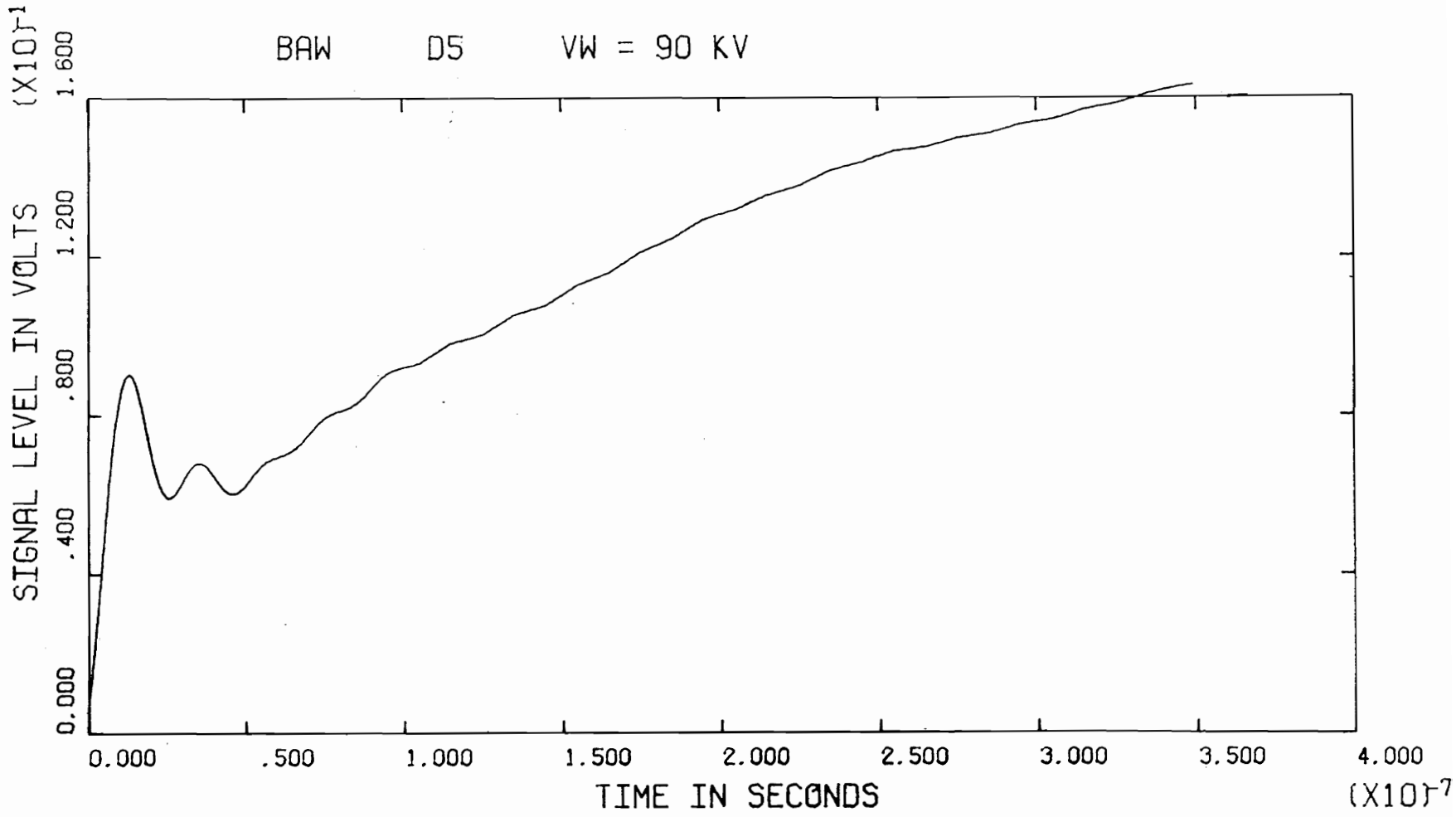

Figure B8

Corrected Test Data

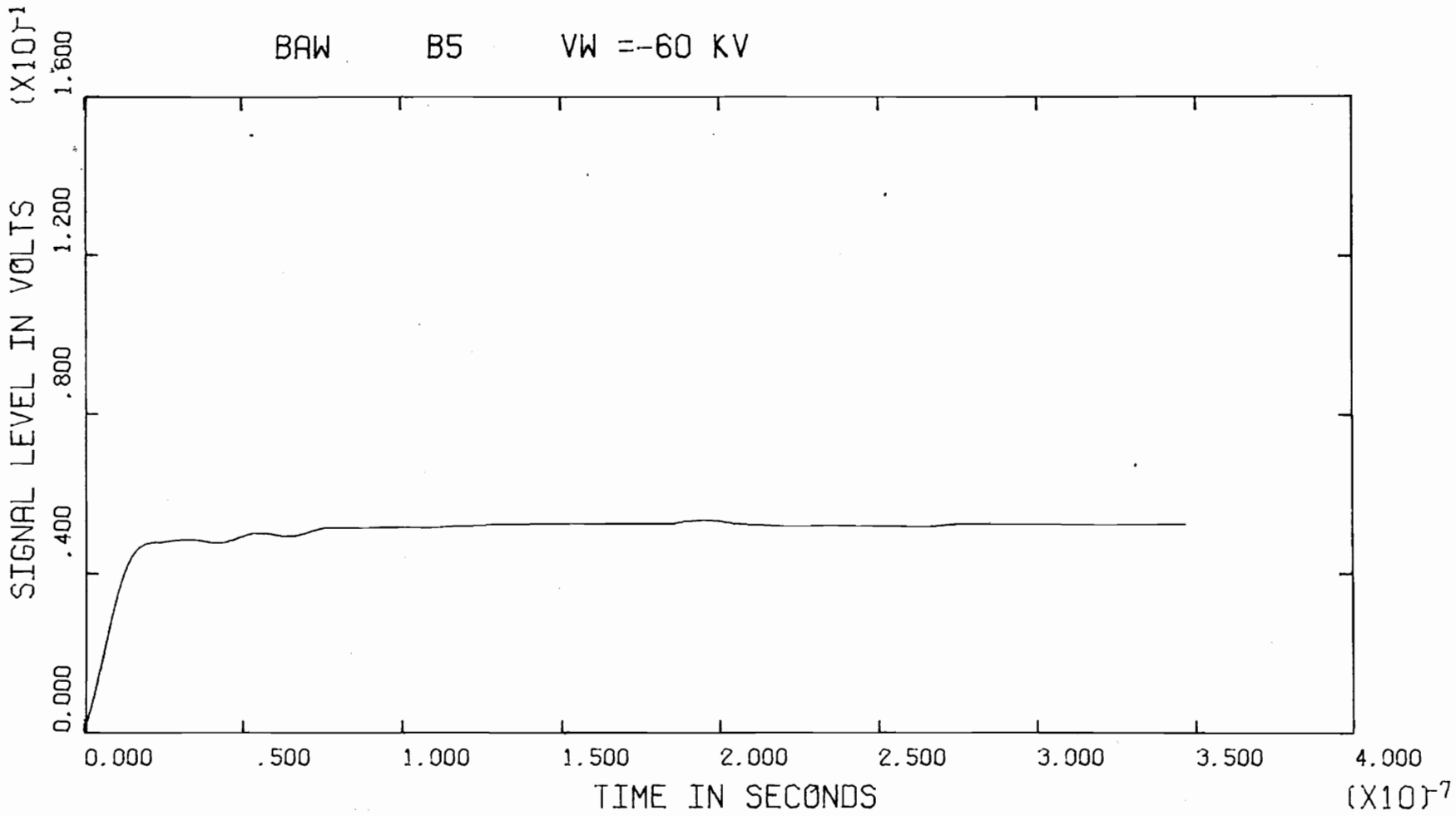

Figure B9

Corrected Test Data

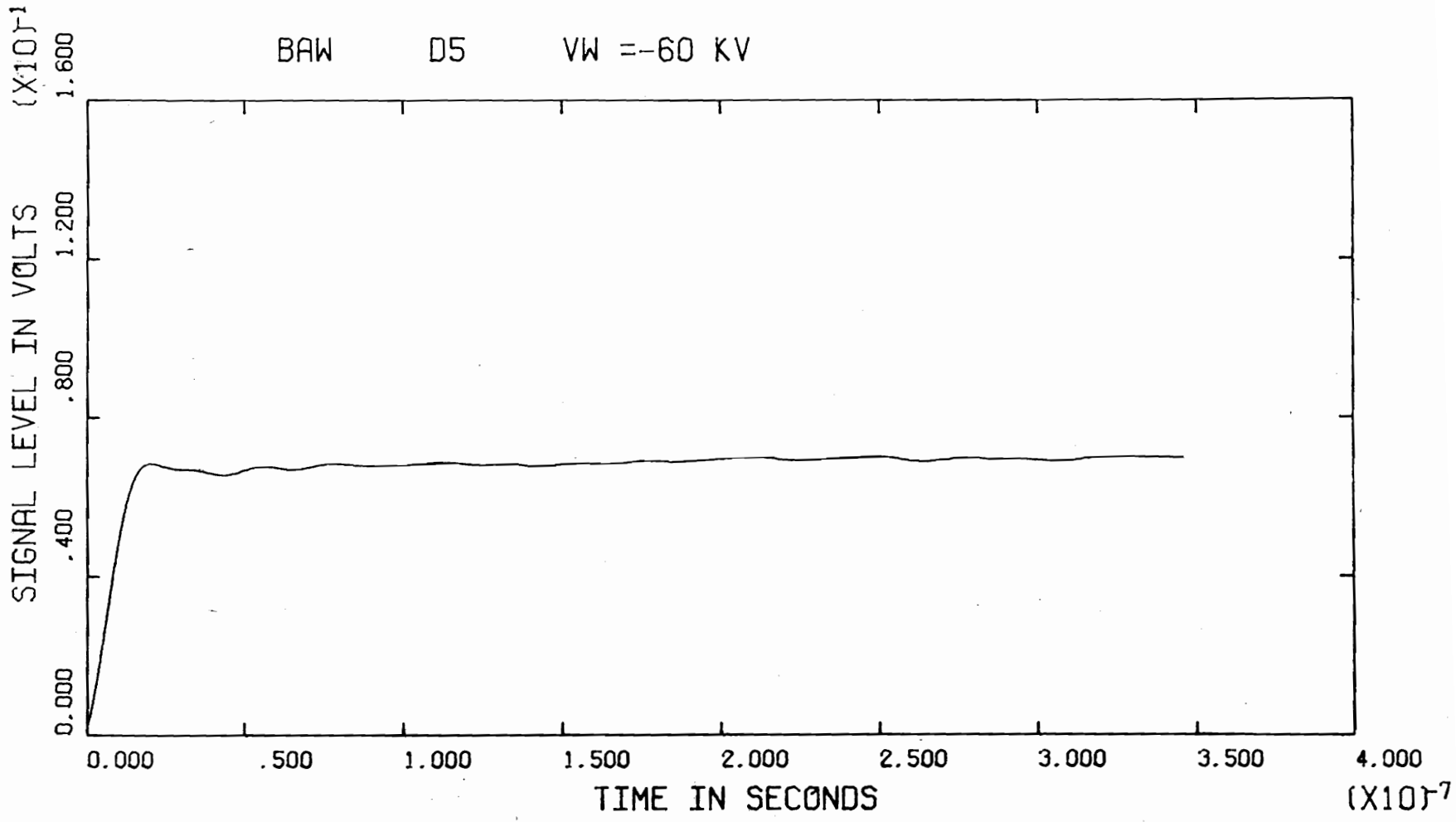

Figure B10

Corrected Test Data

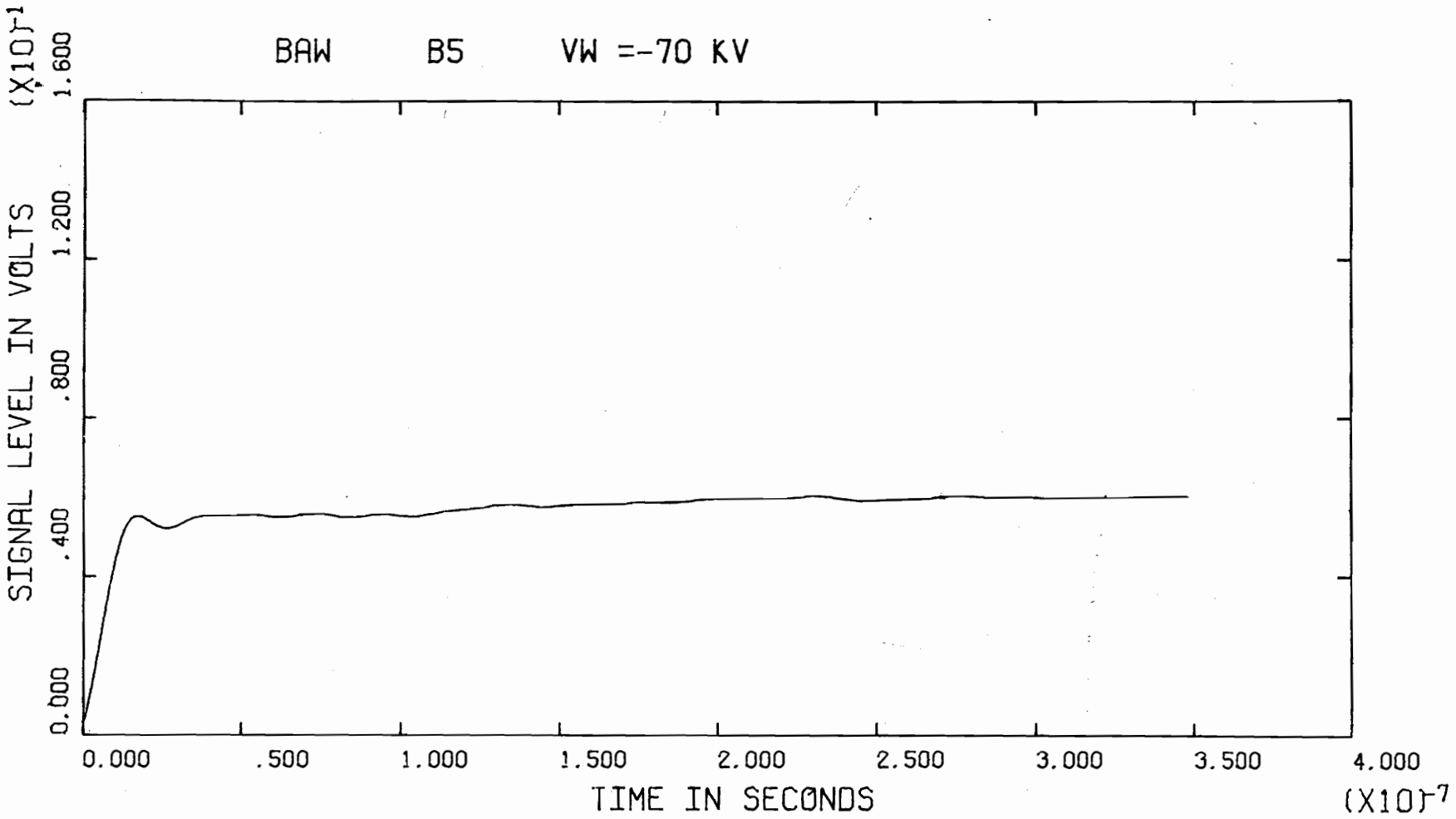

Figure B11

Corrected Test Data

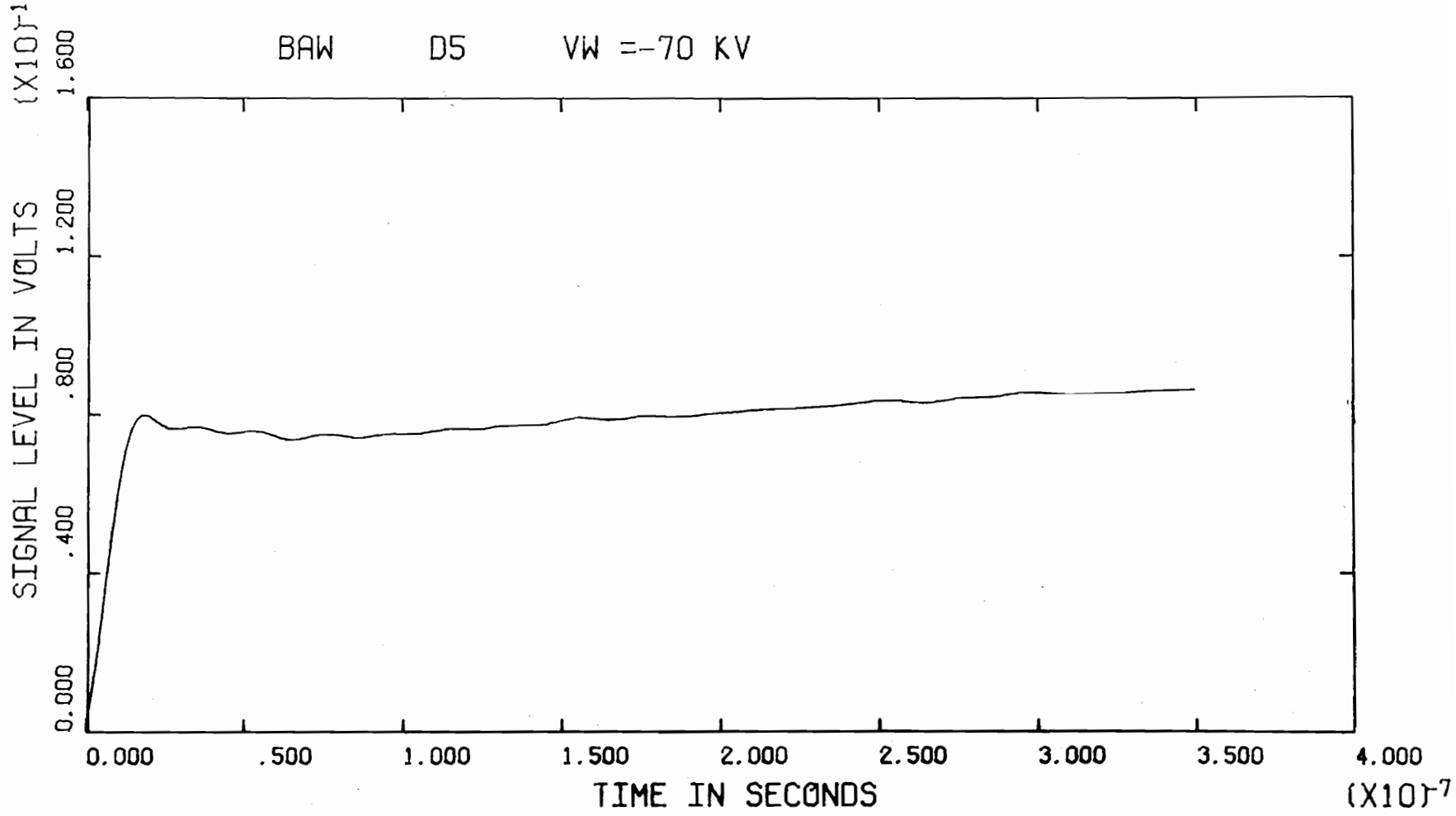

Figure B12

Corrected Test Data

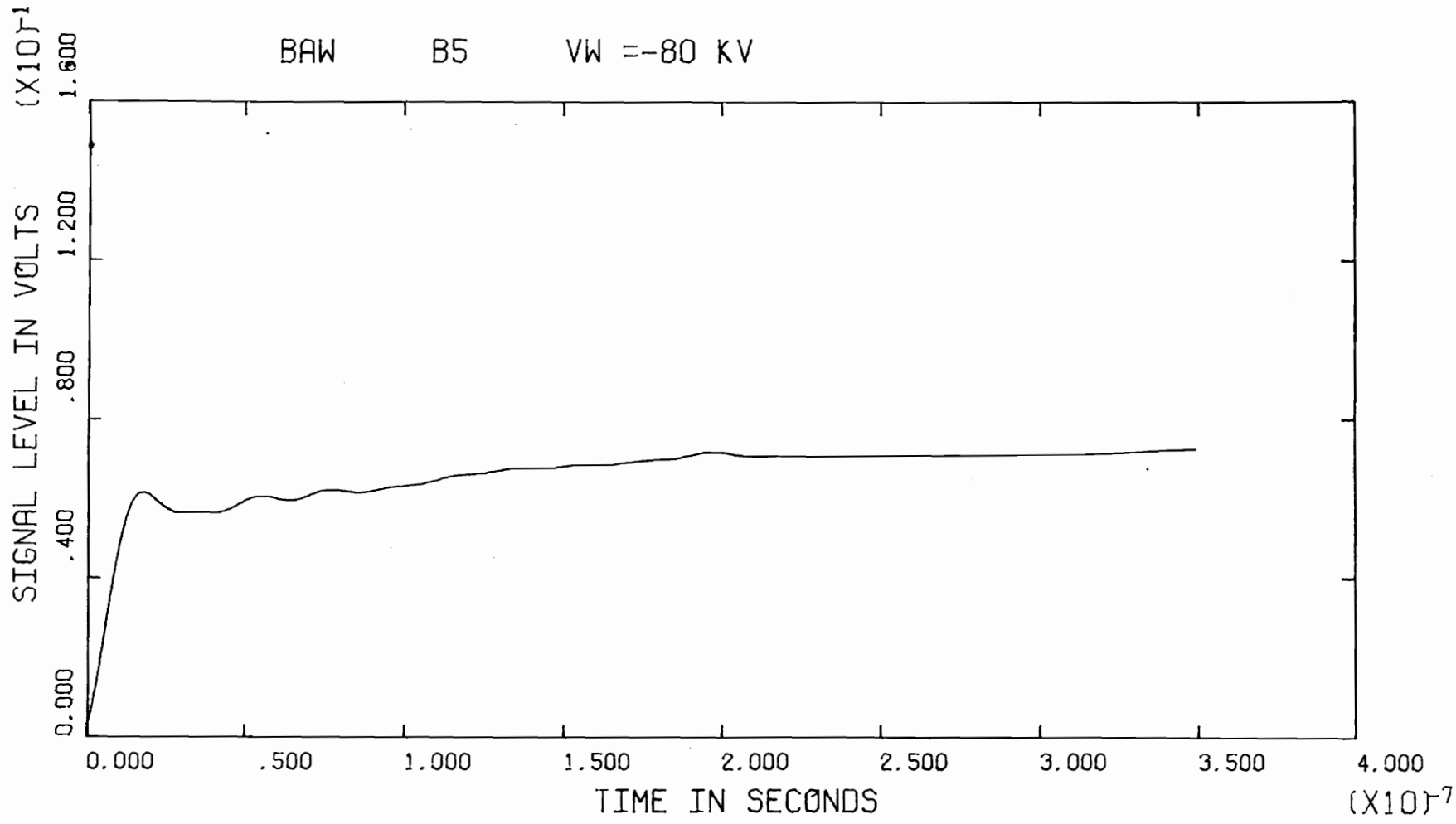

Figure B13

Corrected Test Data

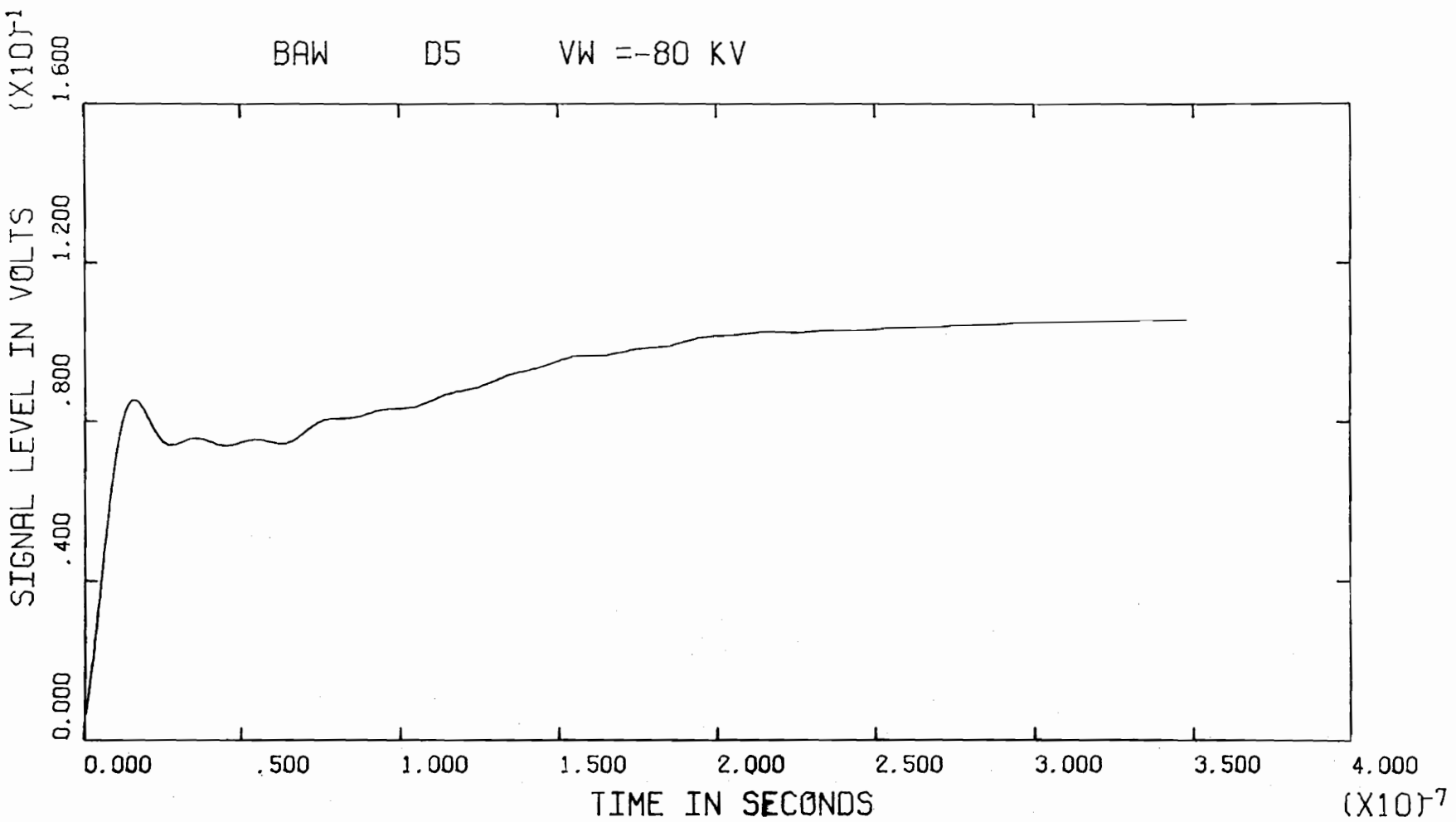

Figure B14

Corrected Test Data

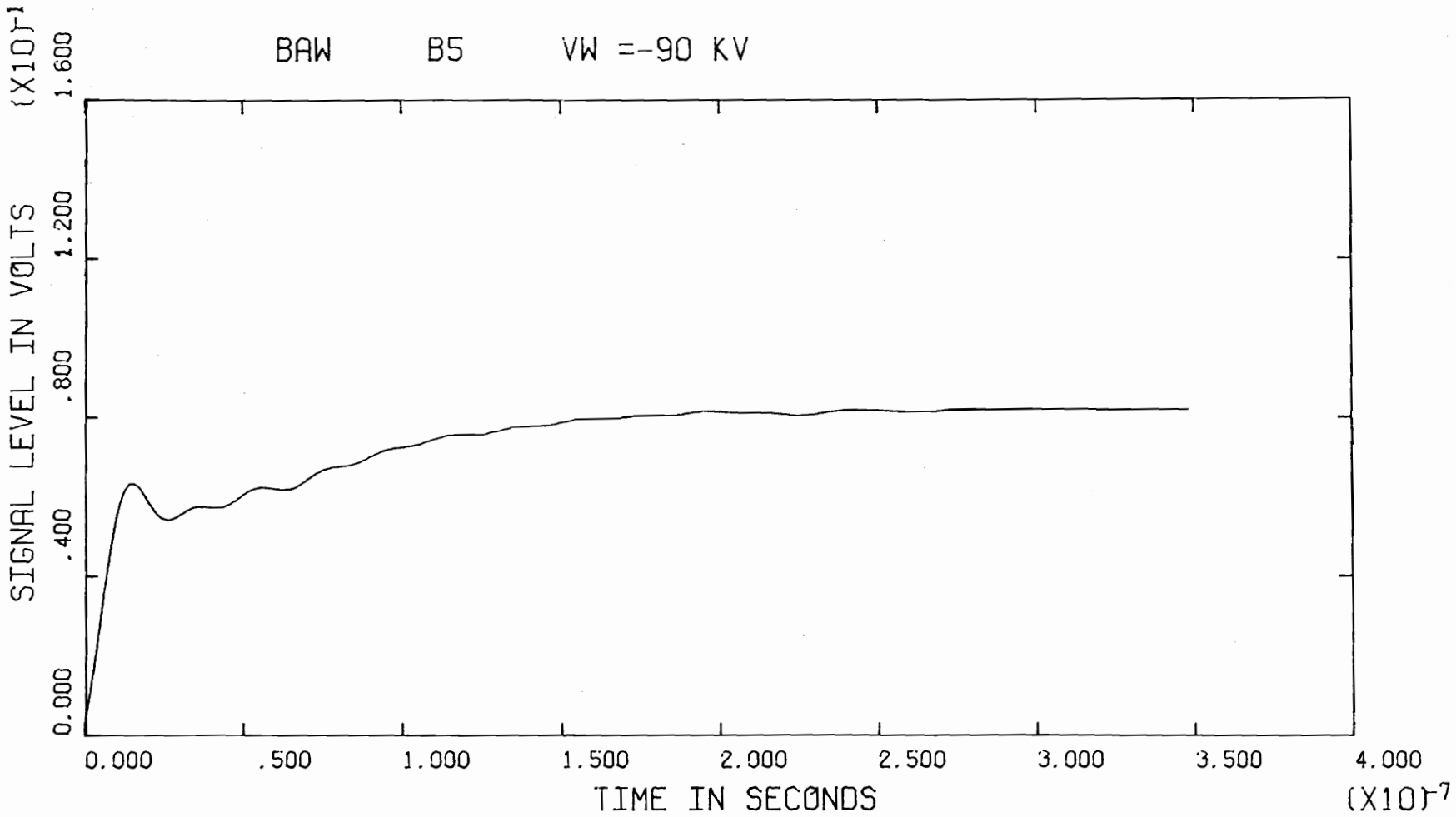

Figure B15

Corrected Test Data

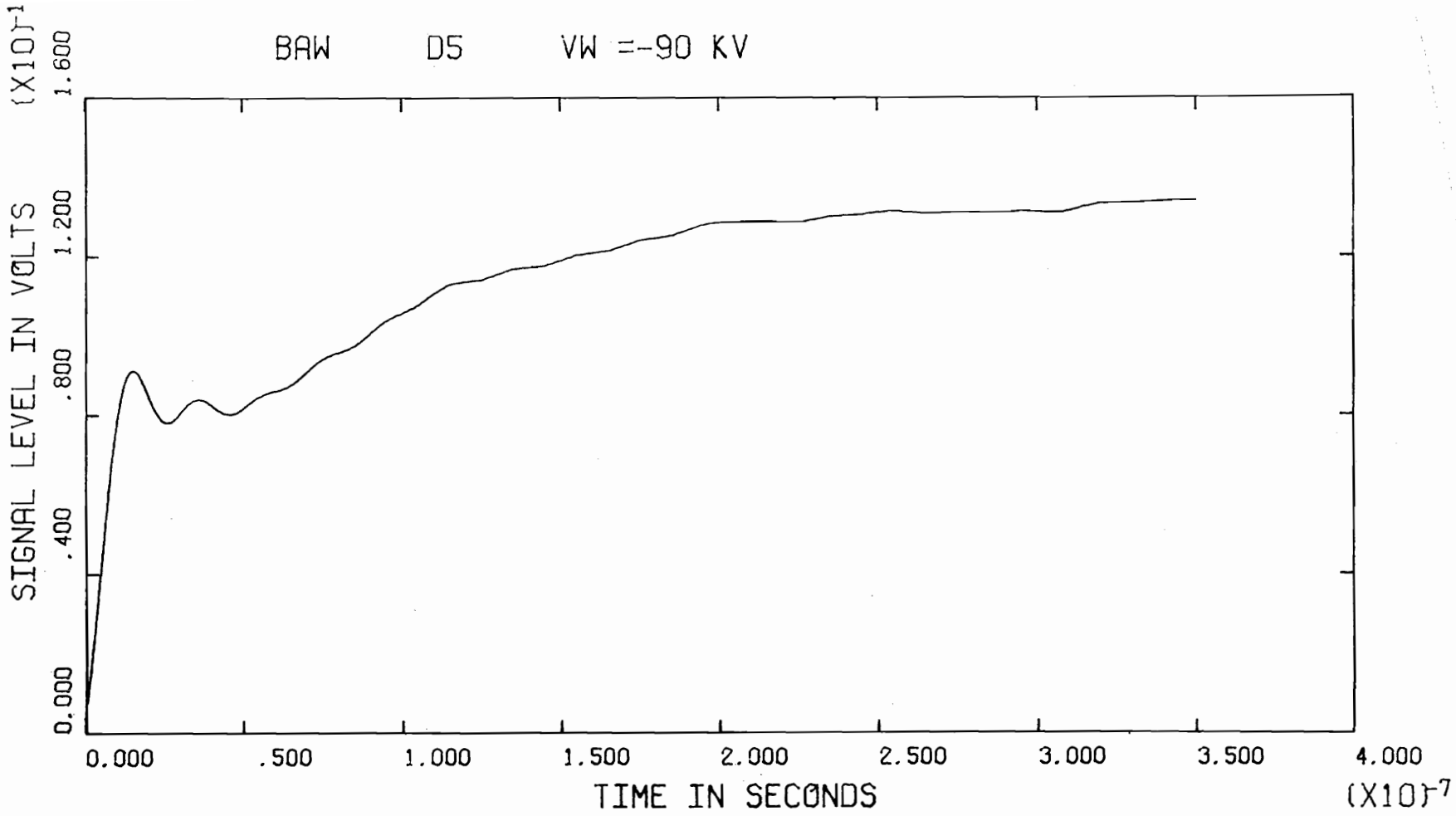

Figure B16

Corrected Test Data

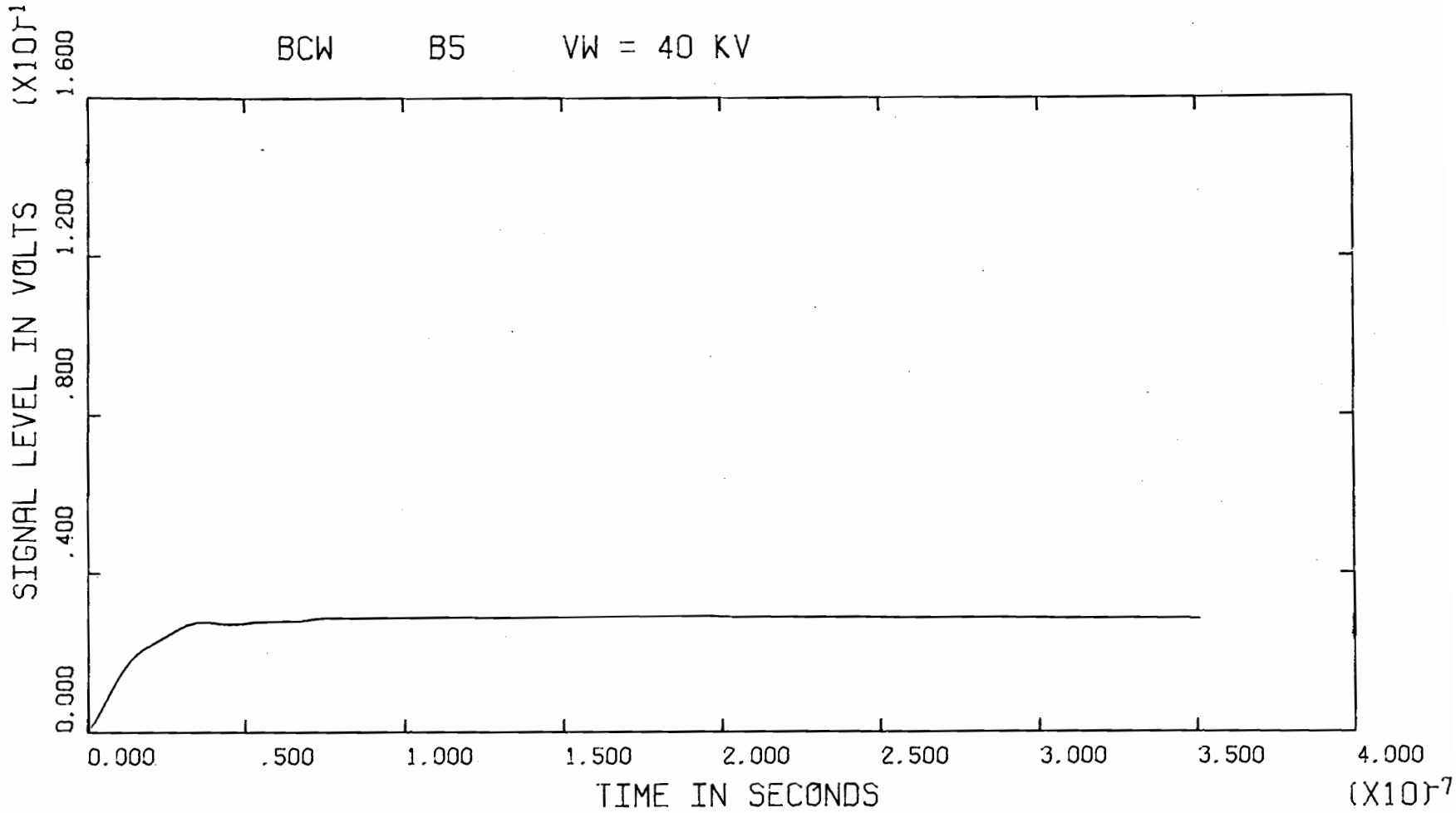

Figure B17

Corrected Test Data

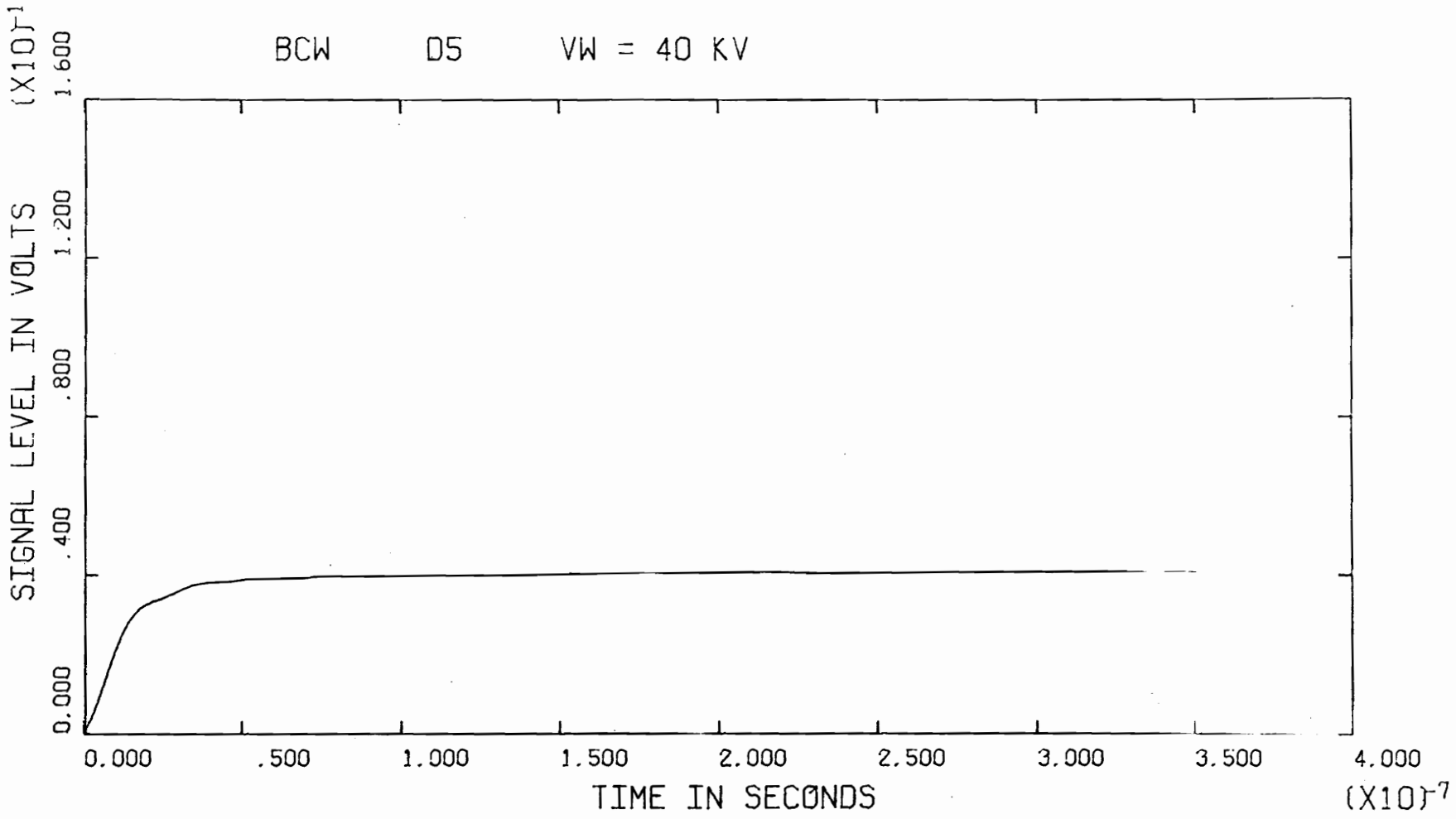

Figure B18

Corrected Test Data

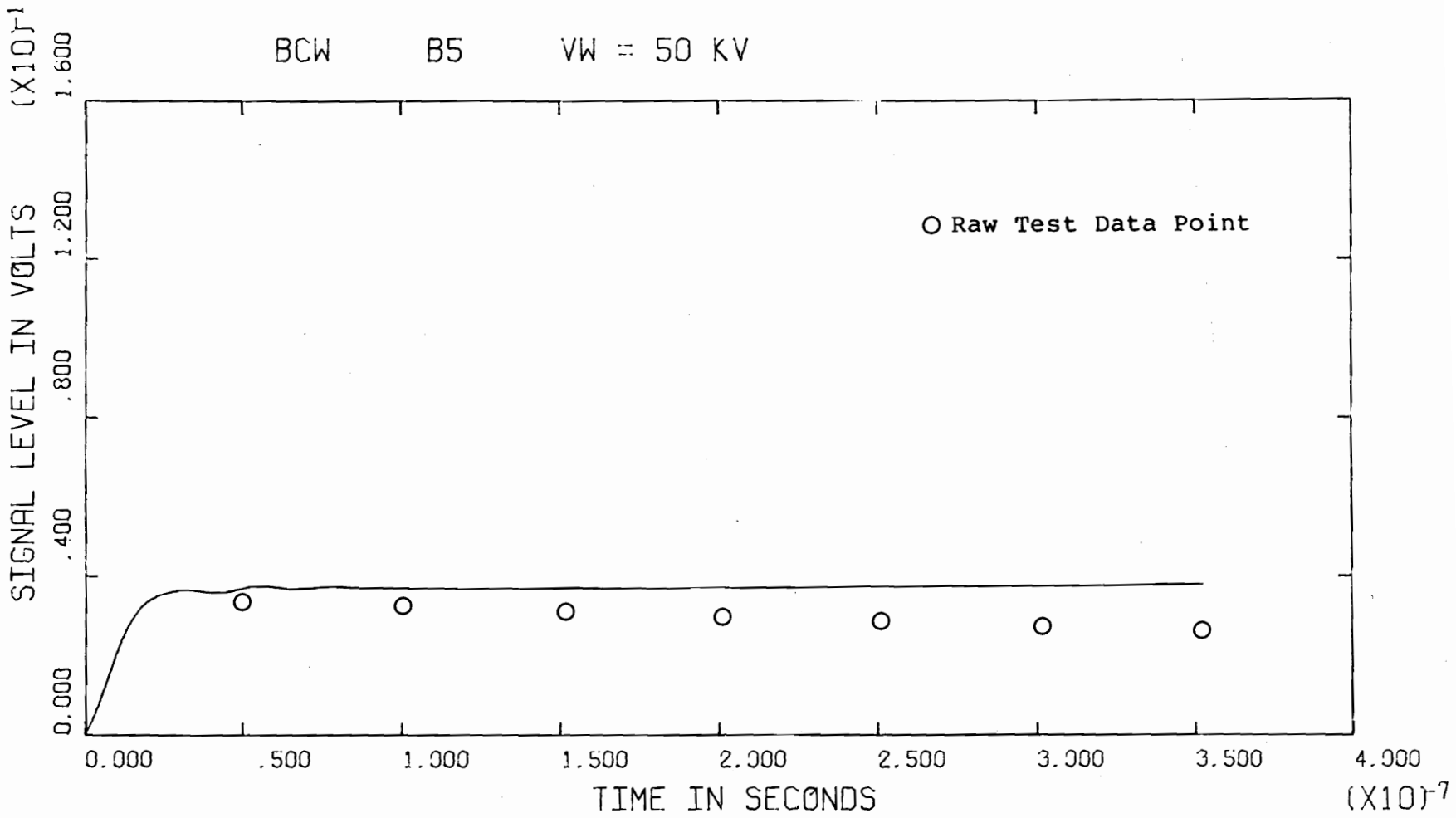

Figure B19

Corrected Test Data

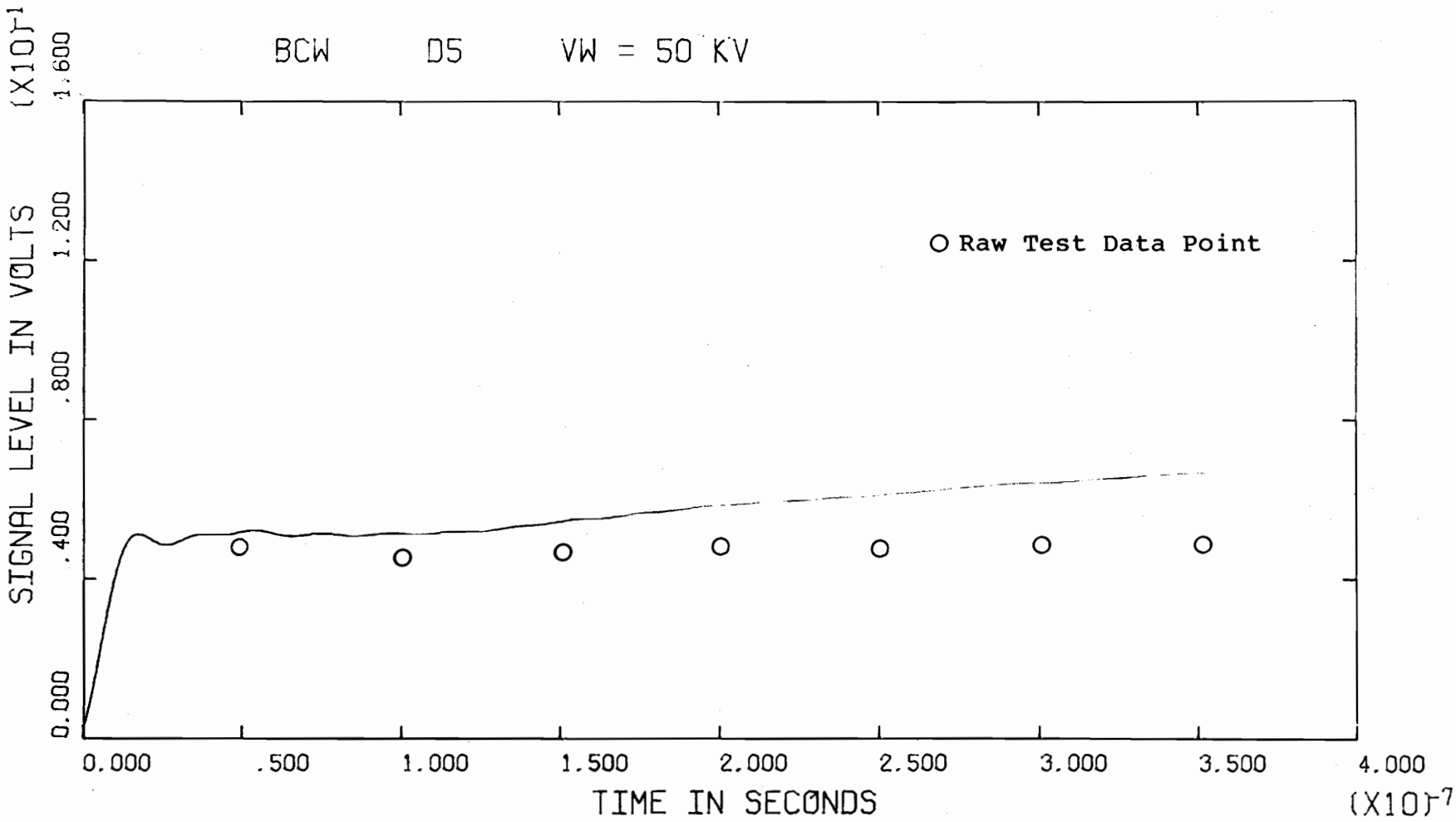

Figure B20

Corrected Test Data

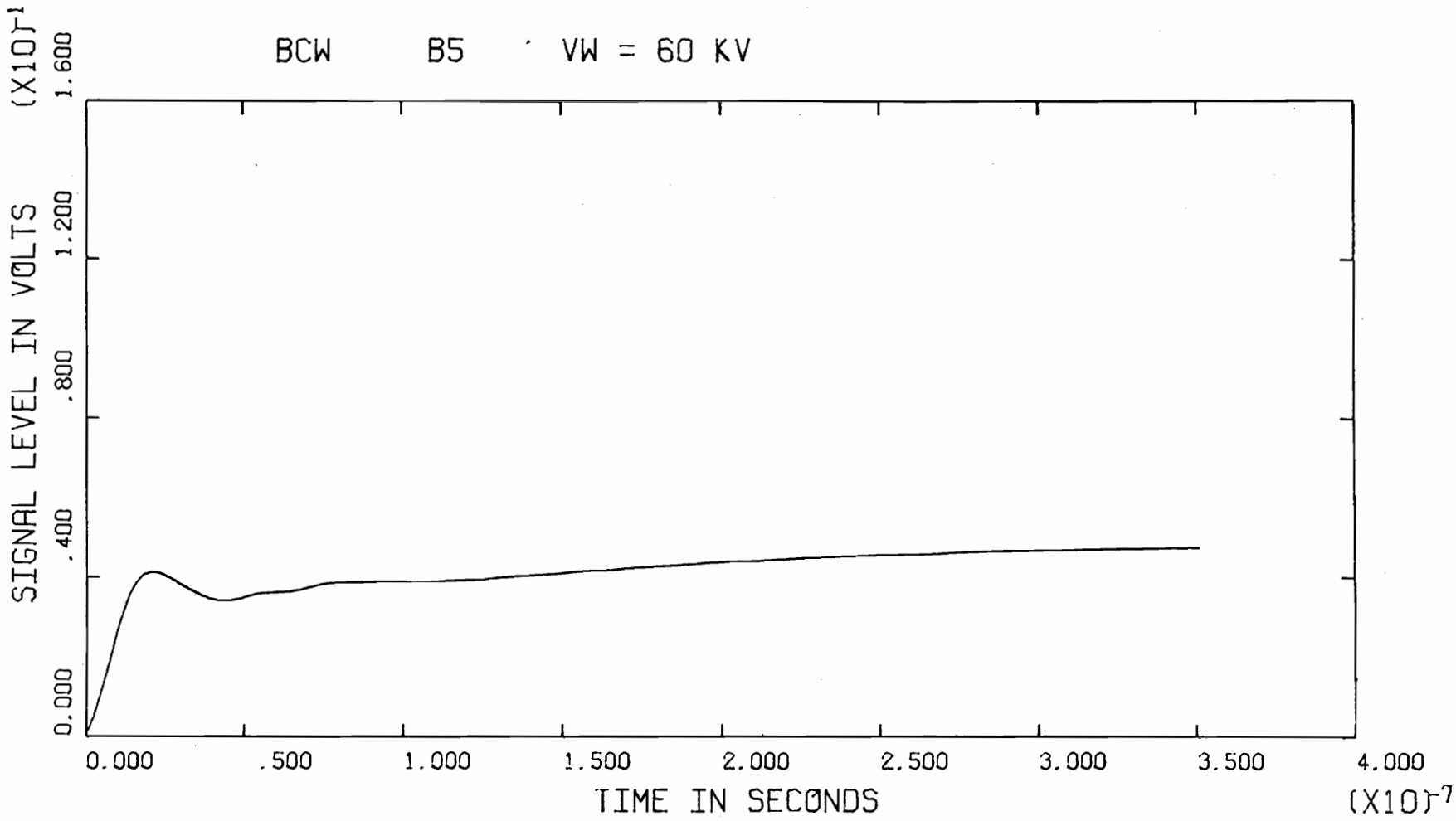

Figure B21

Corrected Test Data

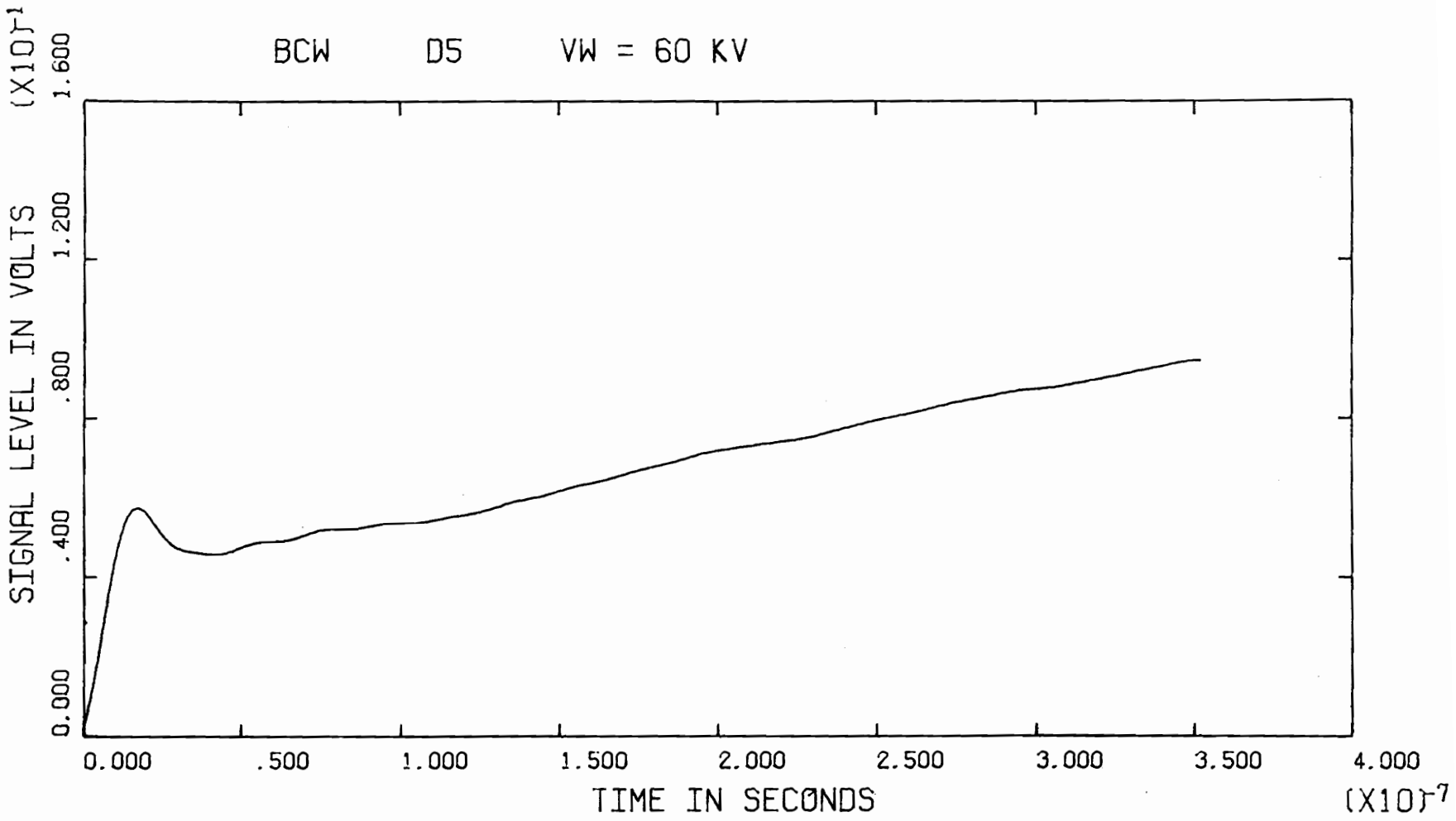

Figure B22

Corrected Test Data

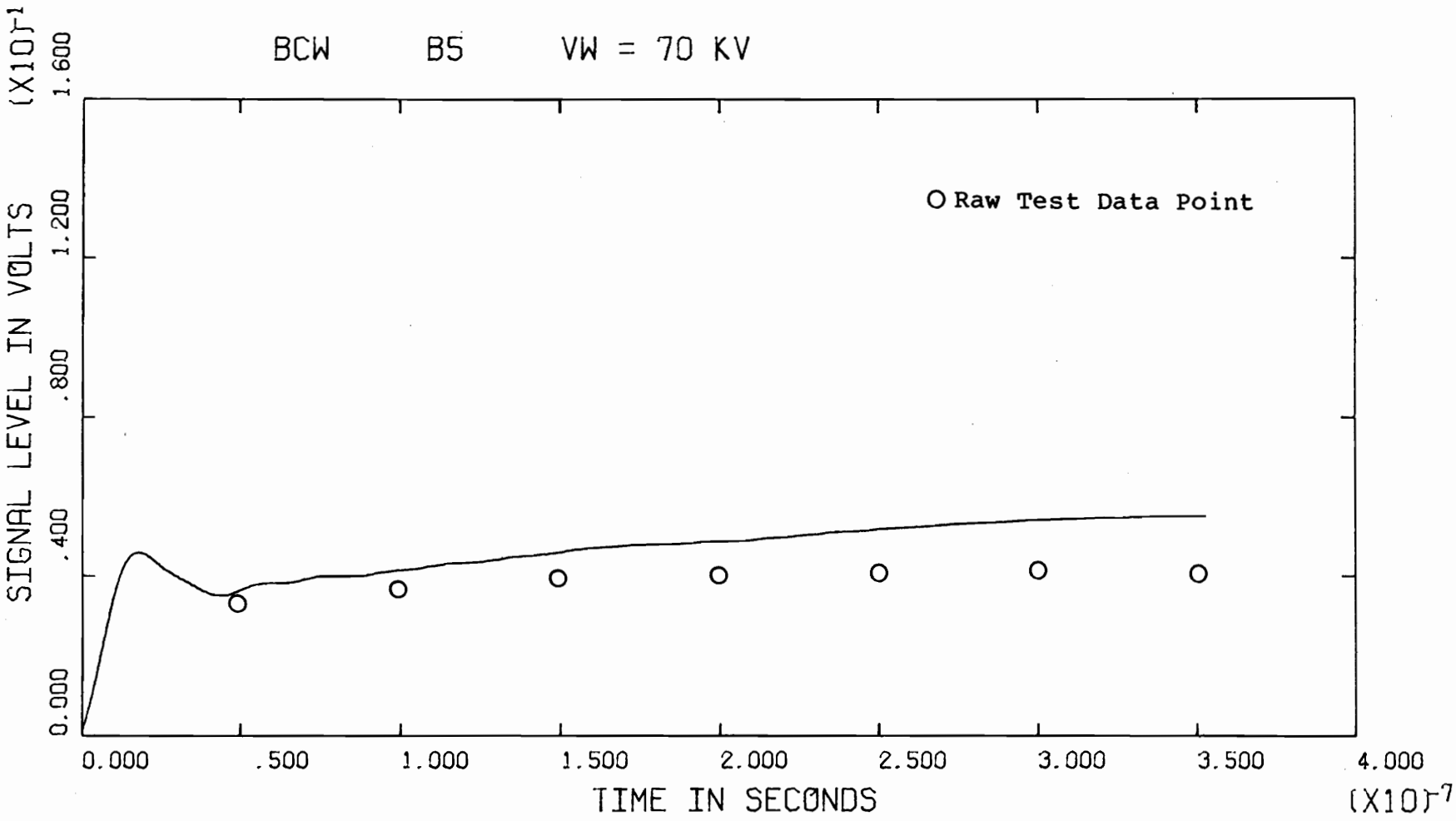

Figure B23

Corrected Test Data

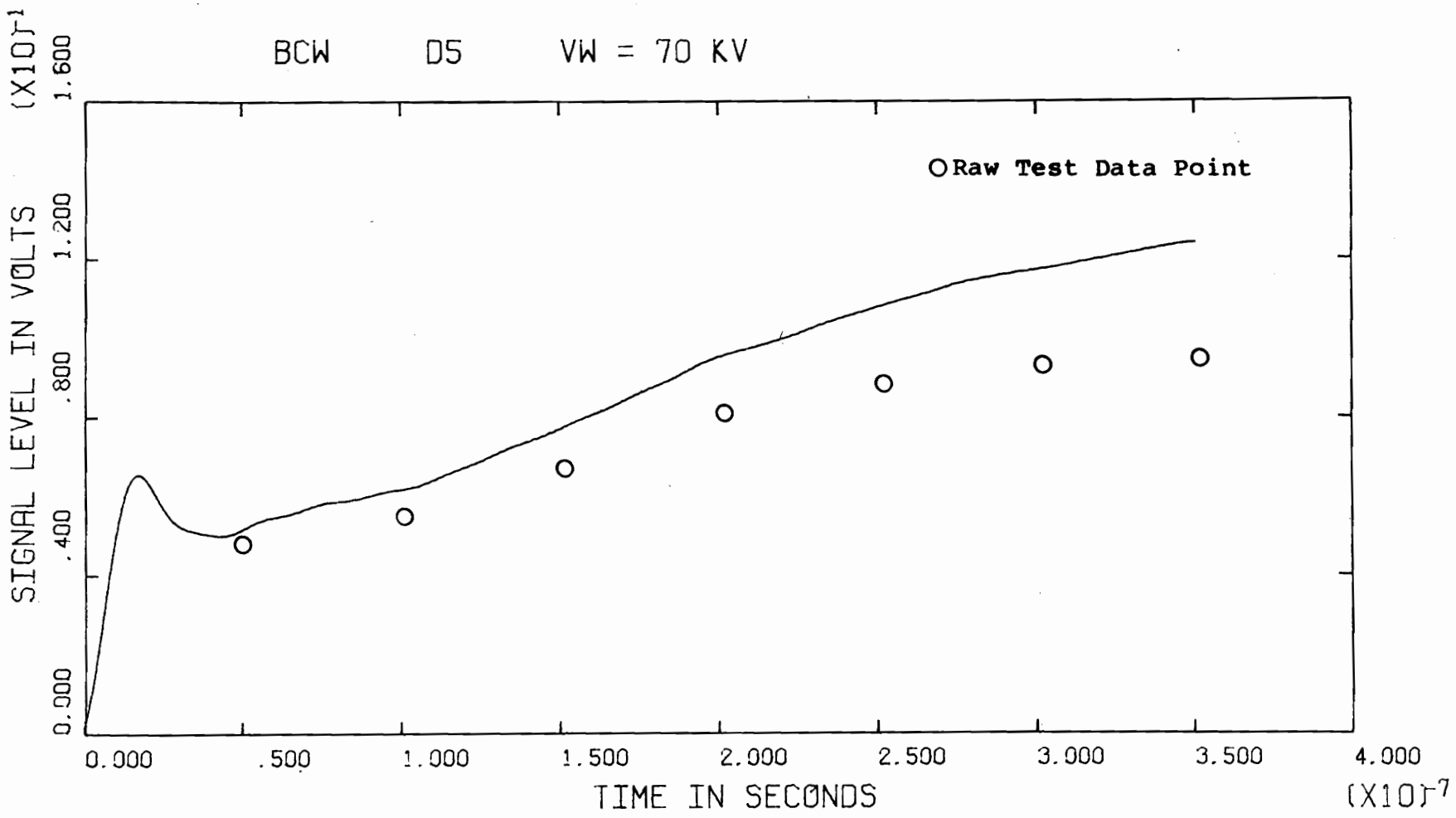

Figure B24

Corrected Test Data

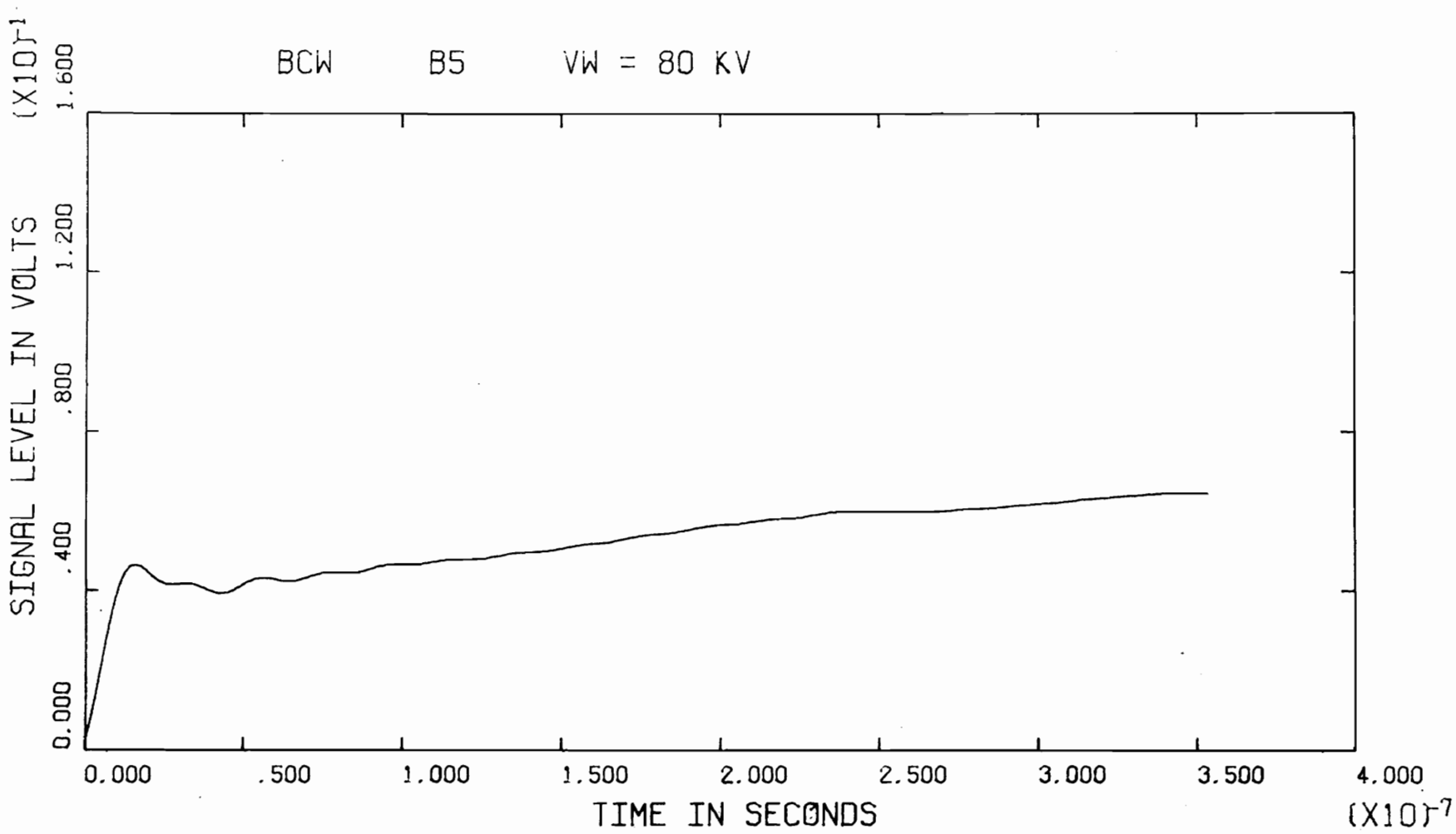

Figure B25

Corrected Test Data

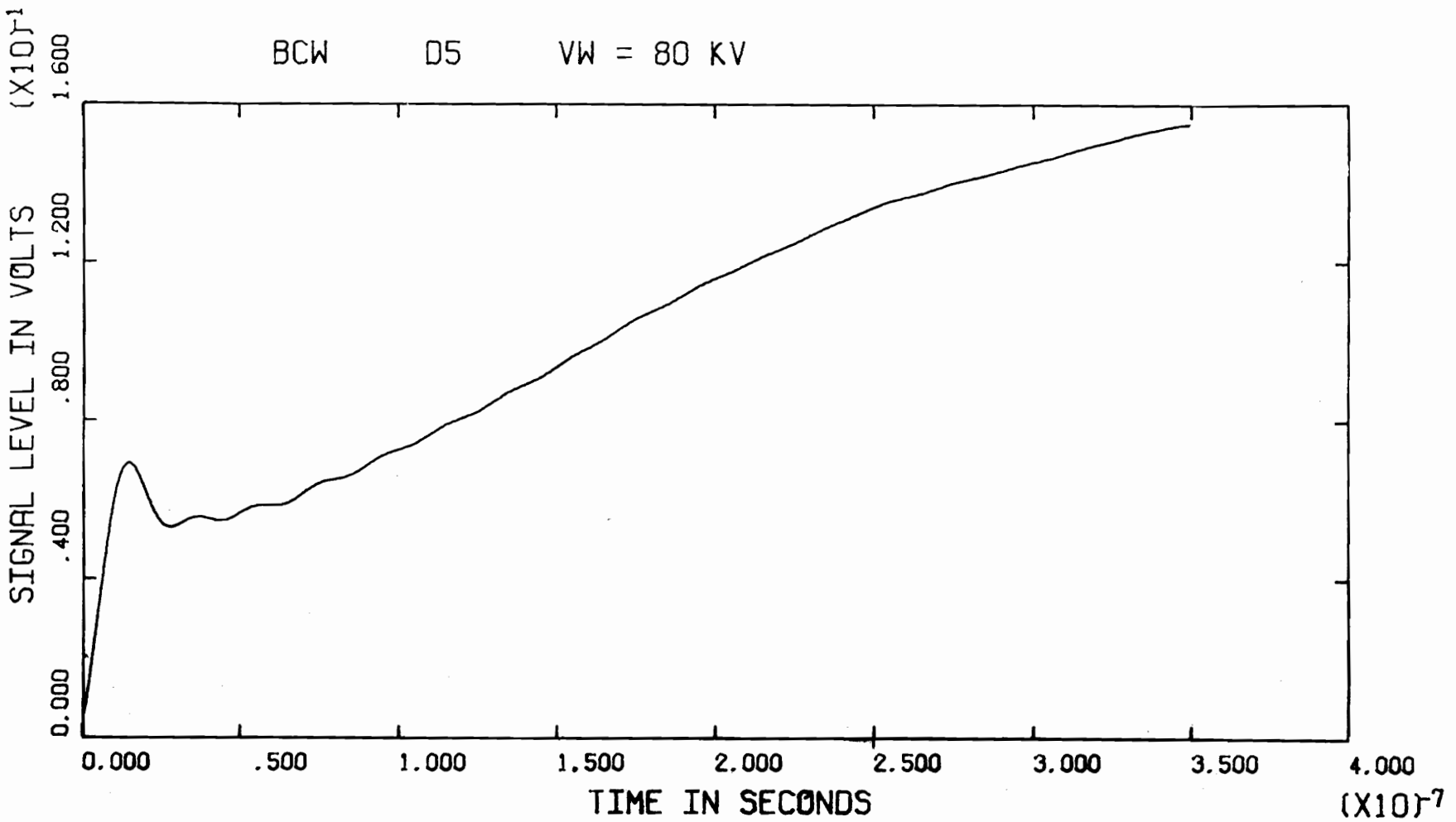

Figure B26

Corrected Test Data

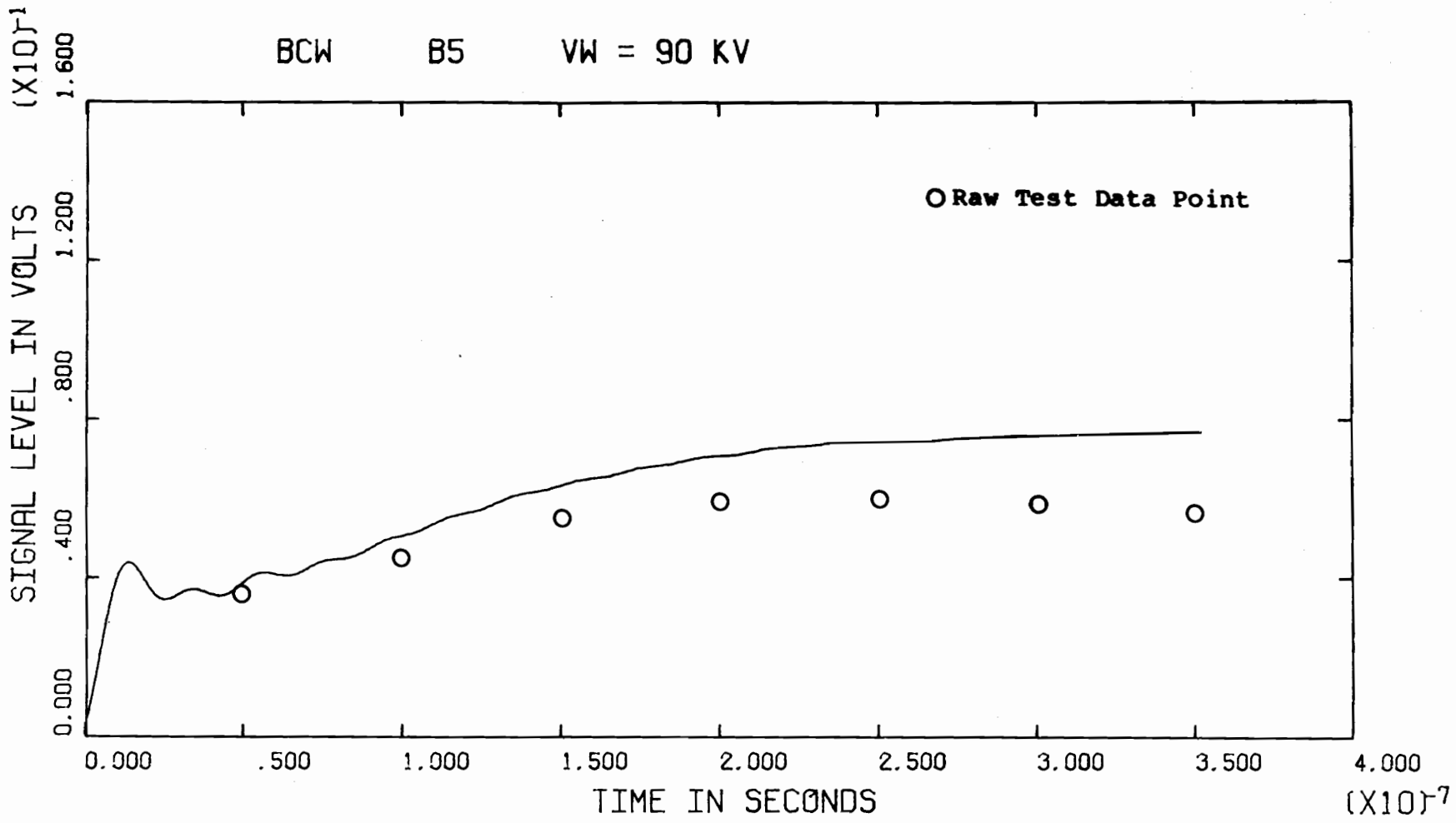

Figure B27

Corrected Test Data

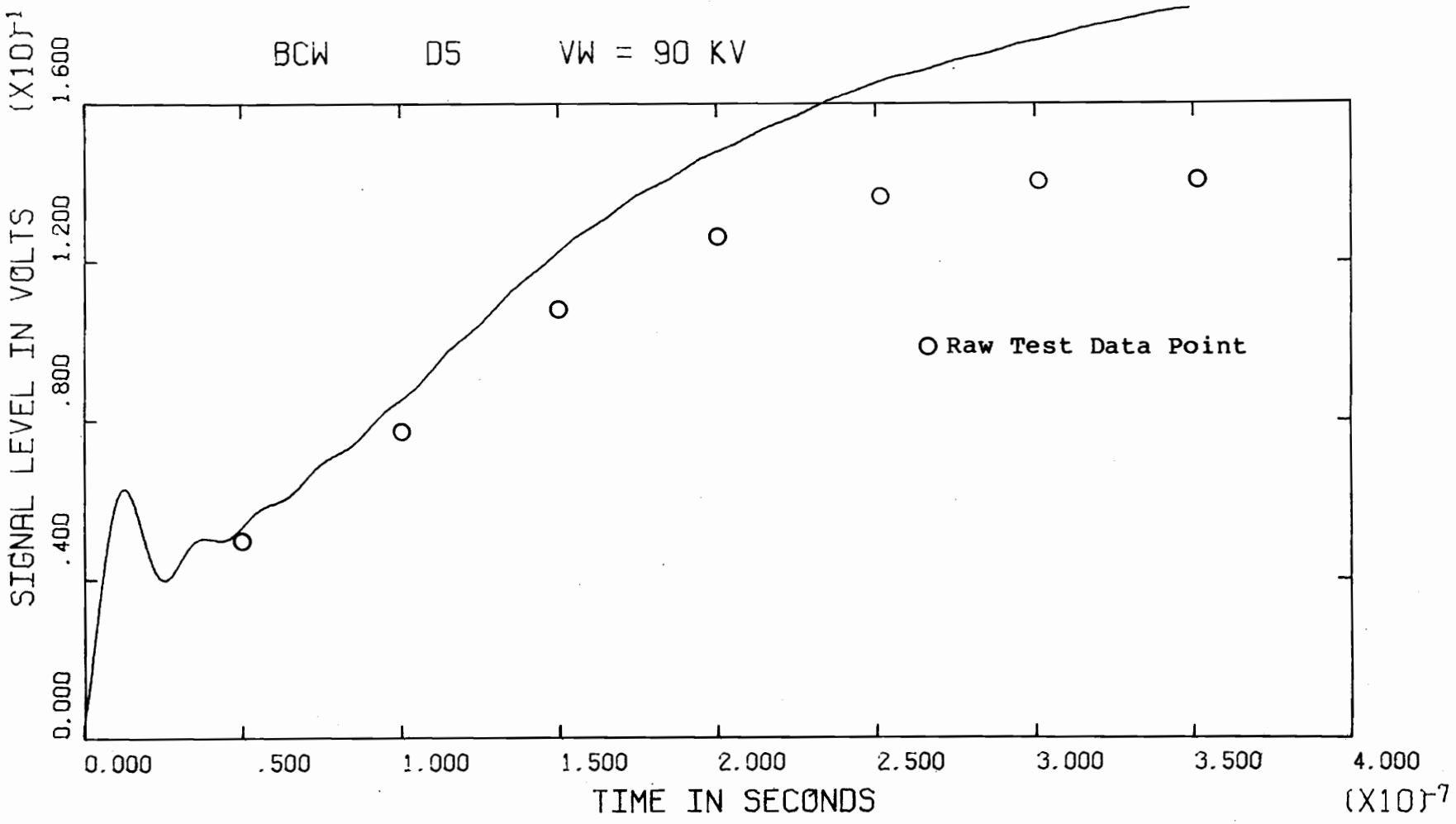

Figure B28

Corrected Test Data

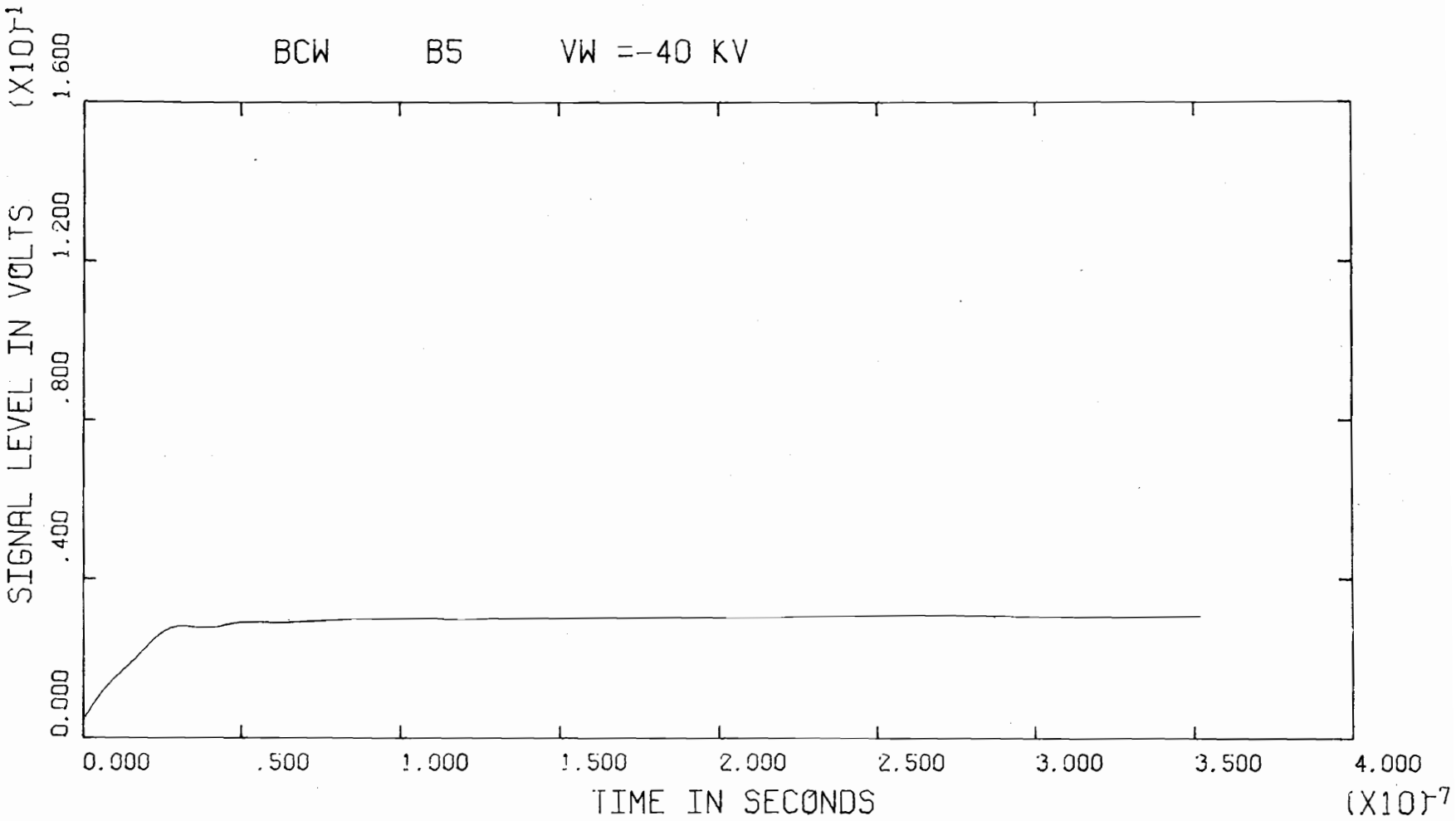

Figure B29

Corrected Test Data

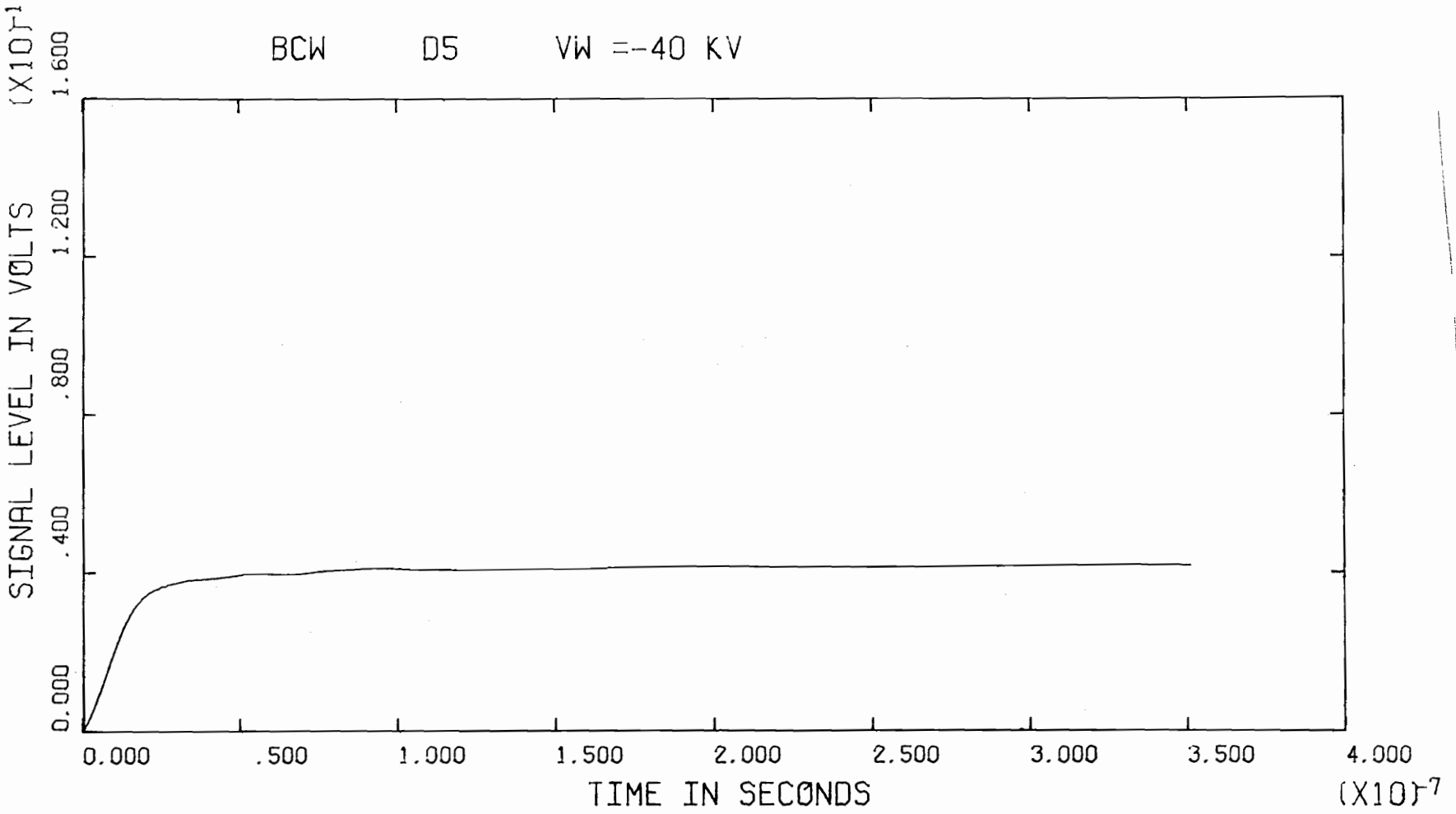

Figure B30

Corrected Test Data

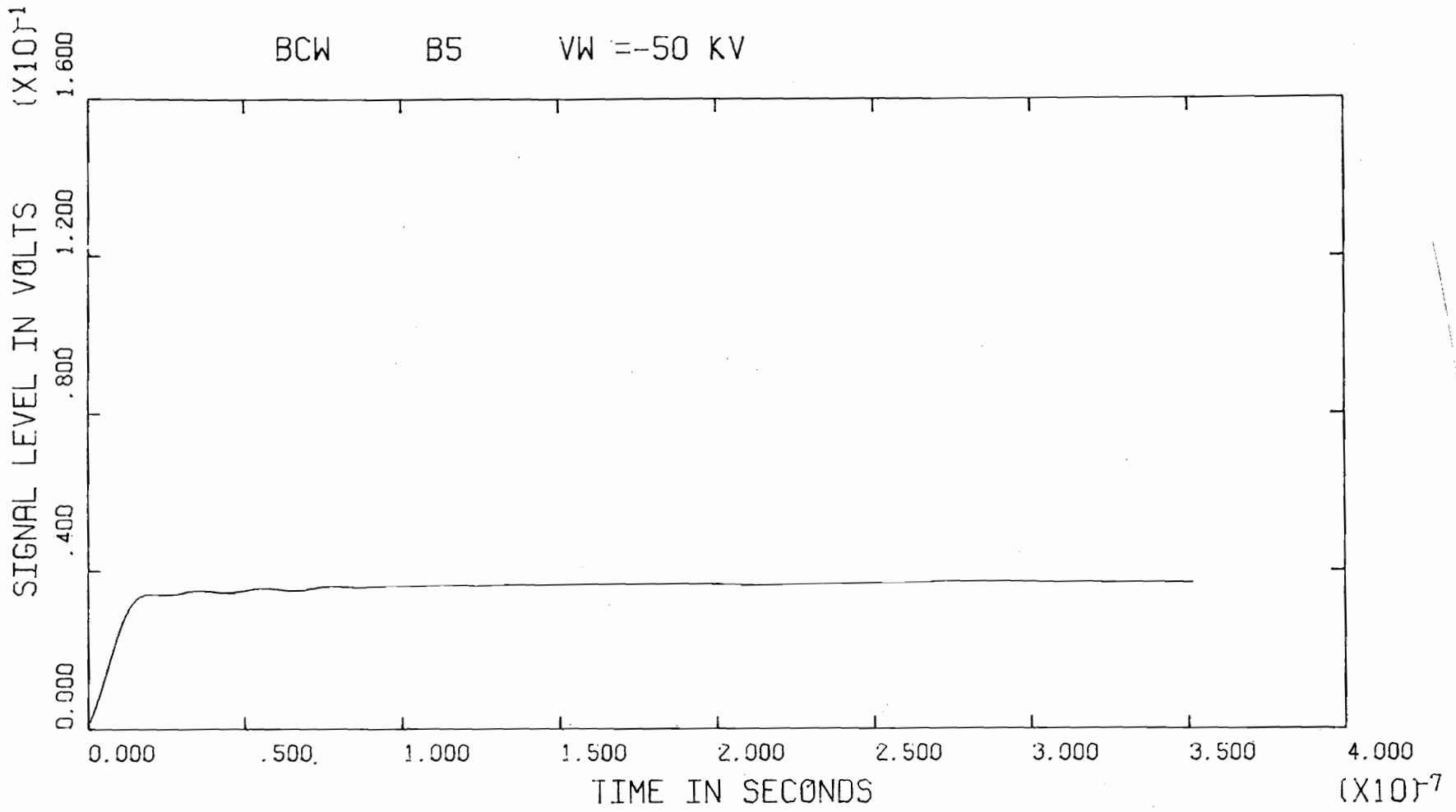

Figure B31

Corrected Test Data

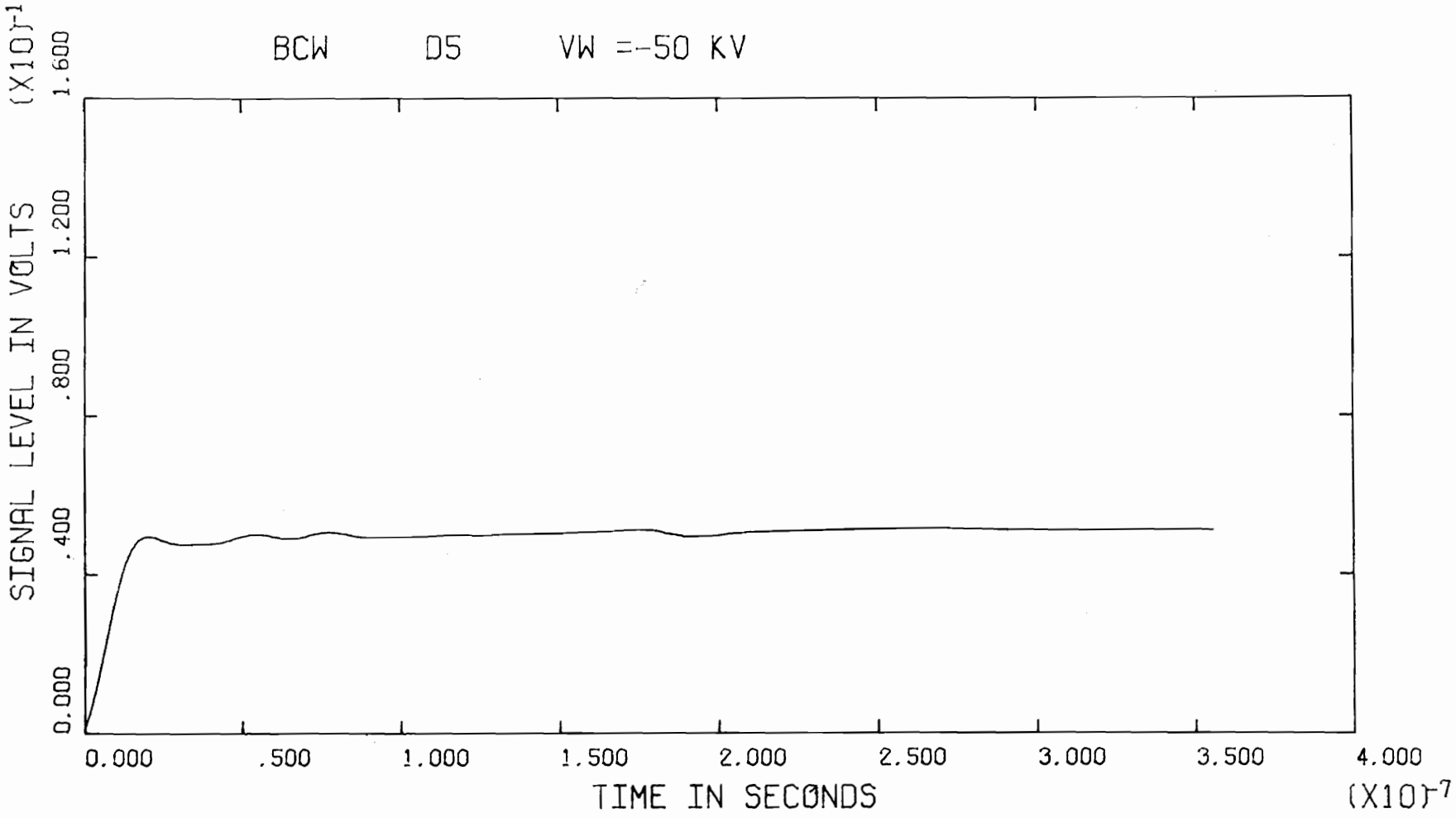

Figure B32

Corrected Test Data

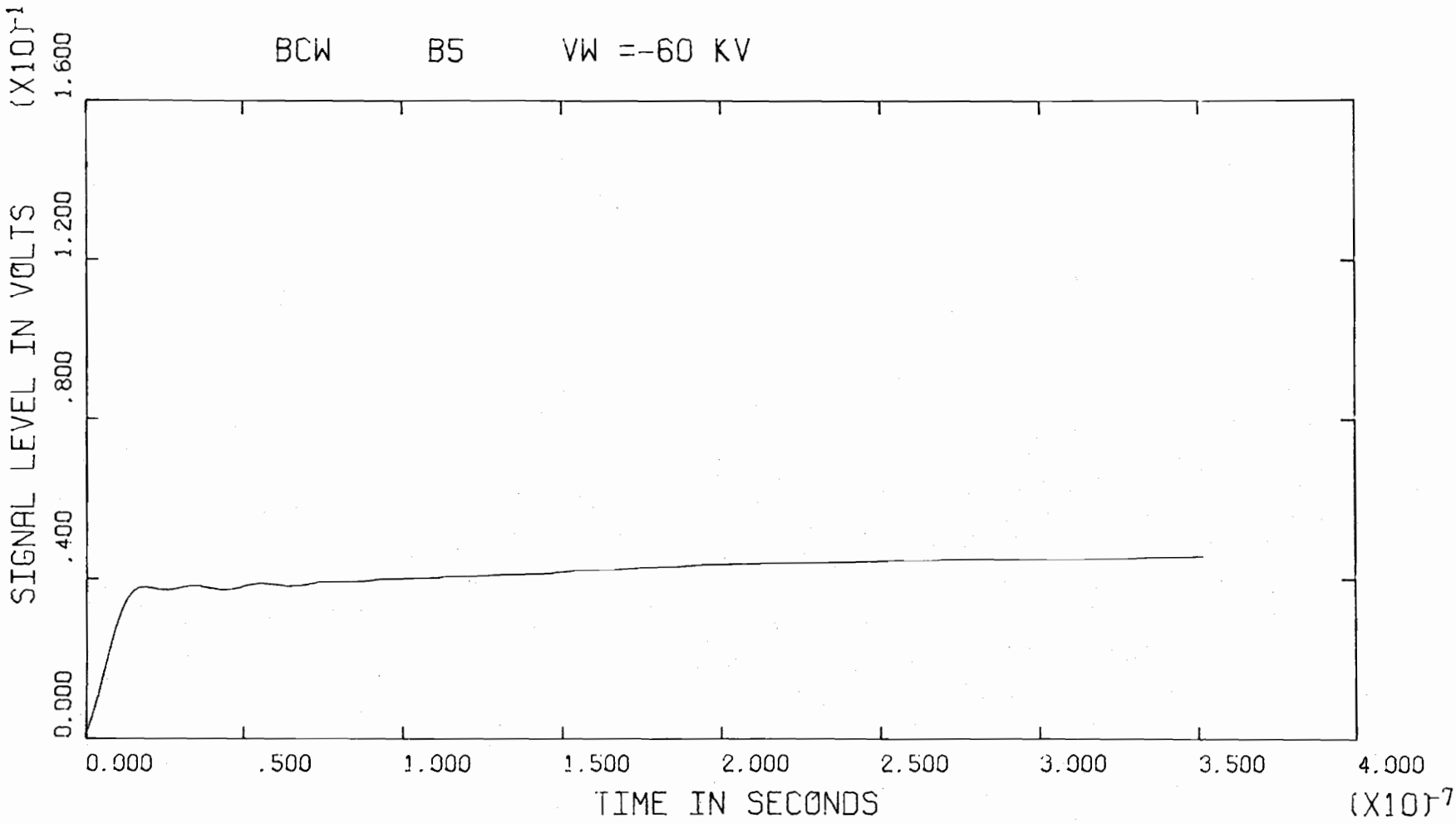

Figure B33

Corrected Test Data

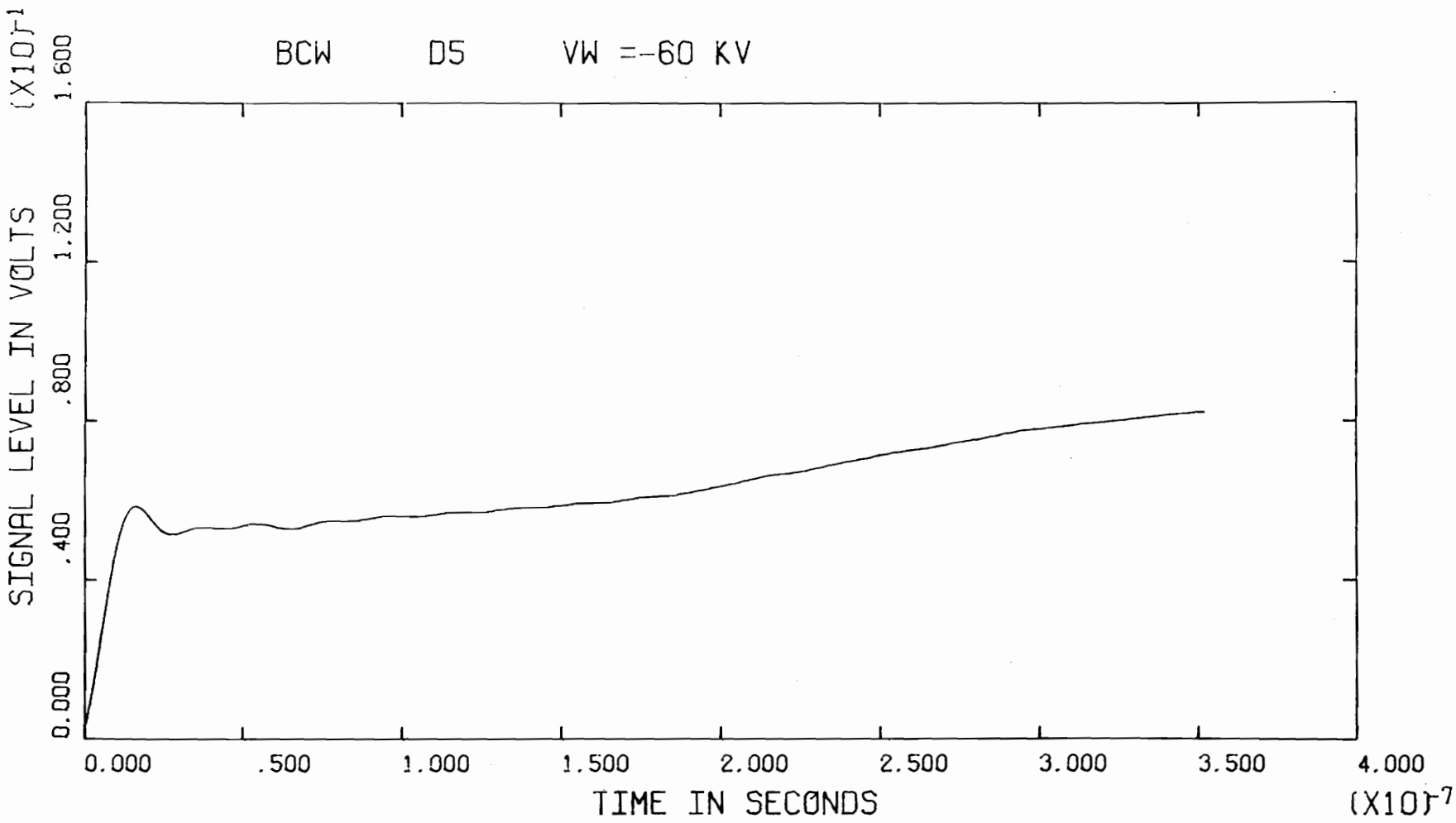

Figure B34

Corrected Test Data

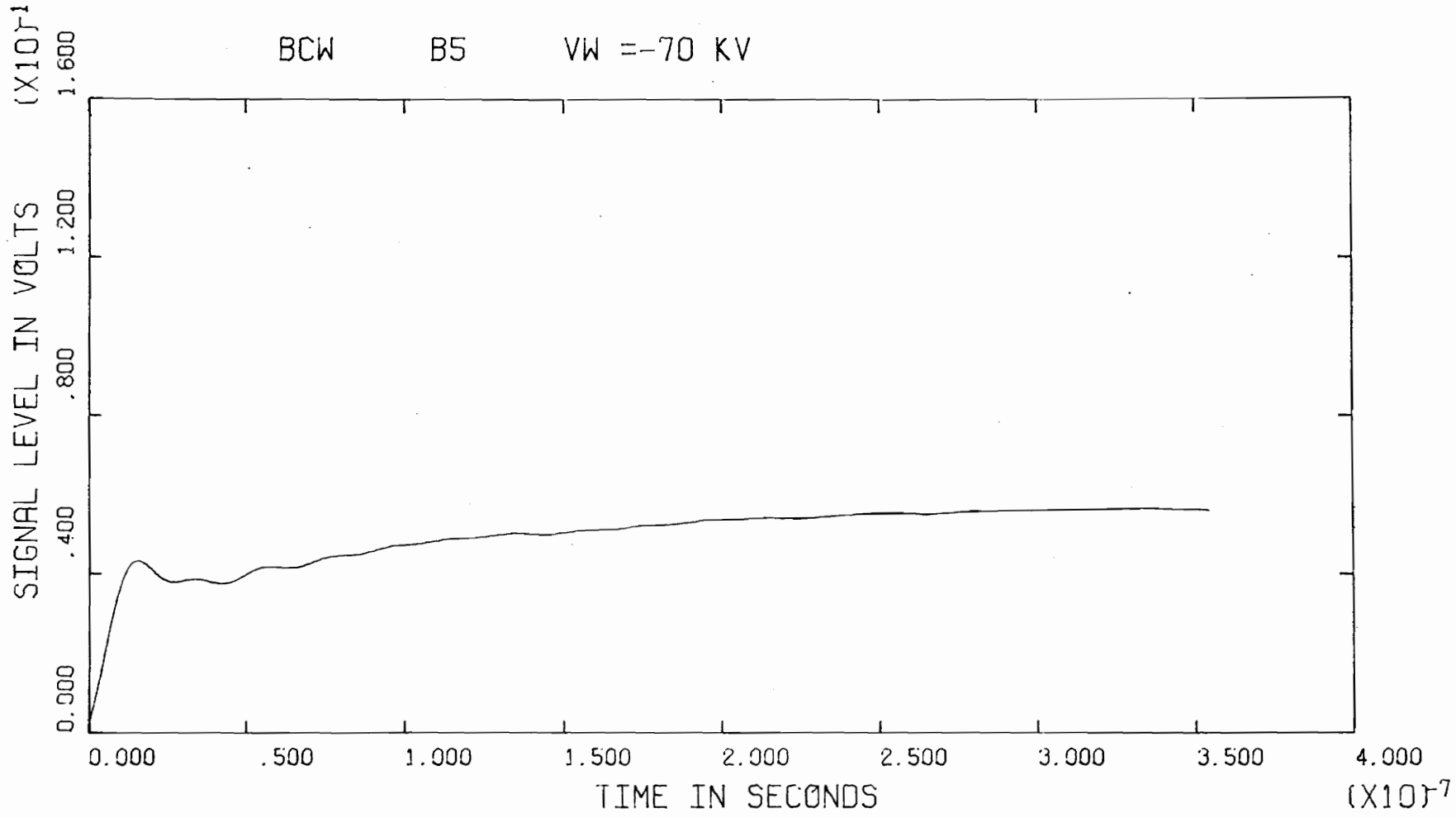

Figure B35

Corrected Test Data

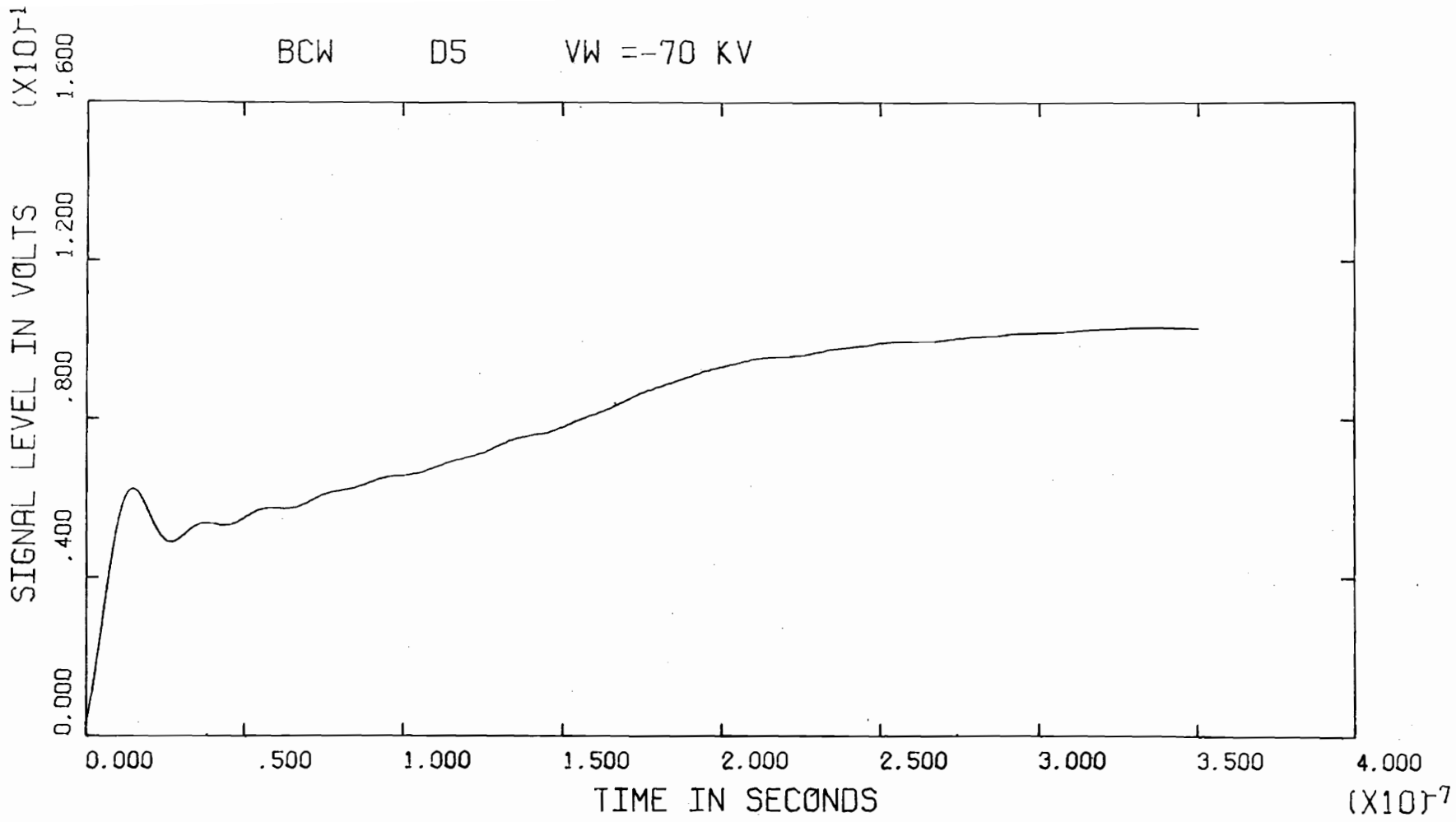

Figure B36

Corrected Test Data

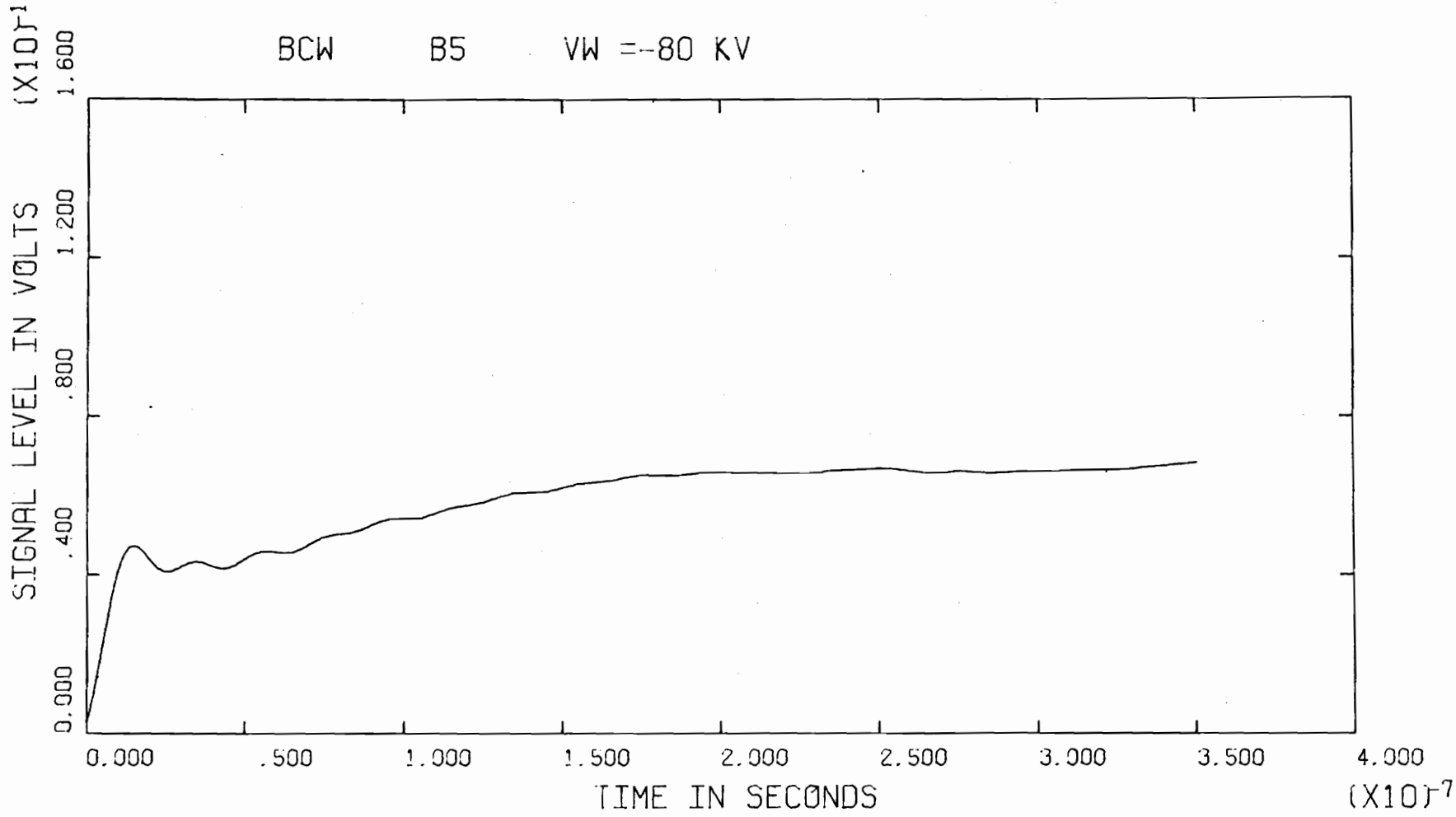

Figure B37

Corrected Test Data

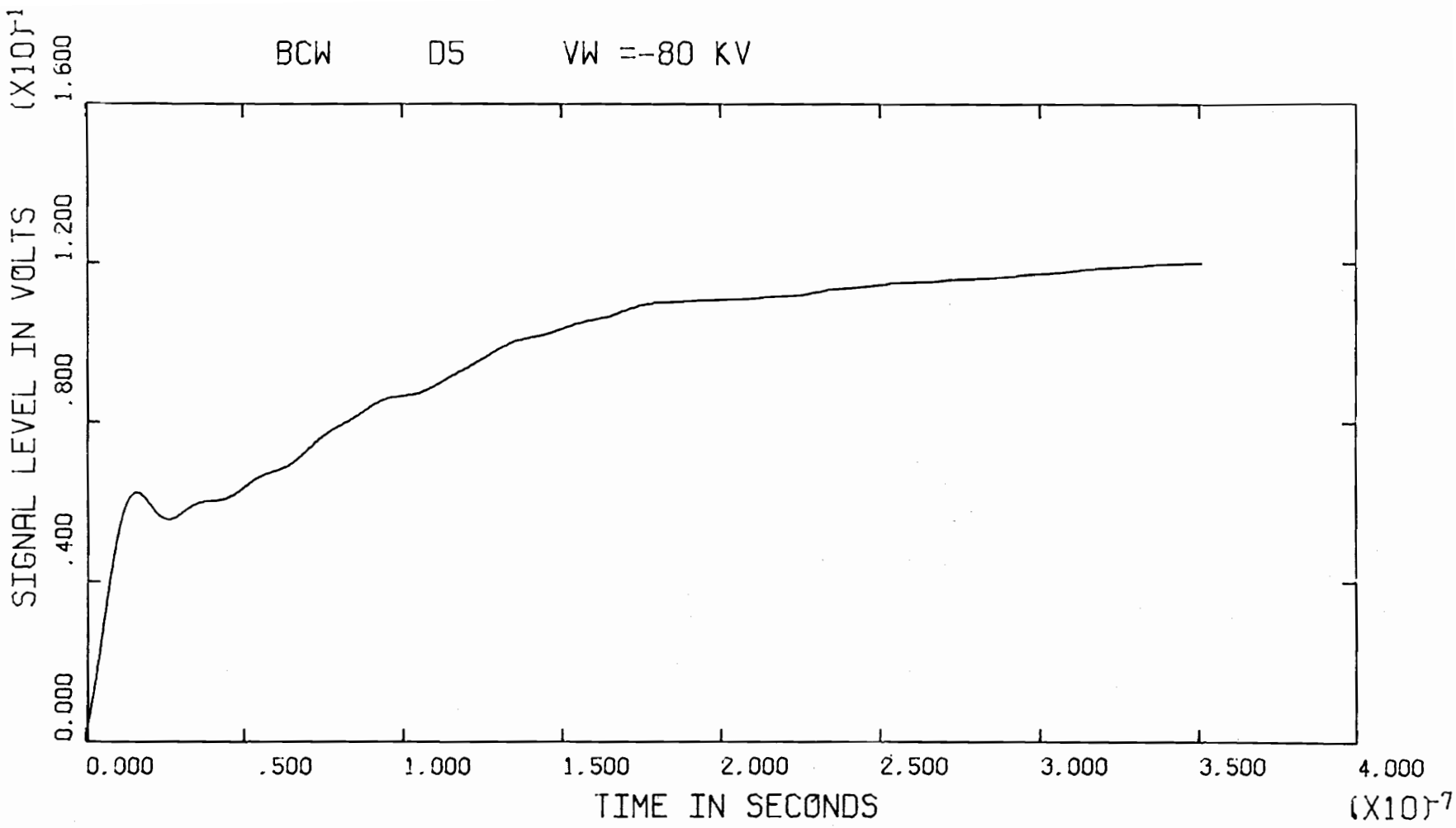

Figure B38

Corrected Test Data

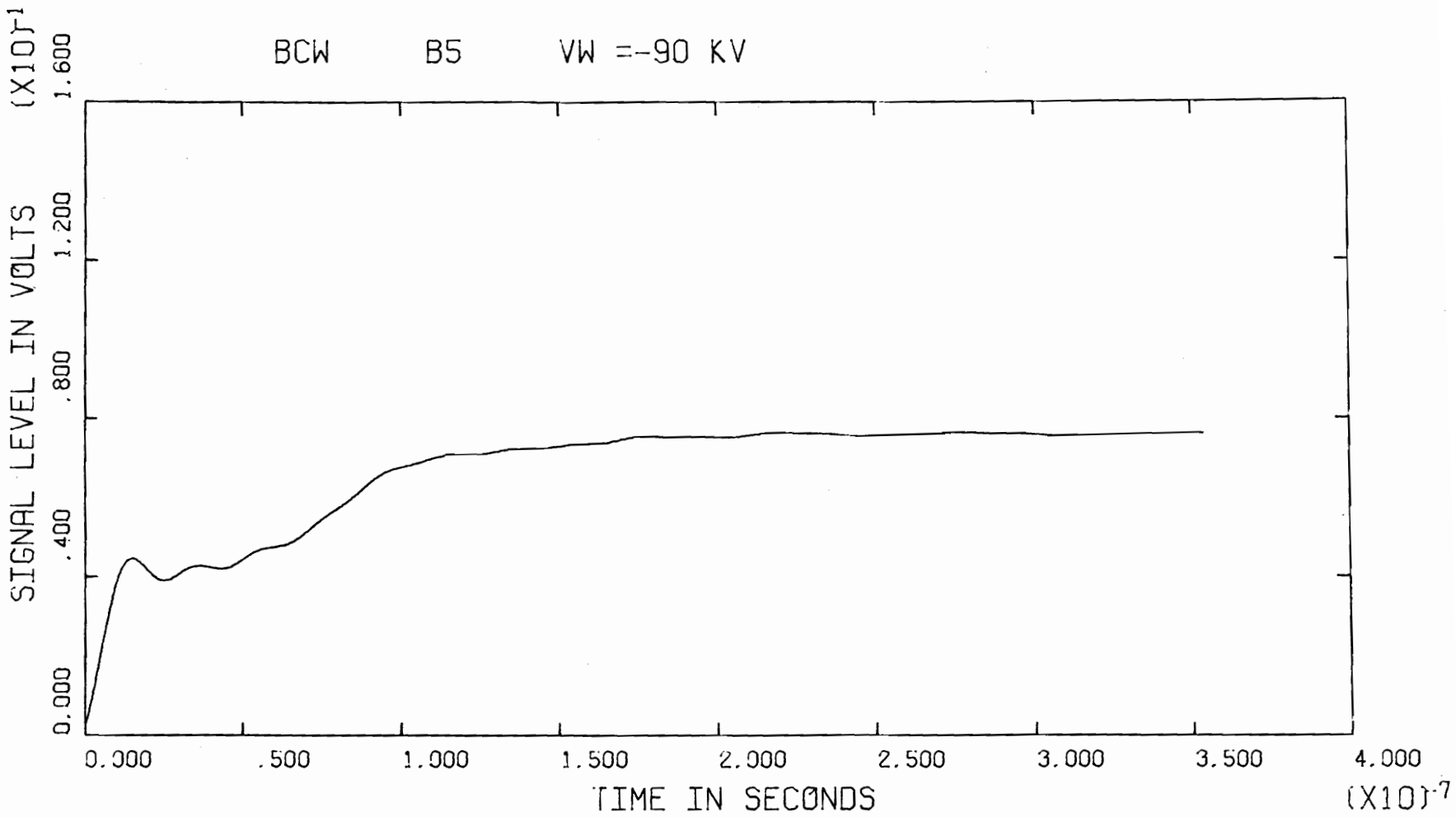

Figure B39

Corrected Test Data

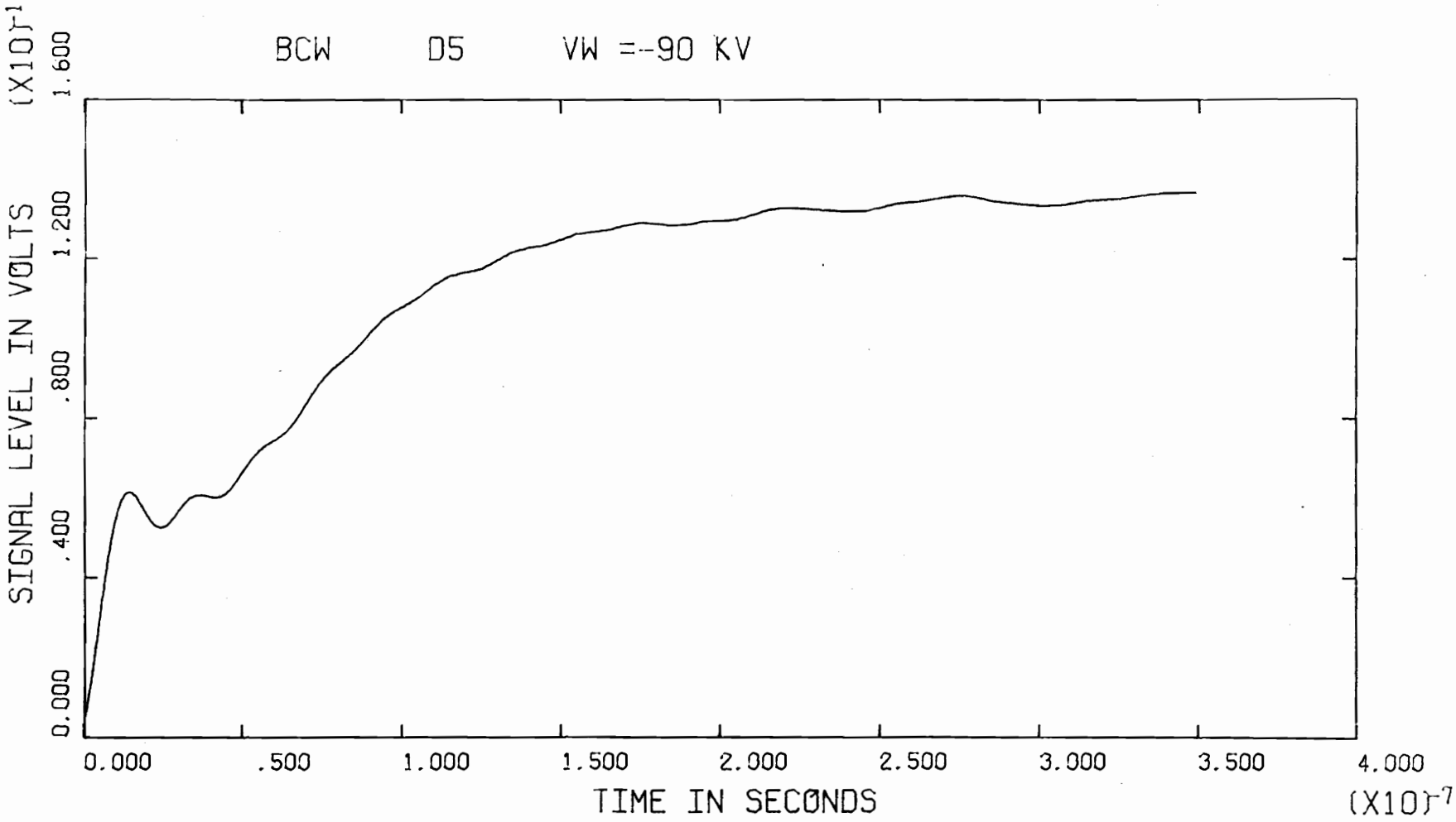

Figure B40

Corrected Test Data